DESIGN, SYNTHESIS, ANTIMALARIAL EVALUATION AND COMPUTATIONAL STUDIES OF SOME CHALCONE DERIVATIVES

BY

Asmau, Nasiru HAMZA

DEPARTMENT OF PHARMACEUTICAL AND MEDICINAL CHEMISTRY,
FACULTY OF PHARMACEUTICAL SCIENCES,
AHMADU BELLO UNIVERSITY,
ZARIA, NIGERIA

JUNE, 2018

DESIGN, SYNTHESIS, ANTIMALARIAL EVALUATION AND COMPUTATIONAL STUDIES OF SOME CHALCONE DERIVATIVES

BY

Asmau, Nasiru HAMZA
B.Pharm (ABU) 2004
MSc Pharmaceutical and Medicinal Chemistry, 2011
PhD/Pharm.Sci/10320/2011-2012

A THESIS SUBMITTED TO THE SCHOOL OF POSTGRADUATE STUDIES, AHMADU BELLO UNIVERSITY ZARIA,
IN PARTIAL FULFILLMENT OF THE REQUIREMENTS FOR THE AWARD OF DOCTOR OF PHILOSOPHY IN PHARMACEUTICAL AND MEDICINAL CHEMISTRY

DEPARTMENT OF PHARMACEUTICAL AND MEDICINAL CHEMISTRY,
FACULTY OF PHARMACEUTICAL SCIENCES,
AHMADU BELLO UNIVERSITY,
ZARIA, NIGERIA

JUNE, 2018

DECLARATION

I declare that the work in this thesis entitled "Design, Synthesis, Antimalarial Evaluation and Computational Studies of Some Chalcone Derivatives" has been performed by me in the Department of Pharmaceutical and Medicinal Chemistry, Ahmadu Bello University, Zaria. The information derived from the literature has been duly acknowledged in the text and a list of references provided. No part of this dissertation has been previously presented for another degree or diploma at this or any other Institution.

_____ _____

Asmau Nasiru HAMZA Date

CERTIFICATION

This thesis entitled 'DESIGN, SYNTHESIS, ANTIMALARIAL EVALUATION AND COMPUTATIONAL STUDIES OF SOME CHALCONE DERIVATIVES' by Asmau Nasiru HAMZA meets the regulations governing the award of the degree of Doctor of Philosophy of the Ahmadu Bello University, and is approved for its contribution to knowledge and literary presentation.

Prof. A.Y Idris Chairman, Supervisory Committee	Date
Prof. A.M Musa Member, Supervisory Committee	Date
Prof. A.K Haruna Member, Supervisory Committee	Date
Prof. A.M Musa Head of Department	Date
Prof. A. Z. Abubakar Dean, School of Postgraduate Studies	Date

DEDICATION

This work is dedicated to my department: Department of Pharmaceutical and Medicinal Chemistry, Ahmadu Bello University, Zaria.

ACKNOWLEDGEMENT

All praise and thanks is due to Almighty Allah the most Beneficent, the most Merciful and, the Exalted. May the peace and blessings of Almighty Allah be upon our Nobel Prophet Muhammad (SAW), his family and his companions.

I wish to express my sincere gratitude and appreciation to my diligent supervisors, Prof. A.Y. Idris, Prof. A. M. Musa and, Prof A.K. Haruna for their constant support, encouragement and guidance academically, morally and financially. I pray that Allah reward them abundantly. I would also like to sincerely appreciate Prof. M. I. Sule, Prof. U.U. Pateh and Mal I. M. Iliyasu for their assistance towards the realization of this project; thank you all and May Allah reward you abundantly.

I am also grateful to Prof. Mahmoud Soliman of Kwa-Zulu Natal University, Durban and his team, especially Mal Umar Ndagi for giving me the opportunity to actualize my dreams, thank you for the training on computational chemistry. I am also highly indebted to Prof Uzairu of Chemistry Department, A.B.U, Zaria, for his guidance and encouragement on computational aspect of the work.

To the staff of Phamaceutical and Medicinal Chemistry, A.B.U, Zaria, you were all there for me throughout the struggle, I really appreciate it all. I am also grateful to Dr. (Mrs) Amina Busola Olorukooba, Mrs Aisha Shehu and Mal Aliyu for assisting in the pharmacological screening, Mr Dilip, Mal Buhari and Anita of Chemistry Department, Kwa-Zulu Natal University, Durban for the spectroscopic analysis.
My special appreciation goes to the family of Late Alkali Hamza Muh'd Bichi, my husband: Muh'd Nasiru Nasarawa, my children and my friends, far too numerous to mention.
I also thank the Tertiary Education Trust Fund (TETFund) for the financial sponsorship of the computational work.

TABLE OF CONTENTS

TITLE PAGE ..... **ii**

DECLARATION ..... **iii**

CERTIFICATION ..... **iv**

DEDICATION ..... **v**

ACKNOWLEDGEMENT ..... **viii**

TABLE OF CONTENTS ..... **ix**

LIST OF TABLES ..... **xv**

LIST OF FIGURES ..... **xvi**

LIST OF APPENDICES ..... **xix**

ABBREVIATION ..... **xxiv**

ABSTRACT ..... **xxvii**

CHAPTER ONE **1**

1.0 INTRODUCTION **1**

1.1 Statement of Research Problem **6**

1.2 Justification of the Study **7**

1.3 Aim and Objectives of the Study **8**

1.4 Research Hypothesis **9**

CHAPTER TWO **10**

2.0 LITERATURE REVIEW **10**

2.1 Malaria **10**

2.1.1 Pathogenesis 10

2.1.2 Chemotherapy 12

2.1.3 Novel malaria targets 13

2.2 The Proteases 13

2.2.1 Cysteine protease 14

2.2.2 Aspartic proteases 16

2.2.3 Mechanism of hemoglobin degradation by the protease 18

2.2.4 Protease inhibitors 20

2.3 Chalcones 21

2.3.1 Chemistry of chalcones 21

2.3.2 Chemical synthesis 23

2.3.3 Chalcones as protease inhibitors 24

2.3.4 Present work 31

2.4 Computational Chemistry 32

2.4.1 Computer-assisted drug design (CADD) 35

2.5 Theoretical Oral Bioavailability 42

CHAPTER THREE 43

3.0 MATERIALS AND METHODS 43

3.1 Materials 43

3.1.1 Equipment and glassware 43

3.1.2 Reagents, solvents and standard drugs 44

3.1.3 Experimental Animals 44

3.1.4 Malarial parasite 44

3.1.5 Computer hardware and software 45

3.1.6 Protein crystal structure 45

3.2 Methods 45

3.2.1 Design strategy 45

3.2.2 Evaluation of theoretical oral bioavailability 47

3.2.3 Synthesis of chalcones (Claisen –Schmidt Condensation) 47

3.2.4 Procedure for the synthesis of the substituted chalcones 48

3.2.5 Characterization 50

3.2.6 Evaluation of *in vivo* antiplasmodial activity 51

3.2.7 *In vit*ro determination of hematin polymerization inhibitory activity 52

3.2.8 Data analysis 53

3.2.9 Computational studies 53

CHAPTER FOUR 58

4.0 RESULT 58

4.1 Designed Substituted Chalcones 58

4.2 Analysis of Theoretical Oral Bioavailability 59

4.3 Synthesis and Characterization of the Substituted Chalcones 64

4.3.1 Yield and some physical properties of substituted chalcones. 64

4.3.2 ^{1}H and ^{13}C NMR Data of P1, P2 and P13 66

4.3.3 ^{1}H and ^{13}C NMR data of P3, P4 and P8 68

4.3.4 ^{1}H and ^{13}C NMR Data of P11, P12 and P17 70

4.3.5 ^{1}H and ^{13}C NMR Data of P15, P16 and P23 72

4.3.6 ^{1}H and ^{13}C NMR assignment of P19, P24 and P25 74

4.3.7 ^{1}H and ^{13}C NMR data of P21, and P22 76

4.3.8 FT-IR spectral data of the substituted chalcones 78

4.3.9 Mass spectral data of the substituted chalcones 78

4.4 Antiplasmodial Studies on the Substituted Chalcones in Mice 79

4.4.1 Effect of P1, P2, P3, P4, P23, P24 and P25 on established *P. berghii* infection in mice ……79

4.4.2 Effect of P11, P12, P13, P15, P16, P17, P19, P21 and P22 on established *P. berghii* infection in mice 81

4.5 Effect of Substituted Chalcones on Inhibition of *β-hematin* Synthesis 82

4.6 Molecular Docking Studies of P3 and P4 Complexes on FP-2, FP-3, Plm-II, and Plm-IV 84

4.6.1 Validation of docking procedure 84

4.6.2 The binding energies of the co-crystallized ligands and 17 substituted Chalcones against four enzymes (FP-2, FP-3, Plm-II, and, Plm-IV) 86

4.6.3 The binding pose and binding interaction analysis of P3 and P4 against FP-2, FP-3, Plm-II, and Plm-IV. 90

4.7 Molecular Dynamics Simulation Studies of P3 and P4 Complexes of FP-2, FP-3, Plm-II, and Plm-IV. 99

4.7.1 System stability 99

4.7.2 Per-residue energy decomposition analysis 104

4.7.3 Binding free energy (BFE) analysis of P3 and P4 in complex with FP-2, FP-3, Plm-II and Plm-IV 109

CHAPTER FIVE 111

5.0 DISCUSSIONS 111

5.1 Design of Substituted Chalcones 111

5.2 Theoretical Oral Bioavailability 112

5.3 Synthesis and Characterization 112

5.3.1 Synthesis and characterization of 2,3,4–trimethoxy benzaldehyde Chalcones (P1,P2 and P13) ……112

5.3.2 Synthesis and characterization of 3-quinolinyl benzaldehyde Chalcones (P3, P4 and P8) ……114

5.3.3 Synthesis and characterization of 2,4–dimethoxy benzaldehyde Chalcones (P11, P12 and P17) ……116

5.3.4 Synthesis and characterization of 4–methoxy benzaldehyde Chalcones (P15, P16, P23 and P25)..... 118

5.3.5 Synthesis and characterization of un-substituted (benzaldehyde) Chalcones (P19 and P24) ……...119

5.3.6 Synthesis and characterization of 4-triflouromethyl benzaldehyde Chalcones (P21 and P22) 120

5.4 Antimalarial Studies..... 121

5.4.1 *In-vivo* antimalarial studies (Curative test)..... 121

5.4.2 *In-vitro* antimalarial study (*β-hematin* inhibition assay) 123

5.5 Computational Studies..... 124

5.5.1 Docking Studies..... 124

5.5.2 Molecular dynamics simulation..... 126

CHAPTER SIX..... 132

6.0 SUMMARY, CONCLUSION AND RECOMMENDATION..... 132

6.1 Summary of Findings..... 132

6.2 Conclusion..... 134

6.3 Contribution to Knowledge..... 135

6.4 Recommendation..... 135

REFERENCES 137

APPENDICES 150

LIST OF TABLES

Table 3.1: Reagents for the synthesis of the substituted chalcones 49

Table 3.2: Grid-box parameters for the enzymes 55

Table 4.1: Chemical description P1, P2, P3, P4 and, P8 59

Table 4.2: Chemical description of P11, P12, P13, P15, P16 and P17 60

Table 4.3: Chemical description of P19, P21, P22, P23, P24 and P25 61

Table 4.4: Analysis of theoretical oral bioavailability 63

Table 4.5: Yield and Some Physical Properties of the substituted chalcones 65

Table 4.6: ^{1}H and ^{13}C NMR Data of P1, P2 and P13 67

Table 4.7: ^{1}H and ^{13}C NMR Data of P3, P4 and P8 69

Table 4.8: ^{1}H and ^{13}C NMR Data of P11, P12 and P17 71

Table 4.9: ^{1}H and ^{13}C NMR Data of P15, P16 and P23 73

Table 4.10: ^{1}H and ^{13}C NMR Data of P19, P24 and P25 75

Table 4.11: ^{1}H and ^{13}C NMR Assignment of P21, and P22 77

Table 4.12: Effect of P2, P3, P4, P8, P11, P12, P17, P21 and P25 on inhibition of β-hematin synthesis 83

Table 4.13: Showing the crystal structure of enzyme complexes and re-docked ligand super-imposed on the crystal structure for validation. 85

Table 4.14: Binding free energy analysis of P3 and P4 in complex with FP-2, FP-3, Plm-II and Plm-IV 110

LIST OF FIGURES

Figure 1.1: Chalcone..... 5

Figure 2.1: The life cycle of *Plasmodium falciparum*. 11

Figure 2.2: Cartoon representation of the structure of falcipain-2..... 15

Figure 2.3: Ribbon diagram of the complex of plasmepsins II with EH58. 17

Figure 2.4: The degradation process of hemoglobin in the *P. falciparum* food vacuole. 20

Figure 2.5: (E) and (Z) chalcone..... 22

Figure 3.6: Claisen-Schmidt condensation. 23

Figure 2.7: Based catalyzed reaction mechanism for chalcone formation 24

Figure 2.8: oxalic bis[(2-hydroxy- 1-naphthylmethylene)hydrazide] 25

Figure 2.9: Licochalcone A 27

Figure 2.10: 2,4- dimethoxy-4'-butoxychalcone..... 27

Figure 2.11: Quinolinyl substituted chalcone..... 29

Figure 2.12: 1,2,4-triazole substituted chalcones 29

Figure 2.13: (E)-1-(4-bromophenyl)-3-(2,4,5-trimethoxyphenyl)prop-2- en-1-one 30

Figure 3.1: Design of methoxy substituted chalcones..... 46

Figure 3.2: Hybrid design of quinolinyl chalcones 47

Figure 3.3: Scheme for the synthesis of substituted chalcones 48

Figure 4.1: 2”,3”,4”-tri-methoxy substituted chalcones (P1, P2 and, P13) 66

Figure 4.2: 3-quinolinyl-substituted chalcones (P3, P4 and, P8)..... 68

Figure 4.3 : 2”,4”-di-methoxy-substituted chalcones (P11, P12 and, P17)..... 70

Figure 4.4 : 4”-methoxy substituted chalcones (P15, P16 and, P23)..... 72

Figure 4.5: 4”-methoxy substituted chalcone (P25) and un-substituted ring A chalcones (P19 and, P24)..... 74

Figure 4.6: 4” triflouromethyl - substituted chalcones (P21 and, P22)..... 76

Figure 4.7: Effect of P1, P2, P3, P4, P8, and P23-P25 on the parasitaemia level of *P. bergheii* infected mice. 80

Figure 4.8: Effect of P11, P13, P17, P18, and P21-P22 on the parasitaemia level of *P. bergheii* infected mice. 81

Figure 4.9: The binding energies of the ligands across all the enzymes.. 87

Figure 4.10: Compound P3 [(E)-3-(2-chloro-6-methoxyquinolin-3-yl)-1-(2, 4-dimethoxyphenyl) prop-2-en-1-one]..... 88

Figure 4.11: Compound P4 [(E)-3-(2-chloroquinolin-3-yl)-1-(2, 4 dimethoxyphenyl) prop-2-en-1-one..... 89

Figure 4.12 : 3D binding pose and interaction of P3 and P4 in relation to various sub sites of FP-2 binding cavity. 91

Figure 4.13: (A) 2D interaction diagram of FP-2 and P3 (B) 2D interaction diagram of FP-2 and P4. 92

Figure 4.14: 3D binding pose and interaction of P3 and P4 in relation to various sub sites of FP-3 binding cavity. 93

Figure 4.15: (A) 2D interaction diagram of FP-3 and P3 (B) 2D interaction diagram of FP-3 and P4. 94

Figure 4.16: 3D binding pose and interactions of P3 and P4 in relation to various sub sites of Plm-II binding cavity 95

Figure 4.17: (A) 2D interaction diagram of Plm-II and P3 (B) 2D interaction diagram of Plm-II and P4. 96

Figure 4.18: 3D binding pose and interaction of P3 and P4 in relation to various sub sites of Plm-IV binding cavity..... 97

Figure 4.19: (A) 2D interaction diagram of Plm-IV and P3 (B) 2D interaction diagram of Plm-IV and P4. 98

Figure 4.20: RMSD plot of FP-2 (A); FP-3 (B); Plm-II (C); Plm-IV (D) bound to compound P3 and P4. 101

Figure 4.21 : C-α RoG plot of FP-2 (A), FP-3(B), Plm-II (C) and, Plm-IV (D) both in complex with P3 and P4. 102

Figure 4.22 : C-α RMSF of FP-2 (A), FP-3(B), Plm-II (C) and, Plm-IV (D) both in complex with P3 and P4. 103

Figure 4.23 : Per residue energy decomposition plot of (A) FP-2 in complex with P3 and (B) FP-2 in complex with P4..... 105

Figure 4.24: Per residue energy decomposition plot of (A) FP-3 in complex with P3 and (B) FP-3 in complex with P4..... 106

Figure 4.25: Per residue decomposition plot of (A) Plm-II in complex with P3 and (B) Plm-II in complex with P4. 107

Figure 4.26 : Per residue energy decomposition plot of (A) Plm-IV in complex with P3 and (B) Plm-IV in complex with P4. 108

LIST OF APPENDICES

Appendix 1: Effect of compound P1, P2, P3, P4, P8, and P23-P25 on the parasitaemia level of *P. berghei* infected mice. 150

Appendix 2: Effect of compound P11, P12, P13, P15, P16, P17, P19, P21and, P22 on the parasitaemia level of *P. berghei* infected mice. 151

Appendix 3: The binding energy result of the co-crystallized ligands and 17 chalcones against four enzymes (FP-2, FP-3, Plm-II, and, Plm-IV). 152

Appendix 4: MD trajectory showing 30 nanoseconds (ns) molecular dynamic simulation of P3 bound to FP-2. 153

Appendix 5: MD trajectory showing 30 nanoseconds (ns) molecular dynamic simulation of P4 bound to FP-2. 155

Appendix 6: MD trajectory showing 30 nanoseconds (ns) molecular dynamic simulation of P3 bound to FP-3. 155

Appendix 7: MD trajectory showing 30 nanoseconds (ns) molecular dynamic simulation of P4 bound to FP-3. 156

Appendix 8: MD trajectory showing 30 nanoseconds (ns) molecular dynamic simulation of P3 bound to Plm-II 157

Appendix 9: MD trajectory showing 30 nanoseconds (ns) molecular dynamic simulation of P4 bound to Plm-II. 158

Appendix 10: MD trajectory showing 30 nanoseconds (ns) molecular dynamic simulation of P3 bound to Plm-IV. 159

Appendix 11: MD trajectory showing 30 nanoseconds (ns) molecular dynamic simulation of P4 bound to Plm-IV. 160

Appendix 12: FT-IR Spectrum of P1 160

Appendix 13: ^{1}H NMR of compound P1 162

Appendix 14: ^{13}C NMR of compound P1 163

Appendix 15: DEPT spectrum of compound P1 164

Appendix 16: COSY spectrum of compound P1 165

Appendix 17: HMBC spectrum of compound P1 166

Appendix 18: HSQC spectrum of compound P1 167

Appendix 19: Mass spectrum of P1 168

Appendix 20: FT-IR Spectrum of P13 169

Appendix 21: ^{1}H NMR of compound P13 170

Appendix 22: ^{13}C NMR of compound P13 171

Appendix 23: Mass spectrum of P13 172

Appendix 24: FT-IR Spectrum of P3 173

Appendix 25: ^{1}H NMR of compound P3 174

Appendix 26: ^{13}C NMR of compound P3 175

Appendix 27: DEPT spectrum of compound P3 176

Appendix 28: COSY spectrum of compound P3 177

Appendix 29: HMBC spectrum of compound P3 178

Appendix 30: HSQC spectrum of compound P3 179

Appendix 31: FT-IR Spectrum of P4 180

Appendix 32: ^{1}H NMR of compound P4 181

Appendix 33: ^{13}C NMR of compound P4 182

Appendix 34: DEPT spectrum of compound P4 183

Appendix 35: COSY spectrum of compound P4 184

Appendix 36: HMBC spectrum of compound P4 185

Appendix 37: HSQC spectrum of compound P4 186

Appendix 38: Mass spectrum of P4 187

Appendix 39: FT-IR Spectrum of P8 188

Appendix 40: ^{1}H NMR of compound P8 189

Appendix 41: ^{13}C NMR of compound P8 190

Appendix 42: DEPT spectrum of compound P8 191

Appendix 43: COSY spectrum of compound P8 192

Appendix 44: HMBC spectrum of compound P8 193

Appendix 45: HSQC spectrum of compound P8 194

Appendix 46: FT-IR Spectrum of P11 195

Appendix 47: ^{1}H NMR of compound P11 196

Appendix 48: ^{13}C NMR of compound P11 197

Appendix 49: DEPT spectrum of compound P11 198

Appendix 50: COSY spectrum of compound P11 199

Appendix 51: HMBC spectrum of compound P11 200

Appendix 52: HSQC spectrum of compound P11 201

Appendix 53: FT-IR Spectrum of P12 202

Appendix 54: ^{1}H NMR of compound P12 203

Appendix 55: ^{13}C NMR of compound P12 204

Appendix 56: Mass spectrum of P12 205

Appendix 57: FT-IR Spectrum of P17 206

Appendix 58: ^{1}H NMR of compound P17 207

Appendix 59: ^{1}H NMR of compound P17 (Expanded) 208

Appendix 60: ^{1}H NMR of compound P17 (Expanded)..... 209

Appendix 61: ^{13}C NMR of compound P17 210

Appendix 62: Mass spectrum of P17..... 211

Appendix 63: Figure 2: FT-IR Spectrum of P15 212

Appendix 64: ^{1}H NMR of compound P15..... 213

Appendix 65: ^{13}C NMR of compound P15 214

Appendix 66: Figure 2: FT-IR Spectrum of P16 215

Appendix 67: ^{1}H NMR of compound P16..... 216

Appendix 68: ^{1}H NMR of compound P16 (Expanded)..... 217

Appendix 69: ^{13}C NMR of compound P16 218

Appendix 70: Mass spectrum of P16..... 219

Appendix 71: ^{1}H NMR of compound 23..... 220

Appendix 72: ^{1}H NMR of compound 23 (Expanded)..... 221

Appendix 73: ^{13}C NMR of compound 23..... 222

Appendix 74: Mass spectrum of P23..... 223

Appendix 75: ^{1}H NMR of compound P19..... 226

Appendix 76: ^{1}H NMR of compound P19 (Expanded)..... 227

Appendix 77: ^{13}C NMR of compound P19 228

Appendix 78: Mass spectrum of P19..... 229

Appendix 79: ^{1}H NMR of compound 24..... 230

Appendix 80: ^{13}C NMR of compound 24..... 231

Appendix 81: Mass spectrum of P24..... 232

Appendix 82: ^{1}H NMR of compound 25..... 233

Appendix 83: ^{13}C NMR of compound 25..... 234

Appendix 84: FT-IR Spectrum of P21 235

Appendix 85: ^{1}H NMR of compound P21 236

Appendix 86: ^{13}C NMR of compound P21 237

Appendix 87: Mass spectrum of P21 238

Appendix 88: FT-IR Spectrum of P22 239

Appendix 89: ^{1}H NMR of compound 22 240

Appendix 90: ^{13}C NMR of compound 22 241

Appendix 91: TLC plates of substituted chalcones 242

ABBREVIATION

MD	Molecular Dynamics
LBP	Ligand-Based Pharmacophore
QSAR	Quantitative Structure Activity Relationship
SAR	Structure Activity Relationship
3D	3-Dimensional
2D	2-Dimensional
CADD	Computer Assisted Drug Design
SBDD	Structure Based Drug Design
LBDD	Ligand Based Drug Design
TLC	Thin Layer Chromatography
FT-IR	Fourier Transformed Infrared Spectroscopy
MS	Mass Spectrometry
NMR	Nuclear Magnetic Resonance
^{1}H	Proton
^{13}C	Carbon 13
PDB	Protein Data Bank

ADT	AutoDock Tool
GPU	Graphical Processing Unit
MD	Molecular Dynamic
PME	Particle Mesh Ewald
RESP	Restrained Electrostatic Potential
GAFF	General Amber Force Field
NPT	Number of particles, Pressure and Temperature
NVT	Number of particles, Volume and Temperature
Ps	Pico second
Fs	Femto second
ns	Nano second
ΔS	change in entropy
RMSD	Root Mean Square Deviation
RMSF	Root Mean Square Fluctuation
Rg	Radius of Gyration
COSY	Correlated SpectroscopY
HMBC	Heteronuclear Multiple Bond Correlation

HSQC	Heteronuclear Single Quantum Correlation
DEPT	Distortionless Enhancement by Polarization Transfer
QM	Quantum Mechanics
MM	Molecular Mechanics
VS	Virtual Screening
PDB	Protein Data Bank
SBVS	Structure Based Virtual Screening
SBP	Structure Based Pharmacophore
TETFUND	Tertiary Education Trust Fund

ABSTRACT

Inspired by the previous findings on the structural requirements needed for good antimalarial activity by chalcones against *Plasmodium* proteases, seventeen chalcone derivatives were designed and synthesized using Claisen-Schmidt condensation of appropriate aldehydes and methyl ketones. The structures of these compounds were established using various spectroscopic techniques. Based on SciFinder search the compounds; P1, P2, P3, and P8 are new compounds not listed on any chemical data base. The synthesized chalcones were screened in mice against established *P. berghii* infection. Eleven compounds were active and P2 the most active compound exhibited significant percentage inhibition of 90.32% ($p<0.05$) at a dose of 100 mg/kg. An interesting observation was the demonstration of good antimalarial activity with the 3-quinolinyl A ring derivatives- P3, P4 and P8. The potential of the synthesized compounds to inhibit the synthesis of β-hematin was also evaluated but, only compounds P12 and P17 showed modest inhibition of β-hematin synthesis with percent inhibition of 59.28% and 49.04% respectively at a dose of 50 µg/kg. The prospects of dual inhibition of *Plasmodium falciparum* vital proteases; aspartic proteases (plasmepsin II and IV) and cysteine proteases (falcipain-2 and 3) of the seventeen chalcone derivatives was also investigated using *in silico* studies. Structure-based virtual screening using validated molecular docking revealed two potential hits (P3 and P4) with the best binding affinity and broad inhibition across all the proteases used. The crucial driving forces for receptor interaction and key interacting residues of the enzymes by the potential hits were established using molecular dynamics and binding free energy calculations. Simulation experiments revealed the

stability of the docked ligands within all the enzymes. The ligands were found to interact with the residues at the active site and other sub-site regulating specificity for the falcipains system. With the plasmepsin systems, the ligands interact with the flap, covering the active site. From the different energetic contributions of the individual residues, it is evident that the binding process was principally favored by van der Waals and little affected by electrostatic energies while the polar solvation energy impaired it. With regard to the binding interactions, it appeared that the most contributing features of the ligands for receptor interactions are the quinoline ring, carbonyl group and 2- methoxy group. Therefore, the result from this work have identified quinolinyl chalcones with 2-methoxy substitution on ring B as potential candidates for further optimization as antimalarial against *Plasmodium* proteases.

CHAPTER ONE

1.0 INTRODUCTION

Malaria is a devastating infectious disease caused by a parasitic protozoan, Apicomplexan of the genus *Plasmodium (P.).* There are four important species of *Plasmodium* responsible for causing malaria in human; *P.vivax, P.malariae, P.ovale* and *P.falciparum*, with *P.falciparum* being the most virulent and predominant in Africa (Kumar *et al.,* 2009). The disease is transmitted through the bites of infected female Anopheles mosquito.

At the start of 2016, nearly half of the world ‘s population was at risk of malaria. It was considered to be endemic in 91 countries and territories in 2016 (WHO, 2016). In 2015 alone, there were an estimated 212 million new cases of malaria and 429, 000 deaths (WHO, 2016). Although the incidence rate of malaria is estimated to have decreased by 21% globally between 2010 and 2015, the decrease is more pronounced in the World Health Organization (WHO) European Region (100%) and WHO South-East Asia Region (54%). But progress in the WHO African Region, which is the region that carries the heaviest malaria burden has been slow (WHO, 2016).

WHO African Region continues to shoulder the heaviest malaria burden, accounting for an estimated 90% of malaria cases and 92% of malaria deaths in 2015. Three quarters of these cases and deaths are estimated to have occurred in fewer than 15 countries, with Nigeria and Democratic Republic of the Congo accounting for more than a third (WHO, 2016). The vulnerable groups are children under the age of five years and pregnant women (Miller *et al.*, 2013; WHO, 2016). Every 40 seconds a child dies of malaria, resulting in a daily loss of more than 2,000 young lives worldwide (Miller *et al.*, 2013). These estimates

render malaria the pre-eminent tropical parasitic disease and one of the top three killers among communicable diseases (Miller *et al.,* 2013).

Malaria is associated with significant socio-economic burden, as a general rule of thumb, where malaria prospers most; human societies have prospered least (Gallup and Sachs, 2001). Analysis estimating the long-term impacts of malaria on economic growth and development suggests the importance of the economic burden of the disease. The mechanisms through which malaria can impose economic costs include; medical/treatment cost and forgone incomes due to absenteeism at work place, social cost through migration, absenteeism in school and, loss of revenue from trade, tourism and foreign direct investment (Gallup and Sachs, 2001).

The global effort to defeat malaria has expanded greatly in the last few years. In this process, a number of novel strategies to obstruct malarial growth have emerged. Among the most appealing strategies is an attempt to produce a long-lasting vaccine which would help eradicate the disease (Valero *et al.,* 1993). The vaccine developed by Alonso *et al*. (2004) appears promising, but has so far only given limited protection (Lell *et al.,* 2005). Therefore, chemotherapy remains the only solution for malaria prevention and cure.

For decades chloroquine; a 4-aminoquinoline has been the gold standard for malaria chemotherapy due to its high efficacy, low cost and minimal host toxicity. Indiscreet use of chloroquine has led to massive development of resistance by the parasite making it ineffective (Kumar *et al.,* 2010). Consequently, artemisinin and its derivatives which include arteether, artemether and artesunate were introduced for the treatment of drug-resistant as well as drug-sensitive malaria (Wang and Xu, 1985; Lin *et al*., 1987), particularly in cases of deadliest cerebral malaria. And, to avoid or slow down the development of resistance, combination of artemisinin derivatives with other antimalarial agents known as artemisinin-based combination therapies (ACTs) are being advocated and

promoted by WHO (WHO, 2011). Presently, ACT is the first line intervention in *P. falciparum* malaria (WHO, 2016). Unfortunately, there is an alarming report of decrease artemisinin and ACT sensitivity in some parts of the Asia including; Cambodia, Myanmar, Thailand and Vietnam (Phyo *et al.,* 2012; Carrara *et al.,* 2013).

The un-availability of clinically effective vaccine, appearance of insecticide resistant mosquitoes and *Plasmodium* resistance to multiple available antimalarials have motivated scientists to develop new drugs with novel targets. In the wake of full genome sequencing of *P. falciparum*, numerous new drug targets have been proposed. These are quite diverse and include enzymes from the respiratory chain in the parasite mitochondria (Biagini *et al.,* 2006), several transport proteins (Reguera *et al.,* 2005) enzymes in the fatty acid synthetic pathway (Eastman *et al.,* 2006) a number of proteases (Ersmark *et al.,* 2006; Micale *et al.,* 2006) and, DNA replication and regulation (Yanow *et al.,* 2006)

The proteases have been identified as promising drug targets through several experiments (Goldberg *et al.,* 1991; McKerrow *et al.,* 1993; Liu *et al.,* 2005). Proteases are enzymes vital for plasmodium parasite survival. They are said to be responsible for degrading host hemoglobin to provide essential amino acid for the parasite survival (Rosenthal, 2004; 2011) and for maintenance of osmotic balance of the infected erythrocyte during the intra-erythrocytic life cycle (Mauritz *et al*. 2009). Another study has implicated proteases in the erythrocyte egression and subsequent rupturing process (Blackman, 2008). Proteases having key roles in hemoglobin degradation include aspartic (plasmepsins) and cysteine (falcipains) proteases. These proteases are validated as drug targets, but no drug has so far been approved against them (Teixeira *et al.,* 2011).

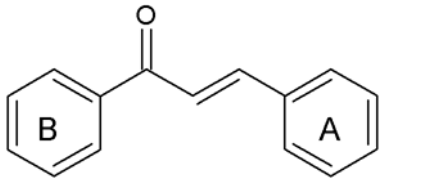
Numerous malarial protease inhibitors have been developed through computational studies (Li *et al.,* 1995; 1996; Gutiérrez-de-Terán *et al.,* 2006), and by chemical synthesis and serendipity (Rosenthal, 1998; Bjelic *et al.,* 2007). One of the major computational

approaches employed in the development of protease inhibitors consists of structure-based design using docking and molecular dynamic (Li *et al.,* 1995). Indeed, complementing experiment and computational techniques increases the rate of success in many stages of the drug discovery, by assessing the interactions between the ligands and the binding site of the protein according to their binding affinity to optimize pharmacodynamics and development of compounds with desired pharmacokinetic properties. Moreover, the use of computers at some conceivable steps is imperative to cut down the expense, number of animals and time needed in the drug discovery process (Gomes *et al.*, 2017)

Interestingly, chalcone (Figure 1.1) was identified through molecular modeling studies as *Plasmodium* parasite cysteine protease inhibitor (Li *et al.,* 1995). At the same time, Licochalcone A isolated from Chinese liquorice roots was identified as potent antimalarial compound (Chen *et al.,* 1994). Since then, there was substantial interest by the scientific community to develop chalcone as effective antimalarial drug. This is augmented by simple chemistry, ease of synthesis and possibility of various substitutions on the chalcone nucleus.

Various derivatives have been synthesized and were found to possess promising antimalarial activity. Several efforts were made to determine the features necessary for the antimalarial activity for optimization through QSAR and molecular modeling studies (Li *et al.,* 1995; Liu *et al.,* 2001; Kumar *et al.,* 2010). The strong dependence of antimalarial activity on specific substitution of rings **A** (Benzaldehyde ring) & **B** (Acetophenone ring) was noted. This led to a proposal which was put forward by Li *et al.,* (1995) on the importance of electron withdrawing substituents on ring A (decreased electron density) and electron donating substituents on ring B (increased electron density) for good antimalarial activity of chalcones. Similarly, Liu *et al*. (2001; 2003) and Go *et al*. (2003) synthesized a series of substituted chalcones and screened them against chloroquine-

susceptible (3D7) and chloroquine resistant (Dd2) strains of *P. falciparum*. From the SAR analysis, size and hydrophobicity of substituents on both rings of chalcones were identified as critical parameters. In addition, most of the hydroxylated chalcones were found to be less active than the corresponding alkoxylated derivatives as reported earlier (Li *et al.*, 1995).



(2*E*)-1,3-diphenylprop-2-en-1-one

Figure 1.1: Chalcone

Conversely, in a study conducted by Kumar *et al.*, (2010) it was observed that chalcones which are methoxylated in their aryl ring **A** and electron deficient at ring **B** are better antimalarials than those in which these groups are interchanged. These observations clearly indicate that increase in the electron density on ring **A** significantly enhanced the antimalarial activity which is evidently in contrast to earlier reports linking potent antimalarial activity with electron deficient ring **A** of chalcones (Li *et al.*, 1995). Thus, there is no clear conclusion of the substitution pattern on the chalcone rings that confer better antimalarial activity.

The present research aimed at designing various chalcone derivatives depicting previous proposals set forward for chalcones as proteases inhibitors, their synthesis and evaluation of their *in vivo* antimalarial activity using mice model. Molecular hybridization design is employed, matching various scaffold of the chalcone moiety denoted from previous studies as significant for antimalarial activity. Additionally, the redundant function of the proteases in hemoglobin degradation prompted this research to also study the potential of the synthesized chalcones to inhibit both aspartic and cysteine proteases using *in silico*

studies and to provide insight into the structural features for dual proteases inhibition. This should help to furnish information for further design of new compounds with improved and dual activity.

1.1 Statement of Research Problem

Despite tremendous progress in medicinal chemistry malaria is still a major threat to public health (WHO, 2016). One of the major hurdles to control malaria is resistance of malaria parasites to most of the commonly used antimalarials. Today, artemisinins and Artemisinin Combination Therapy (ACTs) are the only drugs that cure chloroquine-resistant *Plasmodium falciparum* infections. However, there is reported decrease sensitivity of the ACTs in some parts of Asia (WHO, 2016). In fact, ACTs resistance to *Plasmodium falciparum* is spreading very rapidly (Ashley *et al.,* 2014). Hence, new antimalarials with novel targets are urgently needed to combat the disease.

Inspite the biochemical characterization of proteases as an attractive and potential drug target, no drug has yet been clinically approved (Teixeira *et al.,* 2011; McGillewie and Soliman, 2015). Many potent peptidyl protease inhibitors were discovered, but, their utility as therapeutic agents is limited by their susceptibility to proteolytic degradation and poor absorption through cell membranes (Ettari *et al.,* 2010). Thus, the search for small molecule non-peptide inhibitors continues.

Obviously, since functional redundancy exists among the various *Plasmodial* proteases, attention needs to be targeted at more than one enzyme during drug design and development. Some experimental studies proved dual inhibition of falcipains and plasmepsins is necessary for lethal inhibition to the parasites (Liu *et al.,* 2006; de Oliveira *et al.,* 2013). Many efforts to computationally study interactions between the inhibitors and different proteases are made, using various *in silico* methods (McGillewie and

Soliman, 2015; Musyoka *et al.,* 2016). However, there are limited studies on computational analysis targeting dual inhibition of the different proteases.

1.2 Justification of the Study

Malaria remains one of the most important tropical parasitic diseases, causing great suffering and loss of life. Nigeria suffers the world greatest burden with 97% of the total population, at risk which resulted in 192,284 deaths in 2015 (WHO, 2016). The disease remains a major cause of death in Nigeria followed by diarrhea and HIV/AIDS (Adedotun *et al.*, 2010). Study has shown that children under five years of age have an average of 2-4 attacks of malaria annually (Adedotun *et al.*, 2010). The socio-economic impact of malaria on individual and the economy is enormous. Annually it costs Africa alone, $12 billion (WHO, 2016).

In an effort to combat the mortality and morbidity burdens of malaria arising from development of resistance to the available antimalarials, scientists from many disciplines have initiated an extensive and comprehensive malaria vaccine development program. Yet, there is currently no licensed vaccine against malaria. The vaccine Mosquirix^{TM} (RTS,S/AS01) developed by GlaxoSmithKline in partnership with PATH malaria initiative has been found to be associated with cases of meningitis, seizures and, reduction in efficacy over time (Lell *et al.*, 2009). Moreover, vaccine alone cannot replace the core package of WHO-recommended preventive and treatment measures (WHO, 2017). This suggests that there is still need to search for newer and more effective antimalarials.

The antimalarial potential of the chalcones, their simple structure, low cost synthesis, minimal host toxicity and ease of availability presents them as excellent alternative drug candidates for malaria (Gallup and Sachs, 2001; Sinha *et al.,* 2013). Chalcone template structures have been studied and shown to exhibit activity but, structural refinement and optimization is needed to make a viable potent drug candidate. This is limited by uncertain

SAR analysis and realization of other mechanistic pathways different from protease inhibition. Therefore, more chalcone derivatives are needed until a true SAR is established.

The drug design and discovery process are highly laborious and costly both in terms of resources and time. However, computational studies in drug design and discovery have the advantage of being faster and far less expensive, in addition to saving lives of animals compared to standard high thorough put screening (HTS). Computational methods provide a powerful complement to standard HTS and by combining chemical screening with computational tools, lead discovery and optimization can be made significantly faster and effective. A number of successful examples exist where computational chemistry has made significant contributions to the processes of lead discovery and optimization (Teixeira *et al.,* 2011).

1.3 Aim and Objectives of the Study

The aim of the study was to design, synthesize and, evaluate antimalarial activity of some chalcone derivatives and explores their optimization through computational studies

To achieve the aim, the objectives of the study are;

I. To design some substituted chalcones based on previous studies, synthesize and characterize them using melting point and various spectroscopic techniques (FT-IR, ^{1}H, ^{13}C and 2D NMR and Mass spectrometry).

II. To evaluate the theoretical oral bioavailability of the designed chalcones based on Lipinski ‘s rule of five.

III. To screen them for *in vivo* antiplasmodial activity using curative model in mice infected with *Plasmodium berghei*.

IV. To carry out molecular docking studies using the crystal structure of two cysteine and two aspartic proteases of *P. falciparum* and the synthesized chalcones. And further study the Chalcones with good binding affinity and broad spectrum of inhibition from docking study using molecular dynamic simulation.

V. To evaluate an alternative mechanism of action based on *in vitro* assay of β-hematin inhibition.

1.4 Research Hypothesis

The synthesized derivatives are not inhibitory to the protease of *P. falciparum* and are therefore not potential antimalarial agent.

CHAPTER TWO

2.0 LITERATURE REVIEW

2.1 Malaria

Malaria is one of the earliest known diseases. The French researcher Laveran (Nobel Prize in Medicine 1907) discovered the malaria parasite in human blood. In 1897, the English physician Ross (Nobel Prize in Medicine 1902) and, in 1898, the Italian zoologist Grassi, demonstrated that the parasite was injected into the human bloodstream through the bite of an infected female mosquito (Teixeira *et al.,* 2011). Malaria remains a human disease of global significance and a major cause of high infant mortality in endemic nations (Miller *et al.,* 2013). Parasites of the genus Plasmodium cause the disease by degrading human hemoglobin as a source of amino acids for their growth and maturation (Rosenthal *et al.,* 2002).

2.1.1 Pathogenesis

Understanding the interplay of the Plasmodium parasite with its cellular host provides the biological basis for its control, treatment and eradication (Teixeira *et al.,* 2011). Plasmodium parasites have a complex life cycle, consisting of two basic cycles; an asexual cycle in the human host and a sexual cycle in the mosquito host (Khan and Waters, 2004). The asexual cycle is further divided into a liver stage (or a pre-erythrocytic stage) and an erythrocytic stage. Figure 2.1 is a schematic representation of the transmission cycle of malaria parasite (Hoffman *et al.,* 2002).

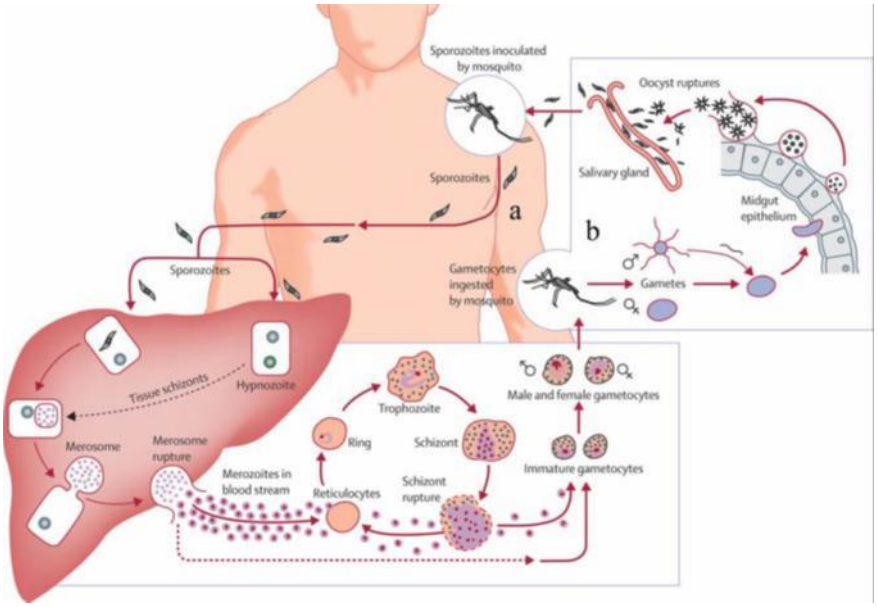


Figure 2.1: The life cycle of *Plasmodium falciparum*, where (a) and (b) represent the asexual cycle in human host and the sexual cycle in the mosquito, respectively.

The parasite enters the bloodstream in the form of sporozoites through the bite of an infected female *Anopheles* mosquito. The sporozoites then travel to the liver and invade hepatocytes, where they are converted, through an asexual transformation, to trophozoites, which in turn divide into several schizonts, eventually generating merozoites. After being multiplied in huge numbers, these merozoites rupture the hepatocytes and are released into the blood stream. The merozoites invade the erythrocytes, initiating the erythrocytic stage and feed on the hemoglobin. After proliferation, the erythrocyte rupture and the liberated merozoites invade other erythrocytes. Sometimes, during this endo-erythrocytic stage, other forms of the parasite emerge as gametocytes, sexually differentiated forms that, when taken up by a feeding mosquito, will complete the sexual cycle within the mosquito gut until new sporozoites are formed and migrate to the insect ‘s salivary glands, for another round in the spreading of infection (Teixeira *et al.*, 2011).

The asexual erythrocytic parasites are responsible for most of the typical clinical symptoms associated with malaria. As the parasites develop in the erythrocytes, numerous

waste and toxic substances accumulate. These are dumped into the blood stream as the infected red blood cells lysed and liberated the merozoites. The waste and toxic substances such as hemozoin and glucose phosphate isomerase (GPI) stimulate microphages and other cells to produce cytokines and other soluble factors which act to produce fever and probably influence other severe pathophysiology associated with malaria.

2.1.2 Chemotherapy

The complex life cycle of the malaria parasite above offer a clue on target for drug development by attacking stages of important development. However, discovery of drugs to combat malaria has to a large extent been serendipitous, and the mechanism of action of many agents is still partially or totally unknown (Kumar *et al.,* 2010). Chloroquine and other quinine alkaloid derivatives have been the mainstay in malaria chemotherapy for decades. Chloroquine appears to act by blocking the bio crystallization of heme, while the mechanisms for related drugs, including quinine, are unknown. Antifolate drugs, such as pyrimethamine, inhibit folate metabolism. (Wiesner *et al.,* 2003; Baird *et al.,* 2005)

Unfortunately, parasite resistance is rendering antimalarial medicines ineffective in most parts of the world. This resistance to antimalarial drugs arises as a result of spontaneously occurring mutations that affect the structure and activity at the molecular level of the drug target in the malaria parasite or affect the access of the drug to that target (Hayton and Su, 2004). To date, clinically relevant resistance has emerged, towards all classes of antimalarial drugs.

Fortunately, quinine has remained the drug of choice for treating the chloroquine and multidrug resistant *P. falciparum* malaria; however, its use is limited because of potential toxicity (Kapoor and Kumar, 2005). Thus, combination therapy of the effective antimalarial drugs available, such as artemisinin and its analogues remain WHO global strategy for malarial treatment (WHO, 2016), in addition to other control measures. It is

therefore evident that extensive scientific effort should be committed to the discovery of additional novel therapeutic targets and to develop drugs aimed at these targets.

2.1.3 Novel malaria targets

Since the unveiling of the *P. falciparum* genome in 2002 (Gardner *et al.,* 2002) a number of potential targets for drug intervention have emerged (Wiesner *et al.,* 2003; Jana and Paliwal, 2007). These potential antimalarial drug targets can be broadly classified into three categories, according to their function in the parasite ‘s life cycle as; i) targets involved in macromolecular and metabolite synthesis, ii) targets engaged in membrane transport and signaling, and iii) targets involved in hemoglobin degradation (Teixeira *et al.,* 2011).

Proteases having key roles on the degradation of host ‘s hemoglobin within the food vacuole of blood-stage parasites, have been increasingly attracting the attention of medicinal chemists worldwide as promising drug targets since *Plasmodium* depends on the hemoglobin degradation for their survival (Rosenthal *et al.,* 2002; Musyako *et al.,* 2016).

2.2 The Proteases

Proteases are enzymes that catalyze the hydrolysis of amide bonds in peptide and protein substrates. They have been identified in biological systems, from viruses to vertebrates. Proteases range from monomers of 10 kDa to multimeric complexes of several hundred kDa. They have been divided into groups based on the catalytic mechanism used during the hydrolysis of peptide bonds. The main catalytic types are serine, threonine, aspartate, metallo and cysteine proteases (Sajid and McKerrow, 2002). Proteases are important therapeutic targets because they play a role in various biological processes, such as protein synthesis, turnover, and function. These critical roles proteases play in the life cycle of parasitic organisms makes them attractive drug-design targets for malaria. Malarial main

proteases include; Falcipains-FP (cysteine proteases) and Plasmepsins-Plm (aspartic proteases).

2.2.1 Cysteine protease

Plasmodium cysteine proteases belong to Clan CA, or papain-like proteases. Cysteine proteases use a cysteine residue in the enzyme active site to catalyze protein hydrolysis *via* nucleophillic attack to the carbonyl carbon of a susceptible bond (Lecaille, *et al.,* 2002).

Plasmodium cysteine proteases adopt the classical papain-like fold in which the protease is divided into L (left) and R (right) domains (Figure 2.2). The catalytic residues CYS42, HIS174 and ASN204 for FP2 and CYS44, HIS176 and ASN206 for FP3 are located at the junction between the L and R domains (Kerr *et al.,* 2009). Thus, the catalytic site is formed by a cysteine and a histidine, whose side chains form a thiolate/imidazolium ion pair, and also by an asparagine, which has a crucial role in the appropriate orientation of the ion pair. The active site of falcipains is generally formed by four pockets: S1, S2, S1‘and S3. The S1 pocket is the least defined of the four grooves and, usually, includes the glutamine of the “oxyanion hole”. The most well-defined pocket is S2, which seems to govern specificity towards falcipains-2 (FP2) and/or falcipains-3 (FP3), and prefer substrates bearing a LEU in the corresponding P2 site. The S1‘pocket contains a highly conserved tryptophan, which is known to participate in hydrophobic interactions with substrates. Finally, a glycine-rich region of the binding site represents the S3 groove (Sajid and McKerrow, 2002; Kerr *et al.,* 2009).

Unique structural features of falcipains are two novel insertions assigned as FP2/3 nose and FP2/3 arm (Figure 2.2). The FP2/3 nose motif, situated at the N-terminus, is required for folding, while the FP2/3 arm contains a C- terminal insertion and mediates interaction between the falcipains and hemoglobin independent of the enzyme ‘s active site (Wang *et*

al., 2006). FP2 and FP3 are single polypeptide chains of 241 and 243 amino acids, respectively.

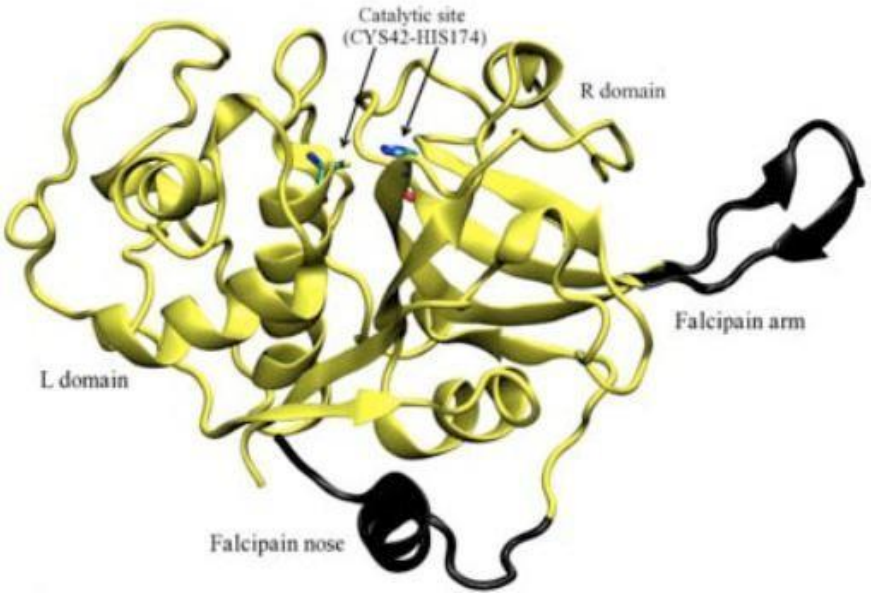


Figure 2.2: Cartoon representation of the structure of falcipain-2 (PDB code: 3BPF) with the L domain (Left) and the R (Right). The N- terminal extension (FP nose) at the most right and the C-terminal insertion (FP arm) at the bottom are colored in dark grey (Wang *et al.*, 2006)

Falcipains are the best characterized cysteine proteases of the malaria parasite. Analysis of the *P. falciparum* genome sequence suggested the existence of a family of four falcipains: falcipain-1 (FP1), falcipain-2 (FP2), falcipain-2‘(FP2‘) and falcipain-3 (FP3). FP1 is encoded on chromosome 14 and is distantly related to the other falcipains in terms of sequence (<40% amino acid identity) and function. Its exact physiological role is yet to be elucidated. However, some studies suggested that FP1 could be important in oocyst production during parasite development in the mosquito mid-gut and also could help in the invasion of the host cell by the *P. falciparum*. FP2, FP2‘and FP3 encoded on chromosome 11, are closely related and appear to be the key hemoglobinases in the acidic food vacuole. Also, they are believed to be involved in the transformation of pro-plasmepsins into the mature active enzymes (Teixeira *et al.*, 2011).

FP2 and FP3 present a high similarity in sequence (68% identity), share similar sized pro-domains and include an unusual amino-terminal extension of the catalytic domain that is not found in FP1. Both enzymes require a reducing environment and acidic pH for optimal activity. At acidic pH, FP3 is more active and stable, presenting a higher activity against native hemoglobin than FP2. It has been discovered that, despite the concentration of FP2 in trophozoites being 1.8 times that of FP3, the latter seems to cleave hemoglobin about twice as rapidly as the former. This indicates that the relative contribution of the two enzymes to hemoglobin degradation is essentially equivalent. The loss of FP2 is probably compensated by the increased expression of FP2‘and/or FP3, thus suggesting the overlapping functions performed by the falcipains (Rosenthal, 2011; Marco and Miguel, 2012). On the other hand, disruption of the FP3 gene is not possible, strongly suggesting that FP3 is essential for erythrocytic parasites.

These findings suggest that drug development focused on falcipains must consider simultaneous inhibition of all the essential falcipains.

2.2.2 Aspartic proteases

Aspartic proteases have aspartic acid as their catalytic apparatus and, use water molecules for proteolysis through a nucleophilic attack on the carbonyl carbon in acidic conditions (Bjelic *et al.,* 2007).

Aspartic proteases (Figure 2.3) are bi-lobed (two assymetrical lobes) molecules (N- and C-terminals) with the active site situated at the interface of the two domains; each lobe contributes an aspartic acid to the catalytic dyad of the active site. The two aspartic acids (Asp34 and Asp214) are located in close geometrical proximity to each other, functioning at an optimum acidic pH which ensures at any given moment one of the aspartic acid residues is protonated (ionized) and the other is deprotonated (unionized) (Asojo *et al.*, 2003; Silva *et al.,* 1996). The mature enzyme is formed by a single chain of 329 amino

acid residues. A unique structural feature of aspartic protease enzymes is the flap region lying perpendicular to the catalytic aspartic acid in the active site and, partially covering the active site. The flap region plays crucial role in ligand recognition and in regulating access to the active site, thereby regulating ligand binding (Bjelic *et al.*, 2007).

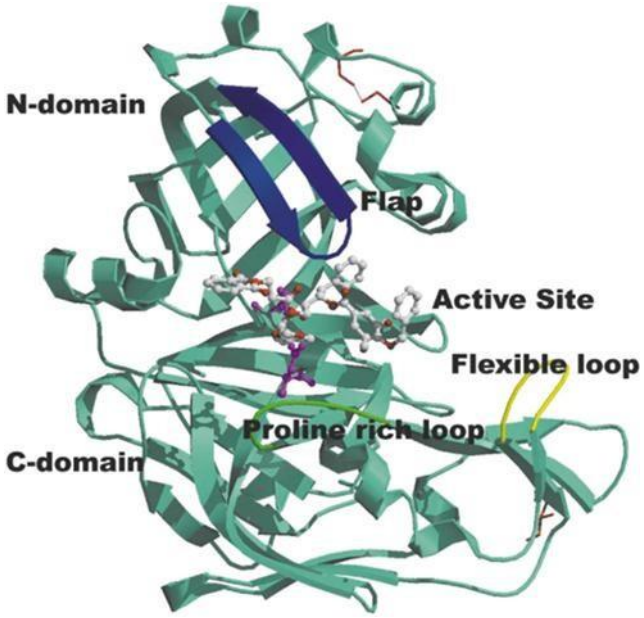


Figure 2.3: Figure 2.3: Ribbon diagram of the complex of plasmepsins II with EH58 showing disulfide bridges, catalytic dyad, inhibitor, flap, flexible loop and proline-rich loop in red, magenta, white, blue, yellow and green, respectively (Asojo *et al.*, 2003).

The mechanism of action of aspartic proteases is through a general acid-base reaction ("push-pull mechanism"), in which a nucleophilic attack occurs through the simultaneous transfer of two protons (between the conserved water molecule, the catalytic dyad and the substrate) leading to the formation of a transient neutral tetrahedral intermediate held non-covalently in the active site until bond cleavage occurs (Bjelic *et al.*, 2007).

With the unveiling of *P. falciparum* genome, ten (I – X) malarial aspartic proteases, also known as plasmepsins (Plm) have been identified. Plasmepsin I, II, IV and histo-aspartic protease (HAP) are situated in the food vacuole (FV) and are responsible for the degradation of hemoglobin, providing nutrients for parasite growth. *P. falciparum* is the

only *Plasmodium* species that actively expresses numerous plasmepsins in the FV, whereas the only aspartic protease in the FV of other *Plasmodium* species is an orthologue of PlmIV. Plasmepsins outside the FV, Plm V – X are highly conserved in all *Plasmodium* species (Banerjee *et al.,* 2002). Their overall structure and general mechanism of action is conserved throughout plasmepsins. However, sequence heterogeneity in regions lining the active site such as the flap and other essential regions that regulate ligand access ensures unique substrate specificity and response to inhibitors (McGillewie *et al.,* 2015). Previous studies (McGillewie *et al.,* 2015; Karubiu *et al.,* 2015) have proposed parameters to accurately describe the twisting motion of the flaps which move away from the active site in the absence of an inhibitor. Upon inhibitor binding, residues in the flap region form hydrogen bonds with the inhibitor pulling it inward towards the active site rendering the enzyme inactive. This could potentially aid in the development of plasmpesin inhibitors as antimalarials.

2.2.3 Mechanism of hemoglobin degradation by the protease

Hemoglobin is the most abundant protein in erythrocytes, and becomes completely degraded after parasite entry. Given that Plasmodia have limited capacity for de novo amino acid biosynthesis, it has been suggested that hemoglobin degradation products are essential for the parasite ‘s own protein biosynthesis, for its survival (Bjelic *et al.,* 2007). Amino acids from hemoglobin proteolysis also appear to be required for energy metabolism (Francis *et al.,* 1997) the regulation of osmotic pressure and the creation of space in the host cell for the growing parasites (Goldberg, 2005).

Reports on malaria both in culture and in animal models have revealed that hemoglobin catabolism takes place in the acidic food vacuole and is essential for parasite survival. Three different classes of enzymes have been found in the acidic food vacuole of the parasite that digest hemoglobin; cysteine protease (falcipains 1, 2, and 3) (Rosenthal *et al.,*

2002), aspartic proteases (plasmepsin I, II, IV, and histoaspartic protease) (Banerjee *et al.*, 2002), and metalloprotease (falcilysin) (Eggleson *et al.,* 1999). The degradation process appears to follow an ordered pathway (Gluzman *et al.,* 1994) which is outlined in (Figure 2.4). Falcipains are implicated for initial cleavage of native hemoglobin (Rosenthal, 1998). However, other studies have shown that native hemoglobin is cleaved by plasmepsin II, but not falcipain, in non- reducing conditions that may be present in the food vacuole (Semenov *et al.,* 1998). It is difficult to determine whether a plasmepsin or falcipain catalyzes the initial cleavage (Liu, 2006). However, it has been suggested that an initial cleavage between Phe33 and Leu34 in the hinge region, of the domain responsible for holding together the oxygen bound tetramer by plasmepsin, unravels hemoglobin to expose it to further cleavage (Coombs *et al.*, 2001).

Subsequent cleavage into smaller peptides is catalyzed by both plasmepsins and falcipains (Semenov *et al.,* 1998). The metallo-protease falcilysin and dipeptidyl aminopeptidase-1 (DPAP1) cleave the resulting small peptides to even shorter oligopeptides that are finally hydrolyzed to free amino acids by aminopeptidases (Coombs *et al.,* 2001). During the hemoglobin degradation process, free heme is released and oxidized from the ferrous (Fe^{2+}) state to the ferric (Fe^{3+}) hematin. Both heme and hematin are potentially toxic to the parasite. To counter this, the parasite has evolved a detoxification system resulting in the formation of β-hemozoin pigment, an inert crystalline hematin polymer (Pagola *et al.,* 2000).

Various evidences support that malarial cysteine and aspartic proteases are mediators of hemoglobin degradation and are therefore plausible novel target for antimalarial drug development (Silva *et al.,* 1996; Rosenthal *et al.,* 1998; Liu *et al.,* 2006). Protease inhibitors are known to block further growth and development of *P. falciparum* (Rosenthal, 1998; Teixeira *et al.,* 2011).

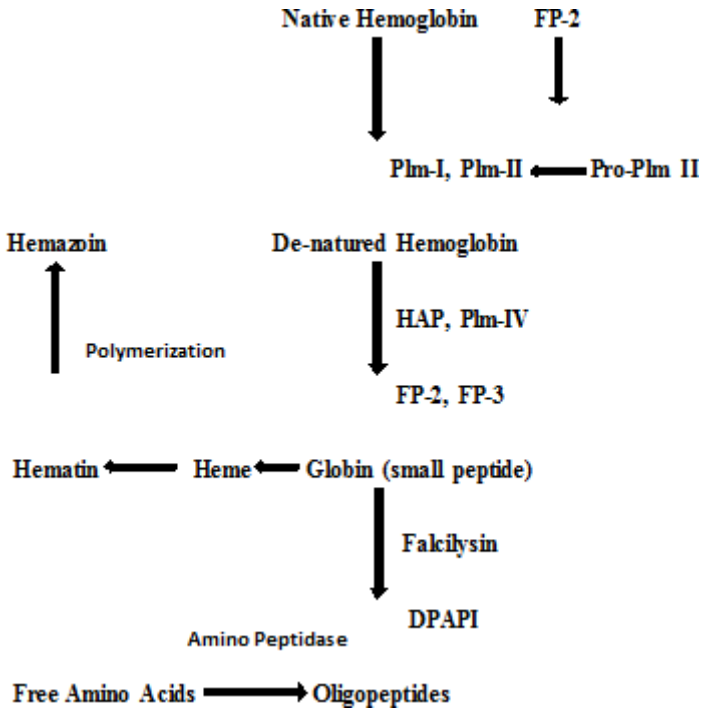


Figure 2.4: The degradation process of hemoglobin in the *P. falciparum* food vacuole (Teixeira *et al.*, 2011).

2.2.4 Protease inhibitors

Several studies revealed that cysteine and aspartic protease inhibitors prevent hemoglobin hydrolysis, block parasite development and cure murine malaria (Rosenthal *et al.*, 1996; 1998; Singh and Rosenthal, 2001; Liu *et al.*, 2006). To date, many compounds have been identified as malarial protease inhibitors which are able to block the parasites enzyme‘s activity by forming a reversible or irreversible covalent bond with the active site cysteine (Silva *et al.*, 1996; Asojo *et al.*, 2003; Liu *et al.*, 2006). Thus, falcipain inhibitors can be broadly divided into three categories (Teixeira *et al.*, 2011): i) peptide-based inhibitors, ii) peptide-mimetic inhibitors and iii) non-peptidic inhibitors.

Most of the falcipain inhibitors identified so far are peptide-based inhibitors. This includes; peptidyl fluoromethyl ketones, peptidyl vinyl sulfones, peptidyl aldehydes and α-ketoamide derivatives, epoxysuccinyl derivatives and peptidyl azirines. Peptidyl aldehydes and α-ketoamides inhibit FPs in a reversible manner, while the others are irreversible

inhibitors (Teixeira *et al.,* 2011). Peptide-based inhibitors were found to be very potent. However, their utility as therapeutic agents is limited because of their limited susceptibility to protease degradation and their poor absorption through cell membranes (Marco and Miguel Coteron, 2012). Peptidomimetic FPs inhibitors include compounds based on 1,4- benzodiazepine and pyridone ring scaffolds, which are able to reversibly block the enzyme. Non-peptide FPs inhibitors include, isoquinolines, thiosemicarbazones and chalcones which are biosynthetic precursors of flavonoids (Teixeira *et al.,* 2011).

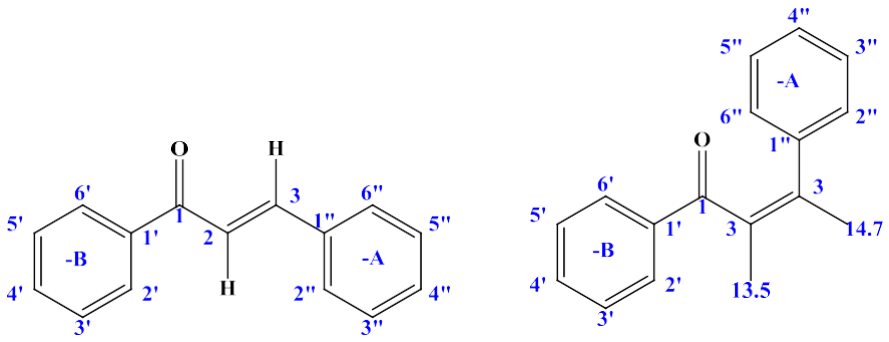
2.3 Chalcones

Chalcones are one of the most important classes of flavonoid family. They are open-chain precursors for biosynthesis of flavonoids and isoflavonoids and occur mainly as polyphenolic compounds, whose colour ranges from yellow to orange (Sahu *et al.,* 2012). They are abundantly present in edible plants. Chalcones exhibit a broad spectrum of biological activities, including antimalarial, anti-inflammatory, cytotoxic, and anticancer properties (Sahu *et al.,* 2012). Two examples of chalcones used in clinical practice are; metochalcone approved as a choleretic drug, and sofalcone as an anti-ulcer agent that increases the amount of mucosal prostaglandin, conferring a gastroprotective effect against *Helicobacter pylori* (Gomes *et al.,* 2017). Thus, medicinal chemists continue to be fascinated by chalcone derivatives because of their simple chemistry, ease of hydrogen atom manipulation, straightforward synthesis, and a variety of promising biological activities (Kumar *et al.,* 2010).

2.3.1 Chemistry of chalcones

Chalcone is a generic term given to compounds bearing the 1, 3-diphenyl-2- propen-1-one in which the three carbon α,β-unsaturated carbonyl system (ketoethylenic group -COCH=CH) is used as an adjunct between two aromatic rings A and B. They are non-chiral small molecules bearing relative molecular mass in the range of 300–600 g/mol with

relatively high lipophilicity (Log P ~5–7). They exist as either *trans* (E) or *cis* (Z) isomers (Figure 2.5). In most cases, the, E isomer is more stable from the perspective of thermodynamics, which makes it the predominant configuration among the chalcones. The configuration of the Z isomer is unstable due to the strong steric effects between the carbonyl group and the A-ring (Aksoz and Ertan, 2011).



(E)-chalcone (Z)-chalcone

Figure 2.5: (E) and (Z) chalcone

All chalcones undergo colored reactions with various reagents such as concentrated sulphuric acid, nitric acid and when a phenolic hydroxyl group is present, they give violet coloration with alcoholic ferric chloride solution. Chalcones on heating with traces of iodine in dimethyl sulphoxide (DMSO) for two hours give the corresponding flavones. Chalcones can be converted into the corresponding flavonols by their oxidation using hydrogen peroxide in methanolic sodium hydroxide solution and these flavonols showed a characteristic greenish yellow fluorescence in ethanol solution as well as with concentrated sulphuric acid (Avupati and Yejella, 2014).

2.3.2 Chemical synthesis

The simple chemistry of chalcones enables easy, efficient and convenient synthesis with multiple substitutions. A variety of methods and schemes are available for the synthesis; in each of these methods, the most important part is condensation of two aromatic systems (with nucleophilic and electrophilic groups) to yield the chalcone scaffold. Amongst all methods, the Claisen- Schmidt condensation (Figure 2.6) is one of the most common. In this reaction equimolar quantities of substituted aromatic aldehydes are condensed with substituted aromatic ketones in aqueous alcoholic alkali. The reaction is usually carried out in the temperature range of 20- 50ºC, and the reaction time is 12-15 hours. Some other condensing agents are also employed e.g. alkali metal alkoxide, magnesium *tert*-butoxide, hydrogen chloride, anhydrous aluminium chloride, boron trifluoride, phosphorus oxychloride, boric anhydride, amino acids, borax and organometallic compounds. The synthesis of chalcones with different substitution patterns on the two aromatic rings further allow to explore a large number of desired potential analogues.

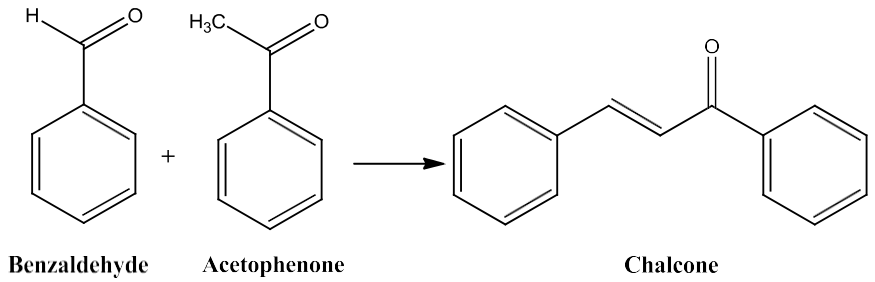


Figure 2.6: Claisen-Schmidt condensation.

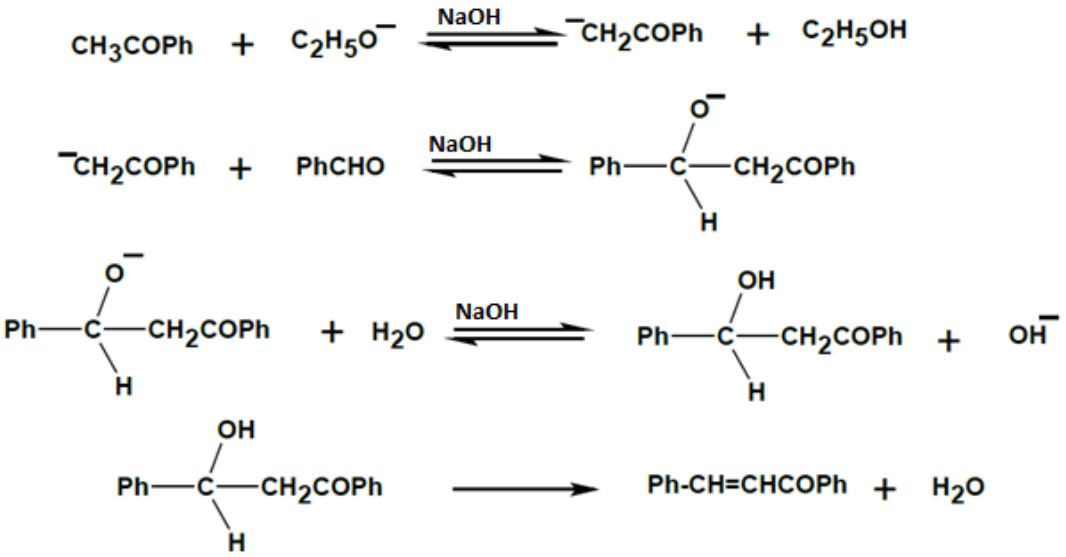
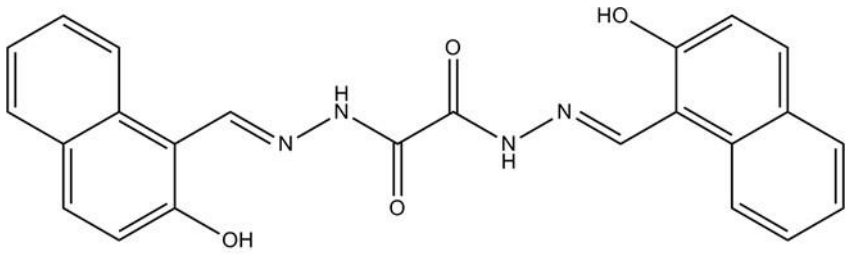


Figure 2.7: Based catalyzed reaction mechanism for chalcone formation

2.3.3 Chalcones as protease inhibitors

Based on the X-ray structures of papain and actinidin, a model structure of falcipain was designed and used as a receptor for ligand docking to search more than 55,000 commercially available small molecules. Thirty-one compounds were chosen for testing against FP-2 (Ring *et al.,* 1993; Li *et al.,* 1994). The most active compound, oxalic bis [(2-hydroxy- 1- naphthylmethylene) hydrazide] (Figure 2.8) inhibited FP-2 of *P. falciparum* with an IC_{50} value of 6 μM. The DOCK v3.0 generated enzyme inhibitor complex showed that one naphthol group fills the hydrophobic S2 site and that the other naphthol group shows a π-stacking interaction with Trp177 of the S1´ site. In addition, each hydroxyl group on the naphthol rings appears to hydrogen-bond to Ser160 at S2 and Gln19 at S1'.



oxalic bis[(2-hydroxy- 1-naphthylmethylene)hydrazide]

Figure 2.8: oxalic bis [(2-hydroxy- 1-naphthylmethylene) hydrazide]

Li *et al.* (1995; 1996) exploited the previous findings to design new improved ligands based on the predicted configuration of the lead compound docked to the 3D-homology model structure of the protease. Despite the lack of a detailed experimental structure of the target enzyme or the enzyme-inhibitor complex, new compounds with increased potency having an IC_{50} values in the nano-molar range emerged (Li *et al.*, 1995, 1996). The length of the backbone was shortened leading to asymmetric acyl hydrazones with less conformational heterogeneity than the symmetric ones. Additionally, the aromatic rings were replaced by nitrogen containing hetero-aromatics in order to improve water solubility and to enhance electrostatic interactions with His67 of the S2 site. To increase chemical and metabolic stability, the hydrazide linker was replaced by an α,ß-unsaturated ketone backbone, leading to chalcones. Furthermore, naphthalene, quinoline, or isoquinoline rings were exchanged for substituted phenyl rings on the α,ß -unsaturated ketone backbone to explore the effective size and electronic character of the sub-site specificity pocket (Li *et al.*, 1995, 1996).

On the basis of antimalarial evaluation, the authors concluded that dichloro or difluoro substitution on the A ring at the 2,3- or 2,4-positions favors the activity, with *para*- mono chloro substitution also giving sub-micromolar activities. This range of potencies were also observed when A ring was a quinolinyl group, either chloro- substituted or non-

substituted. The quinolinyl group probably increases antimalarial activity due to its capacity to protonate under weakly acidic conditions, thus enhancing their interactions with the protease at His67. Furthermore, these nitrogen- containing heterocycles may be somewhat concentrated in the food vacuoles of malarial parasites at pH 5 since pKa values of quinoline and isoquinoline is normally around 4.94 and 5.40 in water at 20 ºC, respectively (Li *et al.,* 1995).

The importance of α, β- unsaturated moiety was also proven, as the corresponding saturated derivatives showed a marked loss of activity or proved inactive. The α, β- unsaturated ketone linker also provided conjugation between aromatic groups on both ends and kept the molecular conformation extended, leading to a better interaction with the active site. Additionally, since inhibition of falcipains most likely occurs in the acidic food vacuole of the malaria parasite, the relative acid stability of α, β- unsaturated ketone linker of chalcones might offer an advantage over the more potentially labile hydrazide linker in the acyl hydrazide series. Such an effect could be responsible, at least in part, for the observed higher potency of chalcones relative to the corresponding acyl hydrazides (Li *et al.,* 1994). Regarding ring B, electron- donating substituents, such as di- or tri-substituted methoxy groups, showed an increase activity regardless of their position (Li *et al.,* 1995; 1996; Liu *et al.,* 2001).

While Li *et al.* (1995) was preparing to publish the finding of chalcones as protease inhibitor and antimalarial agent based on structure-based design, a paper describing licochalcone A (Figure 2.9), isolated from Chinese licorice roots, inhibiting the *in vitro* growth of both chloroquine-sensitive and chloroquine-resistant *P. falciparum* strains at a dose of 5.6 μM was published by Chen *et al.* (1994). *In vitro* results showed that Licochalcone A equally inhibited malaria parasites at all blood stages, suggesting that it acts on metabolic events important for the parasite development throughout the

erythrocytic cycle. The *in vivo* activity of licochalcone A against malaria parasites was also tested in *P. yoelii* model and the result was promising, however, a potential toxicity against human lymphocyte *in vitro* was noted. Therefore, large number of related oxygenated chalcone analogues were synthesized by Chen *et al.* (1997) and screened to test their activity against human malaria parasites *in vivo* and for toxicity against human lymphocytes. The search led to the identification of 2,4- dimethoxy-4'-butoxychalcone (Figure 2.10), having potent antimalarial activity *in vitro*, and *in vivo* against *P. berghei* and *P. yoelii* in mice model.

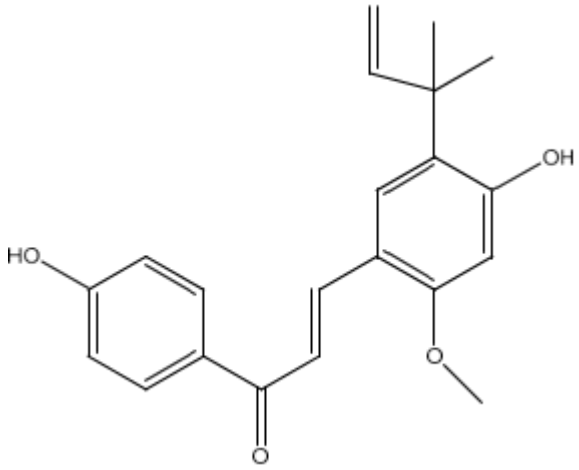
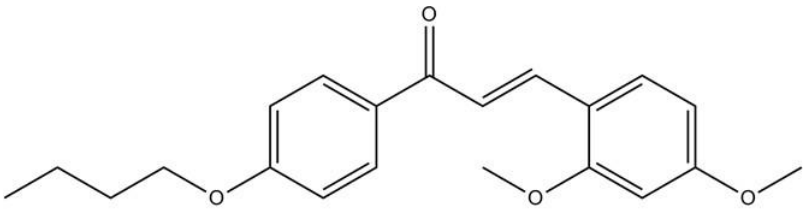


Figure 2.9: Licochalcone A

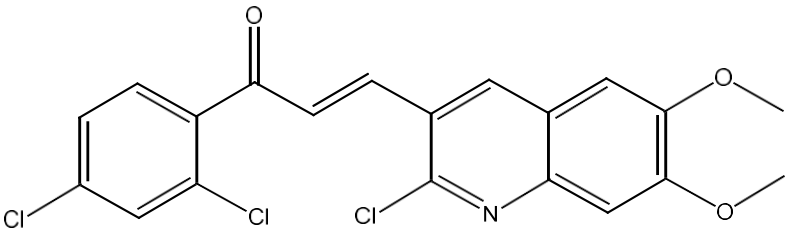


2,4- dimethoxy-4'-butoxychalcone

Figure 2.10: 2,4- dimethoxy-4'-butoxychalcone

The success of Li *et al.* (1995; 1996), the findings of Chen *et al.* (1994; 1995) and the interesting chemistry and biological activity of the chalcone arouse the interest of researchers. Subsequently Liu *et al.* (2001) employing more than 200 analogues, analyzed the influence of substitution on rings A and B of hydroxy or alkoxy chalcone derivatives on their antimalarial activity. It was observed that the selection of substituents on ring A was mainly guided by lipophilicity and electronic considerations. Results showed that there is a good representation of active compounds from the trimethoxy, dimethoxy, and methoxy series, but interestingly, none from the ethoxy series. Once more, the most active compounds presented methoxy substituents on ring B, regardless of its number and positioning. These results point towards the importance of substitution of ring B in determining the type of ring A substituents that would give optimum antimalarial activity. The authors further suggested that size considerations are dominated by ring B while ring A may be more important in influencing hydrophobicity, which in this instance may reflect the polar characteristics of the molecule. Later on, Liu *et al*. (2003) using QSAR methodology studied the physiochemical and structural requirements for antileishmanial activity (*Leishmania donovani*) and antimalarial activity of the chalcones. It was found that good antimalarial effects were found among alkoxylated chalcones as mentioned above. In an elaborate study, Go *et al.* (2004) reported that *in vitro* antimalarial action of chalcones against chloroquine-resistant, *Plasmodium falciparum* (K1) was primarily influenced by the properties of ring B. A few of the alkoxylated chalcones had a very low IC_{50} values.

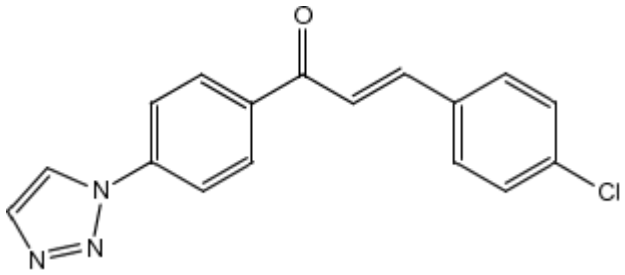
However, Dominguez *et al.,* (2001) reported 1-(2,4-Dichlorophenyl)- 3-[3-(2- chloro-6,7-dimethoxiquinolinyl)]-2-propen-1-one (Figure 2.10) as most promising quinolinyl chalcone with reported IC_{50} value of 19.0 µmol/l against *Plasmodium falciparum* cysteine protease. The compound has electron deficient ring B.



(*E*)-3-(2-chloro-6,7-dimethoxyquinolin-3-yl)-1-(2,4-dichlorophenyl)prop-2-en-1-one

Figure 2.11: Quinolinyl substituted chalcone

In another report, screening of substituted chalcone derivatives for antiplasmodial activity suggested that small or medium sized lipophilic groups containing multiple nitrogen atoms or amine in acetophenone moiety (ring B) favors antiplasmodial potential (Mishra *et al.*, 2008). Among all the tested compounds; 4-chloro, 4-methoxy and 3,4,5-trimethoxy series of 1,2,4-triazole substituted chalcone, the 4-chloro series (Figure 2.12) was found to be the most effective (IC_{50}: 1.52 µg/ml) in inhibiting the growth of *P. falciparum.*



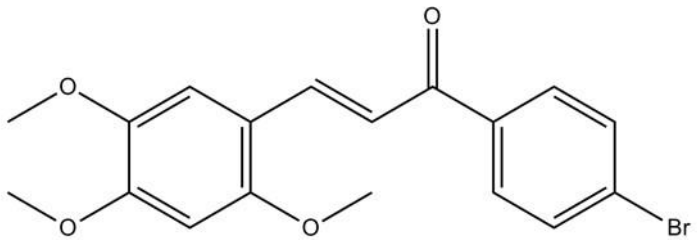
(*E*)-1-(4-(1*H*-1,2,3-triazol-1-yl)phenyl)-3-(4-chlorophenyl)prop-2-en-1-one

Figure 2.12: 1,2,4-triazole substituted chalcones

Kumar *et al.* (2010), attempted to find a potent core skeleton of chalcones having simple substituents and good antimalarial effect. Keeping in mind the well- known antimalarial potency of various chlorinated compounds like chloroquine and previous findings on the importance of electron-rich ring B and electron-deficient ring A, Kumar *et al.* (2010) considered, 3- (4-chlorophenyl)-1-(4-methoxyphenyl) prop- 2-en-1-one as a starting point.

However, test against *P. falciparum* 3D7 strain revealed that it lacks significant potency. Thereafter, molecules with different substituents on each of the two rings were synthesized and evaluated for antimalarial activity. Surprisingly, a reversal of substituents between rings A & B of lead compound (IC_{50}: 88.0 µM) led to a threefold increase in activity (IC_{50}: 28.8 µM) of resulting compound. Therefore, electron density on ring A was increased while, keeping chloro substitution constant on ring B. Interestingly, compounds with 2,4-dimethoxy and 2,4,5-trimethoxy groups on ring A exhibited progressively better antimalarial potential with IC_{50} values of 6 µM and 4 µM respectively (Kumar *et al.*, 2010). These observations clearly indicate that increase in the electron density on ring A significantly enhanced the antimalarial activity which is evidently in contrast to earlier reports linking potent antimalarial activity with electron deficient ring A of chalcones (Li *et al.,* 1995; Liu *et al.*, 2003).

SAR analysis of various derivatives of 2,4,5-trimethoxy chalcone revealed the importance of the 2,4,5-tri-methoxy group. It also shows the importance of keeping ring B electron deficient and bromine (Br) at position -4 of ring A for best activity (Figure 2.13). While, the presence of multiple electron withdrawing groups on the A ring did not lead to any significant increase in activity (Kumar *et al.,* 2010).



(*E*)-1-(4-bromophenyl)-3-(2,4,5-trimethoxyphenyl)prop-2-en-1-one

Figure 2.13: (E)-1-(4-bromophenyl)-3-(2,4,5-trimethoxyphenyl) prop-2- en-1-one

In conclusion there is a strong dependence of antimalarial activity on specific substitution of rings **A** & **B** of the chalcone scaffold, with various opposing views.

2.3.4 Present work

From the above discussion, it is clear that extensive effort for the introduction of chalcones as effective and inexpensive antimalarials are in progress. Various derivatives of chalcones including heterocyclic analogues (with *N*, *S* and *O* containing compounds) have been reported to possess antimalarial activity. However, there is no clear conclusion as to the substitution pattern of the two chalcone rings for better antimalarial activity particularly on inhibition of the plasmodia proteases. While, the initial findings of chalcones as protease inhibitor by Li *et al.* (1995) and other studies point out the significance of electron-rich ring A and electron- deficient ring B, it was found otherwise in some studies. As mentioned earlier structure-activity relationship study conducted by Kumar *et al*. (2010) aimed at exploring the basic chalcone moiety for antimalarial activity revealed that the presence of methoxy substitution, particularly 2,4,5-trimethoxy substitution, on ring A of chalcone and electron withdrawing groups at ring B significantly favors the antimalarial activity, contrary to previous findings.

Therefore, this research looked at previous studies and picked chemical scaffolds important for good activity and matched them, to see if the combination will give a better compound than the individual component. Hybridization of biologically active molecules, based on the combination of complementary pharmacophoric features of two or more known bioactive compounds or moiety, which, through adequate fusion, lead to the design of new hybrid architectures that maintain pre-selected characteristics of the original templates, is a powerful strategy for drug design. Other chalcone derivatives not previously studied with substitution similar or contrary to Li *et al.* (1995) proposal were also designed, synthesized and, evaluated for *in vivo* antimalarial activity.

Although proteases have previously been validated as potential drug targets, studies from knock-out experiments raise questions regarding the validity of either falcipains or

plasmepsins as single drug targets (Liu *et al.,* 2005; 2006; Bonilla *et al.,* 2007). The work of Liu *et al.* (2006) revealed that the doubling time for the malaria parasite was longer for the plasmepsins/ falcipain knock- out (plasmepsin I, plasmepsin IV and falcipain-2) than for either plasmepsin or falcipain knock-outs alone. Thus, effective drug cocktail combining falcipain and plasmepsin inhibitors is important for inhibition to the level that will be lethal to the parasite. Hence, compound combining structural features that can bind favourably to all the key proteases may perhaps be promising as dual target inhibitor. Therefore, this research used *in silico* experiment (docking and molecular dynamic simulation) to study the interaction of the chalcone derivatives with both falcipains (FP2 and FP3) and plasmepsins (Plm-II and Plm-IV). This is to search for compounds with good binding affinity across all the targets (enzymes), with a view to gain insight into the binding orientation, dynamic stability and structural features interacting with each enzyme. Identification of molecular groups involved in the interactions of a chemical moiety with a specific site on a target helps in the understanding of the molecular mechanism(s) responsible for their specific biological activities. Consequently, information acquired can help in re-designing new compounds considering the structural features having favorable interaction with key amino acids of the enzymes. Additionally, the binding orientation and interaction of the different compounds with good binding affinity across all the enzymes might explain the ambiguity regarding the substitution pattern of the chalcone ring for better activity.

2.4 Computational Chemistry

Computational chemistry is a set of techniques for investigating chemical problems on a computer. Problems commonly investigated computationally are: molecular geometry, energies of molecules and transition states, chemical reactivity, IR, UV, and NMR spectra and, the interaction of a substrate with an enzyme (Lewars, 2016).

Computational chemistry is fairly cheap, it is fast compared to experiment, and it is environmentally safe. However, it does not replace experiment, which remains the final arbiter of truth about nature (Lewars, 2016). Furthermore, to have new entity (drug/chemical) experiment is unavoidable. Today, computation has become so reliable in some respects that, more and more scientists are employing it before embarking on an experimental project, and in the future, grants for experimental work might depend on the extent one has computationally explored the feasibility of a proposal (Lewars, 2016).

Computational chemistry encompasses numerous methods and theories, including quantum mechanics, molecular mechanics, conformational analysis, minimization and other computer-based methods for understanding and predicting the behavior of molecular system to solve various chemical and biochemical problems (Cramer, 2013). Molecular modelers employ computational methods to generate large volumes of data and information at an atomic and molecular level on the behavior of atoms and molecules. An understanding of atomic interactions is quite essential. Atomic interactions can be described in two ways; quantum mechanics (QM) and molecular mechanics (MM).

Therefore, from a computational perspective, a researcher has two options when trying to answer questions about a biomolecular system. One is to adhere to the fundamental laws of physics that govern the behavior of electrons such as Schrödinger ‘s equation, solving the problem using quantum chemistry and physics that is the quantum mechanics (QM) approach. The QM approach however, even in its most simplistic form is computationally expensive and time-consuming; and is not feasible for biological systems which contain thousands of atoms. Alternatively, the second approach is to use molecular mechanics (MM) approach, which is essentially a mechanical model of a molecule, envisioned as a collection of balls (atoms) which are held together by springs (bonds); adhering to Newton ‘s laws of classical mechanics. This mechanical system rotates, vibrates and translates

until an energetically favorable conformation is reached while inter- and intra- molecular forces act on the system. MM provides an understanding of the mechanical nature of proteins, and provides insights into the changes in the cellular structure, cellular responses and cellular functions of a protein (Bao and Suresh, 2003). Molecular mechanics is the more popular of the methods used as it is simpler to use and requires considerably less computing time to produce a model. Using this model, total energy of the system may be expressed mathematically by equations known as force fields.

Force fields (interatomic potentials) are the mathematical description that models the interactions between molecules at an atomistic level; it is the functional forms of the potential energy function that predicts the molecular energy of a system in relation to specific particle coordinates. Even though each force field uses different functional forms each equation is always comprised of bonded terms (bond lengths, bond angles and torsions) and non-bonded terms (electrostatic and van der Waals) (Equation 1 and 2) (Jensen, 1999).

$$\boldsymbol{E}_{total} = \boldsymbol{E}_{bonded} + \boldsymbol{E}_{non-bonded} \quad (1)$$

$$\boldsymbol{E}_{total} = \boldsymbol{E}_{stretch} + \boldsymbol{E}_{bend} + \boldsymbol{E}_{torsion} + \boldsymbol{E}_{electrostatic} + \boldsymbol{E}_{vdW} \quad (2)$$

Where, E_{total} represents the total energy of the systems. $E_{stretch}$ is the energy contribution from bond stretching, E_{bend} is the energy contribution from angle bending, $E_{torsion}$ is the energy contribution from torsional motions around single bonds; these make up the energy contributions from bonded interactions, E_{bonded} (Equation 1). $E_{non\text{-}bonded}$, is the interactions between atoms that are not directly bonded together, it is made up of $E_{electrostatic}$ and $E_{van\ der\ Waals}$. Collectively these energies/parameters create the MM force field, and describe the energy contribution of numerous atomic forces. The energy terms above are parameterized

to align to experimental and QM data to ensure systems mimic the behavior of actual molecules in motion (Lewars, 2016).

To date, numerous force fields have been developed and differ in their means of parameterizations; force fields should be selected based on the conditions and the type of system being investigated. The most commonly used biomolecular force fields include CHARMM (Best *et al.*, 2012), AMBER (Case *et al.*, 2005) and GROMOS (Christen *et al.*, 2005). In the present study, the standard AMBER Force Field was used to parameterize the protein systems; and the general AMBER Force Field (GAFF) was used to parameterize the ligands.

2.4.1 Computer-assisted drug design (CADD)

Drug discovery and development is a tedious and time-consuming process and the cost has increased drastically during the past thirty-four years, with few compounds making it into the market. Although expert biological knowledge is indisputably important for successfully guiding drug discovery projects, CADD approaches, with the availability of supercomputers, parallel processing, and the graphics processing unit (GPU), have been playing a pivotal role on prioritizing compounds for synthesis and/or biological evaluation. CADD represents a time-, labor-, and cost-effective strategy to obtain lead compounds in the early stages of drug discovery and for lead optimization (Macalino *et al.*, 2015). CADD employs computational chemistry methods to model both drug molecules and their receptors. Drugs that successfully enter the market through CADD approach include Zanamivir, Amprenavir, Raltitrexed among others (Gomes *et al.*, 2017). CADD is broadly divided into; structure-based drug design (SBDD) and ligand-based drug design (LBDD)

2.4.1.1 Structure-based drug design (SBDD)

In SBDD, 3D structural information of a macromolecule is used to design or evaluate ligands based on their predicted interactions and affinity with protein binding sites. Thus, identification of a valid biochemical target and the acquisition of its structural information are the first vital steps in SBDD. Researchers from computational and structural biology facilitated in the generation of thousands of structures with the use of homology modeling, X- ray crystallography, cryo-electron microscopy (EM), and nuclear magnetic resonance (NMR) (Lionta *et al.,* 2014). Currently, more than 13,000 3D structures have been experimentally solved and stored in the Protein Data Bank (PDB), leading to attractive opportunities for the application of SBDD strategies (Rose *et al.,* 2016)

SBDD can be divided into virtual screening (VS) and *de novo* approaches. In VS large chemical libraries are processed to search for compounds that possess complementarities toward the targets. De novo design exploits information from the 3D model of the receptor to find small fragments that match well with the binding site. These fragments should be linked, providing a structurally novel ligand that can be synthesized for further *in vitro* assays. However, because of its knowledge-based characteristic, SBDD strongly depends on the amount and the quality of information available about the system under investigation. Regardless of what kind of protein will be employed as a molecular target, important issues, such as the suitable assignment of protonation states, solvation, and protein flexibility (Lionta *et al.,* 2014), must be considered. Protein-ligand docking, molecular dynamics simulations and structure-based pharmacophores are the main SBDD tools (Gome *et al.,* 2017).

Protein-ligand docking:

Protein-ligand docking is the most extensively used structure based virtual screening (SBVS) method. It predicts possible binding modes of a compound or fragment in a target binding site and estimates affinity based on its intermolecular interactions in the binding

pocket. Docking is often carried out in two parts. In the first part, the ligand is placed inside the binding site in different orientations and conformations using a search algorithm to facilitate the identification of the binding mode. Then, a scoring function ranks the different poses of the ligand that are generated by the search algorithm and orders them by a score. These scores are features that aid in investigating the interactions between the small molecule and the biological target, thereby providing context about biological activity (Lionta *et al.,* 2014; Ferreira *et al.,* 2015).

Although the concept of docking seems to be precise, it remains a major challenge of this approach. Usually, the scoring functions are found to have limited accuracy in the ranking of compounds and sometimes cannot distinguish between active and inactive molecules. In addition, the insertion of protein flexibility to some active residues can help in identifying new hits with better molecular complementarity, when compared with traditional rigid docking. However, it requires more complex calculations because the proteins of high conformational energy score would result in idealistic binding mode (Ferreira *et al.,* 2015).

Consequently, some streamlined strategies have been developed to solve these methodological limitations. To incorporate protein flexibility, ensemble methods make use of multiple input conformations of a target using a set of different 3D structures experimentally determined (X-ray crystallography or NMR) or computationally produced using molecular dynamics simulations. Instead of single rigid structure, carefully chosen 3D conformations of the target can be used to represent conformational changes in the protein backbone and/or side chain. On the other hand, averaging the results from two or more scoring functions and forming a consensus has proved to be more beneficial in scoring and ranking compounds. In addition to consensus scoring, post-processing

techniques such as the molecular mechanics Poisson–Boltzmann surface area methods can be used to better estimate the free binding energies (Gomes *et al.,* 2017)

Molecular dynamics (MD) simulations:

MD uses MM to generate the forces acting on molecules, which is then used to calculate their motions in time. Structures generated from NMR and crystallographic studies, represent a static view of biomolecular systems; these structures alone are insufficient in understanding the wide range of biological activity. Molecular dynamics programs allow the dynamic nature of molecules to be studied by simulating the natural motion of the atoms in a structure (Lewars, 2016). In essence, MD is a deterministic method that strives to mimic the time dependent behavior of molecules in space. The assumption is that the atoms in a given molecule will interact with each other in accordance to the force field applied; resulting in a MD trajectory. A trajectory is a data set that represents the positions (coordinates) and velocities of particles in the system over time; containing the structural and dynamic properties of the system (Kalyaanamoorthy and Chen, 2014).

Molecular dynamics is based on an integrated approach of Newton ‘s laws of motion (F = m.a), which solves the equation of motion for atoms on an energy surface. Therefore, motion can be simulated for a molecule as it changes conformations over time, or upon ligand binding. The trajectories generated are defined by both location and velocity vectors which describe the time progression of the biomolecular system through phase space. The location (changing through time) for each particle in space and the velocities are used to determine the thermodynamics (temperature and kinetic energy) of the biomolecular system. The functional properties of a system can be affected by dynamic events, which can be detected at an atomic level. MD has been particularly useful in the structural refinements of post-docking complexes, such that the complementarity between the ligand and the receptor is enhanced in the complex state, allowing better

complementarities. MD can provide information on physiological conformations of target proteins, which are, in many cases, not even accessible through experimental techniques (Kalyaanamoorthy and Chen, 2014). Methodologically, MD regards atoms as solid spheres and the bonds connecting them as springs. The trajectories of atoms and molecules are determined by numerically solving Newton ‘s equations of motion for a system of interacting particles, where forces between the particles and their potential energies are calculated using force fields with predefined parameters.

Structure-Based Pharmacophores (SBPs):

In addition to docking, 3D structural information may be used to derive pharmacophore hypotheses. Pharmacophore is defined by the International Union of Pure and Applied Chemistry (IUPAC) as “an ensemble of steric and electronic features necessary to ensure the optimal supramolecular interactions with a specific biological target and to trigger (or block) its biological response” and can be used to screen a compound database (Wermuth *et al.*, 1998). A typical pharmacophore features include hydrophobic centroids, aromatic rings, hydrogen bond acceptors or donors, cations, and anions. Hence, SBPs describe the spatial arrangement of essential ligand-macromolecule interactions directly from the 3D structural data. This approach determines chemical features based on complementarities between a ligand and its binding site. Nonetheless, the selection of features in SBPs is a more complex effort than in ligand-based, since there are more possibilities of conformational and spatial states (Pirhadi *et al.*, 2013). Typically, SBPs can be created using ligand- macromolecule complexes (holo) or using ligand-free macromolecules (apo). The generation of models using holo structures allows complete exploration of the ligand interactions with the binding site, and the inclusion of shape and volume information derived directly from the structural data (Pirhadi *et al.*, 2013). In the absence of a ligand in the binding site, pharmacophores can be obtained using functional groups or

small fragments, also referred to as molecular probes, to map possible interaction sites or hot spots within a binding site. Selected hot spots can then be converted into pharmacophoric features to generate a structure-based pharmacophore model.

2.4.1.2 Ligand-Based Drug Design (LBDD).

In some cases, usually when data pertaining to the 3D structure of a target protein are not available, CADD can instead be based on processes using the known ligands of a target protein or known active compounds in phenotypic assays as starting points. This approach is known as LBDD (Pirhadi *et al.,* 2013). Similarity search, ligand-based pharmacophores, and quantitative structure-activity relationship (QSAR) analysis are the most popular methods in the LBDD process.

Similarity search:

The major principle of medicinal chemistry is the assumption that structurally similar compounds exhibit similar biological activities (Gomes *et al.,* 2017). Based on this premise, similarity search techniques have been applied to chemical structures to allow rapid structural comparison in an effort to identify structurally similar compounds or to cluster collections based on structural similarity.

Methodologically, both query ligand and the database of compounds could be represented and further compared using molecular fingerprints (a string made up of binary digits that account for the presence (1) or absence (0) of representative fragments or atoms in the chemical structure). These fingerprints vary greatly in length and complexity ranging from simple topological representations to complicated multi-point 3D pharmacophore arrangements (Muegge and Mukherjee, 2016).

Ligand-Based Pharmacophores (LBPs):

The pharmacophore approach aims to identify molecules containing different scaffolds, but with a similar 3D arrangement of key interacting functional groups. LBPs identify key common features (e.g., hydrogen bond donors or acceptors, aromatic rings, partial charges, and hydrophobicity) and the relative orientations of known active ligands not shared by inactive ligands. Its elucidation involves two main stages: (i) the analysis of the training set molecules to identify common pharmacophoric points and (ii) the alignment of the bioactive conformations of these molecules to determine the best overlay of corresponding features. During this process, molecular features, which are not consistently observed in active compounds should be made optional or removed from the model. Furthermore, spatial constraints can be employed in moieties occupied by inactive compounds and refined to avoid making the model too restrictive. After model refinement, validation studies using statistical metrics must be performed to determine the ability of the model to discriminate between known active and inactive compounds (Vuorinen *et al.,* 2015).

Quantitative structure activity relationship (QSAR):

QSAR is a mathematical model describing the relationship between chemical structure and respective biological activity of a set of compounds. QSAR modeling could be presented as a two-part process. Firstly, chemical structures are converted into a vector of features, which are also known as descriptors and represented generically by the symbol x. Thousands of descriptors, both freely available and commercial, encode a compound as a feature vector. Then, machine learning methods are used to establish quantitative relationships between descriptors and biological activities. This involves empirically discovering a function that maps between the feature vectors and activities. Nevertheless, the resulting QSAR model is useful if and only if it is predictive. Hence, the quality of the resulting QSAR model is measured by using the appropriate metrics regarding its ability to correctly predict the activities of compounds experimentally determined. The influence of

various factors on QSAR performance decreases in the following row: data quality > molecular descriptors > machine learning approach (Cherkasov *et al.*, 2014).

Once validated, this model can be applied to untested chemical compounds for numerical prediction of biological activity (continuous model) or the discrimination between active and inactive compounds (binary model).

2.5 Theoretical Oral Bioavailability

The drug ability of chemical compounds, that is their ability to be orally available is an important point of consideration during a drug design project and can be predicted theoretically using Lipinski rule of five which states that a compound is highly likely (>90 %) to be orally unavailable, if it has two or more of the following:

1. Molecular weight >500

2. Log P >5

3. More than 5 H-bond donors (OH and NH)

4. More than 10H-bond acceptors (O and N)

5. Number of rotatable bonds≤ 10

CHAPTER THREE

3.0 MATERIALS AND METHODS

3.1 Materials

3.1.1 Equipment and glassware

Pyrex made glassware were used. The glassware were properly cleaned with distilled water and dried in an oven before use. Most of the equipment were sourced from the Department of Pharmaceutical and Medicinal Chemistry, Ahmadu Bello University (ABU), Zaria. Fourier Transform Infrared (FT-IR) and Nuclear Magnetic Resonance (NMR) experiments were performed at the Multi-User Laboratory, Chemistry Department, ABU, and Zaria. Mass Spectrometry (MS) and some NMR experiments were performed at the School of Chemistry and Physics, University of KwaZulu-Natal, Durban South Africa.

Some of the equipment and glassware used include; conical flask, spatula, test tubes, beakers, measuring cylinder, glass rod, funnel, pipette, watch glass, sintered glass, microscopic slides, syringes, capillary tubes, TLC tank, magnetic stirrer, stirring bar, refrigerator, gallenklamp melting point apparatus, centrifuge, incubator, centrifuge, microtitre plate, eppendorf tubes, analytical balance, microscope, agilent FT-IR spectrometer, 400 MHz Agilent and 500 MHz Bruker NMR spectrometer.

3.1.2 Reagents, solvents and standard drugs

The reagents were purchased from Sigma-Aldrich, Germany. All the starting reagents and solvents used for the experiments were of analytical grade and were used without further purification, these include; 4-methoxybenzaldehyde, 2, 4-dimethoxyacetophenone, Sodium hydroxide (50%), Acetophenone, haem- chloride, sodium acetate, glacial acetic acid, iodine crystals, chloroform, ethylacetate, N-hexane, ethanol, hydrochloric acid, 10% giemsa stain, acacia, chloroquine phosphate, quinine, and arthemether.

3.1.3 Experimental Animals

Adult Swiss albino mice (18-22 g) of either sex, locally bred in the Department of Pharmacology and Therapeutics, Ahmadu Bello University (ABU), Zaria were used for the experiment. The animals were housed in clean polypropylene cages under standard laboratory conditions (optimum temperature and humidity, and 12 hr of light/dark circle) and allowed free access to standard rodent pellet diet and water ad libitum. All experimental protocol on animals was in accordance with Ahmadu Bello University Research Policy and guides for the use and care of laboratory animals as accepted internationally. Ethical approval was sought from the ABU committee on animal use and care.

3.1.4 Malarial parasite

Chloroquine-sensitive malaria parasites (Plasmodium berghei NK 65) were obtained from the Department of Microbiology- National Medical Research Institute (NMRI), Lagos. The parasites were maintained viable in new groups of mice by continuous intraperitoneal injection of 0.2 ml of infected erythrocytes every four days (Adzu *et al.*, 2007).

3.1.5 Computer hardware and software

AutoDock Vina (Trott and Olson, 2011), Ligplot (http://www.ebi.ac.uk/thornton srv/software/LIGPLOT/), Molegro Molecular Viewer (MMV) (www.nlcbio.com), MGL tools (Sanner, Olson, and Spehner, 1996), UCSF Chimera (Pettersen *et al.*, 2004), Amber (Case *et al*., 2012), ChemDraw ultra.12, Accelerys Discovery Studio, Spartan 04, Ligand Scout, Origin data analysis, software version 6 (http://www.originlab.com/), Mac OSX, Windows (Intel processor, coi7)

3.1.6 Protein crystal structure

High resolution, non-mutant crystal structure files of the following enzymes were obtained from RCSB Protein Data Bank (http://www.rcsb.org/pdb); Falcipain-2 [FP-2; PDB ID: 3BPF] (Kerr *et al.*, 2001), Falcipain-3[FP-3; PDB ID: 3BWK] (Kerr *et al.*, 2001), Plasmepsin-II [Plm-II; PDB ID: ILF3] (Asojo *et al.*, 2003), Plasmepsin-IV [Plm-IV; PDB ID: 1LS5] (Asojo *et al.*, 2003).

3.2 Methods

3.2.1 Design strategy

Spurred by the previous findings on substitutions type and pattern of the two aromatic rings (ring A: from the aldehyde and B: from acetophenone) of chalcone for potent antimalarial activity (Li *et al.*, 1995; Liu *et al.*, 2001; Dominguez *et al.*, 2001; Shikha *et al.*, 2009), six series of chalcones, broadly classified according to the substitution pattern of the A ring were designed. In series; one, three and four, ring A was substituted with 2,3,4 trimethoxy, 2,4 dimethoxy and 2-methoxy groups respectively (varying electron

density), and series five have un-substituted A ring (Figure 3.1). The other aromatic ring (ring B) in the series was substituted with groups of varying electronic character. In series two, ring A was replaced by 2-chloroquinoline ring with and without 6- methoxy group and ring B comprises of 2,3,4 trimethoxy and, 2,4 dimethoxy substitutions (Figure 3.2). Furthermore, series six have electron deficient ring A with ring B of varying electron densities.

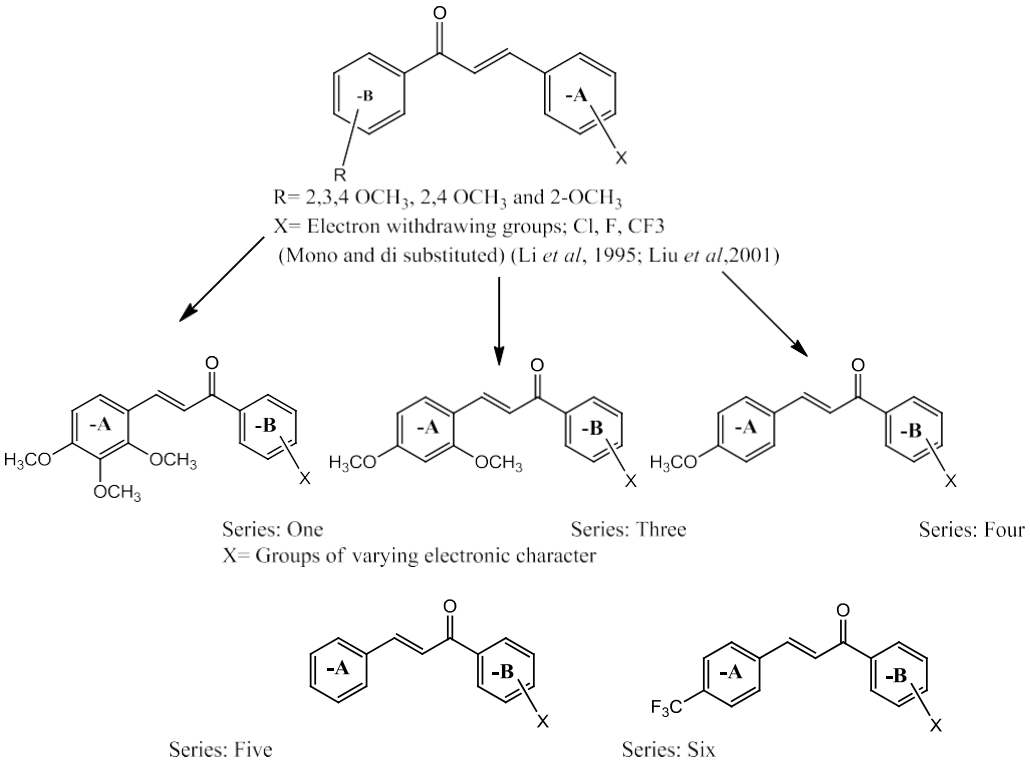


Figure 3.1: Design of methoxy substituted chalcones

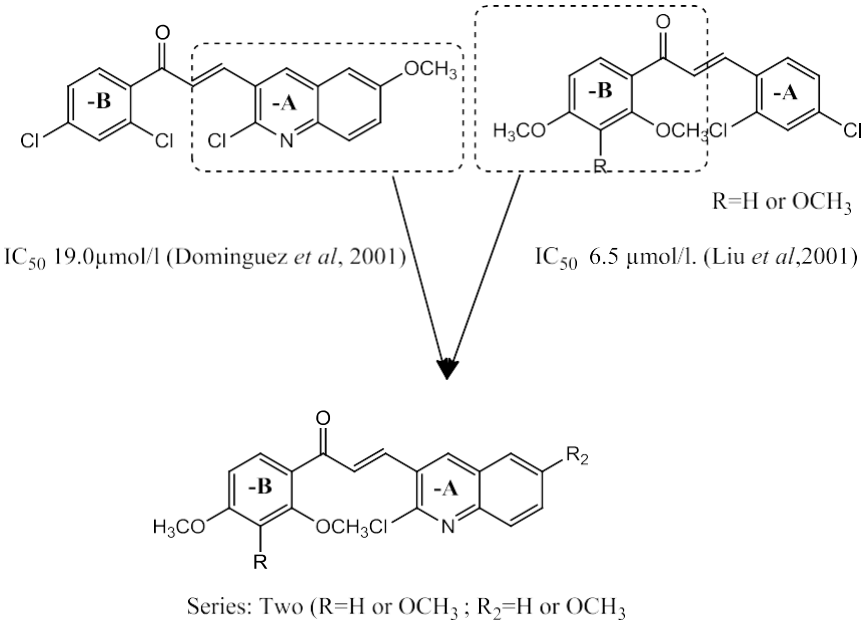


Figure 3.2: Hybrid design of quinolinyl chalcones

3.2.2 Evaluation of theoretical oral bioavailability

The oral bioavailability of the designed chalcones was predicted theoretically using Lipinski ‘s rule of five, prior to synthesis with SWISS ADME software (http://www.swissadme.ch).

3.2.3 Synthesis of chalcones (Claisen –Schmidt Condensation)

All the chalcones were synthesized via base catalyzed condensation of respective equimolar amounts of substituted acetophenone and substituted benzaldehyde using NaOH as catalyst. The chemical equations for the synthesis are as shown in Figure 3.3. Silica gel thin layer chromatography (TLC) was used to monitor the progress of the reaction with ethylacetate: n-hexane (7:3) as developing solvent (Kumar *et al.,* 2010). Appearance of a single new spot and disappearance of the reactants spot indicate the formation of the product, which were visualized under 254 nm ultra violet light and iodine vapor.

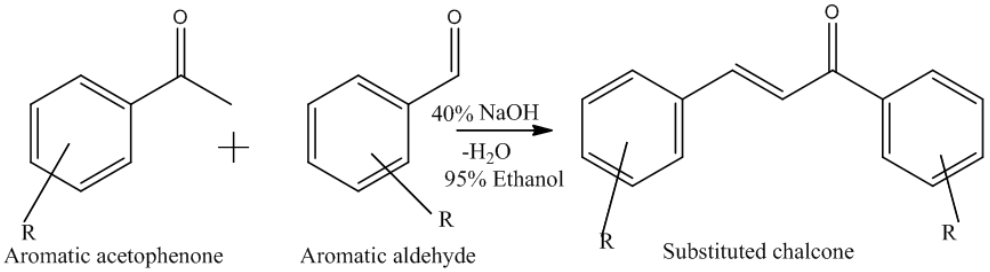


Figure 3.3: Scheme for the synthesis of substituted chalcones

3.2.4 Procedure for the synthesis of the substituted chalcones

Equimolar amounts of substituted acetophenone (0.01 moles) and substituted benzaldehyde (0.01 moles) (Table 3.1) were mixed with 20 ml ethanol in round bottom flask. To this 10 ml of 40% sodium hydroxide solution was added drop wise with continuous stirring for 30 mins while, keeping the mixture cold. The mixing was then continued for another 2 hrs at room temperature using magnetic stirrer and kept in refrigerator overnight until it formed an orange solid mass. Drops of 10% HCl were added to stop the reaction. The mixture was diluted using 40 ml ice-cold distilled water and then filtered; the residue was washed well with more ice-cold distilled water, and dried in air. The product was re-crystallized with ethanol, dried, final weight taken and the percentage yield was calculated. P3 and P8 were however purified using anti-solvent recrystallization. The final products have various color and forms and they were confirmed using TLC.

Table 3.1: Reagents for the synthesis of the substituted chalcones

Compound	Substituted aldehyde	Substituted acetophenone
P1	2,3,4-trimethoxy Benzaldehyde	2,3,4-trimethoxy acetophenone
P2	2, 4-dimethoxy Benzaldehyde	2, 4-dimethoxy acetophenone
P3	2-chloro-6-methoxy-3-quinoline carbaldehyde	2, 4-dimethoxy acetophenone
P4	2-chloro-3-quinoline carbaldehyde	2, 4-dimethoxy acetophenone
P8	2-chloro-6-methoxy-3-quinoline carbaldehyde	2,3,4-trimethoxy acetophenone
P11	2, 4-dimethoxy benzaldehyde	2, 4-dichloro acetophenone
P12	2, 4-dimethoxy Benzaldehyde	Acetophenone
P13	2,3,4-trimethoxy aldehyde	2, 4-dichloro acetophenone
P15	4-methoxy Benzaldehyde	2, 4-dimethoxy acetophenone
P16	4-methoxy benzaldehyde	Acetophenone
P17	2, 4-dimethoxy Benzaldehyde	2,3,4-trimethoxy acetophenone

P19	Benzaldehyde	2, 4-dimethoxy acetophenone
P21	4-triflouro-methyl benzaldehyde	2, 4-dimethoxy acetophenone
P22	4-triflouro-methyl benzaldehyde	Acetophenone
P23	4-methoxy Benzaldehyde	2,3,4-trimethoxy acetophenone
P24	Benzaldehyde	2,3,4-trimethoxy acetophenone
P25	4-methoxy Benzaldehyde	2, 4-dichloro acetophenone

3.2.5 Characterization

3.2.2.1 Melting point determination

All melting point were determined using a Gallenkamp melting point apparatus and were uncorrected.

3.2.5.2 Spectroscopic analysis

Detailed structural analysis of the synthesized compounds was performed using Fourier Transformed Infrared Spectroscopy (FT-IR), Mass Spectrometry (MS) and, Nuclear Magnetic Resonance (NMR) which include; proton (^{1}H) NMR, carbon-13 (^{13}C) NMR, Correlated SpectroscopY (COSY), HSQC and, HMBC

FT-IR data are reported in terms of frequency of absorption cm-1. Data for ^{1}H NMR and ^{13}C NMR are reported as: chemical shift (δ ppm), multiplicity (s = singlet, d = doublet, dd = doublet of doublet, m = multiplet), integration *(J)*. Data for ^{13}C NMR reported in terms of chemical shift (δ ppm).

3.2.6 Evaluation of *in vivo* antiplasmodial activity

3.2.6.1 Inoculation of Plasmodium berghei parasite

Blood was collected into a heparinized capillary tube via the tail vein from donor mouse with *P. berghi* Parasitemia level of about 20-25% and then transferred into a sterile plain bottle. About 2 ml of the blood was diluted with 10 ml normal saline such that 0.2 ml contained approximately $1x10^{7}$ infected red blood cells. Each mouse was then inoculated intraperitoneally with 0.2 ml of blood suspension (Kalra *et al*., 2006).

3.2.6.2 Curative test in mice

Evaluation of the curative potential of compounds against established plasmodia infection was carried out as described by (Ryley and Peters, 1970). Briefly (using compound P1), the mice were inoculated with parasites as described above and left untreated until the fourth day post-inoculation. After Parasitemia was established on parasitemia determination, the mice were randomly divided into five groups of five mice each. Groups 1-3 were intraperitoneally administered with 25, 50 and, 100 mg/kg body weight of compound P1 respectively. Group 4 and 5 were administered 5 mg/kg of chloroquine and 0.2 ml of 1%w/v acacia suspension intraperitoneally, respectively. The treatment was

given for four consecutive days. On the fifth day, blood was collected from the tail vein of each mouse and smeared on slide to make a thin film (Saidu *et al.*, 2000) for parasitemia determination.

The same procedure was repeated for the rest of the compounds (P2 – P25) each with three graded doses. The study was conducted at three different times with different set of compounds. At each experiment different dose of the positive controls was used to improve response. Thus, for chloroquine 5, 10 and 25 mg/kg were used and for arthemether 1.65, 2.3 and 5 mg/kg were used.

3.2.6.3 Parasitemia determination

The thin blood film on microscope slide was fixed with absolute methanol for 10 secs and stained with 3% geimsa stain at pH 7.2 for 45 mins. The remaining stain was gently poured off and the slides were rinsed with distilled water and carefully dried on a rack. Each slide was placed on a microscope stage, with one to two drops of inmersion oil placed on the slide. Using X100 objective lens, four immersion fields were viewed and the number of parasites in each field counted using a tally counter. Average percentage parasite suppression relative to the control was calculated for each treatment group using the formula below (Iwalewa *et al.*, 2008):

$$\% \text{ Parasitemia} = \frac{mean\ parasitemia\ (-ve\ control\ )\ -\ mean\ parasitemia\ (+ve\ control)}{mean\ parasitemia\ (-ve\ control)} \times 100$$

3.2.7 *In vit*ro determination of hematin polymerization inhibitory activity

Hematin polymerization inhibition test was investigated by the method of Baelmans *et al.*, (2000). A solution of hemin chloride in 10% dimethyl sulfoxide (50 µL, 5.2 mg/ml) was distributed in 96-well microplates. 50 µL solution of different concentration of each of the test compounds (50, 100 and 200 µg/ml) in DMSO were added in triplicate into the test wells. Controls were DMSO (50 µL) and chloroquine (50 µL, 2.5 mM). Beta-hematin

synthesis was initiated by the addition of sodium acetate (100 µL, 0.2 M, pH 4.4). Plates were incubated at 37^0C for 48 hrs to allow completion of the reaction and the resultant mixture centrifuged (4,000 rpm for 15 mins). The supernatant was discarded and the pellet was washed three times with 200 µL DMSO and finally dissolved in NaOH solution (200 µL, 0.2N). The solubilized aggregates were further diluted 1:2 with NaOH solution (0.1N) and absorbance recorded at 405 nm using a spectrophotometer. The results were expressed as percentage inhibition of beta-hematin synthesis compared to control using the equation below:

$$\% \text{ Inhibition} = \frac{absorbance\ of\ negative\ control\ -\ absorbance\ of\ test\ compound}{absorbance\ of\ negative\ control} \times 100$$

3.2.8 Data analysis

Statistical software (SPSS) was used to determine the mean parasitemia level and standard error of mean. The mean values of the control group were compared with the mean values of the groups treated with the test compounds using one-way analysis of variance (ANOVA) test, followed by Benferroni post-hoc test for statistical significance and P values <0.05 were considered significant. % parasitemia suppression for each group was computed.

3.2.9 Computational studies

3.2.9.1 Protein structure preparation

The crystal structures were obtained from protein data bank as mentioned earlier. Only protein crystallized from *P. falciparum* with available published data were selected. Other filters include proteins co-crystallized with small molecule inhibitors (Plm-IV is an exception).

Prior to docking, residues surrounding the ligands at distance of <5.0Å were noted and, all crystallographic water molecules, ions and bound ligands were removed on all 3D

structures obtained from PDB using Chimera UCSF (Pettersen *et al.,* 2004). The separated co-crystallized ligands were prepared on Chimera and saved as Lig.mol, and the isolated receptors prepared too and saved as rec.pdb. The output files of Chimera was input to ADT (Sanner, Olson, & Spehner, 1996), were Lig.mol and rec.pdb were edited by adding polar hydrogen and Gastier charges then saved as pdbqt files.

3.2.9.2 Ligand structure preparation

All the ligands studied (17 chalcones) were designed and synthesized in-house as mentioned earlier. The 2D structures were generated using Chem Draw. And, Spartan was used to convert the 2D structures to 3D. Geometrical optimization using the AMI semi-empirical method was performed on all the compounds using the Spartan software and saved as mol2 file. Hydrogen and Gasteir charges were added on ADT and mlo2 file converted to pdbqt.

3.2.9.3 Evaluation of docking methodologies

Docking procedure for each enzyme was validated prior to docking the test compounds by separating the co-crystallized ligand from the enzyme crystal structure and re-docking it using the set-up parameters. Procedure that gives conformation superimposable with geometrical conformation of the co-crystallized ligand in the active site was chosen (de Oliveira *et al.,* 2013).

3.2.9.4 Molecular docking

Molecular docking was performed considering a flexible ligand and rigid receptor (Eder de Oliveira *et al.,* 2013; Syahri *et al.,* 2017). Docking was carried out using virtual screening software AutoDock vina (Trott and Olson, 2010). Seventeen (17) substituted

chalcones were docked on the active site of each enzyme. The grid box parameter for each enzyme is as shown on the Table below:

Table 3.2: Grid-box parameters for the enzymes

Enzyme	Gridbox size			Center		
	X	Y	Y	X	Y	Z
FP-2	**10**	**16**	**12**	**-36.75**	**31.05**	**-47.07**
FP-3	**16**	**16**	**12**	**5.96**	**-22.35**	**50.07**
Plm-II	**12**	**20**	**18**	**16.22**	**6.85**	**27.61**
Plm-IV	**20**	**8**	**16**	**-24.49**	**37.80**	**41.2**

The gridbox parameter was used to write configuration file (config.txt). AutoDock Vina generated results in the pdbqt pdbqt format. Compounds having the best binding energy, optimal geometric conformation and, broad inhibition across all the enzymes studied were selected from the ViewDock feature of Chimera and saved in complex with the reference enzyme. The enzyme and ligand for each system was prepared using Chimera (Pettersen *et al.*, 2004), and MMV molecular modeling suites and subsequently subjected to molecular dynamic simulations and BFE calculations.

3.2.9.5 Molecular dynamics simulation

To determine stability and map intermolecular interactions between the hit compounds (P3 and P4) and the enzymes MD simulation was performed using the GPU version of the PMEMD engine provided with the Amber 14 package. The FF14SB force field of the Amber software package (Nair and Miners, 2014) was used to describe the complex. ANTECHAMBER module (Wang *et al.*, 2006) was used to generate atomic partial

charges for the ligands by employing the Restrained Electrostatic Potential (RESP) and the General Amber Force Field (GAFF) procedures. The Leap module of Amber 14 was used to add missing hydrogen atoms to the systems as well as Na^+ and Cl^- counter ions for neutralization. The system was suspended implicitly within an orthorhombic box of TIP3P water molecules such that any solute atoms were within 10 Å of any box edge during the simulation. Particle mesh Ewald method was used to treat long-range electrostatic interactions with a direct space and van der Waals cutoff of 12 Å.

An initial minimization of 2000 steps of steepest descent were carried out with an applied restraint potential of 500 Kcal/mol for both complexes. An additional full minimization of 1000 steps were further carried out by conjugate gradients algorithm without restrain. A gradual heating of the systems from 0 K to 300 K with a 5 Kcal/mol Å harmonic restrain potential and a Langevin thermostat of collision frequency of 1/ps using a canonical ensemble constant volume and temperature (NVT). MD simulation was then carried out. All the systems were then equilibrated at 300 K in a constant pressure and temperature (NPT) ensemble for 500 ps without restrain and the pressure of the system were maintained at 1 bar pressure using Berendsen barostat. All hydrogen bonds (HBs) were constrained using the SHAKE algorithm in a time step of 2 fs and all MD runs were done using SPFP precision model. A 30 ns production run was performed without any restrain on the systems in an NPT ensemble at a temperature of 300 K with target coupling constant of 2 ps and pressure at 1 bar

Trajectories from all system simulations were saved and analyzed in every 1 ps. Post-MD analyses, such as root mean square deviation (RMSD), radius of gyration (Rg), and root mean square fluctuation (RMSF), were performed using the CPPTRAJ and PTRAJ modules (Roe and Cheatham, 2013) of the Amber 14 suites. All plots were constructed

using Origin data analysis tool (http:/www.originlab.com). Molecular modeling suite Chimera (Petersen *et al.*, 2004) and Discovery studio suite were used for all visualizations.

3.2.9.6 Binding free energy calculations

To estimate the binding affinities of each system, the binding free energies were calculated using the Molecular Mechanics/Generalized-Born Surface Area method (MM/GBSA) (Genheden and Ryde, 2015). Binding free energies were averaged over 30000 snapshots extracted from the 30 ns trajectory. The free binding energy (ΔG) computed by this method for each molecular species (complex, ligand and receptor) can be represented as:

$$\Delta G_{bind} = G_{complex} - G_{receptor} - G_{ligand} \quad (1)$$

$$\Delta G_{bind} = E_{gas} + G_{sol} - T\,\Delta S \quad (2)$$

$$E_{gas} = E_{int} + E_{vdw} + E_{elec} \quad (3)$$

$$G_{sol} = G_{GB} + G_{SA} \quad (4)$$

$$G_{SA} = \gamma SASA \quad (5)$$

The term E_{gas} denotes the gas-phase energy, which consist of the internal energy (E_{int}); Coulomb energy (E_{elec}), and the van der Waals energies (E_{vdw}). The E_{gas} was directly estimated from the FF14SB force field terms. The solvation free energy (G_{sol}), was estimated from the energy contribution from the polar states (G_{GB}) and non-polar states (G_{SA}). The non-polar solvation energy (G_{SA}), was determined from the solvent accessible surface area (SASA), using a water probe radius of 1.4 Å, whereas the polar solvation, (G_{GB}) contribution was estimated by solving the GB equation. ΔS and T denote the total change in entropy of the solute and temperature respectively. To obtain the contribution of each residue to the total binding free energy profile between the ligands (P3 and P4) and

the enzymes, per residue free energy decomposition was carried out at the atomic level for imperative residues using the MM/GBSA method in Amber 14.

CHAPTER FOUR

4.0 RESULT

4.1 Designed Substituted Chalcones

The molecular formula, 2D structure and IUPAC names of the seventeen (17) chalcones synthesized were presented in Tables 4.1 – 4.3. Compounds P3, P4 and P8 are quinolinyl

chalcones from series two while, others represent various substituted chalcones. P1, P2, P3 and P8 are new compounds not reported in any literature/data base as ascertain from SciFinder search.

4.2 Analysis of Theoretical Oral Bioavailability

Table 4.4 present the molecular weight, hydrogen bond donor, hydrogen bond acceptor, number of rotatable bond and MLogP value of the synthesized chalcone for predicting theoretical oral bioavailability based on Lipinski ‘s rule of five.

Table 4.1: Chemical description P1, P2, P3, P4 and, P8

Compound ID	Molecular formula	2D- Representation/IUPAC Name

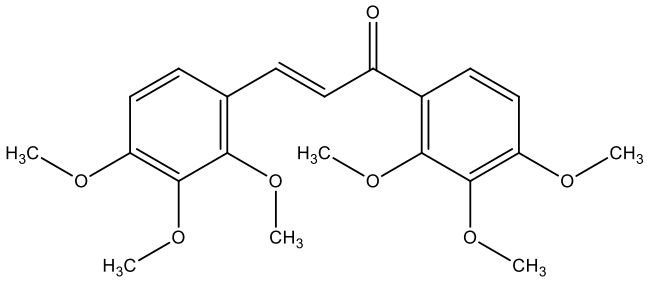
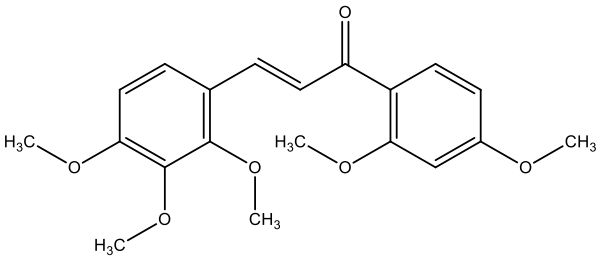
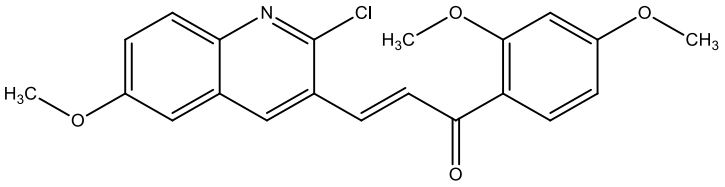
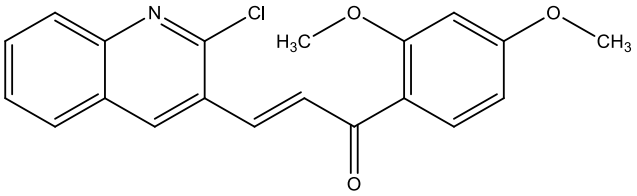
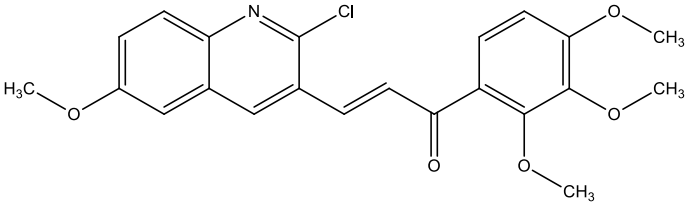
P1	$C_{21}H_{24}O_7$	 (*E*)-1,3-bis(2,3,4-trimethoxyphenyl)prop-2-en-1-one
P2	$C_{20}H_{22}O_6$	 (*E*)-1-(2,4-dimethoxyphenyl)-3-(2,3,4-trimethoxyphenyl)prop-2-en-1-one
P3	$C_{21}H_{18}ClNO_4$	 (*E*)-3-(2-chloro-6-methoxyquinolin-3-yl)-1-(2,4-dimethoxyphenyl)prop-2-en-1-one
P4	$C_{20}H_{16}ClNO_4$	 (*E*)-3-(2-chloroquinolin-3-yl)-1-(2,4-dimethoxyphenyl)prop-2-en-1-one
P8	$C_{22}H_{20}ClNO_5$	 (*E*)-3-(2-chloro-6-methoxyquinolin-3-yl)-1-(2,3,4-trimethoxyphenyl)prop-2-en-1-one

Table 4.2: Chemical description of P11, P12, P13, P15, P16 and P17

Compound ID	Molecular formula	2D- Representation

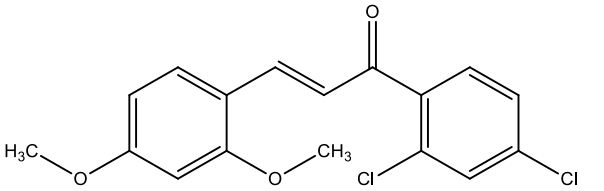
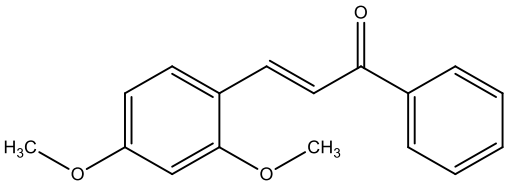
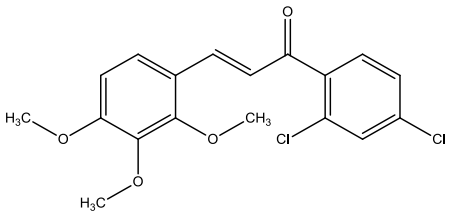
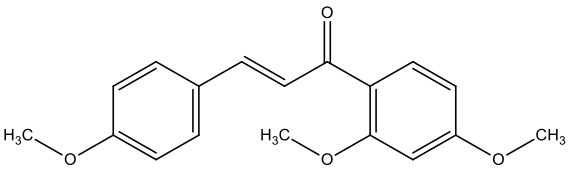
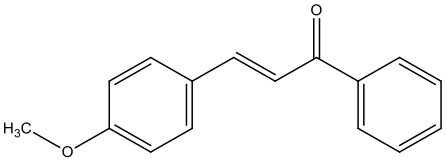
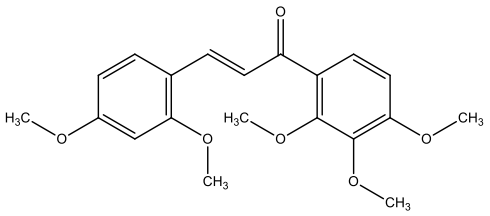
P11	$C_{17}H_{14}Cl_2O_3$	 (*E*)-1-(2,4-dichlorophenyl)-3-(2,4-dimethoxyphenyl)prop-2-en-1-one
P12	$C_{17}H_{16}O_3$	 (*E*)-3-(2,4-dimethoxyphenyl)-1-phenylprop-2-en-1-one
P13	$C_{18}H_{16}Cl_2O_4$	 (*E*)-1-(2,4-dichlorophenyl)-3-(2,3,4-trimethoxyphenyl)prop-2-en-1-one
P15	$C_{18}H_{18}O_4$	 (*E*)-1-(2,4-dimethoxyphenyl)-3-(4-methoxyphenyl)prop-2-en-1-one
P16	$C_{16}H_{14}O_2$	 (*E*)-3-(4-methoxyphenyl)-1-phenylprop-2-en-1-one
P17	$C_{2O}H_{22}O_6$	 (*E*)-3-(2,4-dimethoxyphenyl)-1-(2,3,4-trimethoxyphenyl)prop-2-en-1-one

Table 4.3: Chemical description of P19, P21, P22, P23, P24 and P25

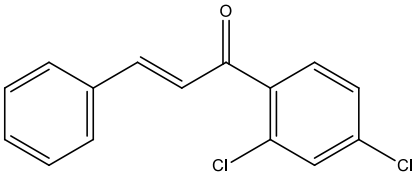
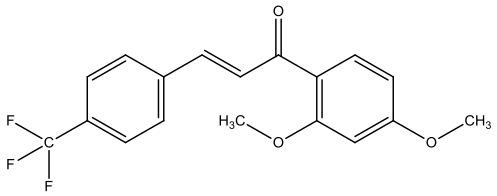
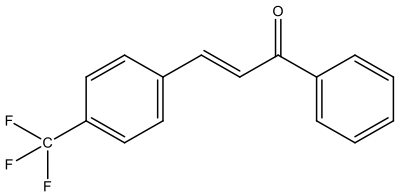
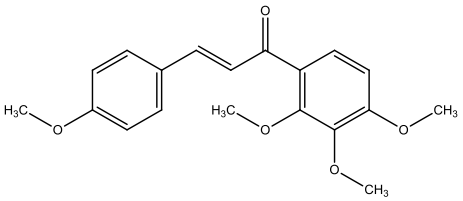
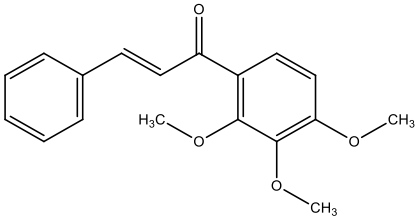
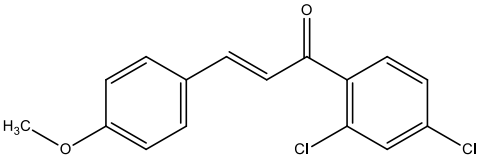
Compound ID	Molecular formula	2D- Representation
P19	$C_{17}H_{16}O_3$	 (*E*)-1-(2,4-dichlorophenyl)-3-phenylprop-2-en-1-one
P21	$C_{18}H_{15}F_3O_3$	 (*E*)-1-(2,4-dimethoxyphenyl)-3-(4-(trifluoromethyl)phenyl)prop-2-en-1-one
P22	$C_{16}H_{11}F_3O$	 (*E*)-1-phenyl-3-(4-(trifluoromethyl)phenyl)prop-2-en-1-one
P23	$C_{19}H_{20}O_5$	 (*E*)-3-(4-methoxyphenyl)-1-(2,3,4-trimethoxyphenyl)prop-2-en-1-one
P24	$C_{18}H_{18}O_4$	 (*E*)-3-phenyl-1-(2,3,4-trimethoxyphenyl)prop-2-en-1-one
P25	$C_{16}H_{12}Cl_2O_2$	 (*E*)-1-(2,4-dichlorophenyl)-3-(4-methoxyphenyl)prop-2-en-1-one

Table 4.4: Analysis of theoretical oral bioavailability of the substituted chalcones based on Lipinski's rule of five

Compound ID	Lipinski's rule of five[b]					
	Mol.Wt[a]	HbA	HbD	nRB	MLogP	Inference
P1	388.41	7	0	9	1.36	Pass
P2	358.39	6	0	8	1.67	Pass
P3	383.82	5	0	6	2.35	Pass
P4	353.80	4	0	5	2.69	Pass
P8	413.85	6	0	7	2.01	Pass
P11	337.20	3	0	5	3.67	Pass
P12	268.31	3	0	5	2.66	Pass
P13	367.22	4	0	6	3.31	Pass
P15	298.33	4	0	6	2.31	Pass
P16	238.28	2	0	4	3.03	Pass
P17	358.39	6	0	8	1.67	Pass
P19	268.31	3	0	5	2.66	Pass
P21	336.31	6	0	6	3.51	Pass
P22	276.25	4	0	4	4.32	Pass[c]
P23	328.36	5	0	7	1.99	Pass
P24	298.33	4	0	6	2.31	Pass
P25	307.17	2	0	4	4.05	Pass

(a) Molecular weight in g/mol, (b) Lipinski *et al.,* 2001 (Mwt≤500, MLogP≤4.15, N or O≤10, NH or OH≤5 and number of rotatable bonds≤ 10), (c) pass with one violation (MLogP>4.15).

4.3 Synthesis and Characterization of the Substituted Chalcones

4.3.1 Yield and some physical properties of substituted chalcones.

The yield and some physical properties of the synthesized compounds are presented in Table 4.5. The yield of the various chalcones ranges from low to high, with P11, P12, P22, P23 and P25 having the highest yield. Most of the compounds appeared as crystals after purification, only P1 occurred as a viscous gum. Color of the compounds is mostly yellow.

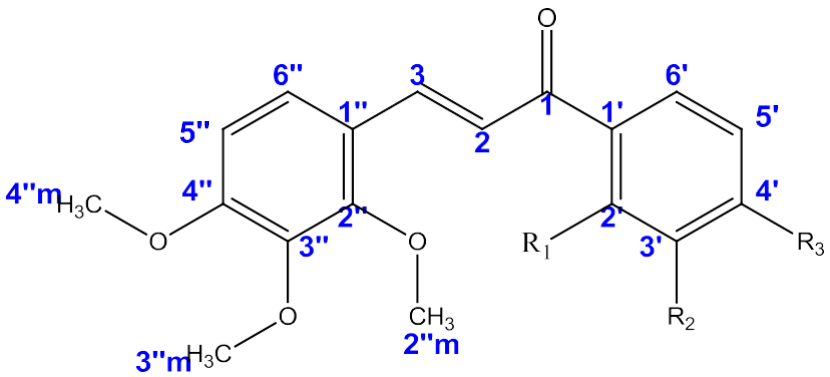
Table 4.5: Yield and Some Physical Properties of the substituted chalcones

Compound ID	Color/appearance	R_f Value[a]	Melting point (^{0}C)	% Yeild
P1*	Yellow viscous oil	0.38	39-40	57.00
P2*	Orange crystal	0.64	120-123	78.08
P3*	Light yellow crystal	0.40	109-111	50.64
P4	Yellow cotton-like	0.55	80-81	28.27
P8*	Yellow cotton-like	0.43	88-89	50.29
P11	Light yellow solid	0.59	114-116	87.00
P12	Yellow wax-like	0.61	48-50	83.93
P13	Yellow gummy solid	0.67	92-94	65.40
P15	Pale yellow crystals	0.25	82-84	36.87
P16	Yellow crystals	0.65	71-74	30.00
P17	Yellow crystals	0.68	66-68	37.50
P19	Light yellow powder	0.32	75-78	76.0
P21	Light yellow crystals	0.45	78-80	58.63
P22	Light yellow crystals	0.47	124-128	97.01
P23	Yellow soft crystals	0.42	60-61	95.50
P24	Yellow crystals	0.64	96-99	21.10
P25	Yellow wax	0.31	41-42	93.40

(a)Silica Thin layer chromatography plate was used with n-hexane: ethyl acetate (7:3) as development solvent. Rf is retention factor. * New compounds not reported in chemical literature (www. Scifinder.com)

4.3.2 ^{1}H and ^{13}C NMR Data of P1, P2 and P13

The ^{1}H and ^{13}C NMR data of compound P1, P2 and P13 (Figure 4.1) are shown in Table 4.6 and Appendices 13, 14, 21 and 22.



	R_1	R_2	R_3
P1	OCH_3	OCH_3	OCH_3
P2	OCH_3	H	OCH_3
P13	Cl	H	Cl

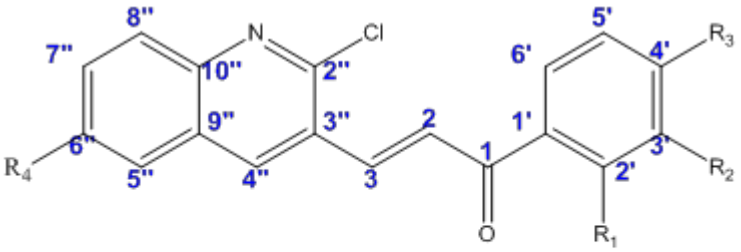
Figure 4.1: 2",3",4"-tri-methoxy substituted chalcones (P1, P2 and, P13)

Table 4.6: ^{1}H and ^{13}C NMR Data of P1, P2 and P13

Carbon Position	P1		P2		P13	
	^{13}C δ(ppm)	^{1}H δ(ppm)	^{13}C δ(ppm)	^{1}H δ(ppm)	^{13}C δ(ppm)	^{1}H δ(ppm)
1	191.35		191.17		192.76	
2	125.70	7. 38 (d, J=15.6(Hz,1H)	126.60	7.48(d, J=16Hz,1H)	123.80	7.42(d, J=16Hz,1H)
3	138.42	7. 86 (d, J=16.0(Hz,1H)	137.62	7.86(d, J=16Hz,1H)	141.89	8.00(d, J=16Hz,1H)
1’	127.17		122.78		136.45	
2’	153.56		160.38		142.20	
3’	142.13		98.85	6.49(d, J=2.0Hz, 1H)	129.94	7.73(d, J=4.0Hz, 1H)
4’	155.56		164.04		121.06	
5’	107.65	6.67(d, J=8.88Hz,1H)	107.75	6.56(dd, J=2.59Hz, 9.0Hz,1H)	127.15	7.64(d, J=7.6Hz,1H)
6’	123.40	7.33(d, J=8.8Hz, 1H)	132.92	7.33(d, J=8.5Hz, 1H)	130.35	7.74(d, J=9.6Hz, 1H)
1”	122.22		122.71		132.11	
2”	153.67		153.79		153.68	
3”	142.43		142.62		137.74	
4”	156.71		155.48		156.27	
5”	107.27	6.70(d, J=8.8Hz, 1H)	105.21	6.70(d, J=9.0Hz, 1H)	107.67	7.02(d, J=7.6Hz, 1H)
6”	125.65	7.41(d, J=9.0Hz, 1H)	123.68	7.34(d, J=9.0Hz, 1H)	124.65	7.64(d, J=7.6Hz,1H)
2’m	61.47	3.87	56.22	3.89	-	-
3’m	60.88	3.87	-	-	-	-
4’m	56.06	3.83	55.90	3.88	-	-
2”m	62.07	3.88	61.58	3.92	61.51	4.25
3”m	61.03	3.87	61.08	3.89	60.80	4.24
4”m	56.10	3.85	55.69	3.86	56.01	4.24

+4.3.3 ^{1}H and ^{13}C NMR data of P3, P4 and P8

The ^{1}H and ^{13}C NMR data of compounds P3, P4 and P8 (Figure 4.2) are as shown in Table 4.7 and Appendices 25, 26, 32, 33, 40 and 41.



	R_1	R_2	R_3	R_4
P3	OCH_3	H	OCH_3	OCH_3
P4	OCH_3	H	OCH_3	H
P8	OCH_3	OCH_3	OCH_3	OCH_3

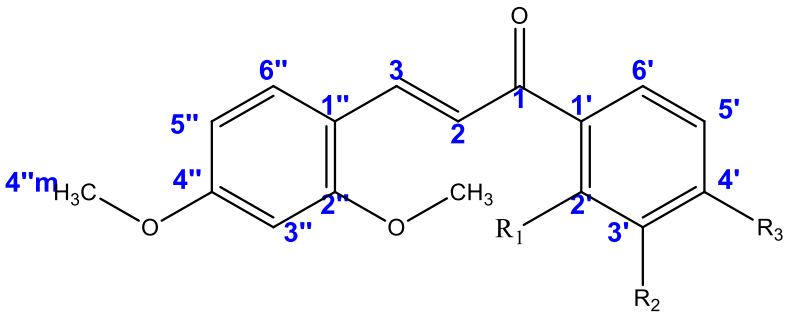
Figure 4.2: 3-quinolinyl-substituted chalcones (P3, P4 and, P8)

Table 4.7: ^{1}H and ^{13}C NMR Data of P3, P4 and P8

Carbon Position	P3		P4		P8	
	^{13}C δ(ppm)	^{1}H δ(ppm)	^{13}C δ(ppm)	^{1}H δ(ppm)	^{13}C δ(ppm)	^{1}H δ(ppm)
1	196.42	-	189.55		197.91	
2	104.86	6.81(d, J=20Hz, 1H)	131.50	7.72(d, J=16Hz, 1H)	104.94	6.82(d, J=16Hz, 1H)
3	135.09	7.84(d, J=21Hz, 1H)	136.24	8.03(d, J=15.9Hz, 1H)	135.08	7.80(d, J=16.0Hz, 1H)
1’	119.75	-	123.84	-	124.53	-
2’	160.39	-	160.75	-	153.35	-
3’	97.89	6.24(d, J=2.12Hz, 1H)	98.67	6.49(d, J=2.00Hz, 1H)	142.32	
4’	164.69	-	164.64	-	158.10	-
5’	105.84	6.45(dd, J=2.68Hz, 9.16Hz, 1H)	105.4	6.57(dd, J=2.1Hz, 8.6Hz, 1H)	122.40	7.21(d, J= 8.84Hz, 1H)
6’	133.24	7.77(d, J=8.68Hz, 1H)	128.27	7.80(d, J=9.00Hz, 1H)	129.59	7.72(d, J=9.20Hz, 1H)
2”	148.88	-	150.51	-	148.84	-
3”	132.91	-	131.38	-	132.12	-
4”	53.09	4.93(d, J=2.40Hz, 1H)	133.24	8.39(d, J=2.40Hz, 1H)	41.73	4.97(d, J=5.10Hz, 1H)
5”	41.44	4.79(d,	128.65	7.82(d, J=10.0Hz, 1H)	51.85	4.86(d, J=6.36Hz, 1H)
6”	158.04	-	127.80	7.61(d, J=9.0Hz, 1H)	157.57	
7”	122.34	7.16(dd, J=2.24Hz, 8.88Hz, 1H)	121.61	7.46(dd, J=4.04Hz, 9.0Hz, 1H)	107.20	6.62(dd, J=4.04Hz, 8.84Hz, 1H)
8’’	129.44	7.19(d, J=9.2Hz, 1H)	133.07	7.72(d, J=9.2Hz, 1H)	126.19	7.42(d, J=8.84Hz, 1H)
9’’	127.92	-	127.12	-	127.82	-
10’’	142.16	-	147.47	-	141.29	-
2’m	55.55	3.76 (3H)	55.84	3.76 (3H)	61.38	4.09 (3H)
3’m	-	-	-		55.60	3.65 (3H)
4’m	55.51	3.74 (3H)	55.61	3.74 (3H)	60.77	3.83 (3H)
6”m	55.09	3.38 (3H)	-	-	56.12	3.73 (3H)

4.3.4 ^{1}H and ^{13}C NMR Data of P11, P12 and P17

The ^{1}H and ^{13}C NMR data of compound P11, P12 and P17 (Figure 4.3) are shown in Table 4.8 and Appendices 48, 49, 54, 55, 58 and 61.



	R_1	R_2	R_3
P11	Cl	H	Cl
P12	H	H	H
P17	OCH_3	OCH_3	OCH_3

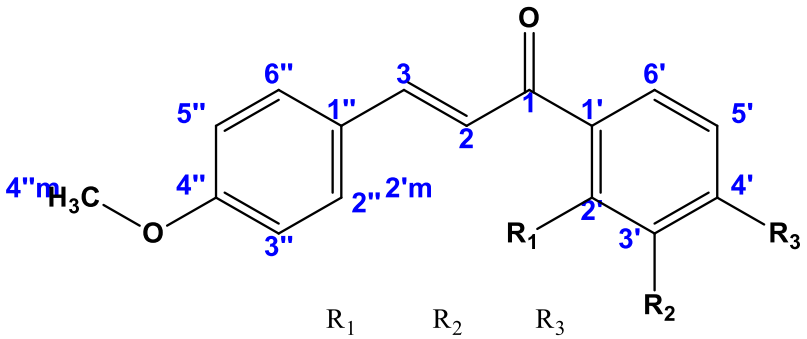
Figure 4.3 : 2”,4”-di-methoxy-substituted chalcones (P11, P12 and, P17)

Table 4.8: ^{1}H and ^{13}C NMR Data of P11, P12 and P17

Carbon Position	P11		P12		P17	
	^{13}C δ(ppm)	^{1}H δ(ppm)	^{13}C δ(ppm)	^{1}H δ(ppm)	^{13}C δ(ppm)	^{1}H δ(ppm)
1	193.28	-	191.12	-	191.47	-
2	124.15	7.42(d, J=16Hz,1H)	128.36	7.48(d, J=14Hz,1H)	125.47	7.93(d, J=16Hz,1H)
3	142.55	8.33(d, J=16.0Hz,1H)	140.53	8.04(d, J=16.0Hz,1H)	138.84	8.46(d, J=15.9Hz,1H)
1’	136.31	-	138.78		117.04	-
2’	138.08	-	128.89	7.98(dd, J=8.0Hz;2.1Hz, 1H)	156.50	-
3’	130.06	7.72(d, J=1.8Hz, 1H)	128.49	7.54(dd, J=8.2Hz:8.1Hz, 1H)	153.38	-
4’	132.29	-	132.34	7.45(dd, J=8.6Hz; 2.0Hz, 1H)	162.89	-
5’	127.09	7.56(d,d J=8.2Hz; 1.8Hz, 1H)	128.42	7.54(dd, J=8.2Hz; 8.1Hz, 1H)	107.19	7.25(d, J=8.1Hz, 1H)
6’	130.32	7.77(d, J=8.2Hz, 1H)	128.82	7.98(dd, J=8.0Hz;2.1Hz, 1H)	124.59	8.06(d, J=7.8Hz, 1H)
1”	116.40	-	116.97		127.29	-
2”	160.46	-	160.37		142.05	-
3”	98.42	6.53(d, J=2.2Hz, 1H)	98.34	6.43(d, J=2.0Hz, 1H)	98.27	6.96(d, J=4.0Hz, 1H)
4”	163.61		163.04		160.13	
5”	105.62	6.76(d, J=8.6Hz; 2.2Hz, 1H)	105.39	6.50(d, J=8.6Hz; 2.2Hz, 1H)	105.49	7.02(d, J=8.6Hz; Hz, 1H)
6”	131.07	8.05(d, J=8.6Hz, 1H)	130.94	7.55(d, J=8.1Hz, 1H)	130.27	7.96(d, J=11.2Hz, 1H)
2’m	-	-	-	-	61.92	4.43 (3H)
3’m	-	-	-	-	60.90	4.43 (3H)
4’m	-	-	-	-	56.01	4.42 (3H)
2”m	55.55	3.82 (3H)	55.48	3.85 (3H)	55.42	4.36 (3H)
4”m	55.53	3.82 (3H)	55.46	3.81 (3H)	55.37	4.33 (3H)

4.3.5 ^{1}H and ^{13}C NMR Data of P15, P16 and P23

The ^{1}H and ^{13}C NMR data of compounds P15, P16 and P23 (Figure 4.4) are as shown in Table 4.9 and Appendices 64, 65, 67, 69, 71 and 73.



	R_1	R_2	R_3
P15	OCH_3	H	OCH_3
P16	H	H	H
P23	OCH_3	OCH_3	OCH_3

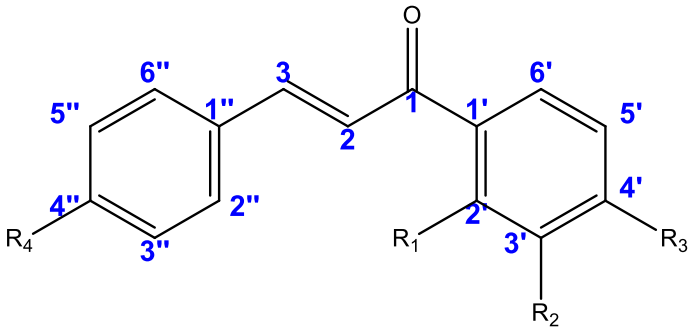
Figure 4.4 : 4”-methoxy substituted chalcones (P15, P16 and, P23)

Table 4.9: ^{1}H and ^{13}C NMR Data of P15, P16 and P23

Carbon Position	P15		P16		P23	
	^{13}C δ(ppm)	^{1}H δ(ppm)	^{13}C δ(ppm)	^{1}H δ(ppm)	^{13}C δ(ppm)	^{1}H δ(ppm)
1	189.81	-	189.96	-	191.31	-
2	124.21	7.36(d, J=15.7Hz,1H)	119.24	7.39(d, J=16.0Hz,1H)	124.61	6.31(d, J=15.8Hz,1H)
3	141.23	7.65(d, J=15.7Hz,1H)	144.20	7.76(d, J=15.5Hz,1H)	143.45	6.59(d, J=15.7Hz,1H)
1’	121.67	-	138.05		127.32	-
2’	160.42	-	128.78	7.98(d, J=8.0Hz,1H)	153.93	-
3’	97.85	6.48(d, J=1.8Hz, 1H)	128.05	7.51(d, J=12Hz, 1H)	142.40	-
4’	163.14	-	132.13	7.55(dd, J=7.2Hz;12Hz, 1H)	161.74	-
5’	104.32	6.54(dd, J=8.2Hz;1.4Hz,1H)	127.98	7.51(d, J=12Hz, 1H)	107.57	5.69(d, J=8.8Hz, 1H)
6’	131.90	7.74(d, J=8.4Hz, 1H)	128.13	7.98(d, J=8.0Hz, 1H)	126.05	6.40(d, J=8.2Hz, 1H)
1”	127.35	-	127.14		128.13	
2”	129.45	7.54(d, J=8.5Hz, 1H)	129.82	7.45(d, J=14.6Hz, 1H)	130.92	6.50d, J=8.0Hz, 1H)
3”	113.81	6.90(d, J=8.4Hz, 1H)	114.30	6.88(d, J=8.0Hz, 1H)	115.11	5.85(d, J=7.2Hz, 1H)
4”	159.43		161.25		157.12	
5”	113.48	6.90(d, J=8.4Hz, 1H)	113.99	6.88(d, J=8.0Hz, 1H)	114.66	5.85(d, J=7.2Hz, 1H)
6”	129.16	7.54(d, J=8.5Hz, 1H)	129.50	7.45(d, J=14.6Hz, 1H)	130.46	6.50d, J=8.0Hz, 1H)
2’m	54.92	3.88 (3H)	-	-	62.47	2.85 (3H)
3’m		-	-	-	61.42	2.85 (3H)
4’m	54.70	3.86 (3H)	-	-	56.44	2.85 (3H)
4”m	54.54	3.81 (3H)	54.90	3.78 (3H)	55.72	2.77 (3H)

4.3.6 ^{1}H and ^{13}C NMR assignment of P19, P24 and P25

The ^{1}H and ^{13}C NMR data of compounds P19, P24 and P25 (Figure 4.5) are as shown in Table 4.10 and Appendices 77, 79, 81, 82, 75 and 76.



	R_1	R_2	R_3	R_4
P19	OCH_3	H	OCH_3	H
P24	OCH_3	OCH_3	OCH_3	H
P25	Cl	H	Cl	OCH_3

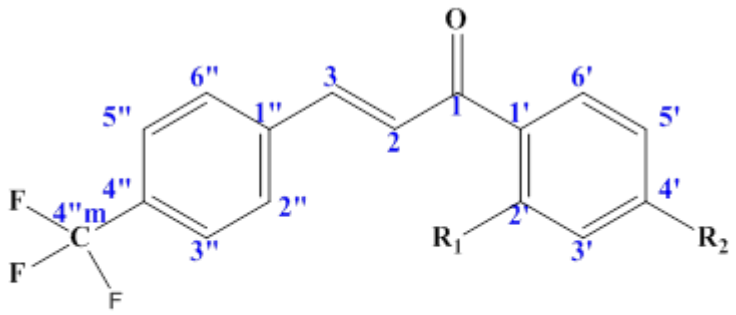
Figure 4.5: 4”-methoxy substituted chalcone (P25) and un-substituted ring A chalcones (P19 and, P24)

Table 4.10: ^{1}H and ^{13}C NMR Data of P19, P24 and P25

Carbon Position	P19		P24		P25	
	^{13}C δ(ppm)	^{1}H δ(ppm)	^{13}C δ(ppm)	^{1}H δ(ppm)	^{13}C δ(ppm)	^{1}H δ(ppm)
1	190.47		190.80		192.60	
2	127.48	7.03(d, J=16Hz,1H)	125.87	7.78(d, J=16Hz,1H)	123.60	7.52
3	142.07	7.19(d, J=15.8Hz,1H)	142.98	7.79(d, J=15.0Hz,1H)	146.71	8.04
1’	122.25		135.10		136.58	
2’	160.80		153.77		137.68	
3’	98.78	5.96(d, J=2.0Hz, 1H)	142.07		130.10	7.93
4’	164.62		157.05		132.23	
5’	105.66	6.03(dd, J=8.5Hz;2.2Hz, 1H)	107.29	6.89(d, J=8.2Hz,1H)	127.23	7.48
6’	133.19	7.29(d, J=8.4Hz, 1H)	126.48	7.82(d, J=8.4Hz, 1H)	130.86	7.98
1”	135.70		126.68		126.85	
2”	129.19	7.08(dd, J=8.5Hz;2.2Hz, 1H)	128.37	7.64(dd, J=11.4Hz;5.6Hz,1H)	130.55	7.86
3”	128.61	6.86(d, J=8.0Hz, 1H)	128.89	7.62(d, J=11.4Hz, 1H)	114.83	7.44
4”	130.33	6.86(d, J=8.0Hz, 1H)	130.23	7.51(dd, J=11.4Hz;1.3Hz, 1H)	162.10	
5”	128.03	6.86(d, J=8.0Hz, 1H)	128.89	7.62(d, J=11.4Hz, 1H)	114.52	7.44
6”	128.87	7.08(dd, J=8.5Hz;2.2Hz, 1H)	128.37	7.64(dd, J=11.4Hz;5.6Hz,1H)	130.34	7.86
2’m	55.97	3.32(3H)	62.12	4.04 (3H)	-	-
3’m	-	-	61.07	4.04 (3H)	-	-
4’m	55.79	3.29(3H)	56.11	4.04 (3H)	-	-
4”m	-	-	-	-	55.44	4.35 (3H)

4.3.7 ^{1}H and ^{13}C NMR data of P21, and P22

The ^{1}H and ^{13}C NMR data of compounds P21 and P22 (Figure 4.6) are as shown in Table 4.11 and Appendices 87, 88, 91 and 92.



	R1	R2
P21	OCH3	OCH3
P22	H	H

Figure 4.6: 4" triflouromethyl - substituted chalcones (P21 and, P22)

Table 4.11: ^{1}H and ^{13}C NMR Assignment of P21, and P22

Carbon Position	P21		P22	
	^{13}C δ(ppm)	^{1}H δ(ppm)	^{13}C δ(ppm)	^{1}H δ(ppm)
1	189.76	-	189.46	-
2	124.75	7.60(d, J=16Hz,1H)	123.73	7.55(d, J=14Hz,1H)
3	139.60	7.80(d, J=17.0Hz,1H)	142.20	7.77(d, J=15.0Hz,1H)
1’	125.71	-	137.32	-
2’	160.60	-	128.05	8.02(dd, J=13.7Hz;6.7Hz,1H)
3’	98.52	6.53(d, J=2.8Hz,1H)	128.27	7.61(d, J=11.0Hz,1H)
4’	164.57	-	132.67	7.69(dd, J=8.2Hz;3.2Hz,1H)
5’	105.35	6.57(dd, J=8.0Hz;2.8Hz,1H)	128.27	7.61(d, J=11.0Hz,1H)
6’	133.13	7.82(d, J=9.0Hz, 1H)	128.05	8.01(dd, J=13.7Hz;6.7Hz,1H)
1”	138.93	-	137.82	
2”	128.57	7.68(d, J=9.0Hz, 1H)	128.10	7.57(d, J=8.0Hz, 1H)
3”	128.16	6.59(d, J=9.3Hz, 1H)	127.78	7.50(d, J=8.0Hz, 1H)
4”	129.33	-	128.50	
5”	127.98	6.59(d, J=9.3Hz, 1H)	127.78	7.49(d, J=8.0Hz, 1H)
6”	128.30	7.68(d, J=9.0Hz, 1H)	128.10	7.56(d, J=8.0Hz, 1H)
2’m	55.73	4.04 (3H)	-	-
4’m	55.57	3.89 (3H)	-	-
4”m	121.66	-	125.43	-

4.3.8 FT-IR spectral data of the substituted chalcones

The FT-IR spectral data of all the compounds synthesized are presented in Appendix VI. In all the spectra, there is appearance of the characteristics strong C=O stretching vibration at 1640 cm^{-1} and an olefinic peak observed at 2995-3008 cm^{-1}.

4.3.9 Mass spectral data of the substituted chalcones

The mass spectral data of all the compounds is also presented in Appendix V. Each mass spectrum present molecular ion peak (M^{+1}) corresponding to the molecular weight of the respective compound. The molecular ion peak in most of the spectrum is the most abundant peak.

4.4 Antiplasmodial Studies on the Substituted Chalcones in Mice

4.4.1 Effect of P1, P2, P3, P4, P23, P24 and P25 on established P. berghii infection in mice

The test compounds showed promising activity with some producing a chemo-suppression comparable to the standard drugs (Figure 4.7). P2 has the highest suppression at 25, 50 and 100 mg/kg of 62.4% ($p<0.05$), 79% ($p<0.05$) and 90 ($p<0.05$) respectively. The quinolinyl chalcones: P3, P4 and P8 significantly reduced the parasitemia level compared to the standard. P25 also showed promising activity with, the smaller dose (25 mg/kg) producing higher chemo-suppression of 72%.

The standard drug chloroquine at 25 mg/kg produced a chemo-suppression of 85.5% ($p<0.05$) compared to the negative control. Arthemeter at 5 mg/kg produced a chemo-suppression of 77% ($p<0.05$) while, quinine produced the highest parasite suppression of 88.5% at 10 mg/kg (Figure 4.7).

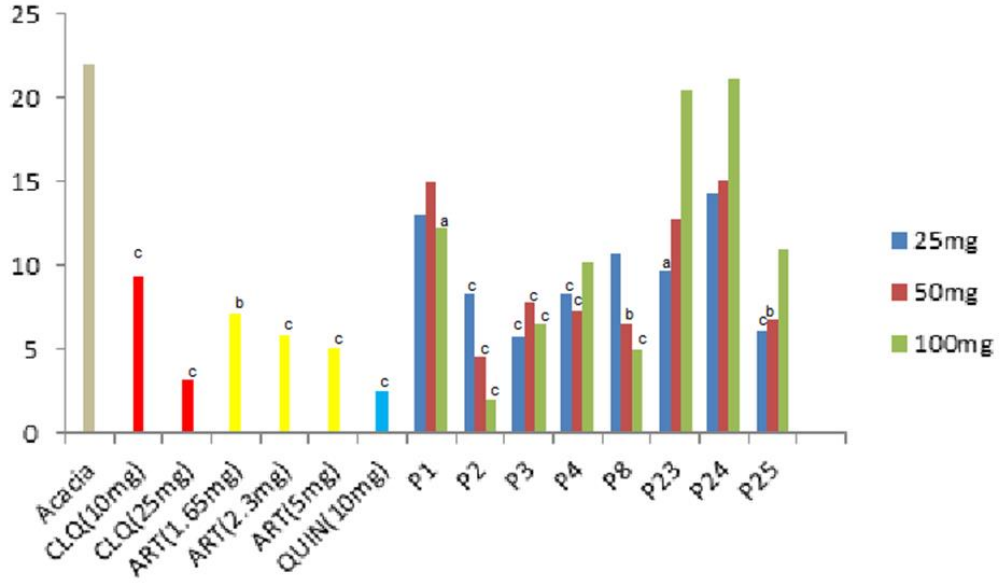


Figure 4.7: Effect of P1, P2, P3, P4, P8, and P23-P25 on the parasitaemia level of *P. bergheii* infected mice.

Values are presented as Mean; Data analyzed by one way ANOVA followed by Bonferroni's post-hoc test; n=5 a=$p<0.05$, b=$p<0.01$, c=$p<0.001$ versus control; CLQ=chloroquine, ART= arthemeter, QUIN= quinine; Route of administration=ip

4.4.2 Effect of P11, P12, P13, P15, P16, P17, P19, P21 and P22 on established *P. berghii* infection in mice

P11, P12 and, P17 at a dose of 100 mg/kg, 300 mg/kg and 50 mg/kg respectively, significantly (p<0.05) suppress parasitaemia in mice, with percent chemosuppression of 82.8%, 89.44% and, 80.3% respectively compared to control (Figure 4.8). The standard drug (chloroquine) at the dose of 25 mg/kg produced significant (p<0.05) parasite suppression of 91.8% compared to control.

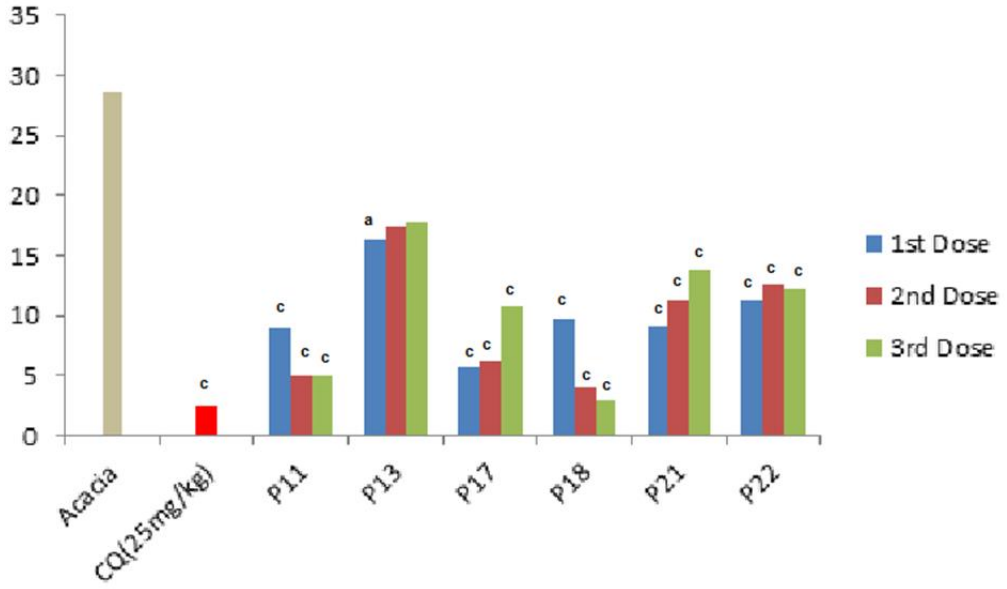


Figure 4.8: Effect of P11, P13, P17, P18, and P21-P22 on the parasitaemia level of *P. bergheii* infected mice.
Values are presented as Mean ± SEM; Data analyzed by one-way ANOVA followed by Bonferroni's post-hoc test; n=5 a=p<0.05, c=p<0.001 versus control; CQ=chloroquine, P11, P13 (25, 50,100 mg/kg); P17 (50,100,200 mg/kg); P18 (75,150,300 mg/kg); P21 (175,350,700 mg/kg); P22 (250,500,1000 mg/kg); Route of administration=*ip*

4.5 Effect of Substituted Chalcones on Inhibition of *β*-hematin Synthesis

With the exception of P12 and P17, none of the compound inhibits the formation of *β*-hematin (Table 4.12). Compounds P12 and P17 showed modest inhibition of *β*-hematin synthesis with percent inhibition of 59.28% and 49.04% respectively at a dose of 50µg/kg. The standard drug (chloroquine) produced 74.58% inhibition of *β*-hematin synthesis (Table 4.12).

Table 4.12: Effect of P2, P3, P4, P8, P11, P12, P17, P21 and P25 on inhibition of *β*-hematin synthesis

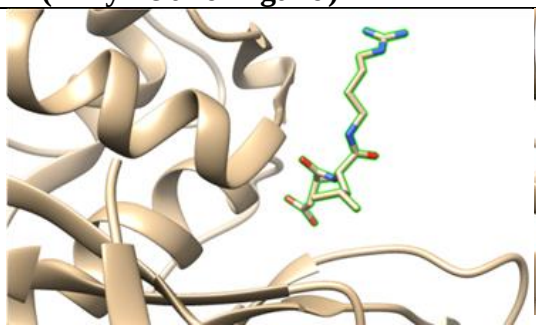
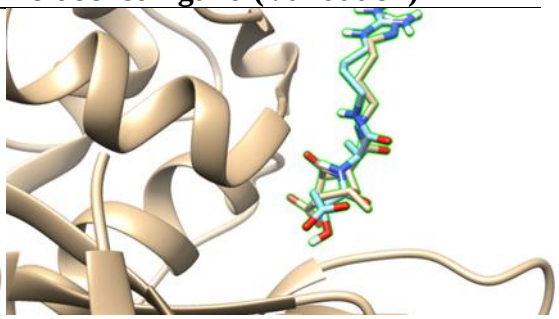
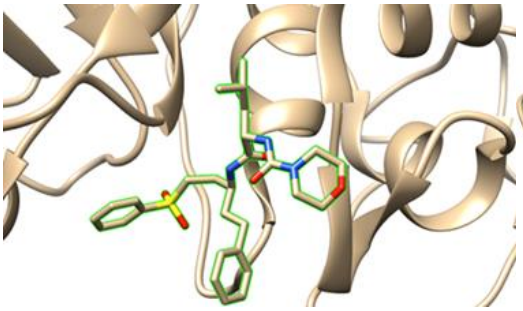
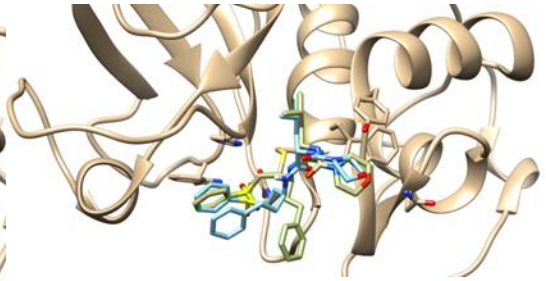
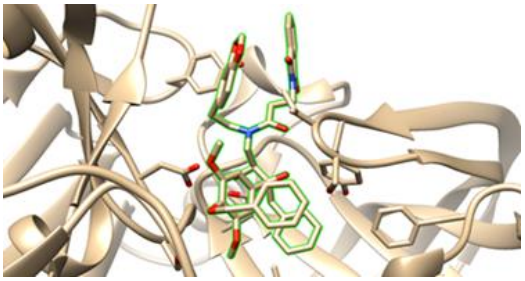
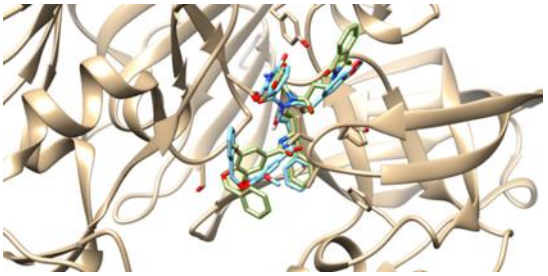
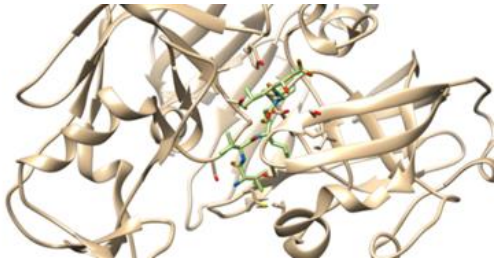
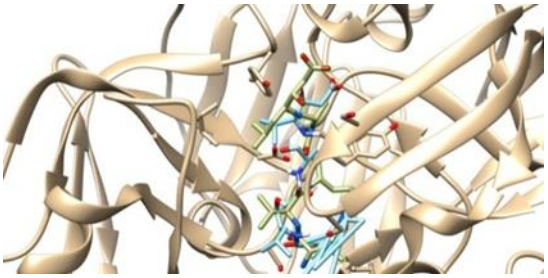
Treatment groups	Dose(µg/kg)	Absorbance	% Inhibition
Acacia	1%w/v	0.830	
Chloroquine	8	0.211	74.58
P2	200	0.711	14.34
P2	100	0.731	11.93
P2	50	0.755	9.04
P3	200	1.098	-32.29
P3	100	0.883	-6.39
P3	50	0.835	-0.60
P4	200	1.011	-21.81
P4	100	1.056	-27.23
P4	50	1.03	-24.10
P8	200	1.066	-28.43
P8	100	1.029	-23.98
P8	50	1.171	-41.08
P11	200	1.137	-36.99
P11	100	1.084	-30.60
P11	50	1.083	-30.48
P12	200	0.395	52.41
P12	100	0.353	57.47
P12	50	0.338	59.28
P17	200	0.456	45.06
P17	100	0.449	45.90
P17	50	0.423	49.04
P21	200	0.509	38.67
P21	100	0.743	10.48
P21	50	1.055	-27.11
P25	200	0.831	-0.12
P25	100	0.845	-1.81
P25	50	1.002	-20.72

4.6 Molecular Docking Studies of P3 and P4 Complexes on FP-2, FP-3, Plm-II, and Plm-IV.

4.6.1 Validation of docking procedure

The docking procedures applied on all the four enzymes were well validated. As shown on Table 4.13 all the co-crystallized ligands re-docked (Cyan color) on their respective proteins are well super imposed on their original Protein Data Bank (PDB) structures.

Table 4.13: Showing the crystal structure of enzymes complexes and re-docked ligand super-imposed on the crystal structure for validation.

Enzyme	Crystal structure complex (Enzyme and Ligand)	Crystal structure complex with Re-docked ligand (Validation)
3-BPF		
3BWK		
1-LF3		
1LS5		

Cyan colour molecule is the re-docked ligand and the green highlighted molecule is co-crystallized ligand.

4.6.2 The binding energies of the co-crystallized ligands and 17 substituted Chalcones against four enzymes (FP-2, FP-3, Plm-II, and, Plm-IV)

Docking results as shown on Figure 4.9 indicated that all the compounds studied exhibited better binding energies to FP-2 than the co-crystallized ligand (5.1 Kcal/mol). However, only compound P8 (quinolinyl chalcone) showed better binding energy (-7.0 Kcal/mol) than the co-crystallized ligand with 6.9 Kcal/mol for FP-3. With the aspartic proteases; Plm-II, the co-crystallized ligand exhibited better binding energy (10.1 Kcal/mol) than all the compounds, nevertheless compound P3, P4, and P8 have a reasonable binding energy of 8.0, 7.9, and 7.7 Kcal/mol respectively. Seven compounds showed better binding energy for Plm-IV as compared to the co-crystallized ligand, with P3 and P4 having remarkable binding energy of 9.3 and 9.1 Kcal/mol respectively.

Interestingly the ranking of the ligands relative to each other and the co-crystallized ligands, point out two chalcones; P3 (Figure 4.10) and P4 (Figure 4.11), possessing high ranking across all the enzymes studied (Figure 4.9)

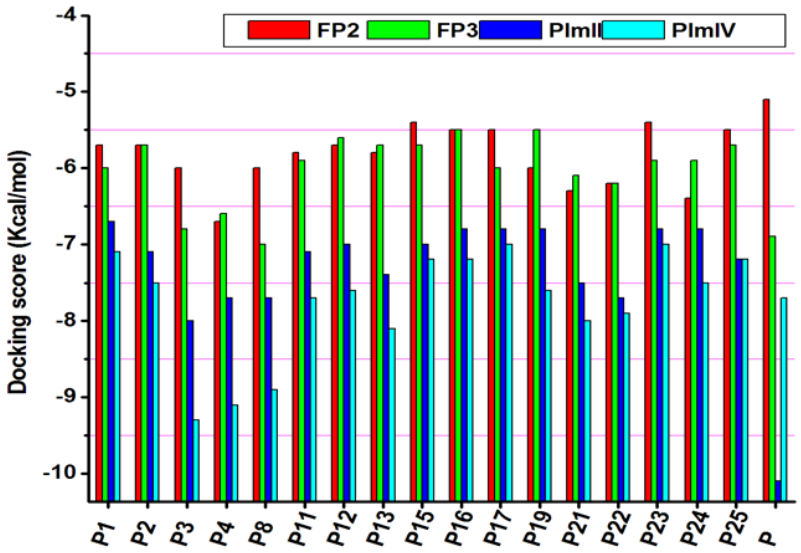


Figure 4.9: The binding energies of the ligands across all the enzymes. P represents the co-crystallized ligand of each enzyme.

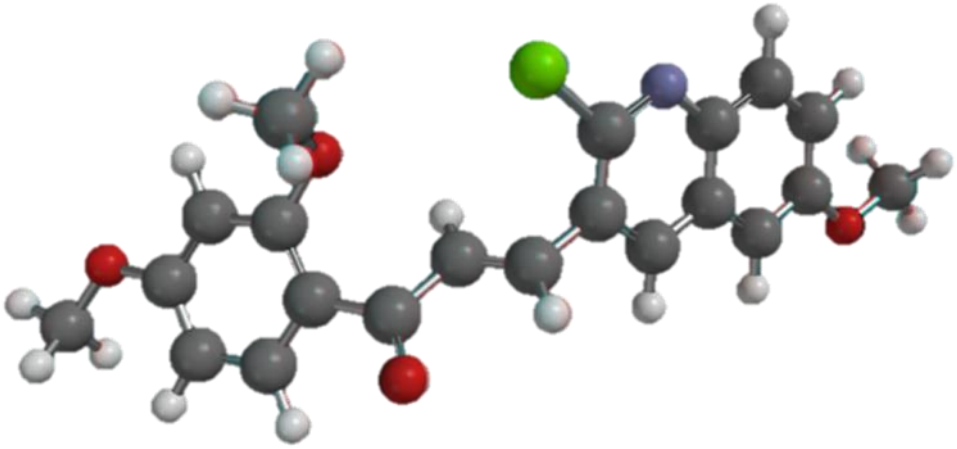


Figure 4.10: Compound P3 [(E)-3-(2-chloro-6-methoxyquinolin-3-yl)-1-(2, 4-dimethoxyphenyl) prop-2-en-1-one]

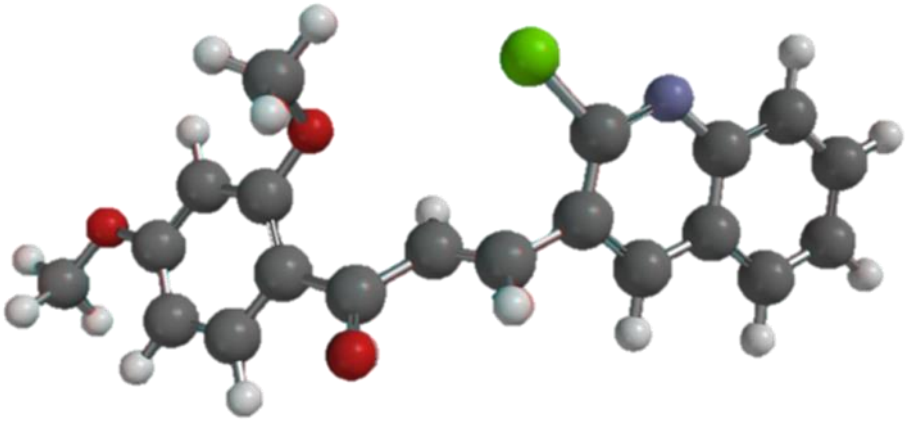


Figure 4.11: Compound P4 [(E)-3-(2-chloroquinolin-3-yl)-1-(2, 4 dimethoxyphenyl) prop-2-en-1-one

4.6.3 The binding poses and binding interaction analysis of P3 and P4 against FP-2, FP-3, Plm-II, and Plm-IV.

The binding conformation and interaction with residues on the active site of the enzymes studied using chimera (Pettersen *et al.,* 2004) and Discovery studio suite (www.accelrys.com) is shown on Figure 4.12-4.19. P3 and P4 fitted well onto the long cleft of FP-2 and FP-3 (Figure 4.12-4.15), extending from S1 subsite to S3, but having more extended conformation in FP-3 (Figure 4.14). On the plasmepsins (Figure 4.16-4.19) the two compounds fit into the binding pocket, resting on the catalytic dyad and fully covered with the flap.

With the exception of Plm-IV (Figure 4.18), the two congeners bind to all the enzymes in an opposite orientation (in different conformation). Nonetheless, the two congeners have similar interactions with the active site residues in the case of each enzyme (Figure 4.13, 4.15, 4.17 and, 4.19).

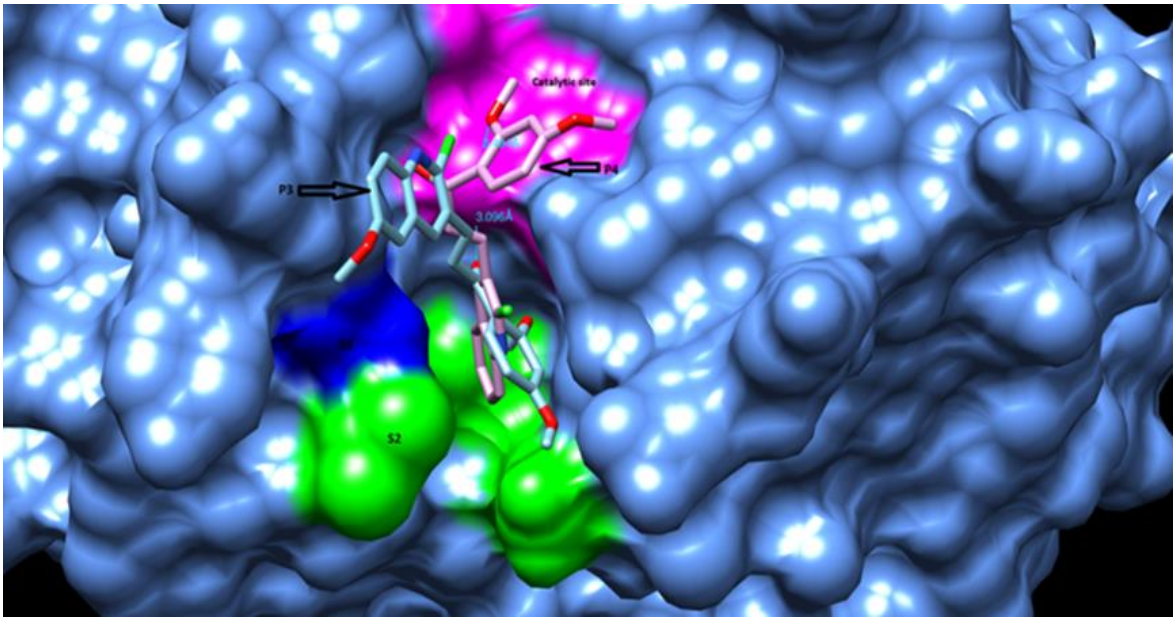


Figure 4.12 : 3D binding poses and interaction of P3 and P4 in relation to various sub sites of FP-2 binding cavity.

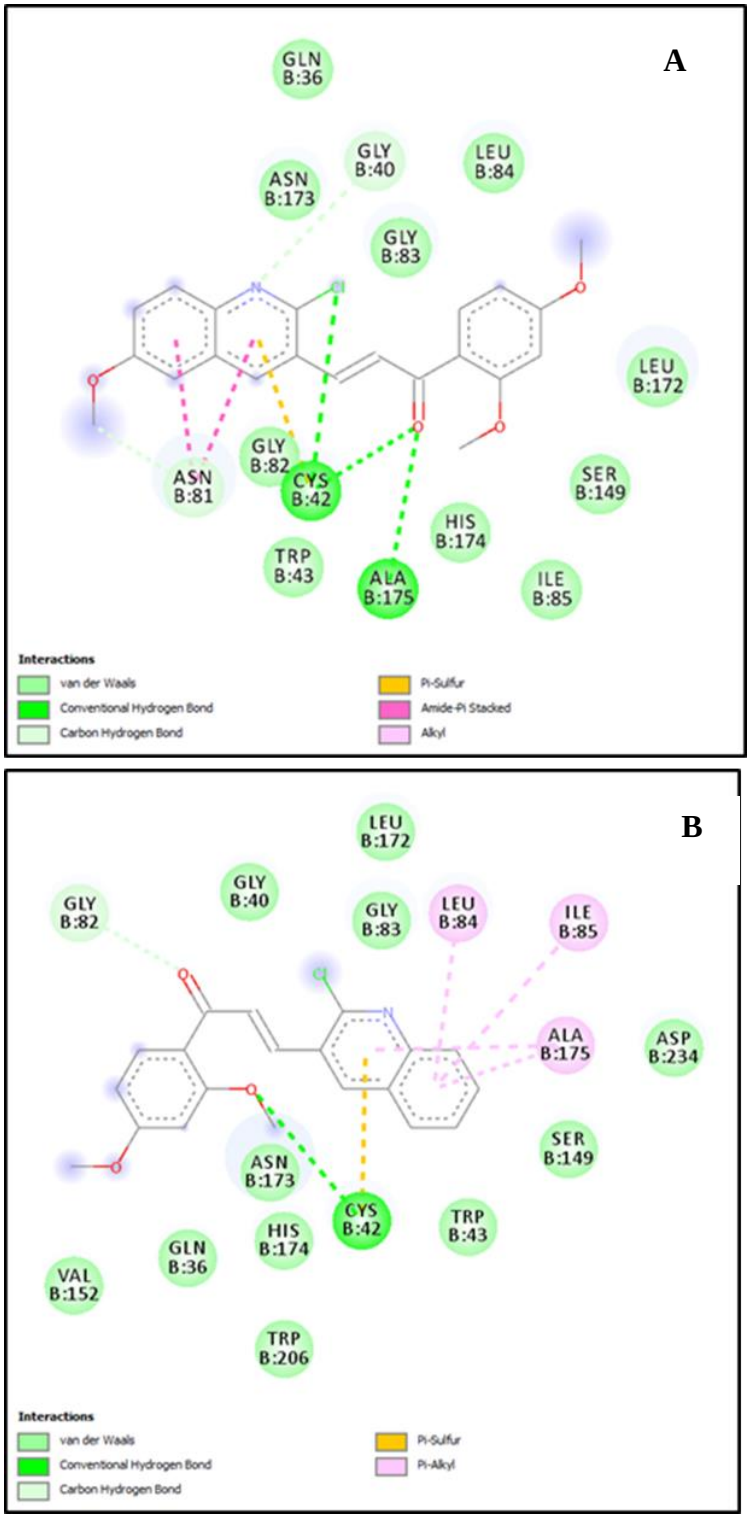


Figure 4.13: (A) 2D interaction diagram of FP-2 and P3 (B) 2D interaction diagram of FP-2 and P4.

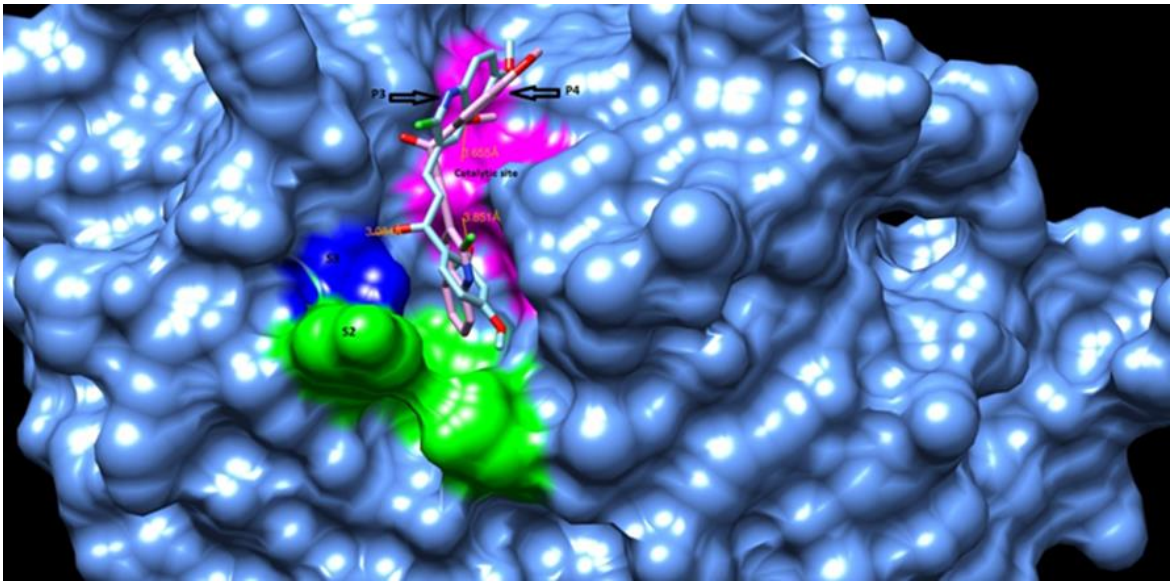


Figure 4.14: 3D binding poses and interaction of P3 and P4 in relation to various sub sites of FP-3 binding cavity.

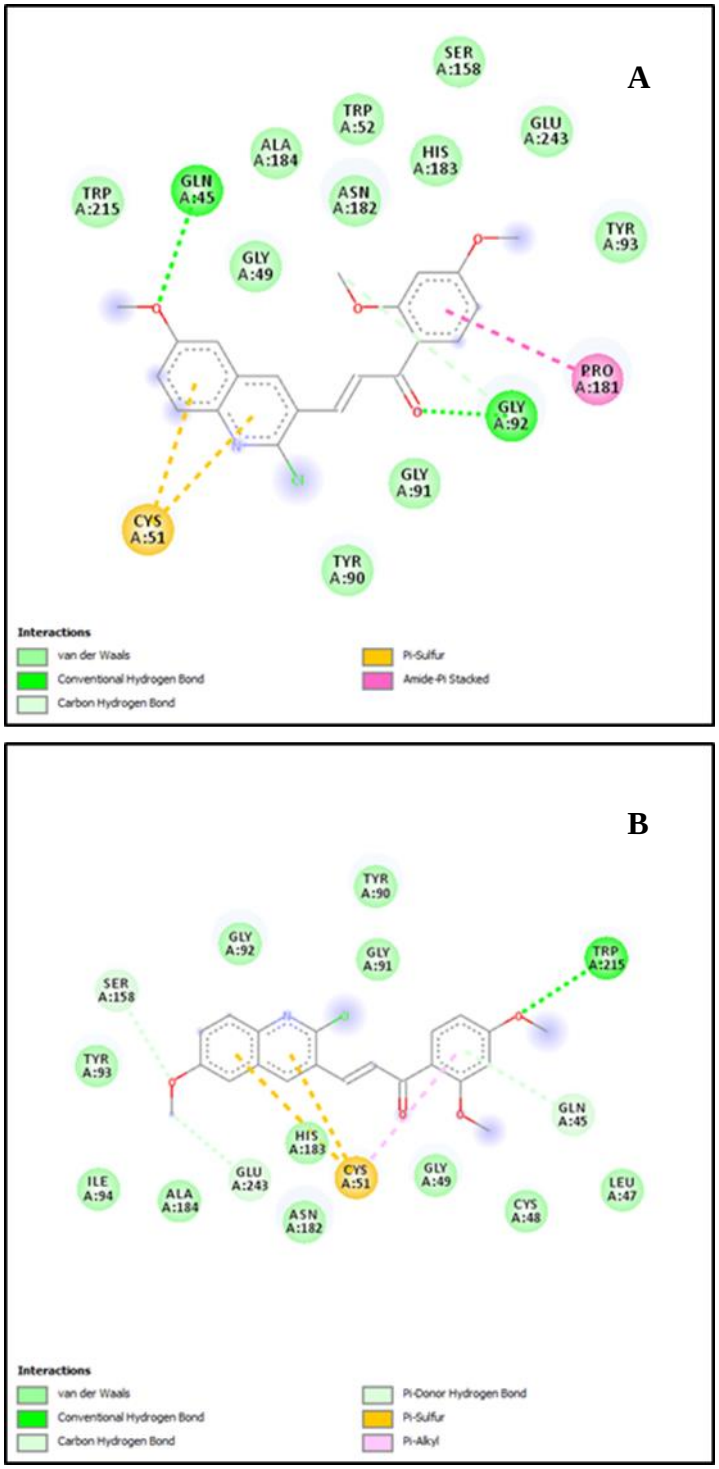


Figure 4.15: (A) 2D interaction diagram of FP-3 and P3 (B) 2D interaction diagram of FP-3 and P4.

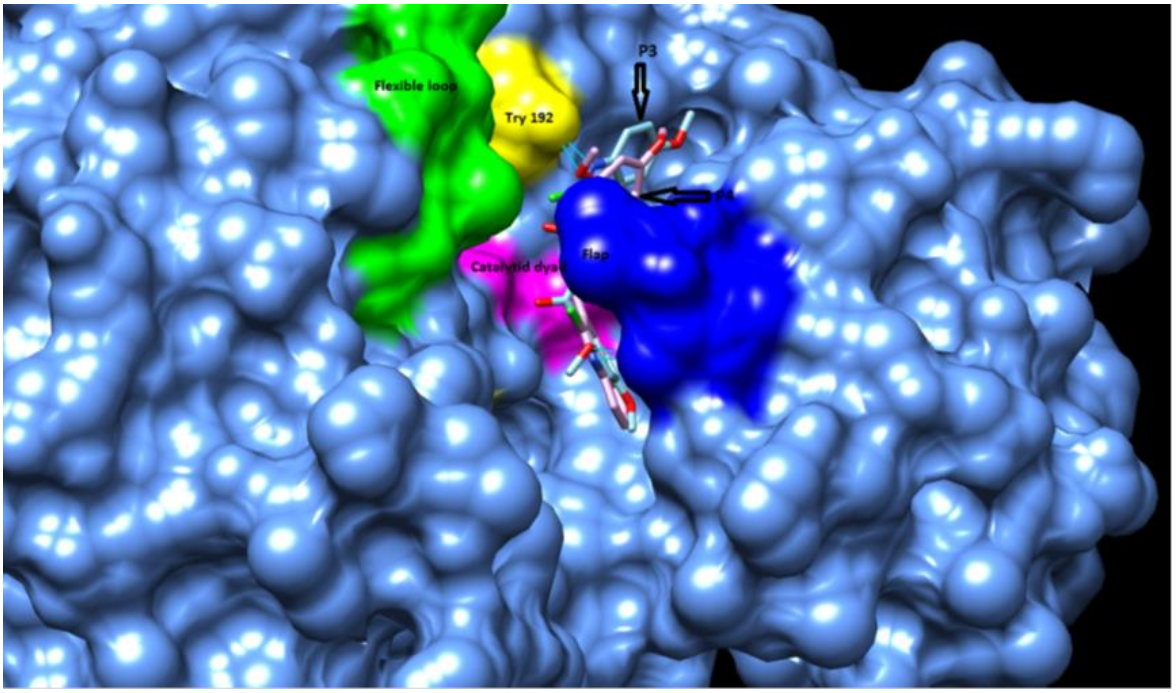


Figure 4.16: 3D binding poses and interactions of P3 and P4 in relation to various sub sites of Plm-II binding cavity

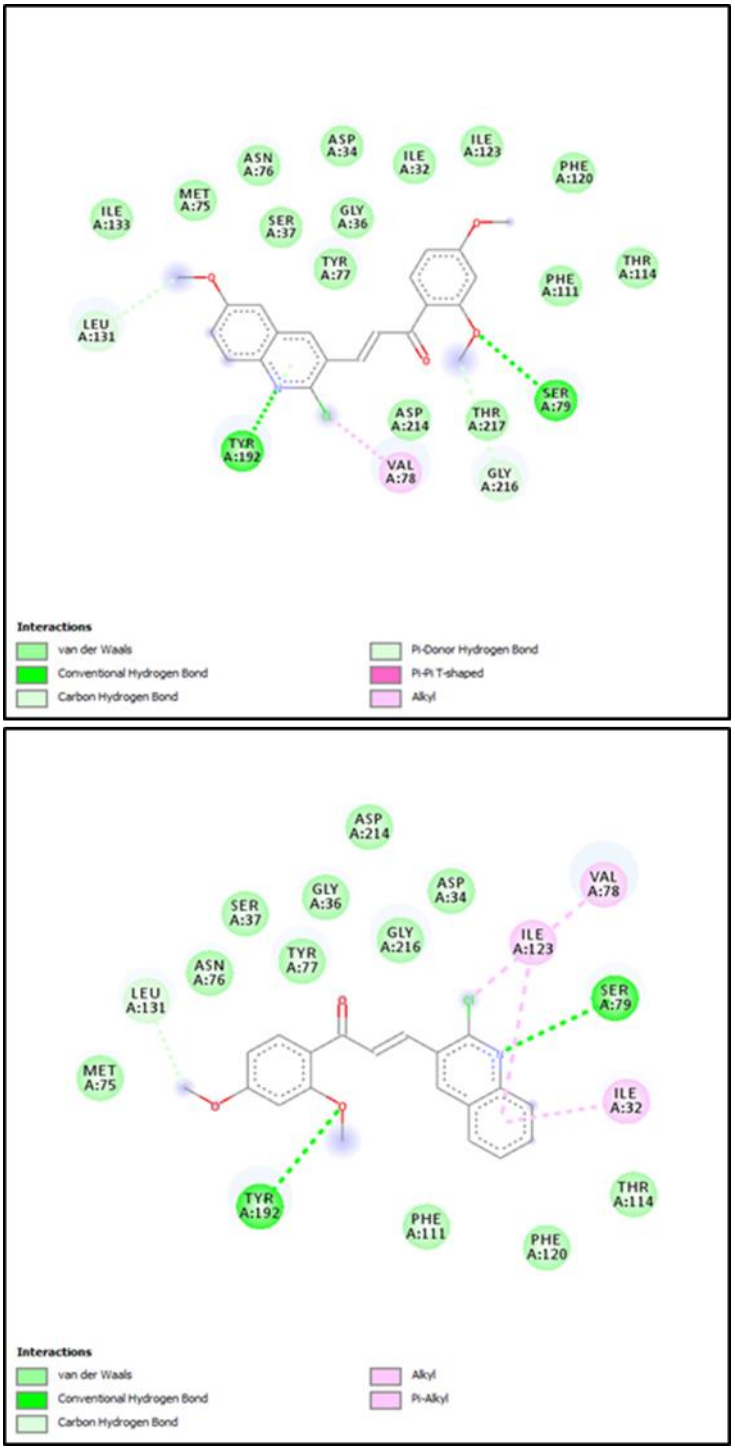


Figure 4.17: (A) 2D interaction diagram of Plm-II and P3 (B) 2D interaction diagram of Plm-II and P4.

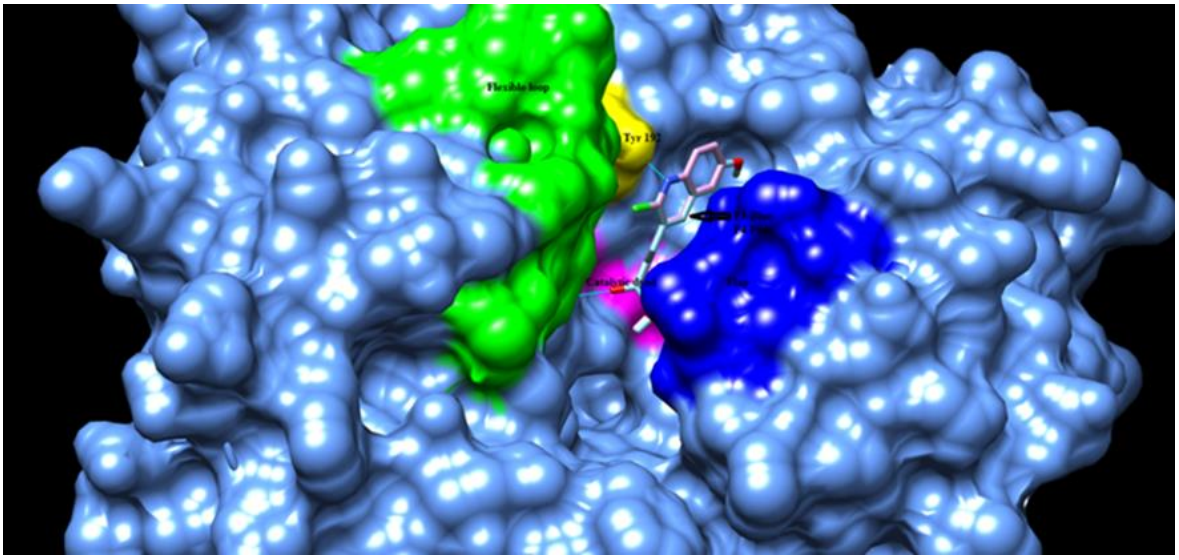


Figure 4.18: 3D binding poses and interaction of P3 and P4 in relation to various sub sites of Plm-IV binding cavity.

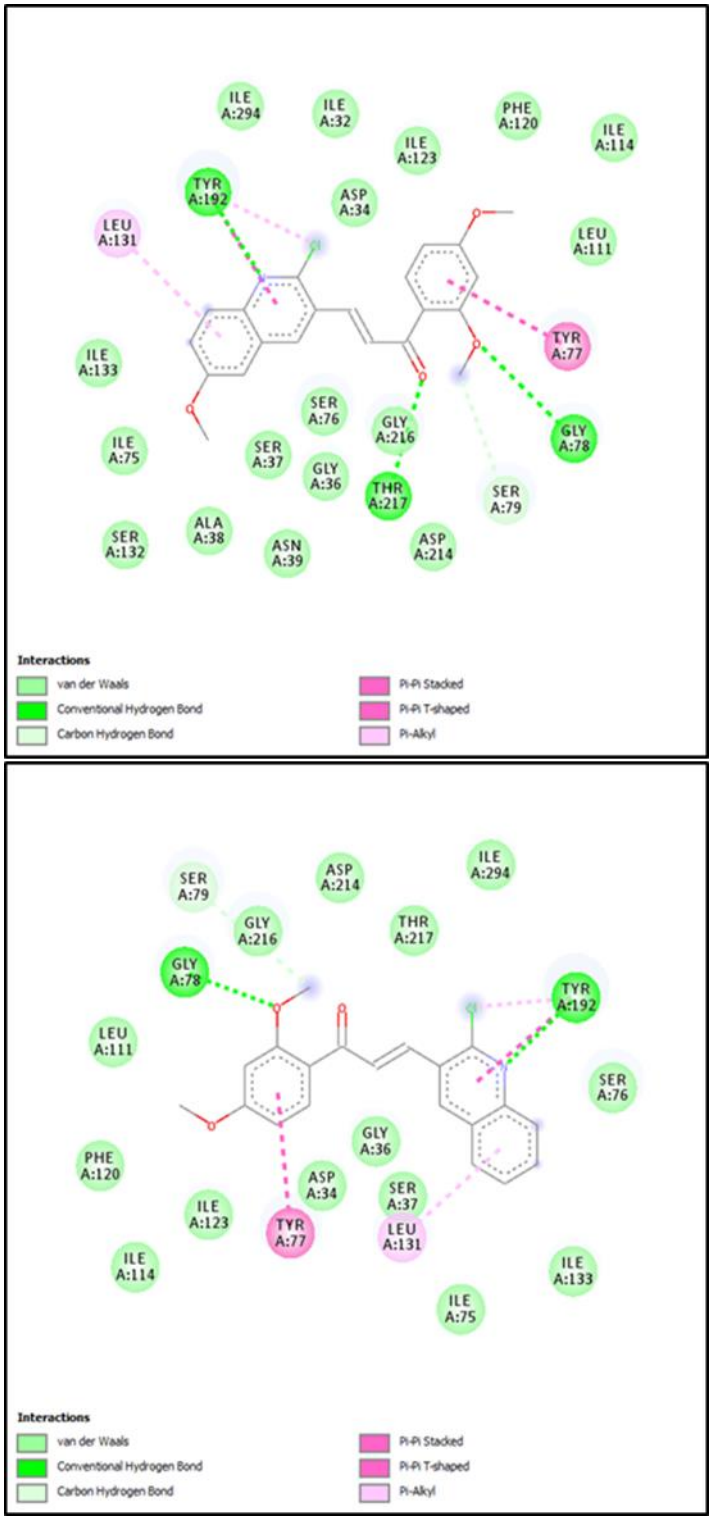


Figure 4.19: (A) 2D interaction diagram of Plm-IV and P3 (B) 2D interaction diagram of Plm-IV and P4.

4.7 Molecular Dynamics Simulation Studies of P3 and P4 Complexes of FP-2, FP-3, Plm-II, and Plm-IV.

4.7.1 System stability

After approximately 10ns, the RMSD trajectories converged and fluctuations did not exceed 3.0Å for either system for the duration of the simulation (Figure 4.20 – 4.22). The average RMSD values for the C-α backbone atoms of FP-2, FP-3, Plm-II and Plm-IV in complex with P3 were 1.481, 1.702, 2.141 and 2.277Å respectively, while that of FP-2, FP-3, Plm-II and Plm-IV in complex with P4 were 1.700, 1.565, 1.602 and 2.010Å respectively. For the C-α Rg, the falcipains complexes showed similar pattern (Figure 4.21, A and B). The average Rg of P3 and P4 are 18.446 and 18.474 Å respectively for FP-3 and 18.278 Å for both P3 and P4 FP-2 complexes. The average Rg displayed by P3 in Plm-II and Plm-IV system are 20.642, and 19.982 Å respectively and that of P4 in Plm-II and Plm-IV system are 20.594 and 20.049. The two systems showed fluctuation in Rg values from the beginning of the simulation but, stabilize and decreased after about 10ns (Figure 4.21, C and D).

The RMSF plots of the falcipains-ligand complexes are similar also (Figure 4.22; A and B). The region showing the highest fluctuation are residues 1-20 representing the N-terminal insertion and the second insertion consisting of residues 175-200 (β-hairpin), been the most flexible regions. From the RMSF plot no fluctuations are observed in the active site (Gln36/45, Cys42/51, His174/183, and Asn204/213 for FP2 and FP3 respectively) thus, the protein–ligand complex system remained stable during the simulation period. The average RMSF of the N-terminus insertion and β-hairpin for the FP2-P3 and FP3-P3 complexes are 11.06 Å, 9.21 Å and 6.95 Å, 7.26 Å respectively, while that of FP2-P4 and FP3-P4 complexes are 7.96 Å, 11.53 Å and 13.39 Å, 7.14 Å respectively.

For the plasmepsins systems (Figure 4.22, C and D), the amino acid residues 225-300 show a higher fluctuation relative to other residues. The region represents the L3 loop (231-244) and L4 loop (277-283) Plm-II numbering, where the flexible loop is situated. There was no significant movement of the flap as the compounds remained embraced by the flap at the active site cavity. The overall average RMSF for Plm-II bound to P3 and P4 are 7.652 Å and 7.138 Å respectively. And, Plm-IV complexes showed an average RMSF of 5.860 Å and 9.111 Å for P3 and P4 respectively. Compound P3 have less residual fluctuation as compared to P4.

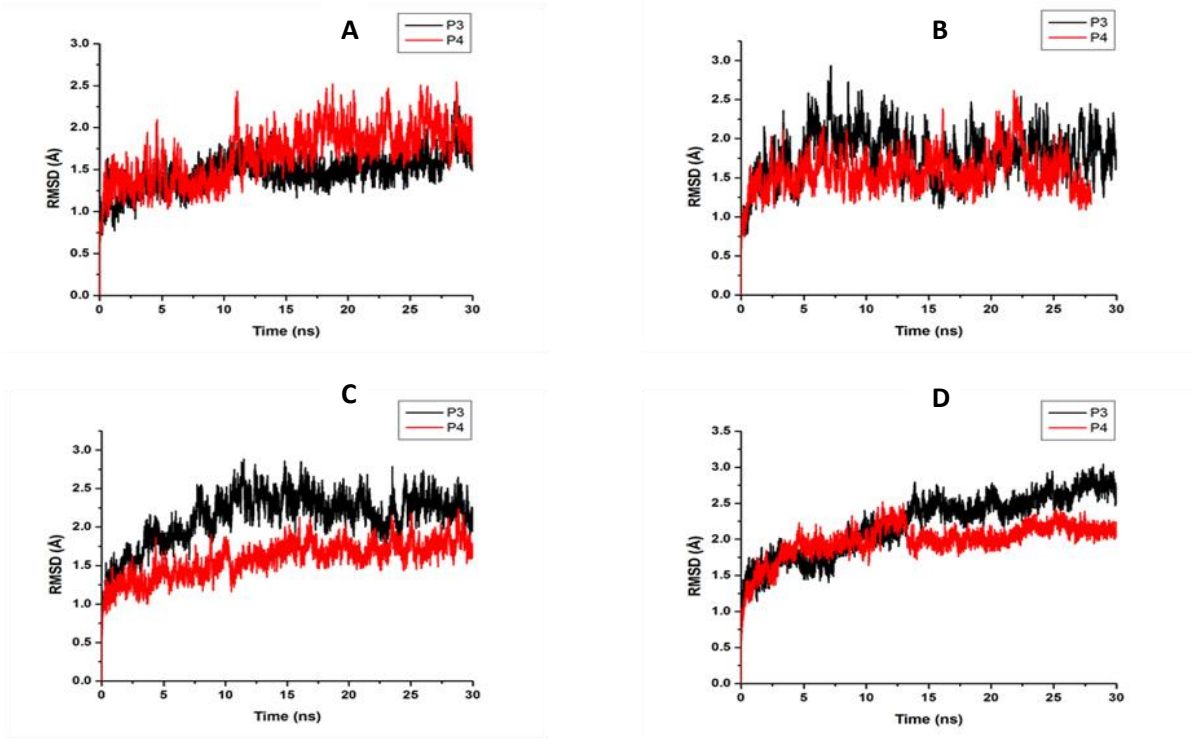


Figure 4.20: RMSD plot of FP-2 (A); FP-3 (B); Plm-II (C); Plm-IV (D) bound to compound P3 and P4 during a 30ns simulation.

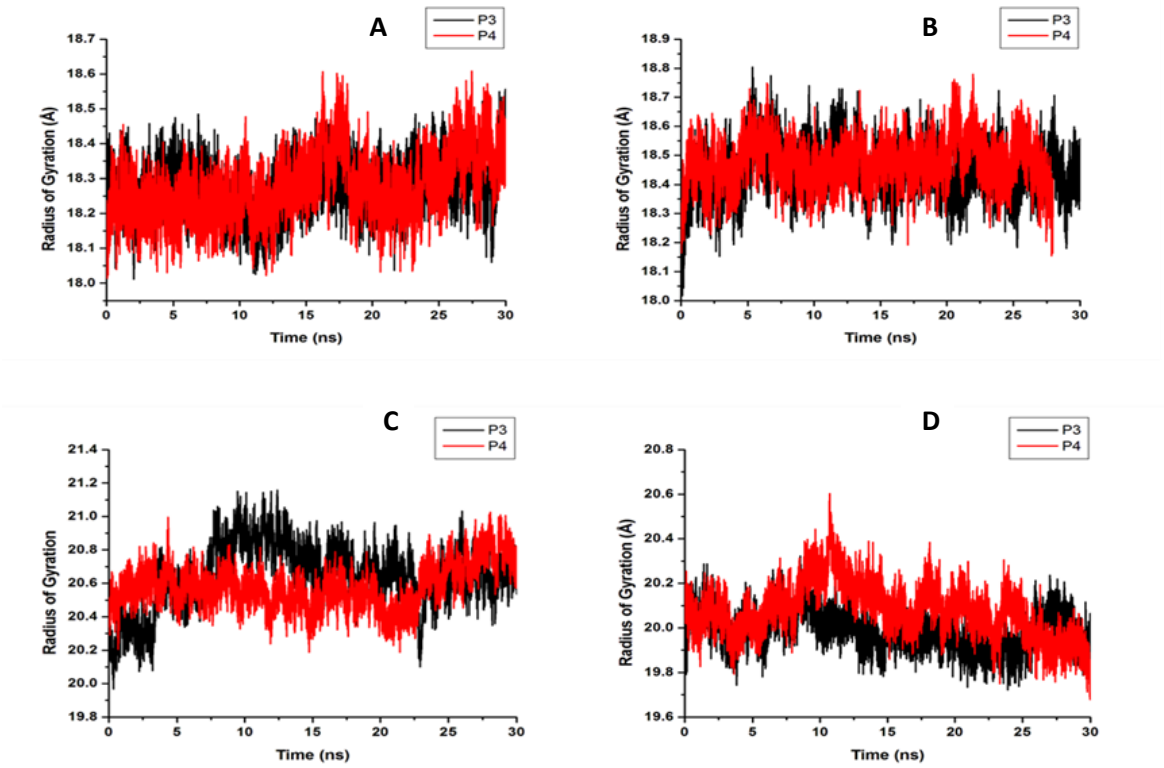


Figure 4.21 : C-α RoG plot of FP-2 (A), FP-3(B), Plm-II (C) and, Plm-IV (D) both in complex with P3 and P4.

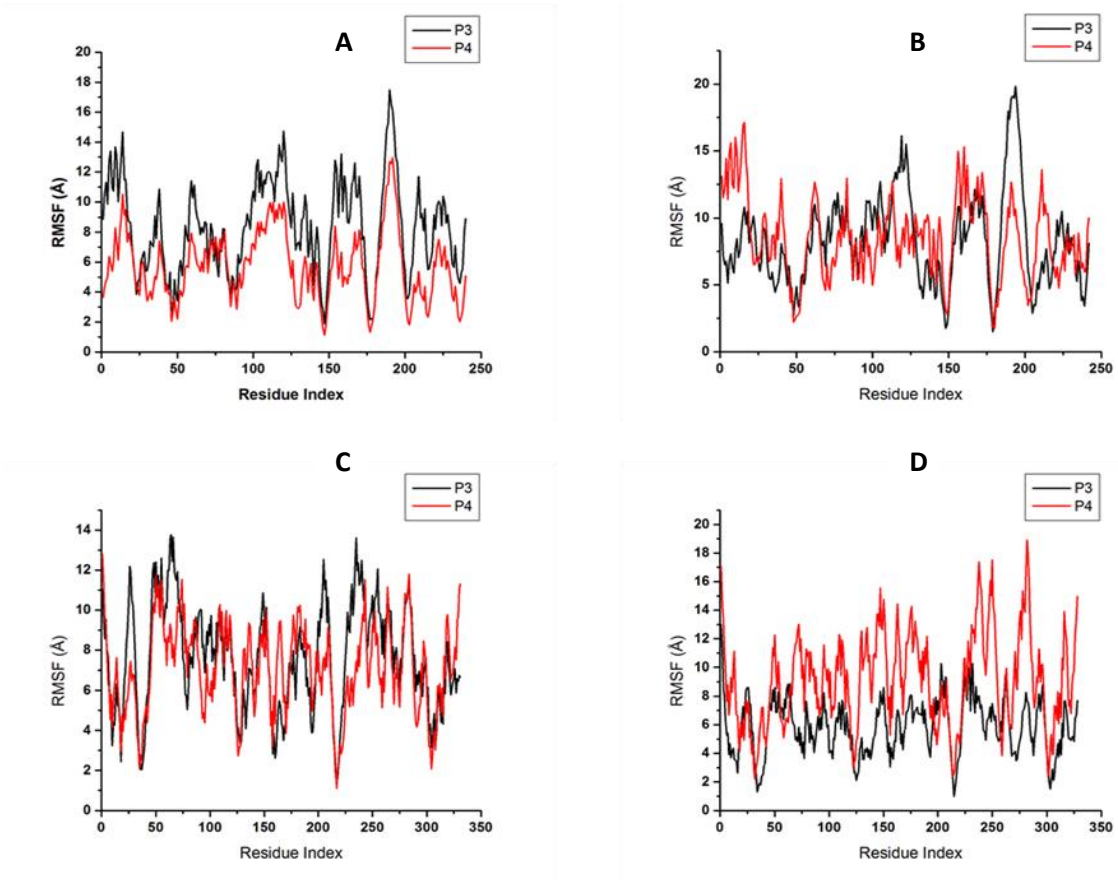


Figure 4.22 : C-α RMSF of FP-2 (A), FP-3(B), Plm-II (C) and, Plm-IV (D) both in complex with P3 and P4.

4.7.2 Per-residue energy decomposition analysis

Per residue energy decomposition plots of each protein ligand complex studied are presented on Figure 4.22 – 4.25. Most of the amino acid residues surrounding the ligand in each complex studied showed favorable binding interaction with the ligand.

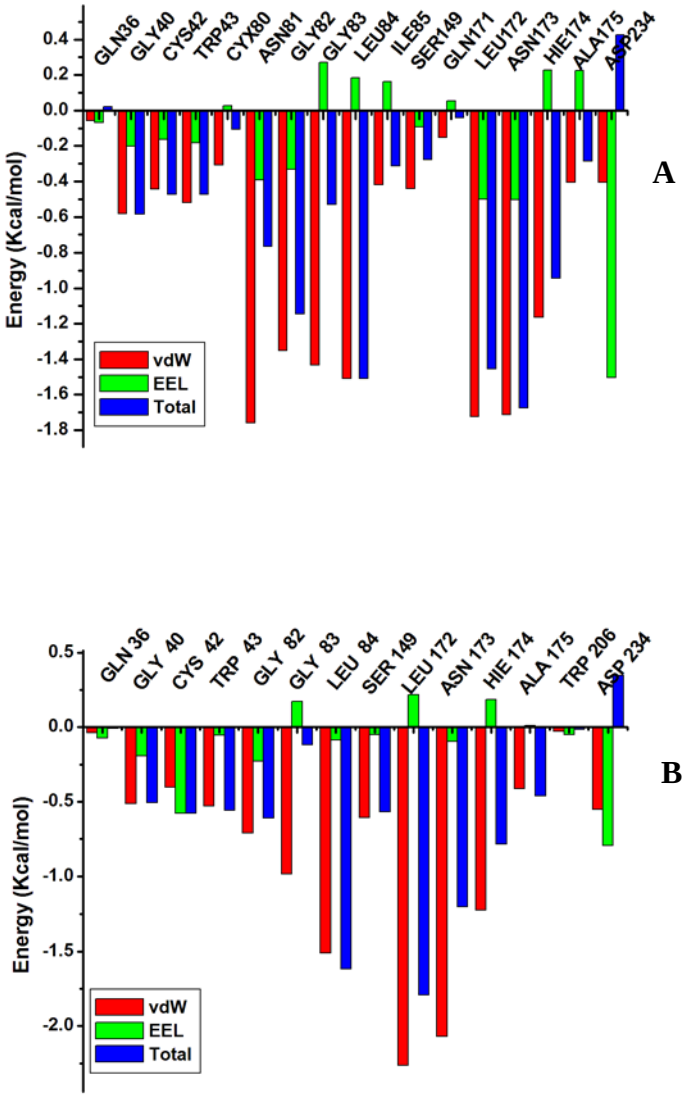


Figure 4.23 : Per residue energy decomposition plot of (A) FP-2 in complex with P3 and (B) FP-2 in complex with P4

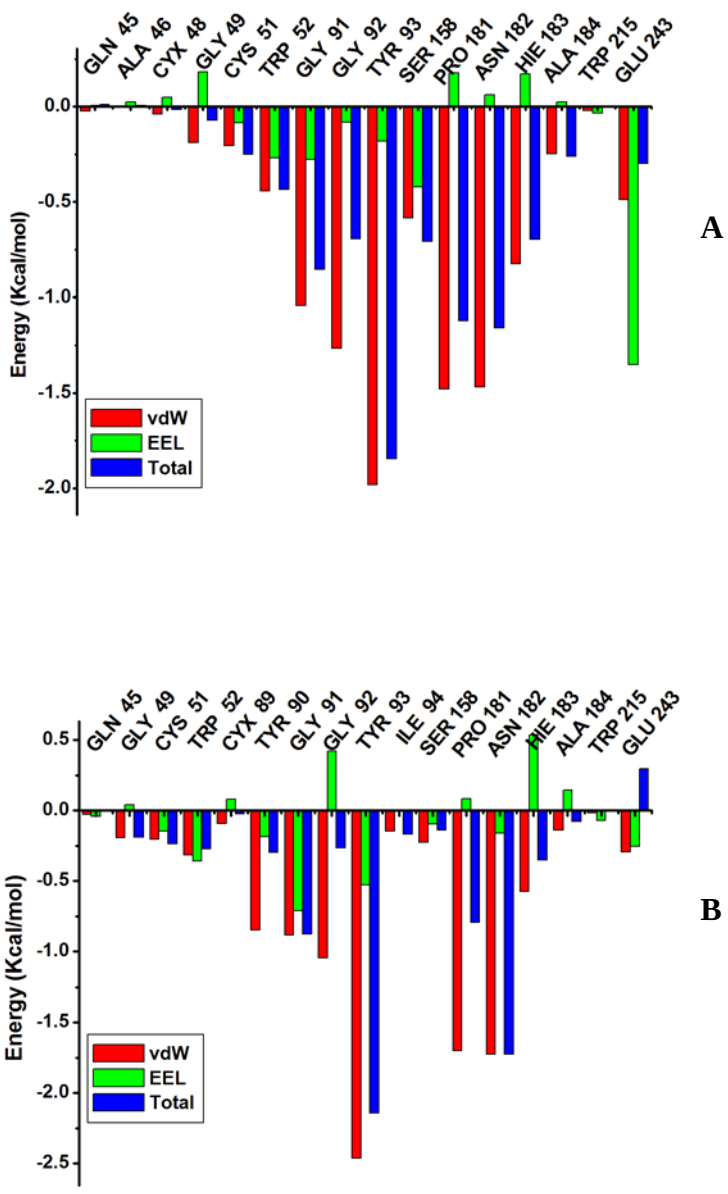


Figure 4.24: Per residue energy decomposition plot of (A) FP-3 in complex with P3 and (B) FP-3 in complex with P4

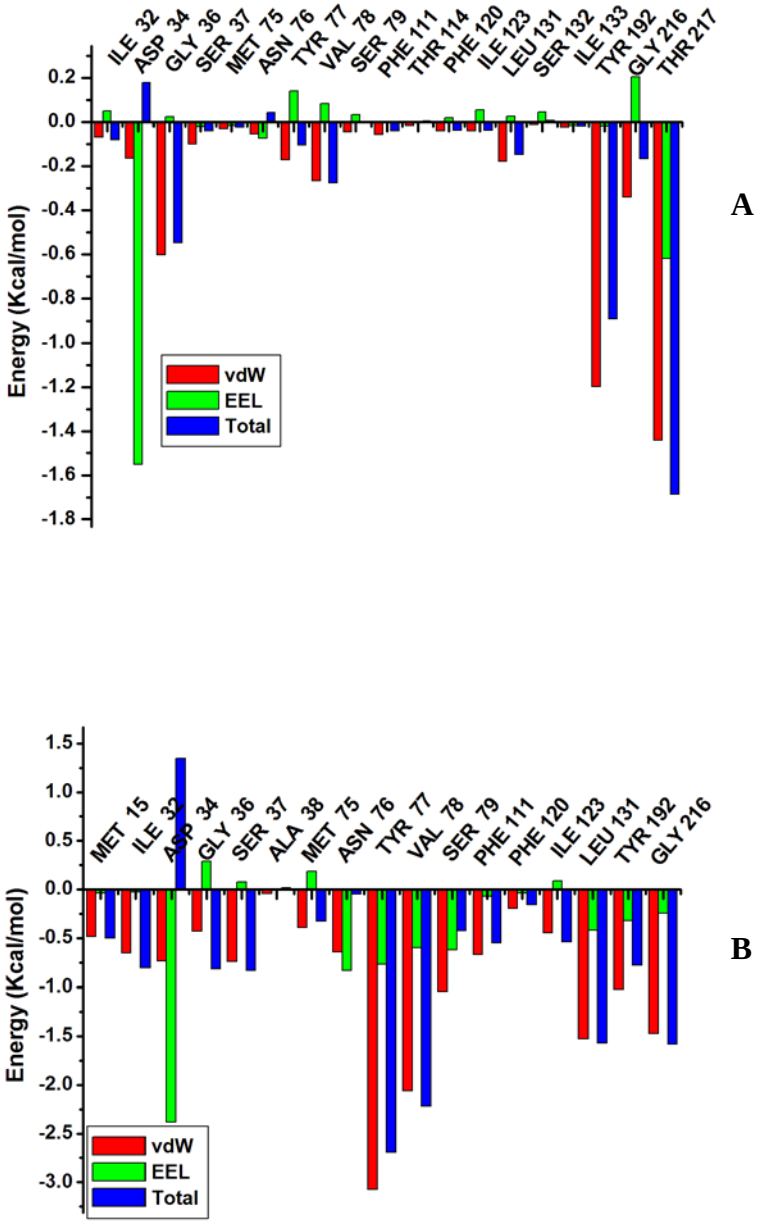


Figure 4.25: Per residue decomposition plot of (A) Plm-II in complex with P3 and (B) Plm-II in complex with P4.

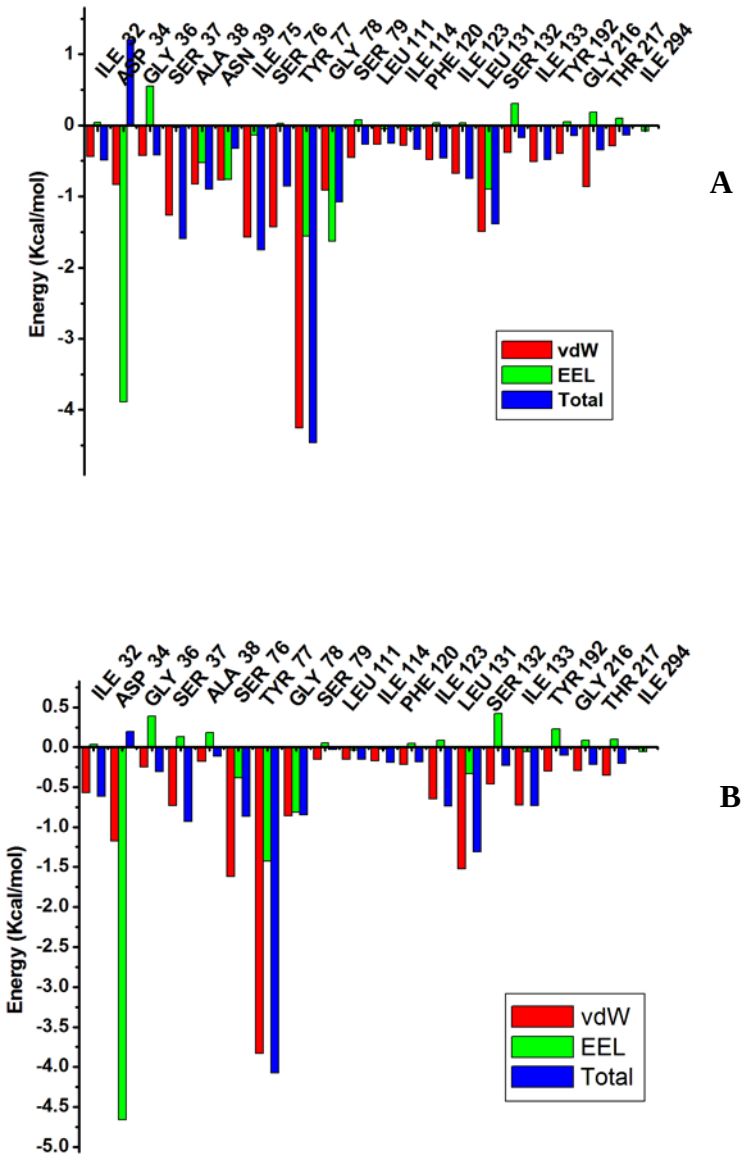


Figure 4.26 : Per residue energy decomposition plot of (A) Plm-IV in complex with P3 and (B) Plm-IV in complex with P4.

4.7.3 Binding free energy (BFE) analysis of P3 and P4 in complex with FP-2, FP-3, Plm-II and Plm-IV

The total binding free energies of all the systems studied are presented on Table 4.14. Plasmepsin complexes showed the most favorable binding energies. With the exception of Plm-II complexes, P3 complexes with all the enzymes have lower binding energies compared to P4 complexes. Van der Waals interactions contribute most favorably to the binding free energy in all the systems.

Table 4.14: Binding free energy analysis of P3 and P4 in complex with FP-2, FP-3, Plm-II and Plm-IV

	Energy Components (kcal/mol)				
Compound	**ΔE_{vdW}**	**ΔE_{elec}**	**ΔG_{gas}**	**ΔG_{solv}**	**ΔG_{bind}**
P3 in complex with FP-2	-34.4215 ±3.9523	-3.0563 ±3.6522	-37.4777 ±4.8821	13.3121 ±3.6631	-24.1657 ±3.6475
P4 in complex with FP-2	-31.9415 ±4.3850	-2.8439 ±3.2947	-34.7855 ± 5.8335	12.0119 ± 3.2910	-22.7735 ± 3.5486
P3 in complex with FP-3	-30.0052 ±4.2458	-3.1560 ± 3.0240	-33.1612 ±5.8761	10.7847 ± 3.1163	-22.3765 ±3.9726
P4 in complex with FP-3	-25.9544 ±4.1852	-0.9678 ± 3.3010	-26.9222 ± 6.0429	9.5954 ± 3.3199	-17.3268 ± 3.4926
P3 in complex with Plm-II	-31.2919 ±4.6702	-16.3381 ±5.5511	-47.6300 ±6.7991	23.3292 ± 5.1865	-24.3008 ±4.2644
P4 in complex with Plm-II	-40.1709 ± 6.3652	-5.0930 ±4.8214	-45.2639 ± 9.5492	13.2342 ±4.5107	-32.0296 ±6.8397
P3 in complex with Plm-IV	-44.2400 ± 2.5772	-18.9574 ± 4.9074	-63.1975 ± 5.2082	27.9581 ± 4.2710	-35.2393 ± 2.7171
P4 in complex with Plm-IV	-36.4033 ± 4.0001	-17.5173 ± 4.2052	-53.9206 ± 5.6791	25.0089 ± 3.7916	-28.9117 ± 4.1073

CHAPTER FIVE

5.0 DISCUSSIONS

5.1 Design of Substituted Chalcones

Novel malaria targets and drugs against such targets are urgently needed to combat the burden of malaria and provide potential solution to the alarming rise of ACTs resistance. Although chalcones have been identified as promising agents against malarial proteases, there was no conclusion on the structural requirement for good activity. The compounds designed in this study are based on features of some active compounds from previous studies, constituting various active chemical scaffolds. Seventeen chalcone derivatives were designed (Tables 4.1 – 4.3), the compounds were represented in six series that differed from each other by the substitution pattern on ring A. The choice of electron dense A ring chalcones for series: one, three and four as a focus for investigation is based on contradictory findings by Kumar *et al.* (2010) suggesting that contrary to previous report (Kumar *et al.,* 2010) linking electron rich B ring with good antimalarial activity, electron deficient B ring and electron dense A ring was found to exhibit potent antimalarial activity. Therefore, to verify these claims substituents on some of the active compounds from Liu *et al* (2001) findings having electron dense B ring were reversed between the two aromatic rings (Table 4.1, 4.2, and 4.3) leading to design of series one, three, four and five. On the other hand, hybrid design was applied in the design of series two, where 2-chloro quinolinyl ring A scaffold, 2,3,4 trimethoxy and, 2,4 dimethoxy ring B scaffold associated from previous studies (Li *et al.,* 1995; Liu *et al.,* 2001; Dominguez *et al.,* 2001; Shikha *et al.,* 2009) with potent antimalarial activity were merged to form a single chemical entity (Table 4.2).

P1, P2, P3, and P8 are new chalcone derivatives not reported in any literature or chemical data base while, P12, P16 and P22 were known compounds but, not previously evaluated for antimalarial activity (www.scifinder.com).

5.2 Theoretical Oral Bioavailability

Prediction of theoretical oral bioavailability is an important step in drug design process. This is to reduce the chances of drug failure at a later stage of the process due to poor pharmacokinetics. All the substituted chalcones designed have passed the criteria put forward by Lipinski *et al.* (2009) for a chemical compound to be orally bioavailable (Table 4.4). The relatively small molecular weight of chalcones coupled with the ease of substitution on the two aromatic rings bestowed on them drug-like properties (Nowakowska, 2007).

5.3 Synthesis and Characterization

5.3.1 Synthesis and characterization of 2,3,4–trimethoxy benzaldehyde Chalcones (P1, P2 and P13)

The procedure using Claisen-Schmidt condensation furnishes good yields; 57%, 78%, and 65% for P1, P3 and P13 respectively (Table 4.5). Completion of the reaction was established by the disappearance of spots due to reactants on the thin layer chromatogram and appearance of single spot for each of the products; P1, P2 and P13 appeared as yellow viscous oil, orange crystal, and yellow gummy solid, respectively. This agrees with the appearance of natural chalcones and other chalcone derivatives reported in the literature (Li *et al.*, 1995; Sinha *et al.*, 2013). The sharp melting point (Table 4.5) observed with the three compounds suggest that the compounds have high degree of purity (Vogel, 1956).

The FT-IR data (Appendices 12 and 20) indicates presence of carbonyl (C=O), ether (C-O-C), aromatic (=C-H), olefinic (=C-H), and aliphatic (-C-H) functional groups in both P1, P2, and P3, as evidenced by the appearance of prominent bands at 1640 cm^{-1} (C=O

stretching vibrations), 1260 and 1095 cm^{-1} (C-O-C stretching vibrations), 3040 cm^{-1} (aromatic C_{sp2}-H stretching vibrations), 3008 cm^{-1} (Olefinic C_{sp2}-H stretching vibrations), 2990 cm^{1} (Aliphatic C_{sp3}-H stretching vibrations), 1580 cm^{-1} (C=C stretching vibrations) for both compounds. The olefinic peak observed in the region 2995-3008 cm^{-1} is evidence that the chalcones have been formed. Also, the characteristic α, β-unsaturated carbonyl group of the chalcones was confirmed by the prominent band in between 1625-1650 cm-$^{1.}$ Additionally, the methoxy function is evidence by coupled strong vibration at 1260 and 1095 cm^{-1} for C-O-C stretching vibrations (Kumar *et al.*, 2010).

The ^{1}H NMR, ^{13}C NMR and 2D NMR spectra was used to elucidate the structures of P1, P2, and P3 (Table 4.6). A noticeable change from the starting materials is the disappearance of the aldehyde and methyl ketone chemical shifts, which appear as singlet around 9.89-10.30 ppm and 2.50 ppm respectively. These protons are replaced by the α,β-unsaturated ketone linker protons observed as doublets in the region of 7.38 – 7.42 ppm (H- α) and 7.86 - 8.00 ppm (H- β) with coupling constants of 15.6-16.0 Hz. It is evident from these coupling constants that the products formed are predominantly the *trans*-isomers (E-form). The configuration of the Z isomer is unstable due to the strong steric effects between the carbonyl group and the A-ring (Gomes *et al.*, 2011). The other noticeable observations in the H NMR are the methoxy proton as singlet at the region of 3.83 – 4.25 ppm. The rest of the protons appear in their expected regions with their usual coupling constants (Table 4.6 and, Appendices 13 and 21).

Additional support for the structures of P1, P2, and P3 comes from the ^{13}C NMR spectra (Table 4.6 and, Appendices 14 and 22), where the carbonyl carbon (C=O) of the α,β-unsaturated ketone linker is observed in the region 191- 192 ppm, compared to the aldehyde carbonyl group (C=O) at 195 ppm and methyl ketone carbonyl group (C=O) which appears in the region 179 ppm. The α and β- carbon atoms with respect to the

carbonyl group give rise to characteristic signals in between δ 123.8-126.6 ppm and δ 137.6-141.9 ppm respectively. The olefinic carbons (α- and β- carbon atoms) are evidence that the chalcone have been formed. As seen in Table 4.6 and, Appendices 14 and 22, the positions of all C atoms in P1, P2, and P3 have been assigned. The nature of carbon atoms (CH_3- or –CH) for P1 and P2 was established by means of the Distortionless Enhancement by Polarization Transfer (DEPT) spectroscopy (Appendix 15 for P1). The DEPT spectra (DEPT 135), showed signals due to OCH_3 and CH above the baseline and the methoxy protons appeared up field (Crews *et al.,* 1998). The two-dimensional (COSY, HSQC and HMBC) NMR spectroscopic data confirm the tentative structural assignment that was made using ^{1}H and ^{13}C NMR for P1 and P2 (new derivatives). COSY correlates two identical ^{1}H NMR spectra; whereas, HSQC and HMBC correlates ^{1}H NMR spectrum and ^{13}C NMR spectrum of the same molecule at short range and long-range distances respectively (Crews *et al.,* 1998). The connection between each carbon atom and the attached hydrogen atom (s) was unambiguously established using HSQC and long-range correlation between protons and carbon was established using HMBC, which led to linking of sub-structural fragments (Table 4.6, Appendix 17). Protons at C2 - C3, C5‘- C6‘and C5”- C6” showed COSY correlation for both P1 and P2 (Appendix 16).

Mass spectral (MS) data further confirmed the structural assignments using the NMR. The MS data of the compounds indicated the molecular ion peak (m/z) corresponding to their molecular weight. The molecular ion peaks $(M+1)^{+}$ are 389 and, 368 for P1 and, P13 respectively (Appendices 19 and 23).

5.3.2 Synthesis and characterization of 3-quinolinyl benzaldehyde Chalcones (P3, P4 and P8)

The percentage yield for P3, P4 and P8 are 57%, 78%, and 65% respectively (Table 4.5). Both compounds precipitate as mixtures and were separated and purified using anti-solvent recrystallization. Completion of the reaction was established by the disappearance

of spots due to reactants on the thin layer chromatogram and appearance of a new spot due to product. P3 appeared as light-yellow crystal, while P4 and P8 are Yellow cotton-like. The sharp melting point (Table 4.5) observed with the three compounds suggest that the compounds have high degree of purity (Vogel, 1956).

The FT-IR data (Appendices 24, 31 and 39) were as described in section 5.3.1, with prominent carbonyl peak C=O appearing at 1613 cm^{-1} and olefinic =C-H vibration at 2983 cm^{-1}. Sharp strong coupled absorption of C-O-C stretching also appeared at 1236 and 1017 cm^{-1}.

The ^{1}H NMR, ^{13}C NMR and 2D-NMR spectra confirmed the structures of P3, P4, and P8 (Table 4.7 and Appendices 25, 32 and 40). In addition to the characteristics α,β-unsaturated ketone linker protons observed as doublets in the region of 6.81 – 7.72 ppm (H- α) and 7.84 - 8.03 ppm (H- β) with coupling constants of 15.9-20 Hz (*trans*-isomers) and the methoxy protons as singlet at the region of 3.38 – 4.09 ppm, the rest of the protons appear in their expected regions with their usual coupling constants. A noticeable observation is the appearance of C4" and C5" protons up-field for P3 and P8. The two protons of P3 are at 4.93 and 4.79 ppm for C4" and C5" respectively. And, for P8 the C4" and C5" protons are at 4.97 and 4.86 ppm respectively. The shift of delta value could be explained by the strong influence of electron donating methoxy group at C6" position causing a shielding effect.

Additional support for the structures of P3, P4, and P8 also comes from the ^{13}C NMR spectra (Table 4.7 and Appendices 26, 33 and 41), where the carbonyl carbon (C=O) of the α,β-unsaturated ketone linker is observed in the region 196.42, 189.55, 197.91 ppm for P3, P4, and P8 respectively. Also, the α and β- carbon atoms with respect to the carbonyl group give rise to characteristic signals in between δ 104.86-131.50 ppm and δ 135.08-136.24 ppm respectively.

The positions of all carbon atoms in P3, P4, and P8 have been assigned (Table 4.7, Appendices 26, 33, and 41). The spectroscopic differences between P4 devoid of methoxy group at C6" and P3, P8 with a methoxy group at the C6" position was noteworthy. Indeed, the presence of the methoxy group had strongly influenced both the ^{1}H NMR, and ^{13}C NMR. The nature of carbon atoms (CH_3- or –CH) was established by means of the Distortionless Enhancement by Polarization Transfer (DEPT) spectroscopy as in section 5.3.1 (Appendices 27, 34 and 42). The two-dimensional (COSY, HSQC and HMBC) NMR spectroscopic data confirmed the tentative structural assignment that was made using ^{1}H and ^{13}C NMR for both compounds (Table 4.7). The connection between each carbon atom and the attached hydrogen atom (atoms) was unambiguously established using HSQC and long-range correlation between protons and carbon was established using HMBC, which led to linking of sub-structural fragments (Table 4.7 and Appendices 29, 30, 36, 37, 44 and 45). COSY correlation was observed on protons at C3'–C5', C5'- C6', C4"- C5"and C7"- C8" for P3 (Appendix 28), C5'- C6', C4"- C5" and C7"- C8" for P8 (Appendix 43) and, C2'–C3', C5'- C6', C5"- C6", C6"- C7" and C7"- C8" for P4 (Appendix 35).

5.3.3 Synthesis and characterization of 2,4–dimethoxy benzaldehyde Chalcones (P11, P12 and P17)

The percentage yield for P11, P12 and P17 are 87%, 83.93%, and 37.50% respectively (Table 4.5). Both compounds were recrystallized using ethanol. Completion of the reaction was established by the disappearance of spots due to reactants on the thin layer chromatogram and appearance of a new spot due to product. P11, P12 and P17 appeared as light-yellow solid, yellow wax-like solid and yellow crystals respectively. The sharp melting point (Table 4.5) observed with the three compounds suggest that the compounds have high degree of purity (Vogel, 1956).

The FT-IR data (Appendices 46, 53 and 57) were as described in section 5.3.1 with prominent carbonyl peak C=O appearing at 1647 cm^{-1} and olefinic =C-H vibration at 3004 cm^{-1}. Sharp strong coupled absorption of C-O-C stretching also appeared at 1207 and 1013 cm^{-1}.

The ^{1}H NMR, ^{13}C NMR and 2D-NMR (P11 only) spectra confirmed the structures of P11, P12 and P17 (Table 4.8). The characteristics α,β-unsaturated ketone linker protons as doublets were also observed in the region of 7.42 – 7.93 ppm (H- α) and 8.04 - 8.46 ppm (H- β) with coupling constants of 14-16 Hz (*trans*-isomers) and the methoxy protons as singlet at the region of 3.81 – 4.43 ppm, the rest of the protons appear in their expected regions with their usual coupling constants (Table 4.8 and, Appendices 47, 54 and 58). For P12 with un-substituted ring A (acetophenone ring) the protons at C2‘and C6‘appeared at the same chemical environment of 7.98 ppm and those at C3‘and C5‘are also on the same environment of 7.54 ppm (Table 4.8 and, Appendices 47, 54 and 58).

Furthermore, the ^{13}C NMR spectra (Table 4.8 and, Appendices 48, 55 and 61) of the P11, P12 and P17 showed the carbonyl carbon (C=O) of the α,β- unsaturated ketone linker in the characteristic region of 193.28, 191.12, 191.47 ppm respectively. Also, the α and β-carbon atoms with respect to the carbonyl group give rise to characteristic signals in between δ 124.15 - 128.36 ppm and δ 138.84 - 142.55 ppm respectively.

Here also, the positions of all C atoms in P11, P12 and P17 have been assigned as shown on Table 4.8 and, Appendices 48, 55 and 61. P11 and P12 with no electron density on the A ring have similar ^{1} H NMR and ^{13} C NMR values compared to P17 having electron-rich ring A (Table 4.8 and, Appendices 48, 55 and 61). Because the compounds are not new derivatives no 2D-NMR experiment was performed. The ^{1} H NMR and ^{13} C NMR values of P11, P12 and P17 agree with what is reported in the literature (Li *et al.,* 1995; Liu *et al.*, 2001; Bandgar *et al.*, 2010).

The mass spectral data of the compounds indicated the molecular ion peak (m/z) corresponding to their molecular weight. The molecular ion peaks $(M+1)^+$ are 269 and 359 for P12 and P17 respectively (Appendices 56 and 62).

5.3.4 Synthesis and characterization of 4–methoxy benzaldehyde Chalcones (P15, P16, P23 and P25)

The percentage yield for P15, P16, P23 and P25 are 36.87%, 30.00%, 95.50% and 93.40% respectively (Table 4.5). Completion of the reaction was established by the disappearance of spots due to reactants on the thin layer chromatogram and appearance of a new spot due to product. P15 appeared as pale-yellow crystals, P25 as yellow wax while, P16 and P23 as yellow crystals. The sharp melting point (Table 4.5) observed with the three compounds suggest that the compounds have high degree of purity (Vogel, 1956).

The FT-IR data (Appendices 63 and 66) were as described in section 5.3.1, with prominent carbonyl peak C=O appearing at 1572 cm^{-1} and olefinic =C-H vibration at 2952 cm^{-1}. Sharp strong coupled absorption of C-O-C stretching also appeared at 1285 and 1025 $cm^{-1.}$

The ^{1}H NMR and ^{13}C NMR spectra confirmed the structures of P15, P16, P23 (Table 4.9) and P25 (Table 4.10). The characteristics α,β-unsaturated ketone linker protons as doublets were observed in the region of 6.31 – 7.52 ppm (H- α) and 6.59 – 8.04 ppm (H- β) with coupling constants of 15.5-16 Hz (trans- isomers) and the methoxy protons as singlet in the region of 2.77 – 4.35 ppm, the rest of the protons appear in their expected regions with their usual coupling constants (Table 4.10 and Appendices 64, 67, 71 and 75). Furthermore, ^{13}C NMR spectra (Table 4.9 and, Appendices 65, 69, and 73) of the P15, P16, P23 and P25 (Table 4.10, Appendix 76) showed the carbonyl carbon (C=O) of the α,β- unsaturated ketone linker in the characteristic region of 189.81, 189.96, 191.31 and 192.60 ppm respectively. Also, the α and β- carbon atoms with respect to the carbonyl

group give rise to characteristic signals in between δ 119.24 - 124.61 ppm and δ 141.23 - 146.71 ppm respectively.

Here also, the positions of all carbon atoms in P15, P16, P23 and P25 have been assigned as shown on Table 4.9 and, Appendices 65, 69, 73 and 76. P15 and P23 with electron density on the A ring have similar ^{1}H NMR and ^{13}C NMR values as compared to P16 having no electron density on ring A. Since the compounds are not new derivatives no 2D-NMR experiment was performed. The ^{1}H NMR and ^{13}C NMR of P15, P16, P23 and P25 agree with what is reported in the literature (Li *et al.*, 1995; Mohammad *et al.,* 2010).

The mass spectral data of the compounds indicated the molecular ion peak (m/z) corresponding to their molecular weight. The molecular ion peaks $(M+1)^{+}$ are 299, 239 and 329 for P15, P16 and P23 respectively (Appendices 63, 70 and 74).

5.3.5 Synthesis and characterization of un-substituted (benzaldehyde) Chalcones (P19 and P24)

The percentage yield for P19 and, P24 are 76.00% and 31.10% respectively (Table 4.5). Completion of the reaction was established by the disappearance of spots due to reactants on the thin layer chromatogram and appearance of a new spot due to product. P1 appeared as light-yellow powder while, P24 as yellow crystals. The sharp melting point (Table 4.5) observed with the three compounds suggest that the compounds have high degree of purity (Vogel, 1956).

The ^{1}H NMR and ^{13}C NMR spectra confirmed the structures of P19 and P24 (Table 4.10). The characteristics α,β- unsaturated ketone linker protons as doublets were observed in the region of 7.03 – 7.78 ppm (H- α) and 7.19 – 7.79 ppm (H- β) with coupling constants of 16 Hz (trans-isomers) and the methoxy protons as singlet in the region of 3.29 - 4.04 ppm, the rest of the protons appeared in their expected regions with their usual coupling constants (Table 4.10 and, Appendices 77 and 81).

^{13}C NMR spectra of P19 and P24 (Table 4.10 and, Appendices 79 and 82) showed the carbonyl carbon (C=O) of the α,β-unsaturated ketone linker in the characteristic region of 190.47 and, 190.80 ppm respectively. Also, the α and β- carbon atoms with respect to the carbonyl group give rise to characteristic signals in between δ 125.87-127.48 ppm and δ 142.07-142.98 ppm respectively. Also, the positions of all carbon atoms in P19 and P24 have been assigned as shown on Table 4.10 and, Appendices 79 and 82. Since the compounds are not new derivatives no 2D-NMR experiment was performed. ^{1}H NMR and ^{13}C NMR data agreed with Liu *et al.* (2001) values.

The mass spectral data of the compounds indicated the molecular ion peak (m/z) corresponding to their molecular weight. The molecular ion peaks $(M+1)^{+}$ are 269 and 299 for P19 and P24 respectively (Appendices 80 and 83).

5.3.6 Synthesis and characterization of 4-triflouromethyl benzaldehyde Chalcones (P21 and P22)

The percentage yield for P21 and, P22 are 58.63% and 97.01% respectively (Table 4.5). Completion of the reaction was established by the disappearance of spots due to reactants on the thin layer chromatogram and appearance of a new spot due to product. P21 and P22 appeared as light-yellow crystals. The sharp melting point (Table 4.5) observed with the three compounds suggest that the compounds have high degree of purity (Vogel, 1956).

The FT-IR data (Appendices 86 and 90) were as described in section 5.3.1, with prominent carbonyl peak C=O appearing at 1658 cm^{-1} and olefinic =C-H vibration at 3008 cm^{-1}.

The ^{1}H NMR and, ^{13}C NMR spectra confirmed the structures of P21 and P22 (Table 4.11). The characteristics α,β- unsaturated ketone linker protons as doublets were observed in the region of 7.55 – 7.60 ppm (H- α) and 7.77 – 7.80 ppm (H- β) with coupling constants of 14 - 17 Hz (*trans*-isomers) and the methoxy protons as singlet in the region of 3.89 – 4.04 ppm, the rest of the protons appeared in their expected regions with their usual coupling

constants (Table 4.11 and, Appendices 87 and 91). ^{13}C NMR spectra of P21 and P22 (Table 4.11 and, Appendices 88 and 92) showed the carbonyl carbon (C=O) of the α,β-unsaturated ketone linker in the characteristic region of 189.76 and 189.46 ppm respectively. Also, the α and β- carbon atoms with respect to the carbonyl group give rise to characteristic signals in between δ 123.73 - 124.75 ppm and δ 139.60 - 142.20 ppm respectively. The positions of all carbon atoms in P21 and 22 have been assigned as shown on Table 4.11 and, Appendices 88 and 92. Since the compounds are not new derivatives no 2D-NMR experiment was performed, and the NMR spectra agree with the literature (Liu *et al.*, 2001).

The mass spectral data of the P21 (Appendix 89) indicated the molecular ion peak (m/z) corresponding to its molecular weight (Table 4.4). The molecular ion peak $(M+1)^+$ is 337 (Appendix 89).

5.4 Antimalarial Studies

5.4.1 *In-vivo* antimalarial studies (Curative test)

Rane's test evaluates the curative capability of test compounds on established infection (Ryley and Peters, 1970). In the curative study the substituted chalcones did not eradicate *P. falciparum* parasite completely on four days treatment, but showed significant parasite suppressive effects. Nine of the compounds showed antimalarial potentials greater than standard drugs used in the study at certain dose (Figure 4.7, Appendix 1). In the first segment of the experiment P3, P4, P8 and P25 showed significant non-dose dependent parasitemia suppression with highest percentage inhibition of 73.9, 67.1, 77.6, and 72.3% respectively. At a dose of 25, 50, 100 and 25 mg for P3, P4, P8 and P25 suppressed the parasitemia better than chloroquine (57.5% inhibition) at a dose of 10 mg/kg, arthemeter (67% inhibition) at a dose of 1.8 mg. However, P2 showed significant suppression (90%, $p<0.05$) comparable to the most potent standard drug in this study; quinine (88.5%

suppression) at a dose of 100 mg/kg. Interestingly, there is a good representation of active compounds from the quinolinyl chalcones (P3, P4, and P8). Quinolones are established chemical scaffold in antimalarials (Sinha *et al.,* 2013). Several quinolinyl chalcones have been reported to possess *in vitro* anti-plasmodial activity (Li *et al.,* 1995; Liu *et al.,* 2001).

In the second segment of the study, with the exception of P13 and P19 all the compounds showed significant *in vivo* activity compared to the negative control. P12 had the most significant parasite suppression (89.44% at a dose of 100 mg) which is close to chloroquine (91.8% inhibition) at a dose of 25 mg/kg. *In vitro* antiplasmodial activity against W2 and D6 plasmodium parasite of P11 was reported by Li *et al.* (1995) where, it showed moderate activity of 3.8 µM (W2) and 3.4 µM (D6) compared to the control: chloroquine with 0.24 µM (W2) and 0,013 µM (D6). Though, *in vitro* results are not always correlated to *in vivo* studies. P17 and P21 were also reported to possessed good *in vitro* anti-plasmodial activity with IC_{50} value of 16.5µM and 5.9µM respectively and P15 reported to displayed modest activity (128 µM) (Liu *et al.,* 2001). However, from the literature P12, P16 and P22 were not evaluated for antimalarial activity (www.scifinder.com). Although they have a simple substitution, having unsubstituted ring B they were found to exhibit significant parasite suppression.

Overall, among the six series studied, chalcones with 2-Cl quinoline ring A were more promising. The most active in the series are P3 and P8 with 6”- OCH_3 substitution on the quinoline ring. Even though, P3 and P4 have di- methoxy substituted ring B and P8 have tri- methoxy substituted ring B, P3 and P8 were more active than P4, indicating the importance of the 6”-OCH_3 substitution. A chalcone with 6,7-dimethoxy quinolinyl ring A and 2,4- dichloro ring B have been reported as the most active compound among the derivatives studied (Dominguez *et al.*, 2001). Similarly, Shikha *et al.* (2009) reported 6-methoxy quinolinyl ring A and 2-bromo, 4-chloro ring B chalcones as the most

active in the series studied. Among the methoxy substituted benzaldehyde chalcones, 2,4-dimethoxy substitution yields more of the active compounds. Even the most active compound in this study; P12 has 2,4-dimethoxy ring B (acetophenone). P15 and P22 having 2,4- dimethoxy ring B but, with 4-methoxy and 4-trifluoromethyl substituted ring A respectively were very active. Triflouromethyl substituted chalcones were also reported to be active against plasmodium parasite *in vitro* (Li *et al.,* 2001; Liu *et al.,* 2009). However, P1 with more electron density on both rings (2,3,4- trimethoxy) exhibited low antiplasmodial activity. This is in contrast to reported good *in vitro* activity (2.1µM) of bis 2,4-dimethoxy chalcones (Liu *et al.,* 2001). From the above observation it seems that electronic factors are not the determinant factor for the antiplasmodial activity, steric factors might be playing more role as proposed by Liu *et al.* (2001).

Additionally, this study contradicts the previous findings on the importance of substitutions of B ring in determining the type of A ring substituents that would give optimum antimalarial activity (Liu *et al.,* 2001). It was reported that, 2,4-dichloro substitution of ring A in the tri-methoxy ring (B) chalcones gave rise to a very active compound (IC_{50} 5.4 uM), but the same substituent gave rise to less active compounds in other series of chalcones. Same scenario was observed with different series of ring A as evidence from the differences in activity of P11, P13 and P25. Thus, conformational and steric factors seem to be more important, which this study further evaluated using *in silico* methods.

5.4.2 *In-vitro* antimalarial study (β-hematin inhibition assay)

Since the chalcone derivatives showed promising antimalarial activity *in vivo,* the possible mechanism of the antimalarial activity was evaluated using the haem polymerization inhibition assay (HPIA). The HPIA has been proposed as possible routine *in vitro* assay for the detection of antimalarial activity. Studies have shown that the ability of the test

compounds to inhibit heme polymerization is directly related to the antimalarial activity (Egan *et al.,* 2000). Compounds that act through this mechanism are considered to have similar action with chloroquine (Rodrigues and Domínguez, 2007). With the exception of P12 and P17 all the compounds showed no activity (Table 4.12). Therefore, the compounds studied act through mechanism other than inhibiting haem polymerization. Thus, they can be considered as potential candidates for treatment of chloroquine resistance malaria. This is in line with the previous findings (Li *et al.,* 1994) and the observed *in silico* inhibitory activity of some compound. The positive standard (chloroquine) has shown appreciable inhibition (Table 4.12).

5.5 Computational Studies

5.5.1 Docking Studies

The docking procedures applied on all the four enzymes were well validated (Table 4.13). From the docking scores it can be deduced that the seventeen chalcones studied have better affinity for FP-2 and Plm-1V, although few have shown appreciable inhibition to all the proteases. Recent report has shown that poly-inhibition of falcipains and plasmepsins is desirable in potential antimalarial to ensure clinical efficacy and combat resistance due to their complementary role (Coombs *et al.,* 2001; Liu *et al.,* 2005; 2006; Sriwilaijaroen *et al.,* 2006). The two enzymes have high significance in hemoglobin degradation activity of *P. falciparum*. FP-2 represents more than 93% of the total cysteine protease activity in the food vacuole during the early and late trophozoite stages of the parasite (Marco and Coteron, 2012). FP-2 is also implicated for the conversion of pro-plasmepsin to plasmepsins (Bjelic *et al.,* 2011). Also, Plm IV is the only plasmepsin located in the food vacuole of *P. falciparum* which has orthologs in the other three *Plasmodium* species infecting humans (Dame *et al.,* 2003).

Indeed 3-quinolinyl ring A chalcones; P3, P4 and P8 were well represented among compounds with the high ranking, with low binding energy across all the enzymes. The quinoline ring is a common scaffold in established antimalarials. It may play a role in facilitating the localization of the drug within the acidic food vacuole of the parasite because of its basic properties (Liu *et al.,* 2001) in addition to the good binding on the active site of the enzymes. Several -3-formyl quinoline chalcones have been reported to possess antimalarial activity (Li *et al.,* 1995; Domínguez *et al., 2001*; Sriwilaijaroen *et al.,* 2006). P3 and P4 are congeners having a dimethoxy phenyl ring B, with P3 possessing additional methoxy group at position six of the quinoline ring (Figures 4.10 and 4.11). The 3D view of the compounds on Spartan (Figures 4.10 - 4.11) showed that they are nearly planar with a torsion angle of 179^0. This feature has been shown to be important in binding onto the long cleft of the active site of cysteine protease (Liu *et al.,* 2001). Thus, P3 and P4 fitted well onto the long cleft of FP-2 and FP-3 (Figures 4.12-4.15), extending from S1 subsite to S3. On the plasmepsins (Figures 4.16-4.19) the two compounds fit into the binding pocket, resting on the catalytic dyad and fully covered with the flap.

With regard to the binding interactions, it appears that the most contributing features of the ligand for receptor interaction are the quinoline ring, carbonyl group and, 2- methoxy group in FP-2 and FP-3 complexes. The hydrogen bonding between the catalytic Cys42 of FP-2 and the oxygen of the carbonyl and 2-methoxy group of ligands is replace by less strong hydrophobic interaction in FP-3 complexes. In which case the catalytic amino acid; Cys51 interact with the quinoline ring of the ligand through hydrophobic interactions. This might be one of the reasons why FP-2 binds more favorably with the ligands than FP-3. Since good binding is associated with higher number of strong interactions (Gallicchio *et al.,* 2011). This interaction between P3 and P4 cannot be interpreted as inhibition in wet experiment unless validated by the experiment. Also, for the plasmepsins (Figure 4.16 and

4.18) more of the active site residues interacted with the ligands. But, there was no interaction with the catalytic amino acid (Asp34 and Asp214), interaction is between the ligands and residues on the flap. Tyr 192 also interacted with the ligands. Most important interactions include; hydrogen bond, carbon-hydrogen bond, Pi-alkyl and van der Waals interaction with the quinoline, Cl, and 2-methoxy group. Could it be that the ligands interacted with the 'gate keepers' to cover the active site?

5.5.2 Molecular dynamics simulation

To ensure stability within the systems and accuracy of successive post dynamic analyses, the roots mean square deviation (RMSD) of the Cα backbone of the trajectories were monitored during the simulation time for all the systems. After approximately 10 ns, the RMSD trajectories converged and fluctuations did not exceed 3.0 Å for either system for the duration of the simulation (Figure 4.20). In three of the enzymes systems (FP-3, Plm-II and Plm-IV), compound P3-protein complex attained a high RMSD value, while P4-protein complex has higher value with FP-2 only (Figure 4.20). The results indicate P4 complexes in those systems as the most stable compared to P3 complexes. The average RMSD values for the C-α backbone atoms of FP-2, FP-3, Plm-II and Plm-IV in complex with P3 were 1.481, 1.702, 2.141 and 2.277Å respectively, while that of FP-2, FP-3, Plm-II and Plm-IV in complex with P4 were 1.700, 1.565, 1.602 and 2.010Å respectively. RMSD values ranging from 1.8Å up to 2.9Å was reported for plasmodial cysteine protease complexes (Musyoka *et al.*, 2016).

To further provide insight into the stability of the protein systems, as well as to determine the compactness of the proteins 3D structure (how folded or unfolded a protein is) upon binding with the two compounds throughout the MD simulation, Rg was calculated and analysed (Figure 4.21). For the falcipains (FP-2 and FP-3) the two complexes showed similar pattern of the Rg (Figure 4.21). In FP-3 the Rg for the two compounds maintain a

relatively steady value over the simulation time indicating a compact and stable system, while in FP-2 system there was stability from the beginning of the simulation for both compounds until after 15ns when it fluctuates increasing slightly then decrease. Overall, the two falcipain systems-maintained compactness and stability of the protein 3D structure upon binding with both P3 and P4, with an average Rg of 18.446 and 18.474 respectively for FP-3 and 18.278 for both in FP-2. This agrees with an average Rg reported by Musyoka *et al.* (2016).

Conversely, with plasmepsins system the two compounds showed different pattern in their Rg. P4 showed lower and more stable values in Plm-II as compared to P3, while it displayed slightly higher values in Plm- IV. Plm-IV system showed fluctuation in Rg values from the beginning of the simulation but, stabilizes and decreased after about 10 ns, with values for both compound smaller than Plm-II system. The pattern of the Rg for both Plm-II and Plm-IV system is similar to that reported by McGillewie and Soliman. (2015). The average Rg displayed by P3 in Plm-II and Plm-IV system are 20.642, and 19.982 respectively and that of P4 in Plm-II and Plm-IV system are 20.594 and 20.049. Rg of apo Plm-II and Plm-IV are 20.48 and 20.66 respectively (McGillewi and Soliman, 2015).

To gain insight into the mobility of the individual residues within the four enzymes system upon binding with P3, and P4 that mediate conformational flexibility and dynamics of the enzyes, per-residue fluctuation (RMSF) was evaluated and analyzed. The RMSF plots of the falcipains-ligand complexes are similar (Figures 4.22, A and B). The region showing the highest fluctuation are residues 1-20 representing the N-terminal insertion, that has previously been reported to mediate folding of the mature enzymes (Rosenthal, 2002) and the second insertion consisting of residues 175-200 that forms the β-hairpin associated with the binding of haemoglobin (Hb) (Pandey *et al.,* 2005; Hogg *et al.,* 2006). Previous studies have shown that these insertions are novel to Plasmodia cysteine proteases and are

more flexible than the rest of the structure (Rosenthal, 2002; Hogg *et al.,* 2006; Wang *et al.,* 2006). Other residues showing fluctuations are located on loop region. From the RMSF plot no fluctuations are observed in the active site (Gln36/45, Cys42/51, His174/183, and Asn204/213 for FP2 and FP3 respectively) thus, the protein–ligand complex system remained stable during the simulation period.

For the plasmepsin systems (Figure 4.22, C and D), the amino acid residues 225-300 show a higher fluctuation relative to other residues. The region represents the L3 loop (231-244 residues) and L4 loop (277-283 residues) Plm-II numbering (McGillewie and Soliman, 2015) where the flexible loop is situated and the fluctuation have been attributed to the coordinated recoiling motion of the flexible loop (Karabiu *et al.,* 2015; McGillewie and Soliman, 2015). There was no significant movement of the flap as the compounds remained embraced by the flap at the active site cavity, but the residues behind the flap fluctuate higher to move the flap over the binding cavity as seen by visual inspection of the trajectories. Less residual fluctuation was reported for bound Plm-II as compared to the apo (Karabiu *et al.,* 2015).

The RMSF pattern is similar to that reported by Karbiu *et al.* (2015) reflecting similar region of higher fluctuations with lower values as compared to the free plasmepsins (Karabiu *et al.,* 2015; McGillewie and Soliman, 2015). The overall average RMSF for the free Plm-II is 9.84 Å and that of Plm-II bound to P3 and P4 are 7.652 Å and 7.138 Å respectively. These indicate lower conformational flexibility as the enzymes bound to the compounds. Also, Plm-IV complexes showed an average RMSF of 5.860 Å and 9.111 Å for P3 and P4 respectively. Compound P3 have less residual fluctuation as compared to P4.

To gain insight into the energetics of P3 and P4 binding to the proteases, the relative BFE and various energy components contributions of the protein- ligand complexes were

averaged over 30,000 snapshots extracted from 30 ns MD trajectories, at an interval of 50 ps using MM-PBSA method. Table 4.14 shows a summary of the overall BFE underlying the binding of P3 and P4 in complex with FP2, FP3, PlmII, and PlmIV. From the results, it was noted that plasmepsins complexes had the lowest binding energies, an indication of stronger interactions compared to the falcipains. The results are in agreement with the docking results with the exception of PlmII system where docking result rank P3 higher than P4 but reverse was observed on the simulation result. Still, the result (Table 4.14) shows a high energy contribution in the gas phase from P3 but with higher solvation energy which docking result could not read, causing the overall BFE to drop. The lower binding energy of the plasmepsins complexes is not a surprise; studies showed that plasmepsins are highly flexible enzymes capable of adopting different conformation to accommodate different ligands (Asojo *et al.,* 2003; McGillewie and Soliman, 2015).

From the different energetic contributions (Table 4.14), it is evident that the binding process was principally favored by van der Waals and little by electrostatic terms while the polar solvation impaired it. Similar finding was reported by Musayako *et al.* (2016) on the falcipain. The low electrostatic energy can be explained by few hydrogen bonds observed in all the system.

Result from the decomposition of the total BPE to individual residue interaction energy revealed that, the significant contribution of the active site residues to the binding of the ligands in energy terms is also van der Waals interactions (Figures 4.23-4.26). Electrostatic interactions and polar solvation energy (in few residues) also contributed favorably (Figures 4.23-4.26).

The residues contributing favorably to the binding of P3 with FP-2 as shown in Fig 4.23 are; GLY40, CYS42, TRP43, ASN81, GLY82, GLY83, LEU84, ILE85, SER149, GLN171, LEU172, ASN173, HIE174 and, ALA175. However, residues GLY36, CYS80,

GLY171 and, ASP234 showed unfavorable energy contribution to P3 binding (Figure 4.23). It appeared that there is favorable interaction with some residue in the active site (CYS42), S2 region (LUE84), S3 region (GLY83), and 'Gate keeper' (LEU172). It was reported that a series of possible hydrophobic interaction with some residues in the nonpolar region (GLY40, GLN82, GLN83, SER149, LEU172 and, ASN173) exist in FP2-E64 crystal structure (Kerr *et al.,* 2009). Also, in the crystal structure, the active site CYS42 forms a covalent irreversible hemi-thioketal with E64 epoxy carbon (Kerr *et al.,* 2009) but, in the current study the interaction with CYS42 is through hydrogen bonding, this suggests mode of inhibition other than irreversible covalent binding to CYS42. Although detecting covalent interactions is beyond the scope of this work. The same trend was observed in P4-FP2 complex with fewer interactions (CYS42). Li *et al.* (1995) have also found non-covalent inhibitors of falcipains through virtual screening and validated their finding experimentally. The unfavorable total BFE of some residues was observed as a result of their high internal energy even though there was reasonable van der Waals and electrostatic energy contribution.

FP-3 complexes have similar residues contribution with few favorable interactions as compared to FP-2 complexes (Figure 4.24). Residues contributing favorably to binding with P3 and P4 are; CYS51, TRP52, GLY91, GLY92, TYR93, SER158, PRO181, ASN182, HIE183 and, GLU243. This also showed favorable interaction with some residue in the active site (CYS51), S2 region (GLU243) and, S3 region (GLY92). Possible hydrophobic interaction with some residues in the nonpolar region (TRY90, GLY91, TYR93, ILE94 and, SER158) was also observed in FP3-leupeptin crystal structure (Kerr *et al.,* 2009). In the light of the above information the lower binding energy from the docking and BFE analysis of P3 and P4 in complex with FP-2 as compared to P3 and P4 in complex with FP3 can be explained. A favorable number of interactions relative to

binding give a stable complex that lead to low negative enthalpy in binding process. This result justifies the high affinity of the compounds for FP2 compared to FP3 as obtained from the docking result (Table 4.13), which was confirmed from the BFE analysis (Table 4.14).

The plasmepsin complexes have few residues contributing favorably to the BFE which include GLY36, TYR77, VAL78, LEU131, TYR192 and THR217 with only GLY36, TYR192 and, THR217 giving the most significant contribution (Figure 4.25). As observed from falcipain systems van der Waals and electrostatic attraction are the major forces contributing favorably to the binding. In the flap region TYR77, VAL78 and SER79 (P4 complex only) contributed favorably to the BFE (Figure 4.25). TYR192 consistently forms hydrogen bond with the compounds in all the plasmepsin systems (Fig 4.25-4.26). It was reported that the hydroxyl groups of SER218 and TYR192 form hydrogen bond with EH58 (the inhibitor) in the crystal structure (Asojo *et al.*, 2003), this interaction was found to be favorable in the present study. Gutierrez-de-Teran *et al.* (2006) studied the interaction of allophenylnorstatine with Plm IV and reported similar residues contribution with this study. P4 complex showed more favourable interaction with the active site residues, probably explaining the high total BFE as compared to P3 complex in addition to other factors. Overall some residues previously reported (Recacha *et al.*, 2015; McGillewie and Soliman, 2015) to interact with known inhibitors have shown favorable binding to the compounds studied.

The same trend as describe above was observed for PlmIV complexes (Figure 4.26) but, there is a favorable BFE from TYR77, GLY78 (replacing VAL78 in PlmII), LEU131, and ILE 133. This is probably the reason for high BFE of PlmIV (Table 4.14) complexes as compared to Plm II complexes, as more favourable interactions stabilizes the system and

gives high negative Gibbs free energy. In this system the energy contribution by TYR 192 and THR217 is small.

CHAPTER SIX

6.0 SUMMARY, CONCLUSION AND RECOMMENDATION

6.1 Summary of Findings

Seventeen chalcone derivatives were designed, successfully synthesized and characterized, four of which (P1, P2, P3 and P8) are new compounds and have not been reported in the literature as ascertained from a search using Scifinder (www.scifinder.com). All the compounds are potential drug candidates as predicted using Lipinski ‘s rule of five.

Chalcone derivatives with promising antimalarial activity comparable with chloroquine at a dose of 25 mg/kg and, arthemeter at a dose of 2.3 mg/kg and quinine at a dose of 10 mg/kg have been identified. Eleven compounds have been identified as ‘actives’ from the present study. The most active compound from this study is P2, with percentage inhibition of 90.32%. An interesting observation is the association of good antimalarial activity with the 3-quinolinyl A ring derivatives.

In silico studies showed that the compounds studied have dual affinity for FP-2 and Plm-1V, although few have shown appreciable inhibition to all the proteases. Recent reports have shown that poly-inhibition of falcipains and plasmepsins is desirable in potential antimalarial to ensure clinical efficacy and combat resistance due to their complementary role (Sriwilaijaroen *et al*., 2006; Bjelic *et al.*, 2007). P3, P4 and, P8 have high rank across all the enzymes. Interestingly they also have good antiplasmodial activity in the experimental *in-vivo* study (Appendix 1). Thus, the dual inhibition of the proteases by the hits is an indication of standing against resistance by the parasite when develop into a drug.

It appears that the most contributing features of the ligand for receptor interaction are the quinoline ring, carbonyl group and, 2- methoxy group. The interactions were between the ligands and the catalytic residues for the falcipains. But, interaction with plasmepsins is only with the residues on the flap and Tyr192. It could be that the ligands interacted with the 'gate keepers' to cover the active site.

The BFE results from simulation agree with the docking results with the exception of PlmII system. From the different energetic contributions, it is evident that the binding process is principally favored by van der Waals and little by electrostatic terms while the polar solvation impaired it. The significant contribution of the active site residues to the binding of the ligands in energy terms is also Van der Waals also interaction. All the simulated system remains stable throughout the simulation

Residues that contributed favorably in all the systems are implicated in binding with an inhibitor. The higher favorable interactions in FP-2 complexes relative to FP-3 complexes justify the high affinity for FP-2, as predicted by docking and BFE analysis. For the Plasmepsin system there were favorable interactions with the residues on the flap.

Although the ligands were stable within the binding cavity throughout the simulation period, no interaction with the active site residue was observed.

Contrary to Liu *et al.* (2001) findings on the importance of electronic feature in modulating antimalarial activity of substituted chalcones, steric features are playing more important role. This has been supported by the evidence from the *in-silico* studies, where the two active compounds having similar features bind to the enzymes on different orientation.

6.2 Conclusion

Seventeen Chalcone derivatives were designed as protease inhibitors and, successfully synthesized and characterized using various spectroscopic techniques. Eleven have shown promising antimalarial activity *in vivo* in mice infected with *P berghii* comparable to some standard drugs. Contrary to Li *et al.* (1995); Liu *et al.* (2001) and Kumar *et al.* (2010) findings, this work suggest that steric features are more important in deciding the antimalarial activity than electronic feature.

In silico studies pointed three quinolinyl chalcones as potential dual inhibitors of aspartic and cysteine proteases. Molecular dynamic simulation has shown that P3 and P4 (quinolinyl chalcones) complexes with the enzymes were stable and there were favorable interactions with the amino acids at the active site.

Most of the chalcones with good *in vivo* activity are not acting through *β*- hematin synthesis inhibition and, are therefore potential candidate in chloroquine resistance malaria. Overall, chalcones with quinolinyl scaffold and 2-methoxy phenyl ring are potential candidates for further optimization.

6.3 Contribution to Knowledge

The study established;

1. Synthesis of seventeen substituted chalcone derivatives, four of which are new; **P1** [(E)-1,3-bis(2,3,4-trimethoxyphenyl)prop-2-en-1-one)], **P2** [(E)-1-(2,4-dimethoxyphenyl)-3-(2,3,4-trimethoxyphenyl)prop-2-en-1-one], **P3** [(E)-3-(2-chloro-6-methoxyquinolin-3-yl)-1-(2,4-dimethoxyphenyl)prop-2-en-1-one] and **P4** [(E)-3-(2-chloro-6-methoxyquinolin-3-yl)-1-(2,3,4-trimethoxyphenyl)prop-2-en-1-one].

2. Nine chalcone derivatives with significant ($p<0.05$) antimalarial activity *in vivo* comparable to standard drugs; chloroquine, and arthemeter at a dose of 25 to 100mg/kg for further studies and optimization

3. Three quinolinyl Chalcones having broad inhibition of aspartic and cysteine proteases *in silico* with binding energy (Kcal/mol) of; P3 [FP-2 (-6.0), FP-3 (-6.8), Plm-II (-8.0), Plm-IV (-9.3)], P4 [FP-2 (-6.7), FP-3 (-6.6), Plm-II (-7.7), Plm-IV (-9.1)], P8 [FP-2 (-6.0), FP-3 (-7.0), Plm-II (-7.7), Plm-IV (-8.9)] as potential drug candidate.

6.4 Recommendation

Both acute and chronic toxicity studies of the compounds should be carried out to determine the safety of the compounds.

The *in silico* studies should be validated with *in vitro* experiment on cysteine and aspartic proteases.

Further structural modification of the quinolinyl chalcones should be carried out to improve binding onto the enzymes and the antimalarial activity.

REFERENCES

Adedotun, A. A., Morenikeji, O. A., and Odaibo, A. B. (2010). Knowledge, attitudes and practices about malaria in an urban community in south-western Nigeria. *Journal of Vector Borne Diseases*, *47*(3), 155.

Adzu, B., Haruna, A. K., Salawu, O. A., Katsayal, U. D., and Njan, A. (2007). *In vivo* antiplasmodial activity of ZS-2A: a fraction from chloroform extract of *Zizyphus spina-christi* root bark against *Plasmodium berghii* in mice. *International Journal of Biological and Chemical Sciences*, *1*(3), 281- 286.

Aksoz, B. E., and Ertan, R. (2011). Chemical and structural properties of chalcones. *FABAD Journal of Pharmaceutical Sciences*, *36*, 223-42.

Alonso, P. L., Sacarlal, J., Aponte, J. J., Leach, A., Macete, E., Aide, P., ... and Guinovart, C. (2005). Duration of protection with RTS, S/AS02A malaria vaccine in prevention of *Plasmodium falciparum* disease in Mozambican children: single-blind extended follow-up of a randomized controlled trial. *The Lancet*, *366*(9502), 2012-2018.

Alonso, P. L., Sacarlal, J., Aponte, J. J., Leach, A., Macete, E., Milman, J., ... and Bassat, Q. (2004). Efficacy of the RTS, S/AS02A vaccine against *Plasmodium falciparum* infection and disease in young African children: randomized controlled trial. *The Lancet*, *364*(9443),1411-1420.

Ashley, E. A., Dhorda, M., Fairhurst, R. M., Amaratunga, C., Lim, P., Suon, S., ... & Sopha, C. (2014). Spread of artemisinin resistance in *Plasmodium falciparum* malaria. *New England Journal of Medicine*, *371*(5), 411-423.

Asojo, O. A., Gulnik, S. V., Afonina, E., Yu, B., Ellman, J. A., Haque, T. S., and Silva, A.M. (2003). Novel uncomplexed and complexed structures of plasmepsin II; an aspartic protease from *Plasmodium falciparum*. *Journal of Molecular Biology*, *327*(1), 173-181.

Avupati, V. R., and Yejella, R. P. (2014). Chalcones: A mini review. *World Journal of Pharmaceutical Sciences*, *278*.

Baelmans, R., Deharo, E., Munoz, V., Sauvain, M., and Ginsburg, H. (2000). Experimental conditions for testing the inhibitory activity of chloroquine on the formation of *β*-hematin. *Experimental Parasitology*, *96*(4), 243-248.

Baird, J. K. (2005). Effectiveness of antimalarial drugs. *New England Journal of Medicine*, *352*(15), 1565-1577.

Banerjee, R., Liu, J., Beatty, W., Pelosof, L., Klemba, M., and Goldberg, D. E. (2002). Four plasmepsins are active in the *Plasmodium falciparum* food vacuole, including a protease with an active-site histidine. *Proceedings of the National Academy of Sciences*, *99*(2), 990-995.

Bao, G., and Suresh, S. (2003). Cell and molecular mechanics of biological materials. *Nature Materials*, *2*(11), 715

Best, R. B., Zhu, X., Shim, J., Lopes, P. E., Mittal, J., Feig, M., and MacKerell Jr, A. D. (2012).Optimization of the additive CHARMM all-atom protein force field targeting improved sampling of the backbone ϕ, ψ and side-chain $\chi 1$ and $\chi 2$ dihedral angles. *Journal of Chemical Theory and Computation*. *8*(9), 3257-3273.

Bhattacharya, A., Mishra, L. C., Sharma, M., Awasthi, S. K., and Bhasin, V. K. (2009). Antimalarial pharmacodynamics of chalcone derivatives in combination with artemisinin against *Plasmodium falciparum in vitro*. *European Journal of Medicinal Chemistry*, *44*(9), 3388-3393.

Biagini, G. A., Viriyavejakul, P., O'Neill, P. M., Bray, P. G., and Ward, S. A. (2006). Functional characterization and target validation of alternative complex I of *Plasmodium falciparum* mitochondria. *Antimicrobial Agents and Chemotherapy*, *50*(5), 1841-1851.

Bjelic, S., Nervall, M., Gutiérrez-de-Terán, H., Ersmark, K., Hallberg, A., and Åqvist, J. (2007). Computational inhibitor design against malaria plasmepsins. *Cellular and Molecular Life Sciences*, *64*(17), 2285-2305.

Blackman, M. J. (2008). Malarial proteases and host cell egress: an 'emerging' cascade. *Cellular Microbiology*, *10*(10), 1925-1934.

Bonilla, J. A., Bonilla, T. D., Yowell, C. A., Fujioka, H., and Dame, J. B. (2007). Critical roles for the digestive vacuole plasmepsins of *Plasmodium falciparum* in vacuolar function. *Molecular Microbiology*, *65*(1), 64-75.

Carrara, V. I., Lwin, K. M., Phyo, A. P., Ashley, E., Wiladphaingern, J., Sriprawat, K., ... and Chu, C. (2013). Malaria burden and artemisinin resistance in the mobile and migrant population on the Thai–Myanmar border, 1999–2011: an observational study. *PLoS Medicine*, *10*(3), 1001398.

Case, D. A., Cheatham, T. E., Darden, T., Gohlke, H., Luo, R., Merz, K. M., ... and Woods, R. J. (2005). The Amber biomolecular simulation programs. *Journal of Computational Chemistry*, *26*(16), 1668-1688.

Chen, M., Christensen, S. B., Blom, J., Lemmich, E., Nadelmann, L., Fich, K., ... and Kharazmi, A. (1993). Licochalcone A, a novel antiparasitic agent with potent activity against human pathogenic protozoan species of *Leishmania*. *Antimicrobial Agents and Chemotherapy*, *37*(12), 2550-2556.

Chen, M., Christensen, S. B., Zhai, L., Rasmussen, M. H., Theander, T. G., Frøkjaer, S., ... and Kharazmi, A. (1997). The novel oxygenated chalcone, 2, 4-dimethoxy-4'-butoxychalcone, exhibits potent activity against human malaria parasite *Plasmodium falciparum in vitro* and rodent parasites *Plasmodium berghei* and *Plasmodium yoelii in vivo*. *Journal of Infectious Diseases*, *176*(5), 1327-1333.

Chen, M., Theander, T. G., Christensen, S. B., Hviid, L., Zhai, L., and Kharazmi, A. (1994). Licochalcone A, a new antimalarial agent, inhibits *in vitro* growth of the human malaria parasite *Plasmodium falciparum* and protects mice from *P. yoelii* infection. *Antimicrobial Agents and Chemotherapy*, *38*(7), 1470-1475.

Cherkasov, A., Muratov, E. N., Fourches, D., Varnek, A., Baskin, I. I., Cronin, M., ... and Consonni, V. (2014). QSAR modeling: where have you been? Where are you going to?. *Journal of Medicinal Chemistry*, *57*(12), 4977-5010.

Christen, M., Hünenberger, P. H., Bakowies, D., Baron, R., Bürgi, R., Geerke, D. P., ... and Peter, C. (2005). The GROMOS software for biomolecular simulation: GROMOS 05. *Journal of Computational Chemistry*, *26*(16), 1719-1751.

Coombs, G. H., Goldberg, D. E., Klemba, M., Berry, C., Kay, J., and Mottram, J. C. (2001). Aspartic proteases of *Plasmodium falciparum* and other parasitic protozoa as drug targets. *Trends in Parasitology*, *17*(11), 532-537.

Cramer, C. J. (2013). *Essentials of Computational Chemistry: Theories and Models*. John Wiley and Sons.

Daina, A., Michielin, O., and Zoete, V. (2017). SwissADME: a free web tool to evaluate pharmacokinetics, drug-likeness and medicinal chemistry friendliness of small molecules. *Scientific Reports*, *7*, 42717.

de Oliveira, M. E., Cenzi, G., Nunes, R. R., Andrighetti, C. R., de Sousa Valadão, D. M., dos Reis, C., ... and Sanchez, B. A. M. (2013). Antimalarial activity of 4-metoxychalcones: Docking studies as falcipain/plasmepsin inhibitors, ADMET and lipophilic efficiency analysis to identify a putative oral lead candidate. *Molecules*, *18*(12), 15276-15287.

Domnguez, J. N., Charris, J. E., Lobo, G., de Domnguez, N. G., Moreno, M. M., Riggione, F., ... and Rosenthal, P. J. (2001). Synthesis of quinolinyl chalcones and evaluation of their antimalarial activity. *European Journal of Medicinal Chemistry*,

36(6), 555-560.

Domínguez, J. N., León, C., Rodrigues, J., Gamboa de Domínguez, N., Gut, J., and Rosenthal, P. J. (2005). Synthesis and evaluation of new antimalarial phenylurenyl chalcone derivatives. *Journal of Medicinal Chemistry*, *48*(10), 3654-3658.

Drew, M. E., Banerjee, R., Uffman, E. W., Gilbertson, S., Rosenthal, P. J., and Goldberg, E. (2008). *Plasmodium* food vacuole plasmepsins are activated by falcipains. *Journal of Biological Chemistry*, *283*(19), 12870-12876.

Eastman, R. T., Buckner, F. S., Yokoyama, K., Gelb, M. H., and Van Voorhis, W. C. (2006). Thematic review series: lipid posttranslational modifications. Fighting parasitic disease by blocking protein farnesylation. *Journal of Lipid Research*, *47*(2), 233-240.

Eggleson, K. K., Duffin, K. L., and Goldberg, D. E. (1999). Identification and characterization of falcilysin, a metallo peptidase involved in hemoglobin catabolism within the malaria parasite *Plasmodium falciparum*. *Journal of Biological Chemistry*, *274*(45), 32411-32417.

Ersmark, K., Nervall, M., Gutiérrez-de-Terán, H., Hamelink, E., Janka, L. K., Clemente, J. C., ... and Hallberg, A. (2006). Macrocyclic inhibitors of the malarial aspartic proteases; plasmepsin I, II, and IV. *Bioorganic and Medicinal Chemistry*, *14*(7), 2197-2208.

Ettari, R., Zappalà, M., Micale, N., Schirmeister, T., Gelhaus, C., Leippe, M., ... and Grasso, S. (2010). Synthesis of novel peptidomimetics as inhibitors of protozoan cysteine proteases falcipain-2 and rhodesain. *European Journal of Medicinal Chemistry*, *45*(7), 3228-3233.

Ferreira, L. G., dos Santos, R. N., Oliva, G., and Andricopulo, A. D. (2015). Molecular docking and structure-based drug design strategies. *Molecules*, *20*(7), 13384-13421.

Forli, S., Huey, R., Pique, M. E., Sanner, M. F., Goodsell, D. S., and Olson, A. J. (2016). Computational protein–ligand docking and virtual drug screening with the AutoDock suite. *Nature Protocols*, *11*(5), 905.

Francis, S. E., Sullivan Jr, D. J., and Goldberg, A. D. E. (1997). Hemoglobin metabolism in the malaria parasite *Plasmodium falciparum*. *Annual Reviews in Microbiology*, *51*(1), 97-123.

Gallicchio, E., Lapelosa, M., and Levy, R. M. (2010). Binding energy distribution analysis method (BEDAM) for estimation of Protein−Ligand binding affinities. *Journal of Chemical Theory and Computation*, 6(9), 2961-2977.

Gallup, J. L., and Sachs, J. D. (2001). The economic burden of malaria. *The American Journal of Tropical Medicine and Hygiene*, *64*(1_suppl), 85-96.

Ganto, M. M. (2004). *Antiprotozoal quinolines containing electrophilic moieties* (Doctoral dissertation, University of Cape Town, Cape Town South Africa).

Gardner, M. J., Hall, N., Fung, E., White, O., Berriman, M., Hyman, R. W., ... and Paulsen, I. T. (2002). Genome sequence of the human malaria parasite *Plasmodium falciparum*. *Nature*, *419*(6906), 498.

Genheden, S., and Ryde, U. (2015). The MM/PBSA and MM/GBSA methods to estimate ligand- binding affinities. *Expert Opinion on Drug Discovery*, *10*(5), 449-461.

Gluzman, I. Y., Francis, S. E., Oksman, A., Smith, C. E., Duffin, K. L., and Goldberg, D. (1994). Order and specificity of the *Plasmodium falciparum* hemoglobin degradation pathway. *The Journal of Clinical Investigation*, *93*(4), 1602-1608.

Go, M. L. (2003), Novel antiplasmodial agents. *Medicinal Research Reviews*, *23*(4), 456-487.

Go, M. L., Liu, M., Wilairat, P., Rosenthal, P. J., Saliba, K. J., and Kirk, K. (2004). Antiplasmodial chalcones inhibit sorbitol-induced hemolysis of *Plasmodium falciparum*-infected erythrocytes. *Antimicrobial Agents and Chemotherapy*, *48*(9), 3241-3245.

Goldberg, D. E. (2005). Hemoglobin degradation. In *Malaria: Drugs, Disease and Post-genomic Biology* Springer, Berlin, Heidelberg. PP. 275-291.

Goldberg, D. E., Slater, A. F., Beavis, R., Chait, B., Cerami, A., and Henderson, G. B. (1991). Hemoglobin degradation in the human malaria pathogen *Plasmodium falciparum*: a catabolic pathway initiated by a specific aspartic protease. *Journal of Experimental Medicine*, *173*(4), 961-969.

Gomes, M. N., Muratov, E. N., Pereira, M., Peixoto, J. C., Rosseto, L. P., Cravo, P. V., ... and Neves, B. J. (2017). Chalcone derivatives: promising starting points for drug design. *Molecules*, *22*(8), 1210.

Gutiérrez-de-Terán, H., Nervall, M., Ersmark, K., Liu, P., Janka, L. K., Dunn, B., ... & Åqvist, J. (2006). Inhibitor binding to the plasmepsin IV aspartic protease from

Plasmodium falciparum. *Biochemistry*, *45*(35), 10529-10541.

Hayton, K., and Su, X. Z. (2004). Genetic and biochemical aspects of drug resistance in malaria parasites. *Current Drug Targets-Infectious Disorders*, *4*(1), 1-10.

Hoffman, S. L., Subramanian, G. M., Collins, F. H., and Venter, J. C. (2002). *Plasmodium*, human and Anopheles genomics and malaria. *Nature*, *415*(6872), 702.

Hogg, T., Nagarajan, K., Herzberg, S., Chen, L., Shen, X., Jiang, H., ... and Schmidt, C. L. (2006). Structural and functional characterization of Falcipain-2, a hemoglobinase from the malarial parasite *Plasmodium falciparum. Journal of Biological Chemistry*, *281*(35), 25425-25437.

http://www.ebi.ac.uk/thornton srv/software/LIGPLOT/

http://www.originlab.com

http://www.rcsb.org/pdb

Iwalewa, E. O., Omisore, N. O., Adewunmi, C. O., Gbolade, A. A., Ademowo, O. G., Nneji, C., ... and Daniyan, O. M. (2008). Anti-protozoan activities of *Harungana madagascariensis* stem bark extract on trichomonads and malaria. *Journal of Ethnopharmacology*, *117*(3), 507-511.

Iyer, J., Grüner, A. C., Rénia, L., Snounou, G., and Preiser, P. R. (2007). Invasion of host cells by malaria parasites: a tale of two protein families. *Molecular Microbiology*, *65*(2), 231-249.

Jana, S., and Paliwal, J. (2007). Novel molecular targets for antimalarial chemotherapy. *International Journal of Antimicrobial Agents*, *30*(1), 4-10.

Jensen, F. (1999). Introduction to Computational Chemistry 2nd edition. Wiley and Sons.

Kalra, B. S., Chawla, S., Gupta, P., and Valecha, N. (2006). Screening of antimalarial drugs: An overview. *Indian Journal of Pharmacology*, *38*(1), 5.

Kalyaanamoorthy, S., and Chen, Y. P. P. (2014). Modelling and enhanced molecular dynamics to steer structure-based drug discovery. *Progress in Biophysics and Molecular Biology*, *114*(3), 123-136.

Kapoor, V. K., and Kumar, K. (2005). Recent advances in the search for newer

antimalarial agents. *Progress in Medicinal Chemistry, 43*, 189-237.

Karubiu, W., Bhakat, S., McGillewie, L., and Soliman, M. E. (2015). Flap dynamics of plasmepsin proteases: Insight into proposed parameters and molecular dynamics. *Molecular BioSystems, 11*(4), 1061-1066.

Kerr, I. D., Lee, J. H., Pandey, K. C., Harrison, A., Sajid, M., Rosenthal, P. J., and Brinen, L. S. (2009). Structures of falcipain-2 and falcipain-3 bound to small molecule inhibitors: implications for substrate specificity. *Journal of Medicinal Chemistry*, *52*(3), 852-857.

Khan, S. M., and Waters, A. P. (2004). Malaria parasite transmission stages: an update. *Trends in Parasitology*, *20*(12), 575-580.

Kumar, R., Mohanakrishnan, D., Sharma, A., Kaushik, N. K., Kalia, K., Sinha, A. K., and Sahal, D. (2010). Reinvestigation of structure–activity relationship of methoxylated chalcones as antimalarials: Synthesis and evaluation of 2, 4, 5-trimethoxy substituted patterns as lead candidates derived from abundantly available natural β-asarone. *European Journal of Medicinal Chemistry*, *45*(11), 5292-5301.

Lecaille, F., Kaleta, J., and Brömme, D. (2002). Human and parasitic papain-like cysteine proteases: their role in physiology and pathology and recent developments in inhibitor design. *Chemical Reviews*, *102*(12), 4459-4488.

Lell, B., Agnandji, S., Von Glasenapp, I., Haertle, S., Oyakhiromen, S., Issifou, S., ... and Demoitie, M. A. (2009). A randomized trial assessing the safety and immunogenicity of AS01 and AS02 adjuvanted RTS, S malaria vaccine candidates in children in Gabon. *PLoS One*, *4*(10), 7611.

Lewars, E. G. (2016). *Computational Chemistry: Introduction to the Theory and Applications of Molecular and Quantum Mechanics*. Springer.

Li, R., Chen, X., Gong, B., Selzer, P. M., Li, Z., Davidson, E., ... and Fletterick, R. J. (1996). Structure-based design of parasitic protease inhibitors. *Bioorganic and Medicinal Chemistry*, *4*(9), 1421-1427.

Li, R., Kenyon, G. L., Cohen, F. E., Chen, X., Gong, B., Dominguez, J. N., ... and Rosenthal, P. J. (1995). *In vitro* antimalarial activity of chalcones and their derivatives. *Journal of Medicinal Chemistry*, *38*(26), 5031-5037.

Li, Z., Chen, X., Davidson, E., Zwang, O., Mendis, C., Ring, C. S., ... and Lee, G. K. (1994). Anti-malarial drug development using models of enzyme structure. *Chemistry and Biology*, *1*(1), 31-37.

Lin, A. J., Klayman, D. L., and Milhous, W. K. (1987). Antimalarial activity of new water-soluble dihydroartemisinin derivatives. *Journal of Medicinal Chemistry*, *30*(11), 2147-2150.

Lionta, E., Spyrou, G., K Vassilatis, D., and Cournia, Z. (2014). Structure-based virtual screening for drug discovery: principles, applications and recent advances. *Current Topics in Medicinal Chemistry*, *14*(16), 1923-1938.

Liu, J., Gluzman, I. Y., Drew, M. E., and Goldberg, D. E. (2005). The role of *Plasmodium falciparum* food vacuole plasmepsins. *Journal of Biological Chemistry*, *280*(2), 1432- 1437.

Liu, J., Istvan, E. S., Gluzman, I. Y., Gross, J., and Goldberg, D. E. (2006). *Plasmodium falciparum* ensures its amino acid supply with multiple acquisition pathways and redundant proteolytic enzyme systems. *Proceedings of the National Academy of Sciences*, *103*(23), 8840-8845.

Liu, M., Wilairat, P., and Go, M. L. (2001). Antimalarial alkoxylated and hydroxylated chalones: structure−activity relationship analysis. *Journal of Medicinal Chemistry*, *44*(25), 4443-4452.

Liu, M., Wilairat, P., Croft, S. L., Tan, A. L. C., and Go, M. L. (2003). Structure–activity relationships of antileishmanial and antimalarial chalcones. *Bioorganic and Medicinal Chemistry*, *11*(13), 2729-2738.

Macalino, S. J. Y., Gosu, V., Hong, S., and Choi, S. (2015). Role of computer-aided drug design in modern drug discovery. *Archives of Pharmaceutical Research*, *38*(9), 1686- 1701.

Marco, M., and Miguel Coteron, J. (2012). Falcipain inhibition as a promising antimalarial target. *Current Topics in Medicinal Chemistry*, *12*(5), 408-444.

Mauritz, J. M., Esposito, A., Ginsburg, H., Kaminski, C. F., Tiffert, T., and Lew, V. L. (2009). The homeostasis of *Plasmodium falciparum*-infected red blood cells. *PLoS Computational Biology*, *5*(4), 1000339.

McGillewie, L., and Soliman, M. E. (2015). Flap flexibility amongst plasmepsins I, II, III, IV, and V: Sequence, structural and molecular dynamics analyses. *Proteins: Structure, Function, and Bioinformatics*, *83*(9), 1693-1705.

McKerrow, J. H., Sun, E., Rosenthal, P. J., and Bouvier, J. (1993). The proteases and pathogenicity of parasitic protozoa. *Annual Reviews in Microbiology*, *47*(1), 821-853.

Micale, N., Kozikowski, A. P., Ettari, R., Grasso, S., Zappalà, M., Jeong, J. J., ... and Chishti, A. H. (2006). Novel peptidomimetic cysteine protease inhibitors as potential antimalarial agents. *Journal of Medicinal Chemistry*, *49*(11), 3064-3067.

Miller, L. H., Ackerman, H. C., Su, X. Z., and Wellems, T. E. (2013). Malaria biology and disease pathogenesis: insights for new treatments. *Nature Medicine*, *19*(2), 156.

Mishra, N., Arora, P., Kumar, B., Mishra, L. C., Bhattacharya, A., Awasthi, S. K., and Bhasin, V. K. (2008). Synthesis of novel substituted 1, 3-diaryl propenone derivatives and their antimalarial activity in vitro. *European Journal of Medicinal Chemistry*, *43*(7), 1530-1535.

Motta, L. F., Gaudio, A. C., and Takahata, Y. (2006). Chalcone Derivatives (1, 3-diphenyl–2–propen–1–one) as Anti *Plasmodium falciparum* Agents (Anti Malaria Agents). *Internet Electronic Journal of Molecular Design*, *5*, 555-569

Muegge, I., and Mukherjee, P. (2016). An overview of molecular fingerprint similarity search in virtual screening. *Expert Opinion on Drug Discovery*, *11*(2), 137-148.

Musyoka, T. M., Kanzi, A. M., Lobb, K. A., and Bishop, Ö. T. (2016). Structure based docking and molecular dynamic studies of *plasmodial* cysteine proteases against a South African natural compound and its analogs. *Scientific Reports, 6,*23690.

Nair, P. C., and Miners, J. O. (2014). Molecular dynamics simulations: from structure-function relationships to drug discovery. *In silico Pharmacology*, *2*(1), 4.

Noedl, H., Se, Y., Schaecher, K., Smith, B. L., Socheat, D., and Fukuda, M. M. (2008). Evidence of artemisinin-resistant malaria in western Cambodia. *New England Journal of Medicine*, *359*(24), 2619-2620.

Noedl, H., Socheat, D., and Satimai, W. (2009). Artemisinin-resistant malaria in Asia. *New England Journal of Medicine*, *361*(5), 540-541

Pagola, S., Stephens, P. W., Bohle, D. S., Kosar, A. D., and Madsen, S. K. (2000). The structure of malaria pigment *β*-haematin. *Nature*, *404*(6775), 307.

Pandey, K. C., Wang, S. X., Sijwali, P. S., Lau, A. L., McKerrow, J. H., and Rosenthal, P. J. (2005). The *Plasmodium falciparum* cysteine protease falcipain-2 captures its substrate, hemoglobin, via a unique motif. *Proceedings of the National Academy of Sciences of the United States of America*, *102*(26), 9138-9143.

Pettersen, E. F., Goddard, T. D., Huang, C. C., Couch, G. S., Greenblatt, D. M., Meng, E. C., and Ferrin, T. E. (2004). UCSF Chimera—a visualization system for exploratory research and analysis. *Journal of Computational Chemistry*, *25*(13), 1605-1612.

Phyo, A. P., Nkhoma, S., Stepniewska, K., Ashley, E. A., Nair, S., McGready, R., ... and Singhasivanon, P. (2012). Emergence of artemisinin-resistant malaria on the western border of Thailand: a longitudinal study. *The Lancet*, *379*(9830), 1960-1966.

Pirhadi, S., Shiri, F., and Ghasemi, J. B. (2013). Methods and applications of structure-based pharmacophores in drug discovery. *Current Topic in Medicinal Chemistry*, *13*(9), 1036-1047.

Recacha, R., Leitans, J., Akopjana, I., Aprupe, L., Trapencieris, P., Jaudzems, K., ... and Tars, K. (2015). Structures of plasmepsin II from *Plasmodium falciparum* in complex with two hydroxyethylamine-based inhibitors. *Acta Crystallographica Section F: Structural Biology Communications*, *71*(12), 1531-1539.

Reguera, R. M., Tekwani, B. L., and Balaña-Fouce, R. (2005). Polyamine transport in parasites: a potential target for new antiparasitic drug development. *Comparative Biochemistry and Physiology Part C: Toxicology and Pharmacology*, *140*(2), 151-164.

Ring, C. S., Sun, E., McKerrow, J. H., Lee, G. K., Rosenthal, P. J., Kuntz, I. D., and Cohen, F. E. (1993). Structure-based inhibitor design by using protein models for the development of antiparasitic agents. *Proceedings of the National Academy of Sciences*, *90*(8), 3583-3587.

Rodrigues, J. R., and de Domínguez, N. G. (2007). *Plasmodium berghei*: *in vitro* and *in vivo* activity of dequalinium. *Experimental Parasitology*, *115*(1), 19-24.

Roe, D. R., and Cheatham III, T. E. (2013). PTRAJ and CPPTRAJ: software for processing and analysis of molecular dynamics trajectory data. *Journal of Chemical Theory and Computation*, *9*(7), 3084-3095.

Rose, P. W., Prlić, A., Altunkaya, A., Bi, C., Bradley, A. R., Christie, C. H., ... and Green, K. (2016). The RCSB protein data bank: integrative view of protein, gene and 3D structural information. *Nucleic Acids Research*, 8(2), 1000.

Rosenthal, P. J. (1998). Proteases of malaria parasites: New targets for chemotherapy. *Emerging Infectious Diseases*, *4*(1), 49.

Rosenthal, P. J. (2002). Hydrolysis of erythrocyte proteins by proteases of malaria parasites. *Current Opinion in Hematology*, *9*(2), 140-145.

Rosenthal, P. J. (2004). Cysteine proteases of malaria parasites. *International Journal for Parasitology*, *34*(13-14), 1489-1499.

Rosenthal, P. J. (2011). Falcipains and other cysteine proteases of malaria parasites. *In Cysteine Proteases of Pathogenic Organisms* (pp. 30-48). Springer, Boston, MA.

Rosenthal, P. J., Olson, J. E., Lee, G. K., Palmer, J. T., Klaus, J. L., and Rasnick, D. (1996). Antimalarial effects of vinyl sulfone cysteine proteinase inhibitors. *Antimicrobial Agents and Chemotherapy*, *40*(7), 1600-1603.

Ryley, J. F., and Peters, W. (1970). The antimalarial activity of some quinolone esters. *Annals of Tropical Medicine and Parasitology*, *64*(2), 209-222.

Sahu, K., Balbhadra, N. S., Choudhary, S., and Kohli, V., D. (2012). Exploring pharmacological significance of chalcone scaffold: A review. *Current Medicinal Chemistry*, *19*(2), 209-225.

Saidu, K., Onah, J., Orisadipe, A., Olusola, A., Wambebe, C., and Gamaniel, K. (2000). Antiplasmodial, analgesic, and anti-inflammatory activities of the aqueous extract of the stem bark of *Erythrina senegalensis*. *Journal of Ethnopharmacology*, *71*(12), 275-280.

Sajid, M., and McKerrow, J. H. (2002). Cysteine proteases of parasitic organisms. *Molecular and Biochemical Parasitology*, *120*(1), 1-21.

Sanner, M. F., Olson, A. J., and Spehner, J. C. (1996). Reduced surface: an efficient way to compute molecular surfaces. *Biopolymers*, *38*(3), 305-320.

Semenov, A., Olson, J. E., and Rosenthal, P. J. (1998). Antimalarial synergy of cysteine and aspartic protease inhibitors. *Antimicrobial Agents and Chemotherapy*, *42*(9), 2254-2258.

Silva, A. M., Lee, A. Y., Gulnik, S. V., Maier, P., Collins, J., Bhat, T. N., ... and Francis, E. (1996). Structure and inhibition of plasmepsin II, a hemoglobin-degrading enzyme from *Plasmodium falciparum*. *Proceedings of the National Academy of Sciences*, *93*(19), 10034-10039.

Singh, A., and Rosenthal, P. J. (2001). Comparison of efficacies of cysteine protease inhibitors against five strains of *Plasmodium falciparum*. *Antimicrobial Agents and Chemotherapy*, *45*(3), 949-951.

Sinha, S., Medhi, B., and Sehgal, R. (2013). Chalcones as an emerging lead molecule for antimalarial therapy: a review. *Journal of Modern Medicinal Chemistry*, *1*(2), 64-77.

Sriwilaijaroen, N., Liu, M., Mei-Lin, G., and Wilairat, P. (2006). Plasmepsin II inhibitory activity of alkoxylated and hydroxylated chalcones. *Southeast Asian Journal of Tropical Medicine and Public Health*, *37*(4), 607.

Syahri, J., Rullah, K., Armunanto, R., Yuanita, E., Nurohmah, B. A., Aluwi, M. F. F. M., and Purwono, B. (2017). Synthesis, biological evaluation, QSAR analysis, and molecular docking of chalcone derivatives for antimalarial activity. *Asian Pacific Journal of Tropical Disease*, *7*(1), 8-13.

Teixeira, C., RB Gomes, J., and Gomes, P. (2011). Falcipains, *Plasmodium falciparum* cysteine proteases as key drug targets against malaria. *Current Medicinal Chemistry*, *18*(10), 1555-1572.

Trott, O., and Olson, A. J. (2010). AutoDock Vina: improving the speed and accuracy of docking with a new scoring function, efficient optimization, and multithreading. *Journal of Computational Chemistry*, *31*(2), 455-461.

Ugwu, D. I., Ezema, B. E., Okoro, U. C., Eze, F. U., Ekoh, O. C., Egbujor, M. C., and Ugwuja, D. I. (2016). Syntheses and pharmacological applications of chalcones: A review. *ChemoInformatics*, *47*(17).

Valero, M. V., Amador, L. R., Galindo, C., Figueroa, J., Bello, M. S., Murillo, L. A., ... and Aponte, J. J. (1993). Vaccination with SPf66, a chemically synthesized vaccine, against *Plasmodium falciparum* malaria in Colombia. *The Lancet*, *341*(8847), 705-710.

Vuorinen, A., and Schuster, D. (2015). Methods for generating and applying pharmacophore models as virtual screening filters and for bioactivity profiling. *Methods*, *71*, 113-134.

Wang, J., Wang, W., Kollman, P. A., and Case, D. A. (2006). Automatic atom type and bond type perception in molecular mechanical calculations. *Journal of Molecular Graphics and Modelling*, *25*(2), 247-260.

Wang, S. X., Pandey, K. C., Somoza, J. R., Sijwali, P. S., Kortemme, T., Brinen, L. S., ... and McKerrow, J. H. (2006). Structural basis for unique mechanisms of folding and hemoglobin binding by a malarial protease. *Proceedings of the National Academy of Sciences*, *103*(31), 11503-11508.

Wang, T.Y., and Xu, R. C. (1985). Clinical studies of treatment of falciparum malaria with artemether, a derivative of qinghaosu. *Journal of Traditional Chinese*, *5*(4), 240-242.

Wermuth, C. G., Ganellin, C. R., Lindberg, P., and Mitscher, L. A. (1998). Glossary of terms used in medicinal chemistry (IUPAC Recommendations 1998). *Pure and Applied Chemistry*, *70*(5), 1129-1143.

Wiesner, J., Ortmann, R., Jomaa, H., and Schlitzer, M. (2003). New antimalarial drugs. *Angewandte Chemie International Edition*, *42*(43), 5274-5293.

World Health Organization. (2011). World Malaria Report 2011. Geneva: WHO; 2011. *www. who. int/malaria/world_malaria_report_2011/en*.

World Health Organization. (2016). *World Malaria Report 2015*. World Health Organization

World Health Organization. (2017). World Malaria Report 2015. Geneva, Switzerland.

Wu, X., Wilairat, P., and Go, M. L. (2002). Antimalarial activity of ferrocenyl chalcones. *Bioorganic and Medicinal Chemistry Letters*, *12*(17), 2299-2302.

www.nlcbio.com

Yadav, N., Dixit, S. K., Bhattacharya, A., Mishra, L. C., Sharma, M., Awasthi, S. K., and Bhasin, V. K. (2012). Antimalarial activity of newly synthesized chalcone derivatives in vitro. *Chemical Biology and Drug Design*, *80*(2), 340-347.

Yanow, S. K., Purcell, L. A., and Spithill, T. W. (2006). The A/T-specific DNA alkylating agent adozelesin inhibits *Plasmodium falciparum* growth in vitro and protects mice against *Plasmodium chabaudi adami* infection. *Molecular and biochemical parasitology*, *148*(1), 52-58

APPENDICES

Appendix 1

Effect of compound P1, P2, P3, P4, P8, and P23-P25 on the parasitaemia level of P. berghei infected mice.

Treatment groups	Dose (mg/kg)	Average parasitemia	Percentage suppression (%)
Acacia	5ml/kg	22.00±1.50	0
CQ	10	9.34±1.01[a]	57.54
CQ	25	3.20±1.01[c]	85.45
Quinine	10	2.52±0.41[c]	88.54
ART	1.8	7.14±0.85[b]	67.54
ART	2.3	5.84±0.68[c]	73.45
ART	5	5.06±1.17[c]	77.00
P1	25	13.05±4.40	40.68
P1	50	14.92±2.29	32.18
P1	100	12.34±1.15[a]	43.90
P2	25	8.28±1.88[c]	62.36
P2	50	4.60±0.68[c]	79.09
P2	100	2.00±0.39[c]	90.90
P3	25	5.74±1.37[c]	73.90
P3	50	7.80±1.31[c]	64.54
P3	100	6.57±3.52[c]	70.15
P4	25	8.34±2.26[a]	62.09
P4	50	7.22±1.24[b]	67.18
P4	100	10.28±1.00	53.27
P8	25	10.76±3.12	51.09
P8	50	6.52±2.25[b]	70.36
P8	100	4.93±0.83[c]	77.61
P23	25	9.70±1.98[a]	55.90
P23	50	12.84±2.73	41.63
P23	100	29.44±5.13	-33.81
P24	25	14.32±4.92	34.90
P24	50	15.04±2.11	31.63
P24	100	29.12±3.42	-32.36
P25	25	6.08±2.10[c]	72.36
P25	50	6.80±1.07[c]	69.09
P25	100	11.05±2.39	49.77

Values are presented as Mean ± SEM; Data analyzed by one way ANOVA followed by Bonferroni 's post-hoc test; n=5 a=$p<0.05$, b=$p<0.01$, c=$p<0.001$ versus control; CLQ=chloroquine, ART= arthemeter, QUIN= quinine; Route of administration=ip

Appendix 2

Effect of compound P11, P12, P13, P15, P16, P17, P19, P21and, P22 on the parasitaemia level of *P. berghei* infected mice.

Treatment groups	Dose (mg/kg)	Average parasitemia	Percentage suppression (%)
Acacia	10ml/kg	28.65±0.95	0
Chloroquine	25	2.33±0.88[c]	91.85
P11	25	8.98±1.42[c]	68.65
P11	50	5.00±0.95[c]	72.54
P11	100	4.93±0.57[c]	72.78
P12	25	9.58±2.93[c]	66.56
P12	50	4.10±1.95[c]	85.68
P12	100	3.03±1.23[c]	89.44
P13	25	16.40±0.40[a]	42.75
P13	50	17.40±0.40	39.26
P13	100	17.74±1.13	38.08
P15	25	11.20±1.24[c]	60.90
P15	50	12.50±2.01[c]	56.36
P15	100	4.93±0.95[c]	82.78
P16	25	9.58±2.53[c]	66.56
P16	50	12.50±2.01[c]	56.36
P16	100	14.50±2.01[c]	46.26
P17	50	5.65±1.75[c]	80.29
P17	100	6.20±1.28[c]	78.35
P17	200	10.80±2.89[c]	62.30
P21	175	9.20±0.58[c]	67.88
P21	350	11.20±1.83[c]	60.90
P21	700	13.80±2.40[c]	51.83
P22	250	11.20±1.24[c]	60.90
P22	500	12.50±2.01[c]	56.36
P22	1000	12.20±2.44[c]	57.41

Values are presented as Mean ± SEM; Data analyzed by one-way ANOVA followed by Bonferroni ‘s post-hoc test; n=5 a=$p<0.05$, c=$p<0.001$ versus control; CLQ=chloroquine

Route of administration=ip

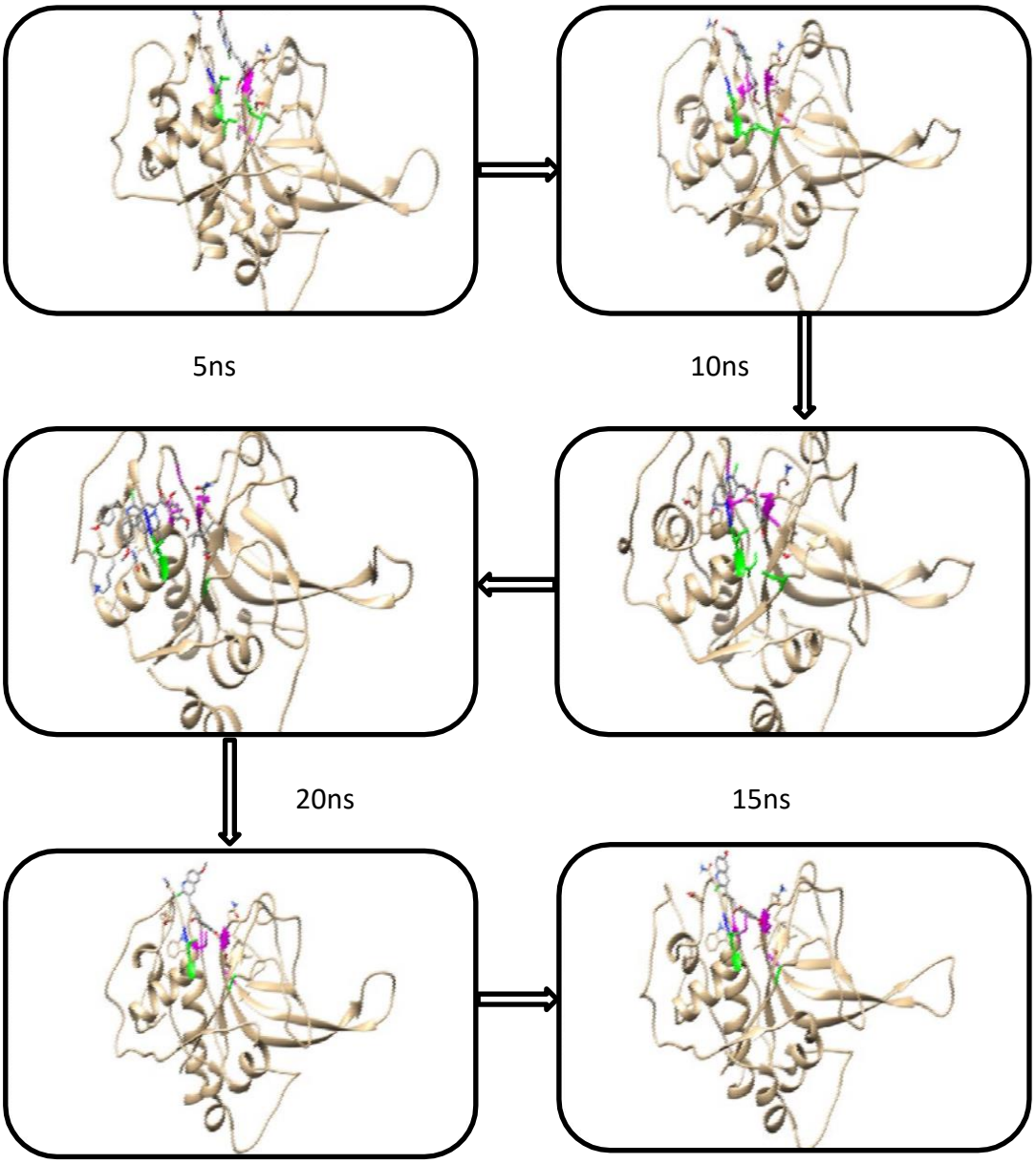
Appendix 3

The binding energy of co-crystallized ligands and 17 chalcones against four enzymes (FP-2, FP-3, Plm-II, and, Plm-IV).

Ligands	Docking score (Kcal/mol)			
	Falcipain-2 (FP-2)	**Falcipain-3 (FP-3)**	**Plasmepsin-II (Plm-II)**	**Plasmepsin-IV (Plm-IV)**
P1	-5.7 (7)	-6.0(7)	-6.7(10)	-7.1(12)
P2	-5.7 (7)	-5.7(9)	-7.1(7)	-7.5(10)
P3*	**-6.0(5)**	**-6.8(2)**	**-8.0(1)**	**-9.3(1)**
P4*	**-6.7(1)**	**-6.6(3)**	**-7.7(3)**	**-9.1(2)**
P8	-6.0(5)	-7.0(1)	-7.7(3)	-8.9(3)
P11	-5.8(6)	-5.9(8)	-7.1(7)	-7.7(8)
P12	-5.7(7)	-5.6(10)	-7.0(8)	-7.6(9)
P13	-5.8(6)	-5.7(9)	-7.4(5)	-8.1(5)
P15	-5.4(10)	-5.7(9)	-7.0(8)	-7.2(11)
P16	-5.5(9)	-5.5(11)	-6.8(9)	-7.2(11)
P17	-5.5(9)	-6.0(7)	-6.8(9)	-7.0(13)
P19	-6.0(5)	-5.5(11)	-6.8(9)	-7.6(9)
P21	-6.3(3)	-6.1(6)	-7.5(4)	-8.0(6)
P22	-6.2(4)	-6.2(7)	-7.7(3)	-7.9(7)
P23	-5.4(10)	-5.9(8)	-6.8(9)	-7.0(13)
P24	-6.4(2)	-5.9(8)	-6.8(9)	-7.5(10)
P25	-5.5(9)	-5.7(9)	-7.2(6)	-7.2(11)
P	-5.1	-6.9	-10.1	-7.7

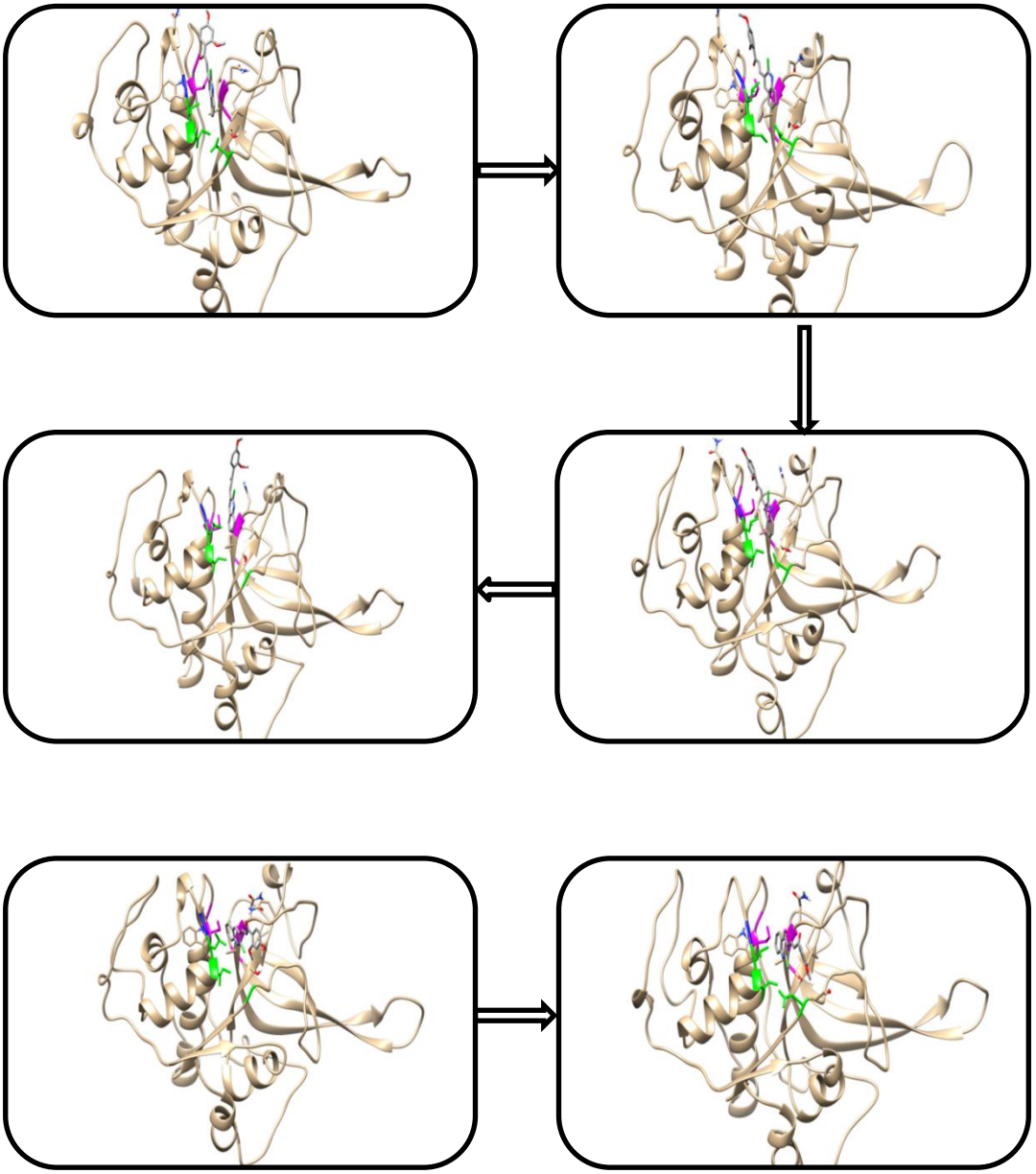
Number in bracket= Ranking, P= Respective ligand co-crytallised with the enzymes (FP2 – E64, FP3- CIP. PlmII- EH5 and, PlmIV- Pepstatin), * Best hits

Appendix 4



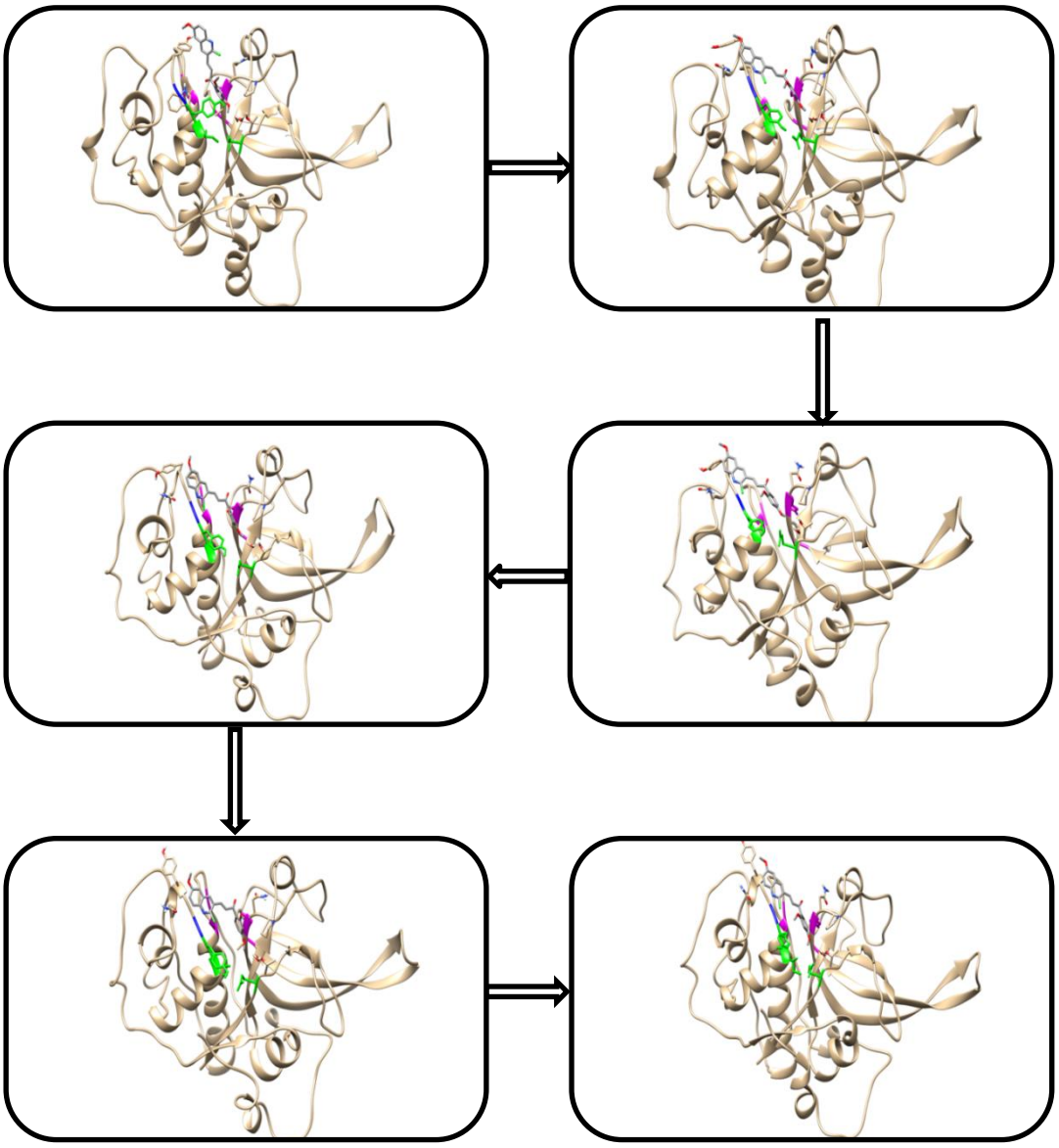
MD trajectory showing 30 nanoseconds (ns) molecular dynamic simulation of P3 bound to FP-2. (Magenta highlights the catalytic amino acids residues, blue is the S3-subsite, green is S2-subsite and P3 colored by element)

Appendix 5



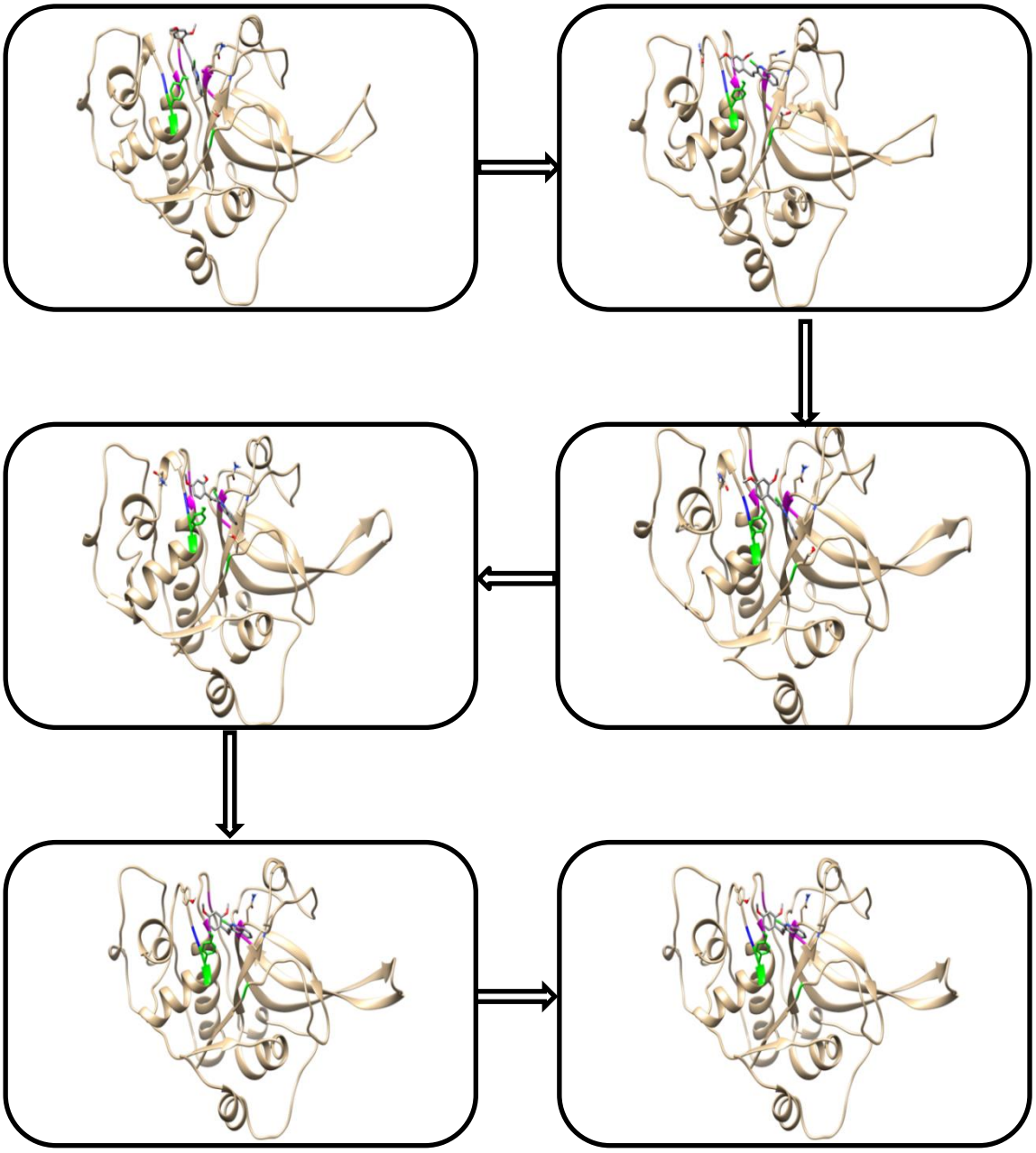
MD trajectory showing 30 nanoseconds (ns) molecular dynamic simulation of P4 bound to FP-2. (Magenta highlights the catalytic amino acids residues, blue is the S3-subsite, green is S2-subsite and P4 colored by element).

Appendix 6



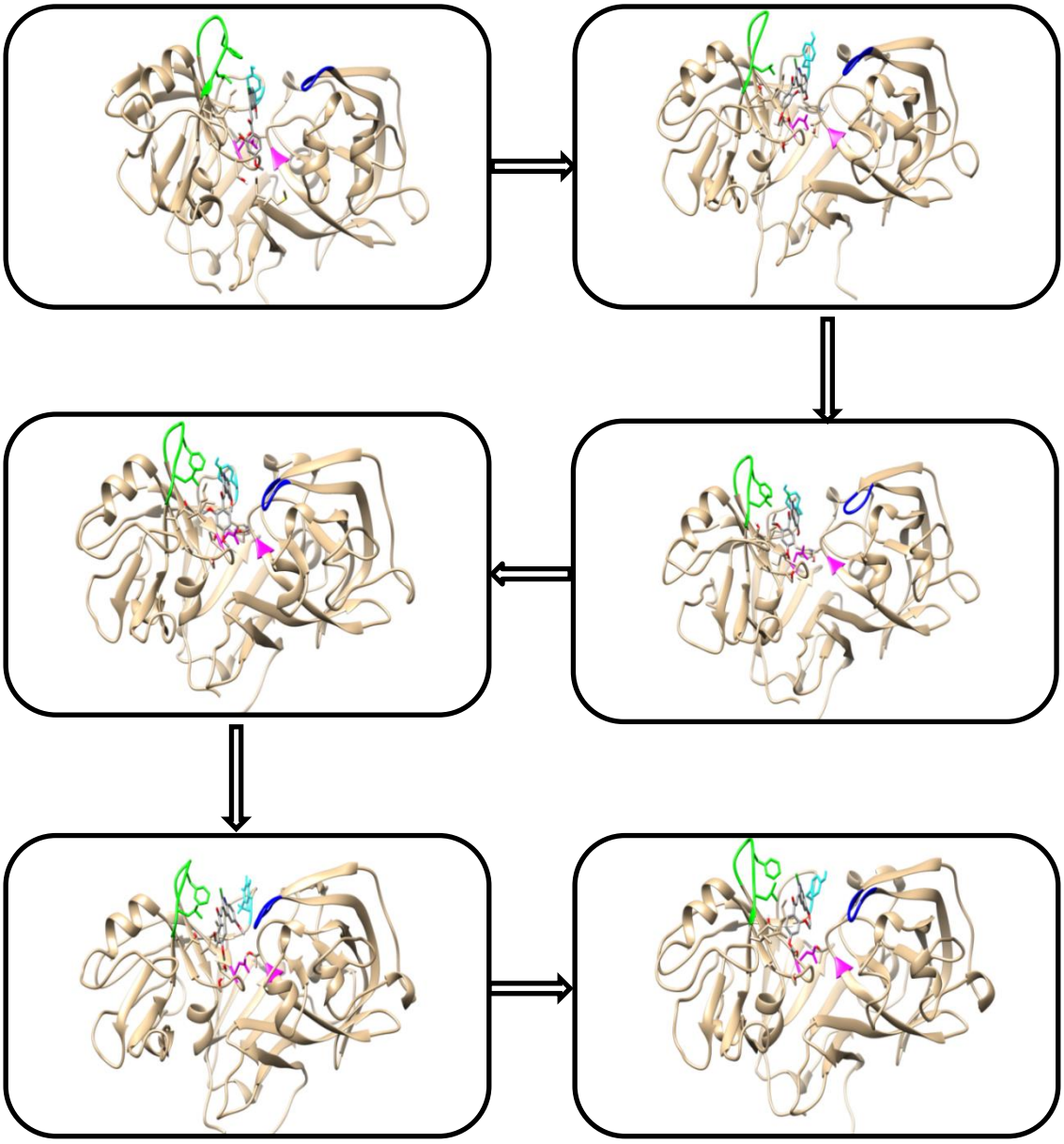
MD trajectory showing 30 nanoseconds (ns) molecular dynamic simulation of P3 bound to FP-3. (Magenta highlights the catalytic amino acids residues, blue is the S3-subsite, green is S2-subsite and P3 colored by element)

Appendix 7



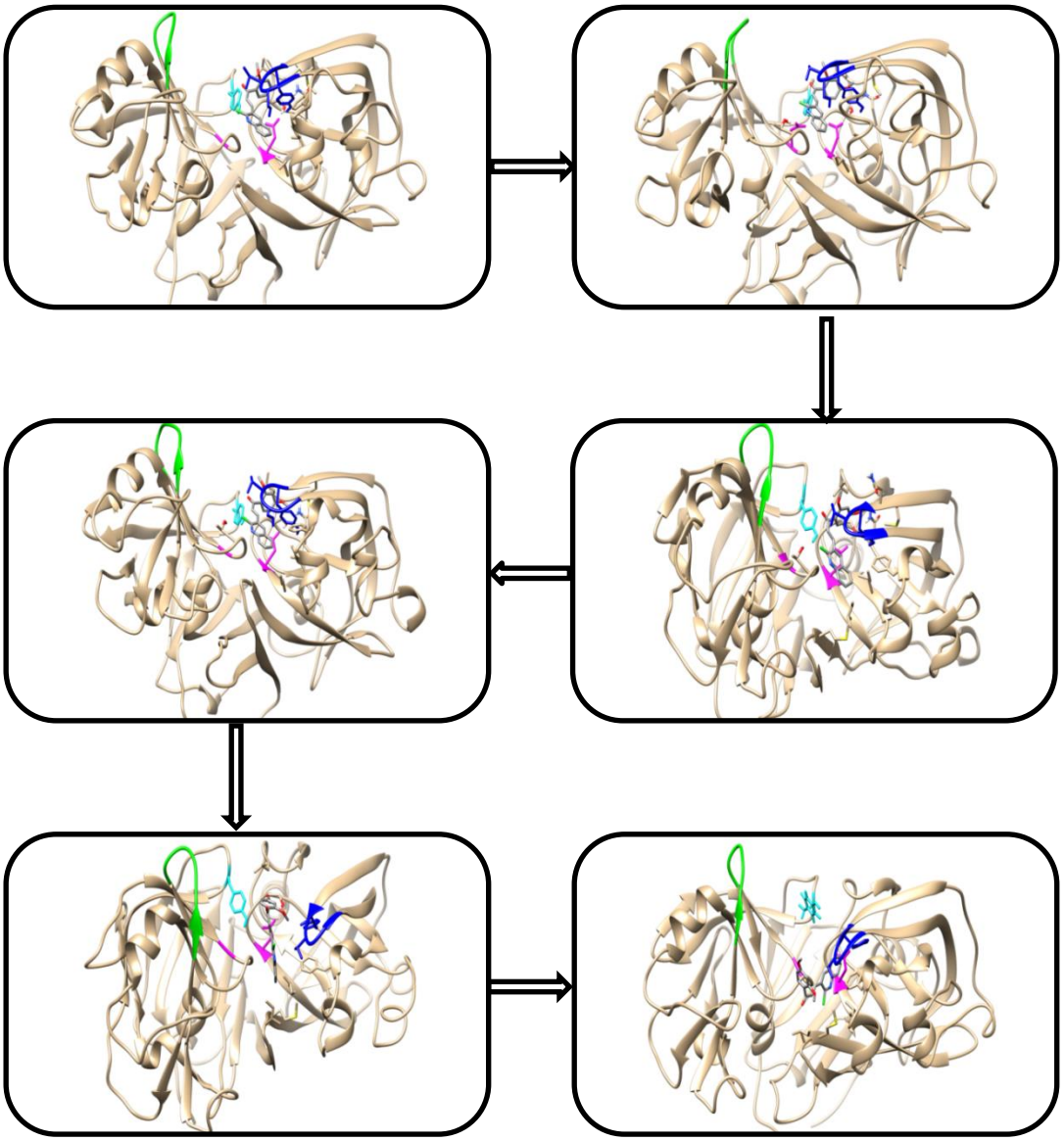
MD trajectory showing 30 nanoseconds (ns) molecular dynamic simulation of P4 bound to FP-3. (Magenta highlights the catalytic amino acids residues, blue is the S3-subsite, green is S2-subsite and P4 colored by element)

Appendix 8



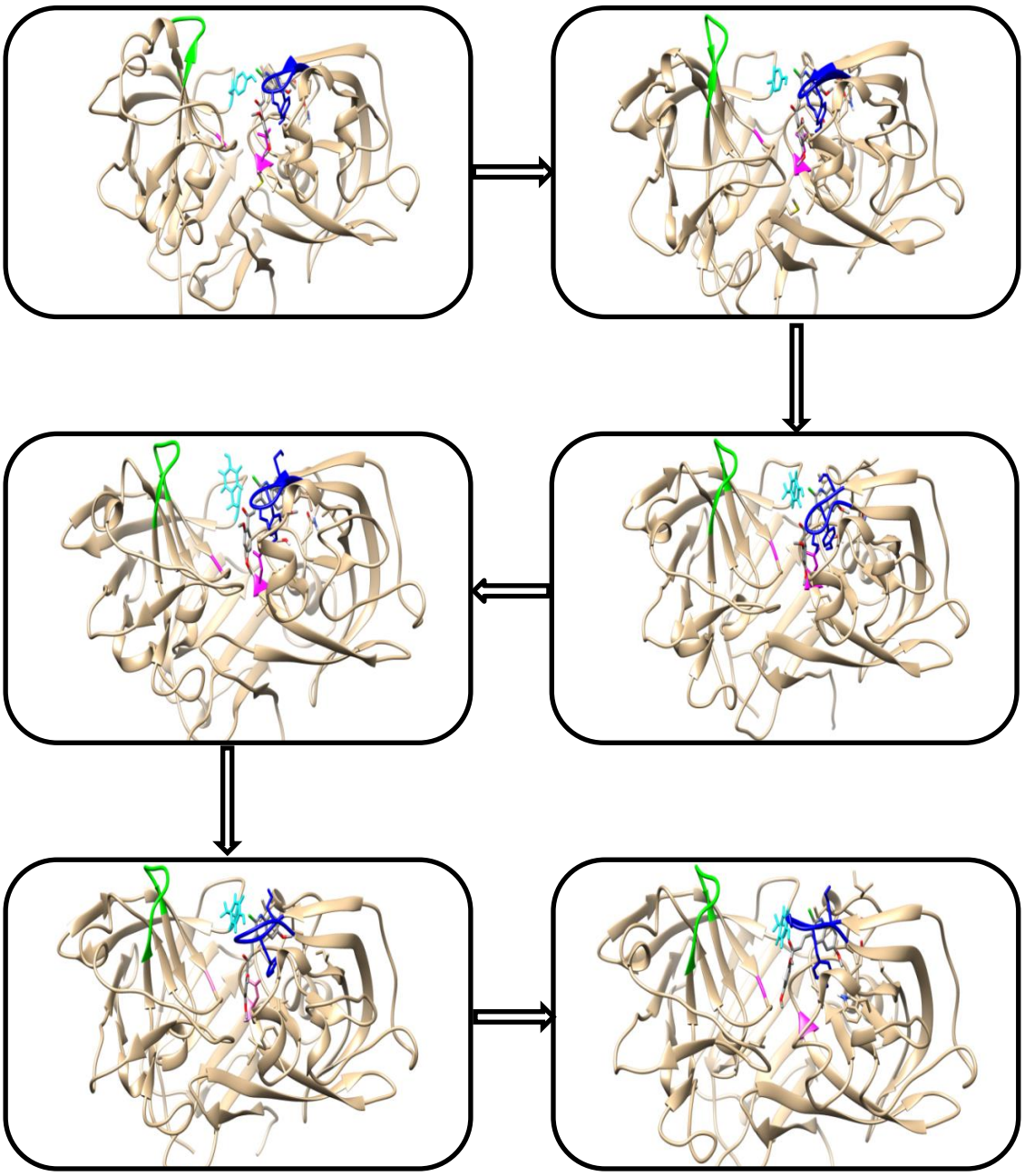
MD trajectory showing 30 nanoseconds (ns) molecular dynamic simulation of P3 bound to Plm-II (Magenta highlights the catalytic aspartic acid residues, blue is the flap, cyan is Tyr 192, green is flexible loop and P3 colored by element)

Appendix 9



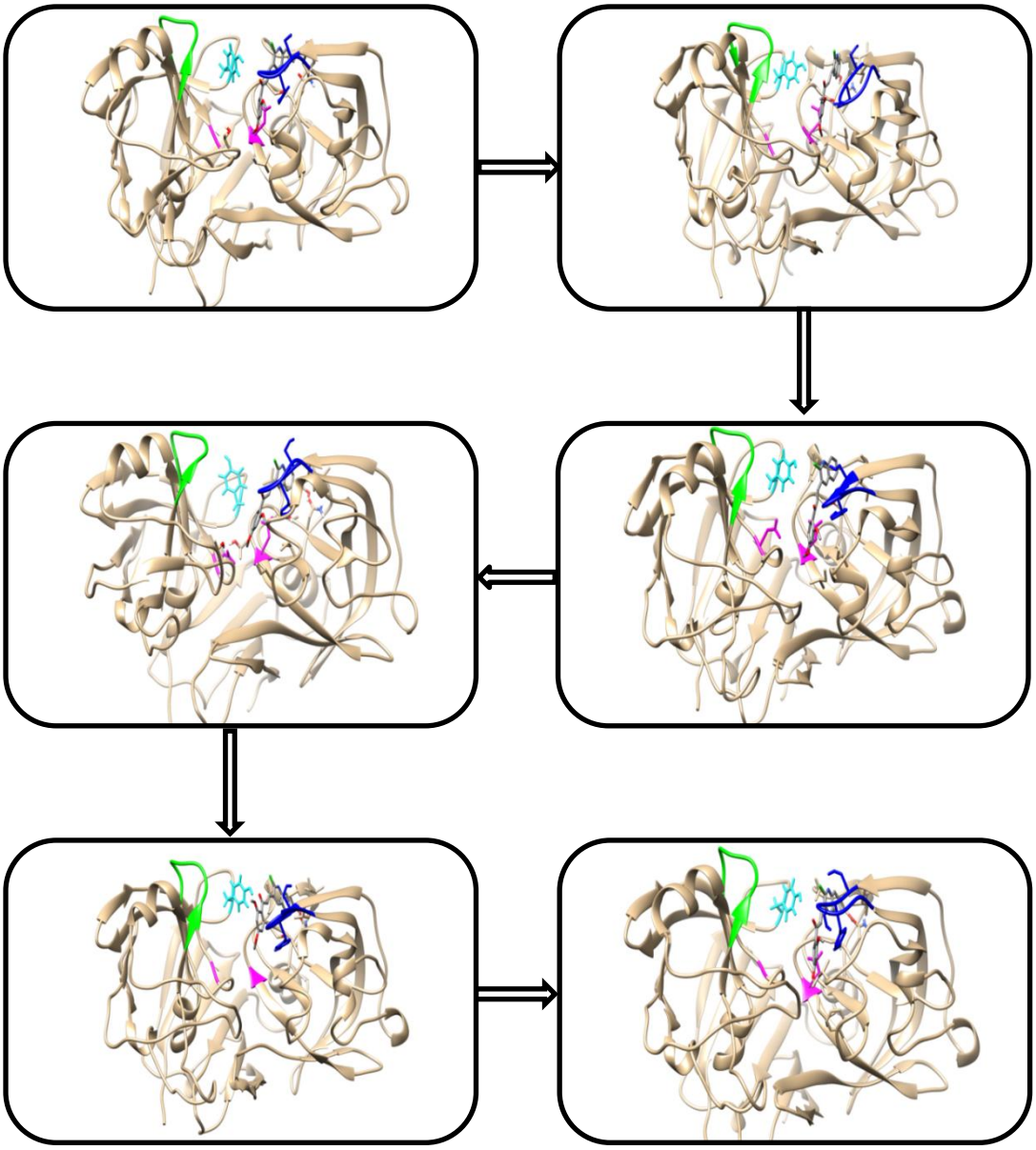
MD trajectory showing 30 nanoseconds (ns) molecular dynamic simulation of P4 bound to Plm-II. (Magenta highlights the catalytic aspartic acid residues, blue is the flap, cyan is Tyr 192, green is flexible loop and P3 colored by element)

Appendix 10



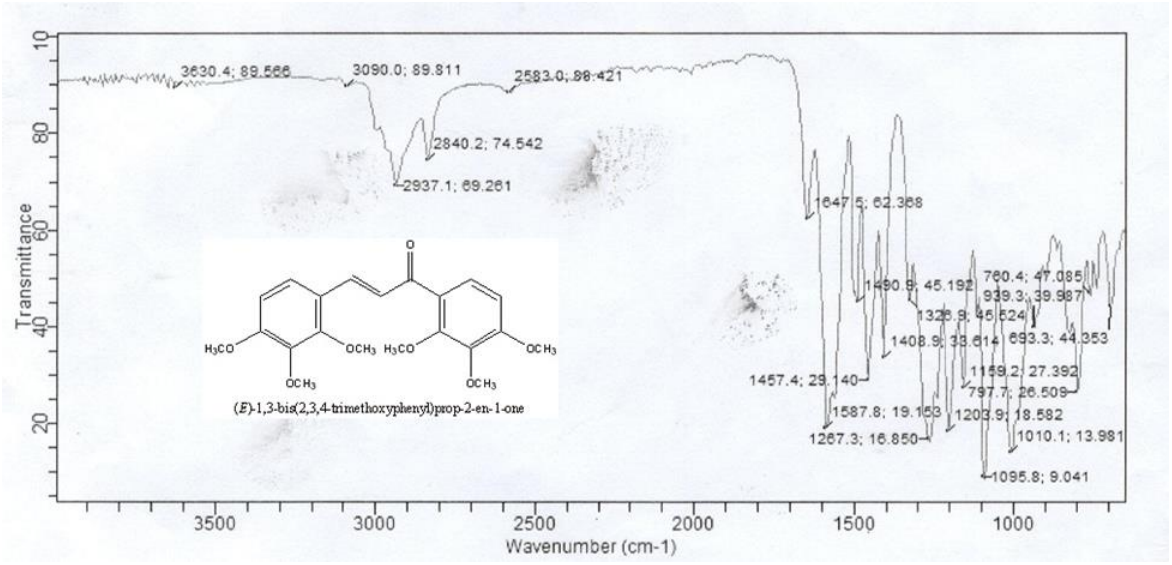
MD trajectory showing 30 nanoseconds (ns) molecular dynamic simulation of P3 bound to Plm-IV. (A magenta highlights the catalytic aspartic acid residues, blue is the flap, cyan is Tyr 192, green is flexible loop and P3 colored by element).

Appendix 11



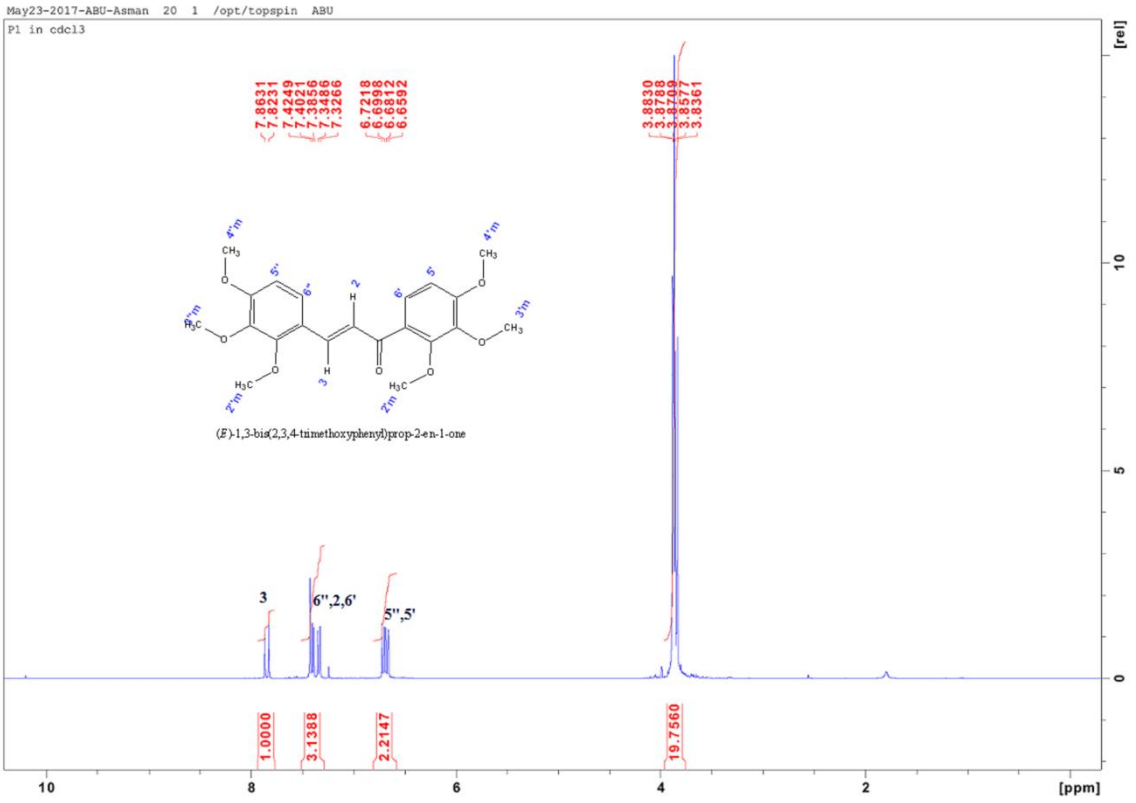
MD trajectory showing 30 nanoseconds (ns) molecular dynamic simulation of P4 bound to Plm-IV. (Magenta highlights the catalytic aspartic acid residues, blue is the flap, cyan is Tyr 192, green is flexible loop and P4 colored by element)

Appendix 12



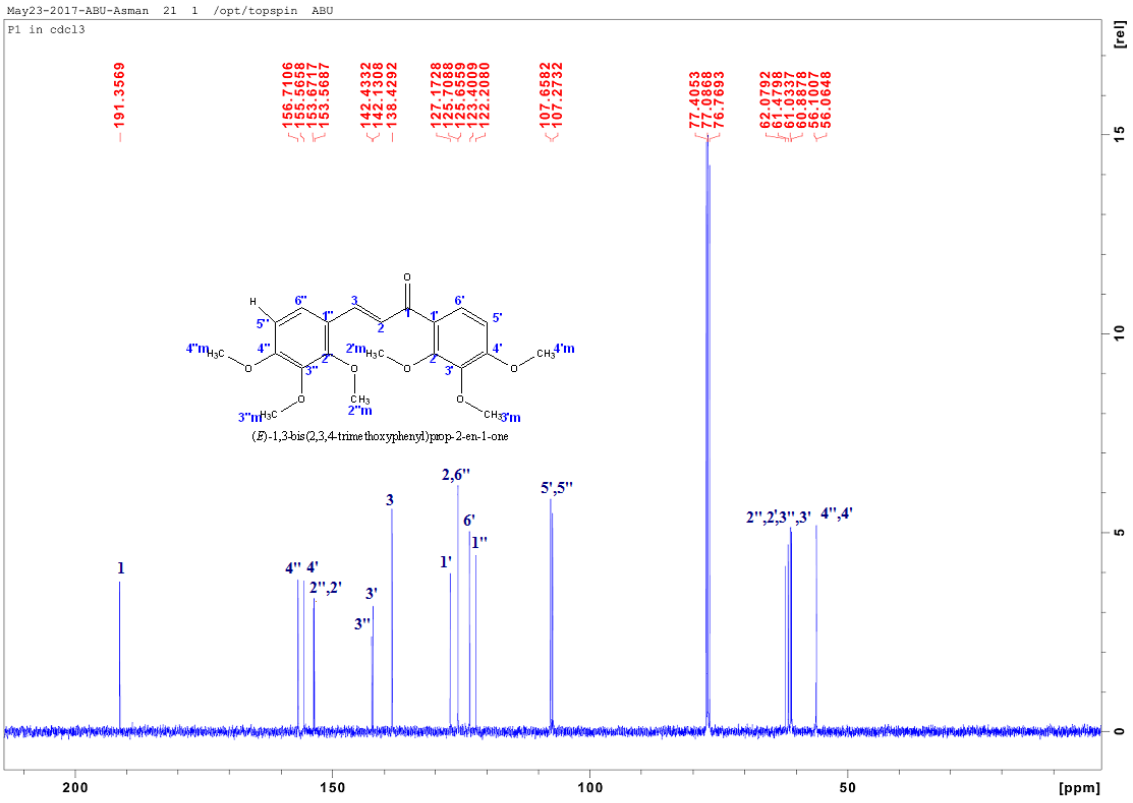
FT-IR Spectrum of P1

Appendix 13



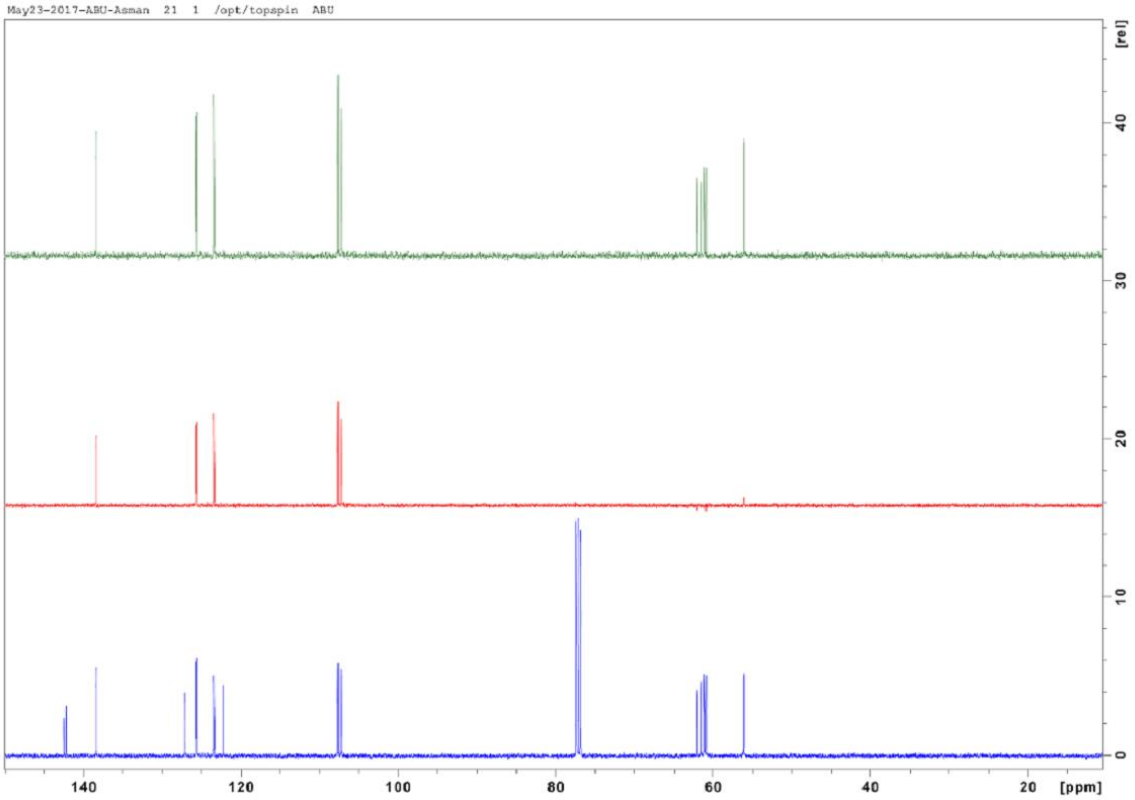
^{1}H NMR of compound P1

Appendix 14



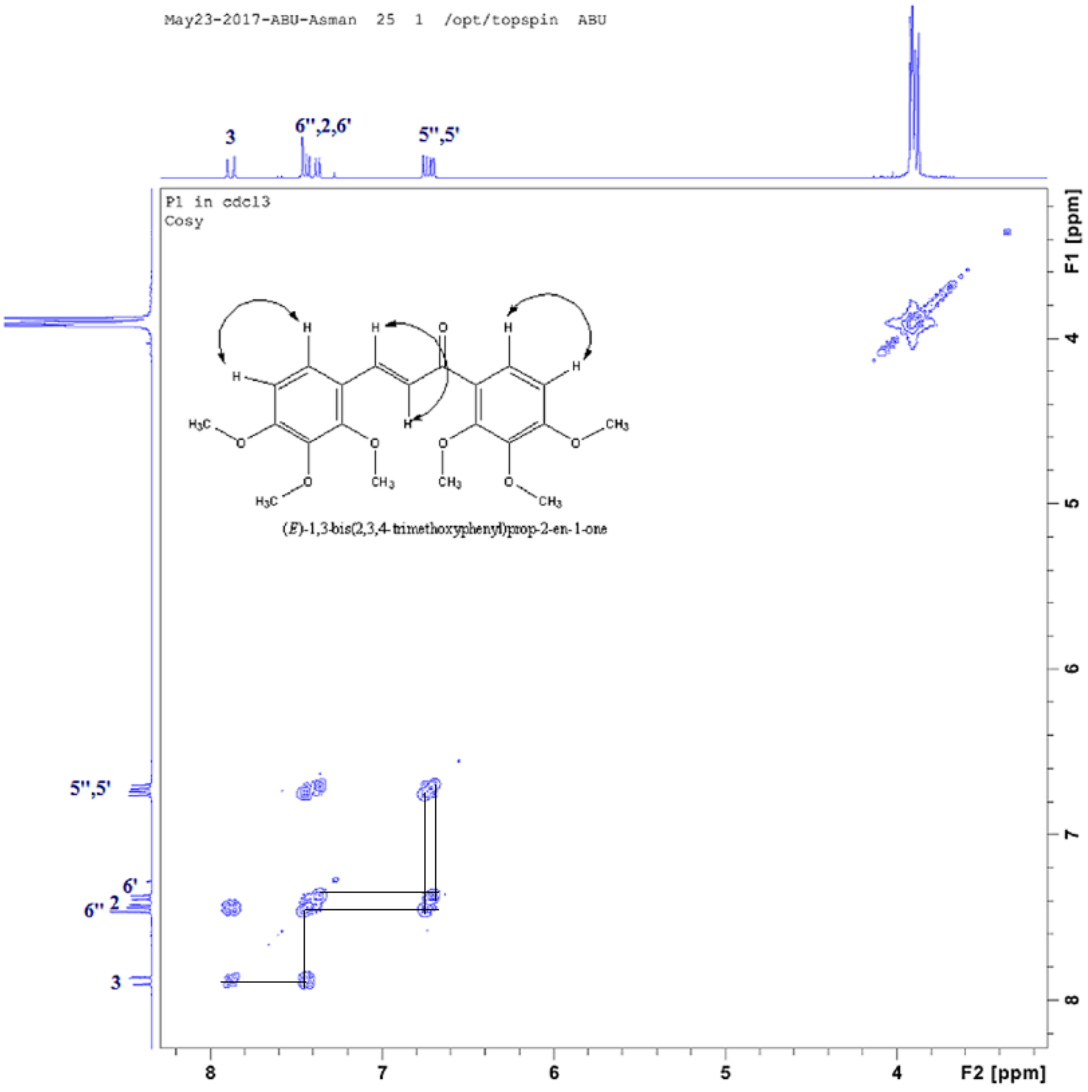
^{13}C NMR of compound P1

Appendix 15



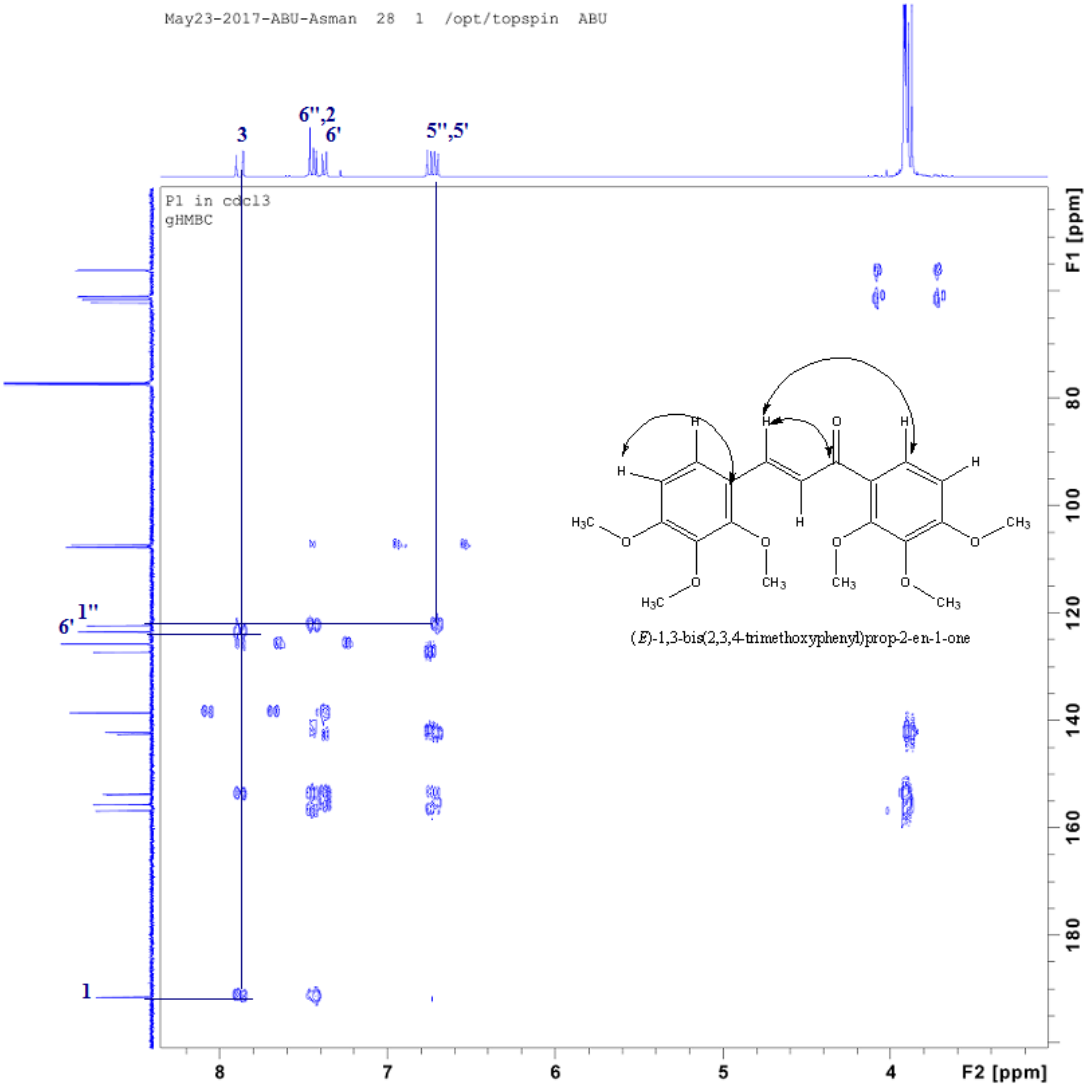
DEPT spectrum of compound P1

Appendix 16



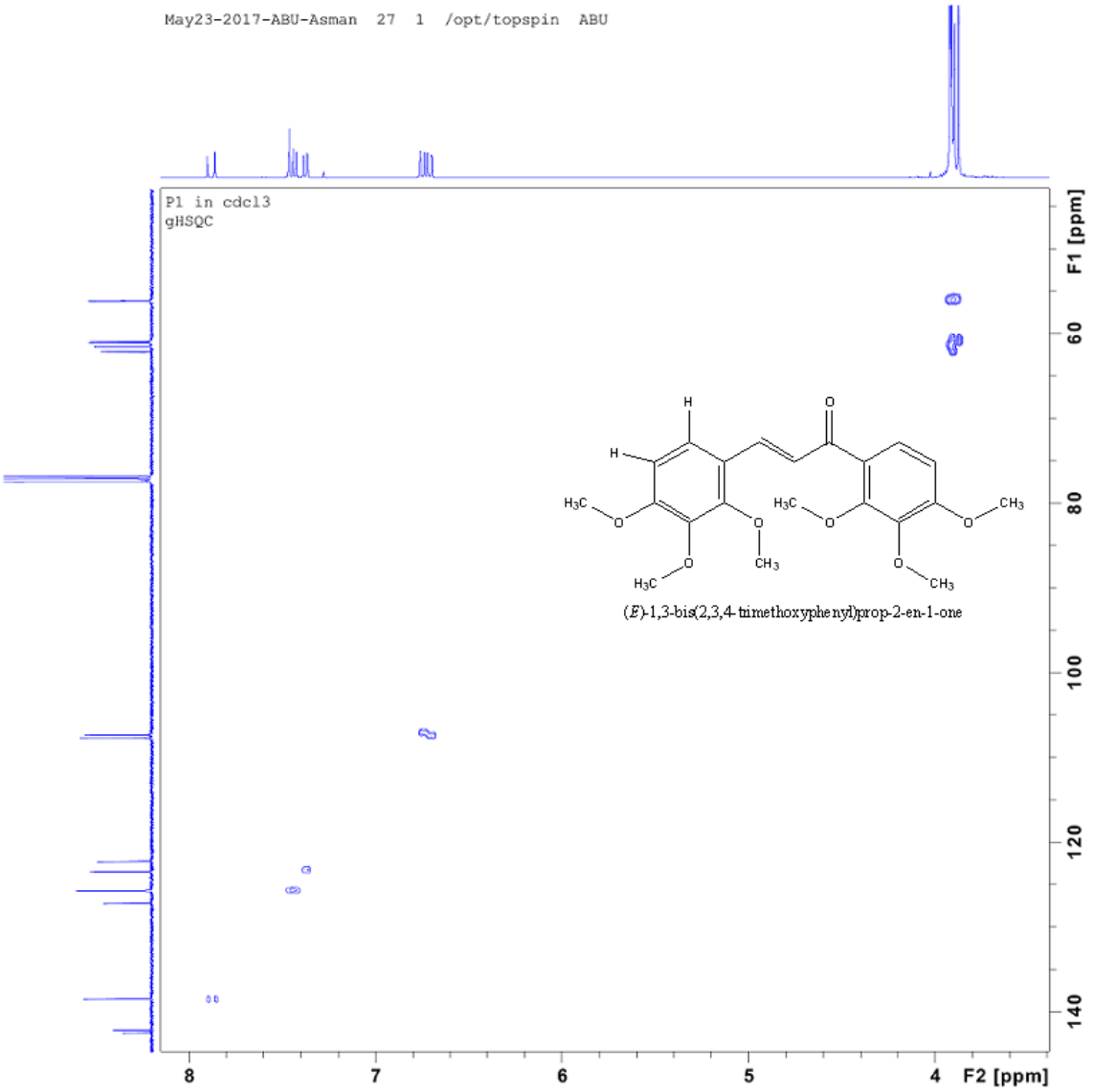
COSY spectrum of compound P1

Appendix 17



HMBC spectrum of compound P1

Appendix 18



HSQC spectrum of compound P1

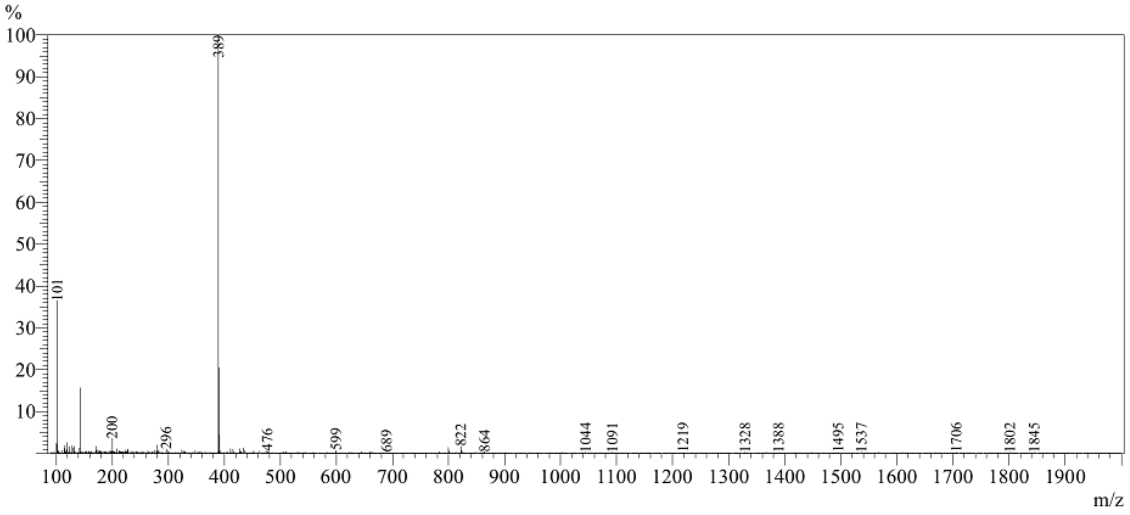
Appendix 19

Sample Information

Date Acquired	: 2017/05/30 08:07:12 AM
Sample Type	: Unknown
Sample Name	: p1
Sample ID	: p1
Data File	: p1.lcd
Method File	: lemien.lcm
Report Format File	: DEFAULT.lsr
Tuning File	: 12042017 repeat repeat.lct

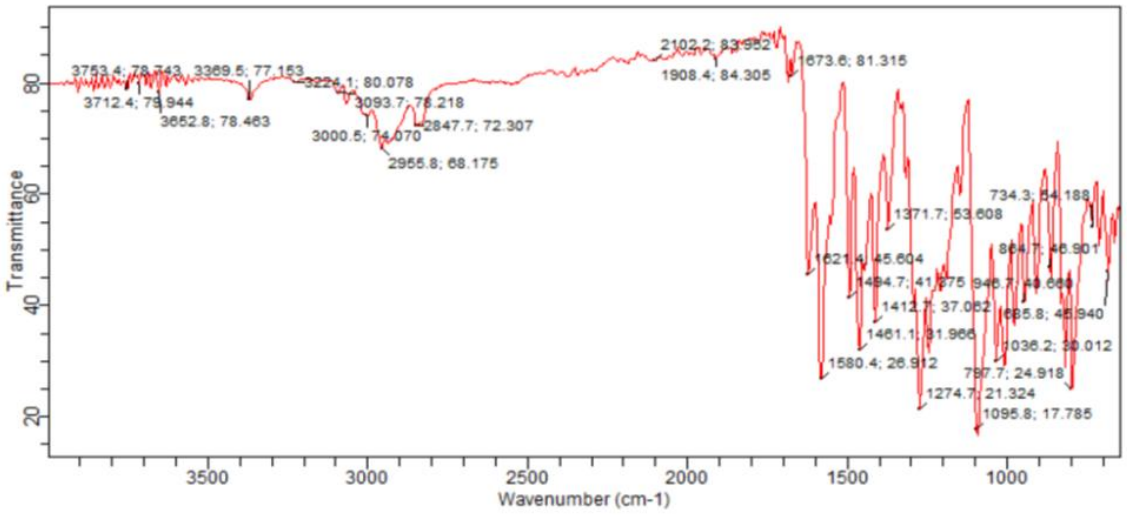
MS Spectrum

R.Time:1.067(Scan#:65)
MassPeaks:1935
Segment 1 - Event 1



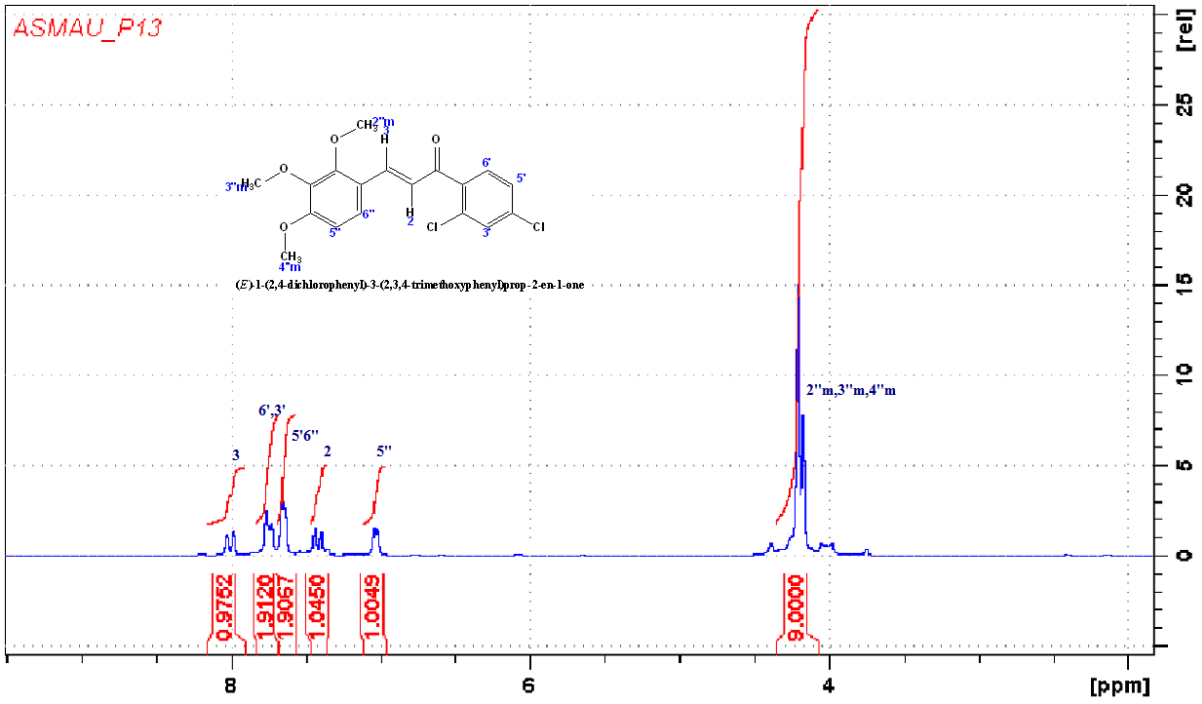
Mass spectrum of P1

Appendix 20



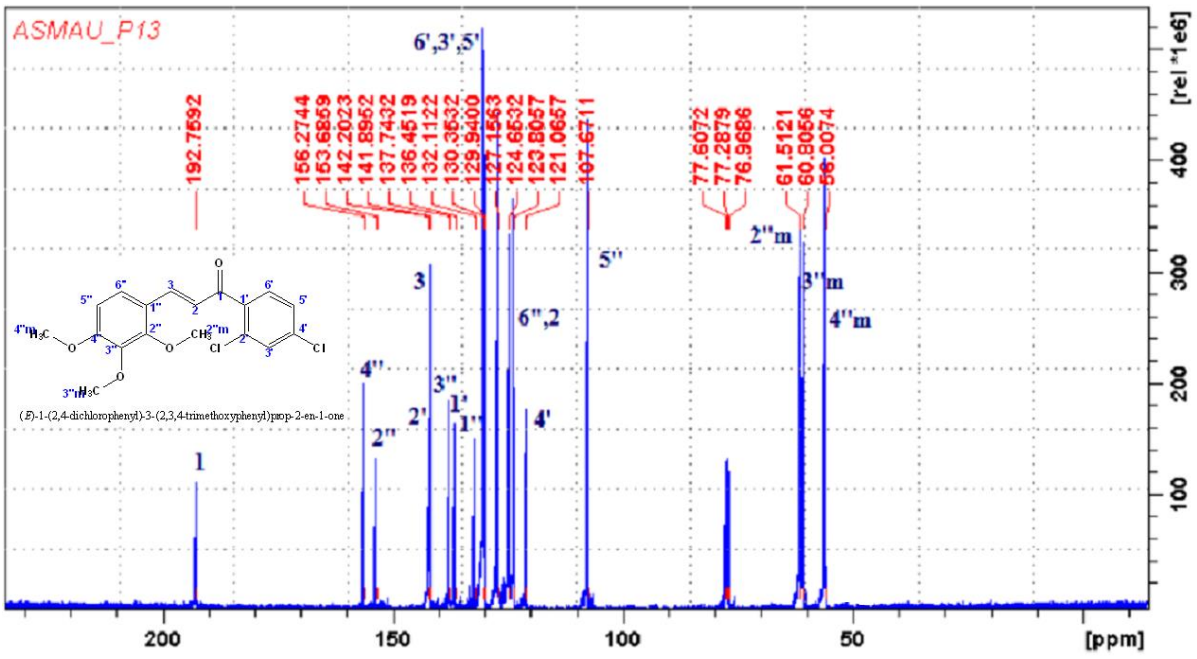
FT-IR Spectrum of P13

Appendix 21



^{1}H NMR of compound P13

Appendix 22



^{13}C NMR of compound P13

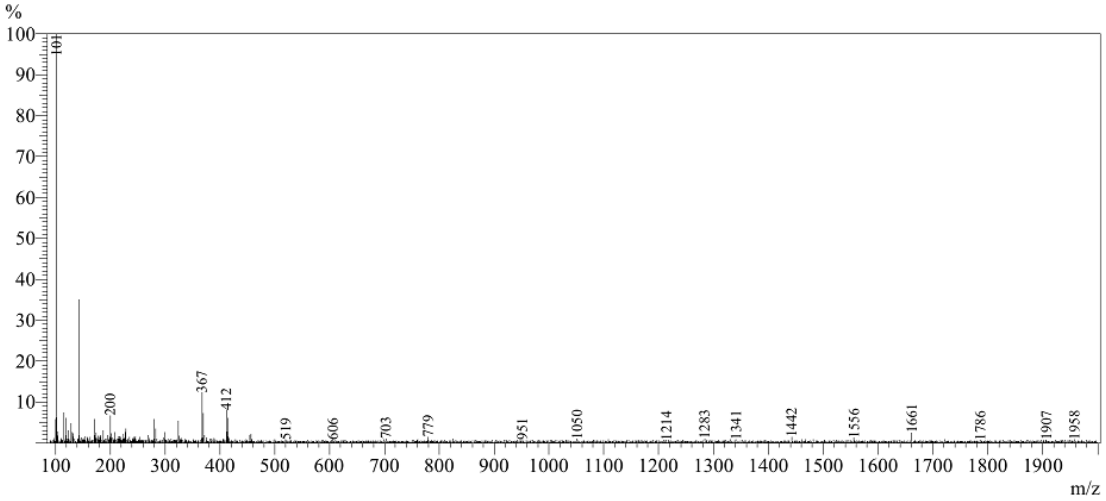
Appendix 23

Sample Information

Date Acquired	: 2017/05/30 09:39:25 AM
Sample Type	: Unknown
Sample Name	: p13
Sample ID	: p13
Data File	: p13.lcd
Method File	: lemien.lcm
Report Format File	: DEFAULT.lsr
Tuning File	: 12042017 repeat repeat.lct

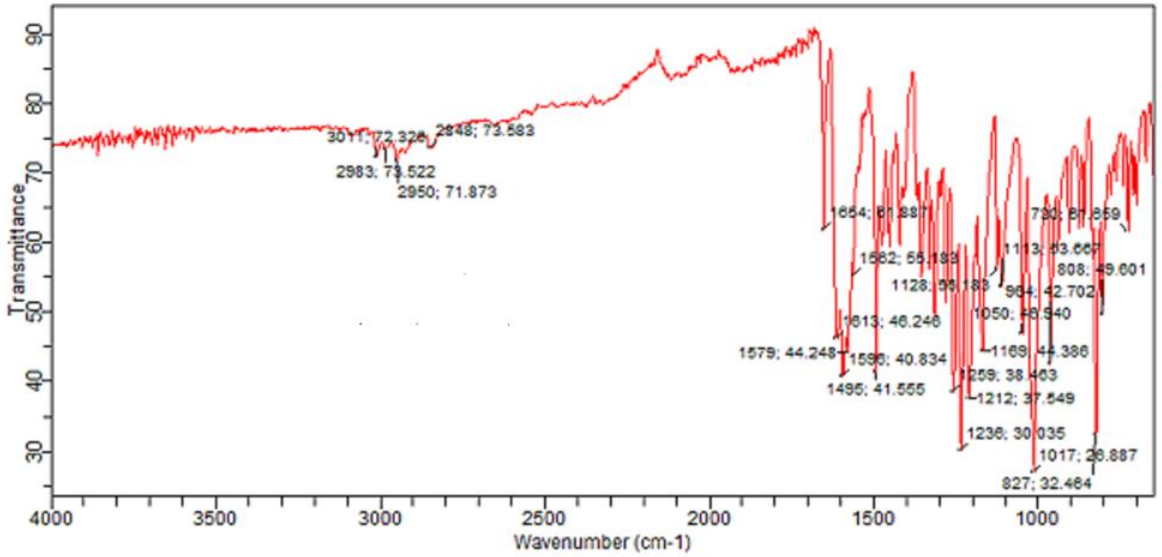
MS Spectrum

R.Time:1.067(Scan#:65)
MassPeaks:1923
Segment 1 - Event 1



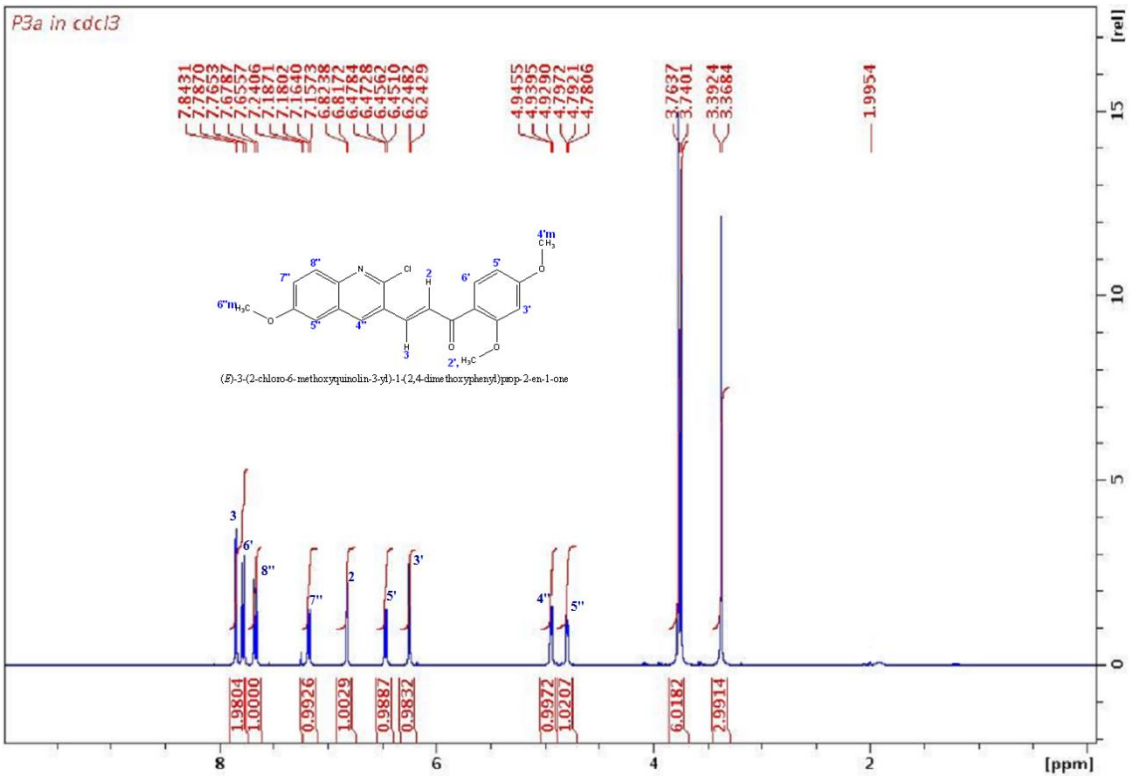
Mass spectrum of P13

Appendix 24



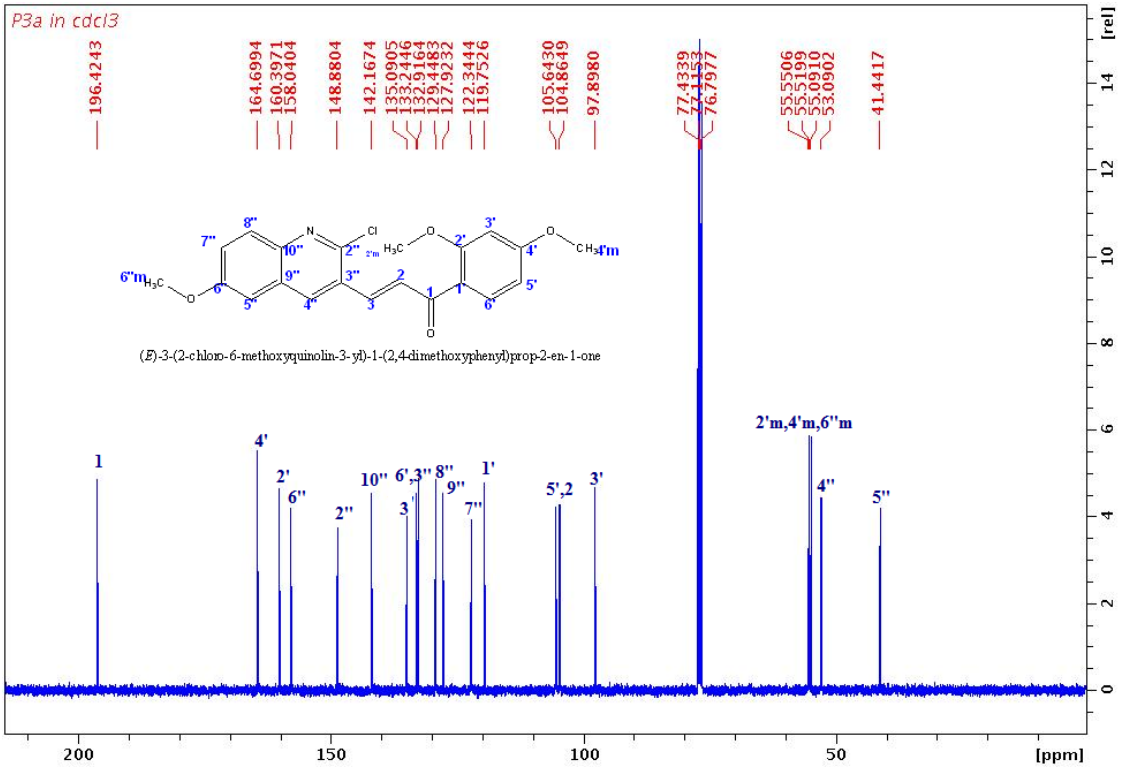
FT-IR Spectrum of P3

Appendix 25



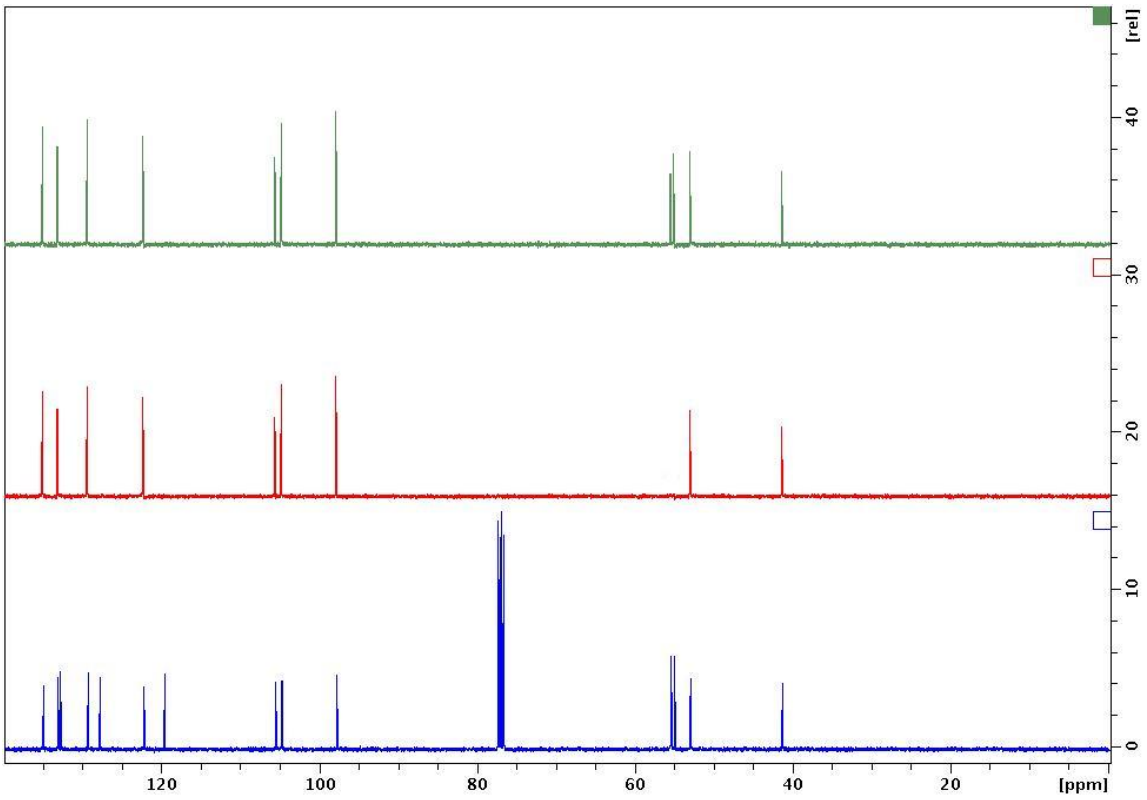
^{1}H NMR of compound P3

Appendix 26



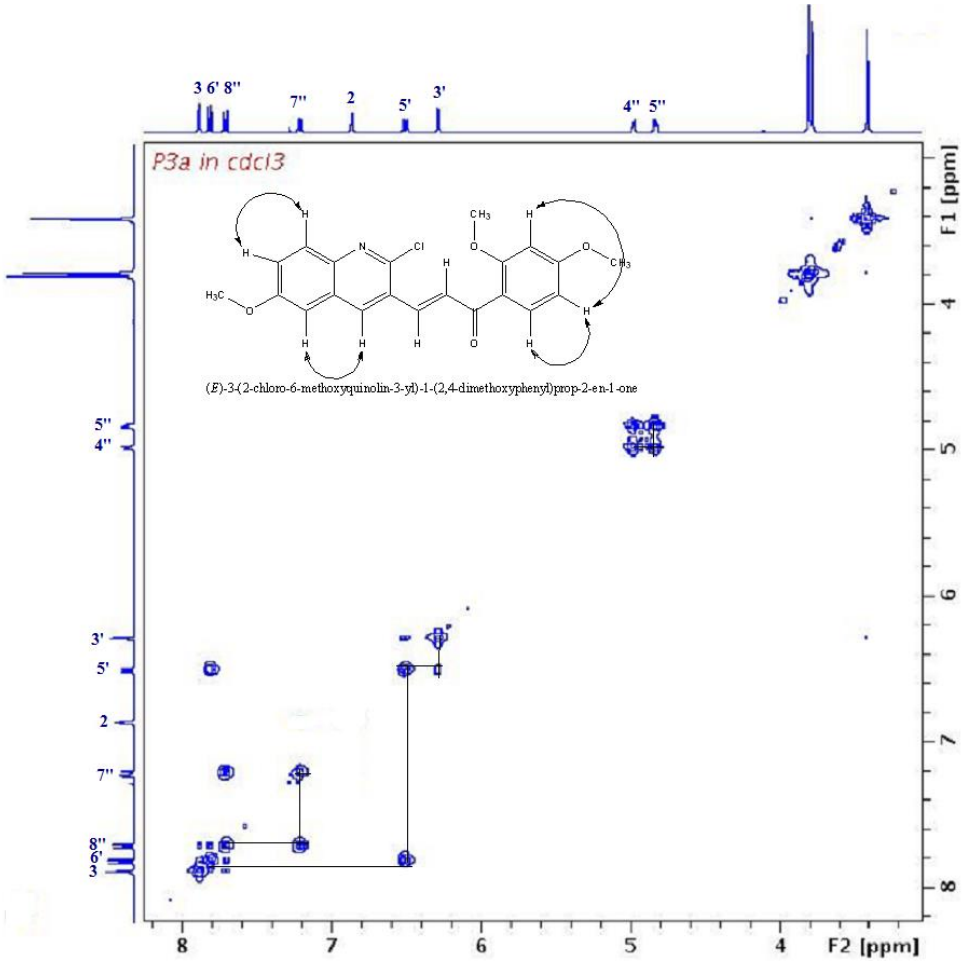
^{13}C NMR of compound P3

Appendix 27



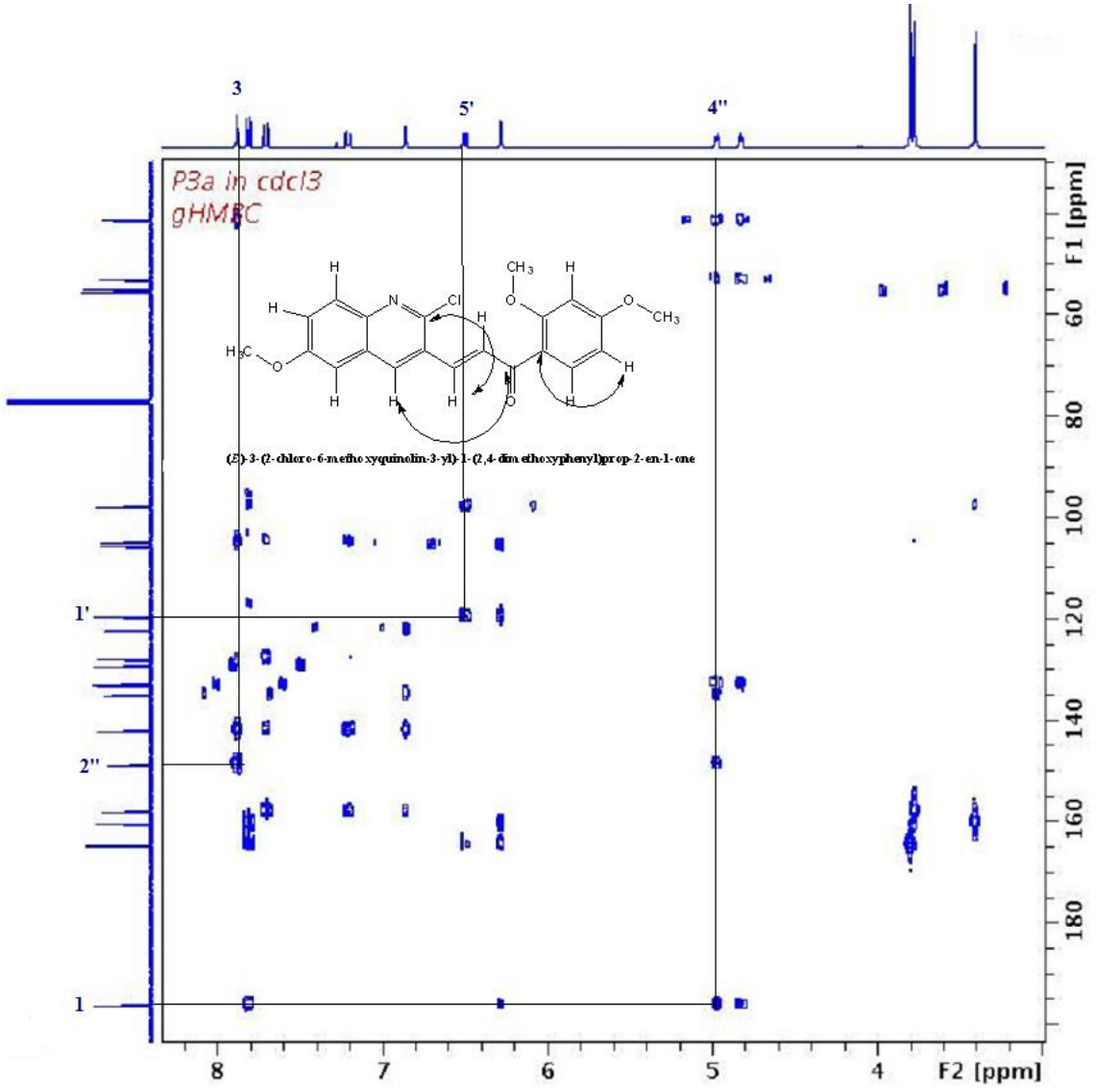
DEPT spectrum of compound P3

Appendix 28



COSY spectrum of compound P3

Appendix 29



HMBC spectrum of compound P3

Appendix 30

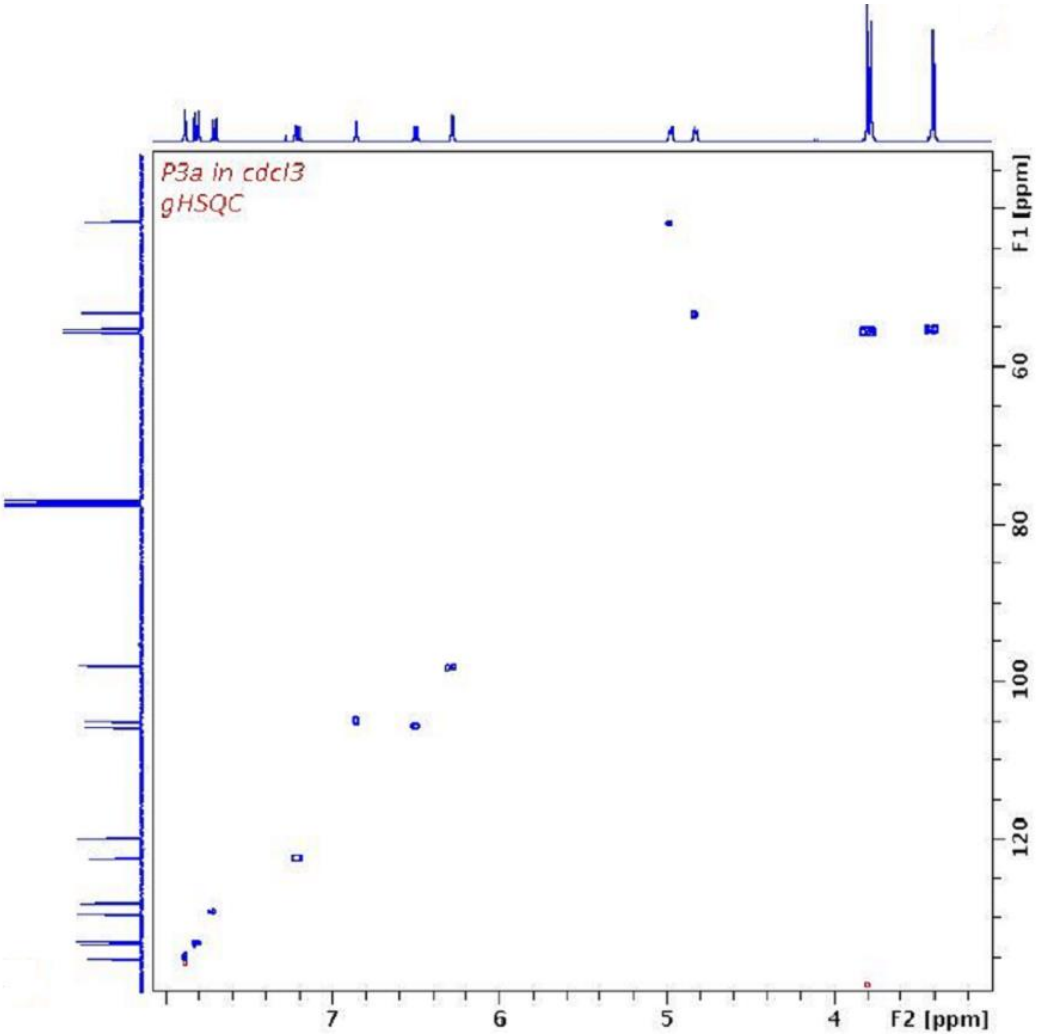
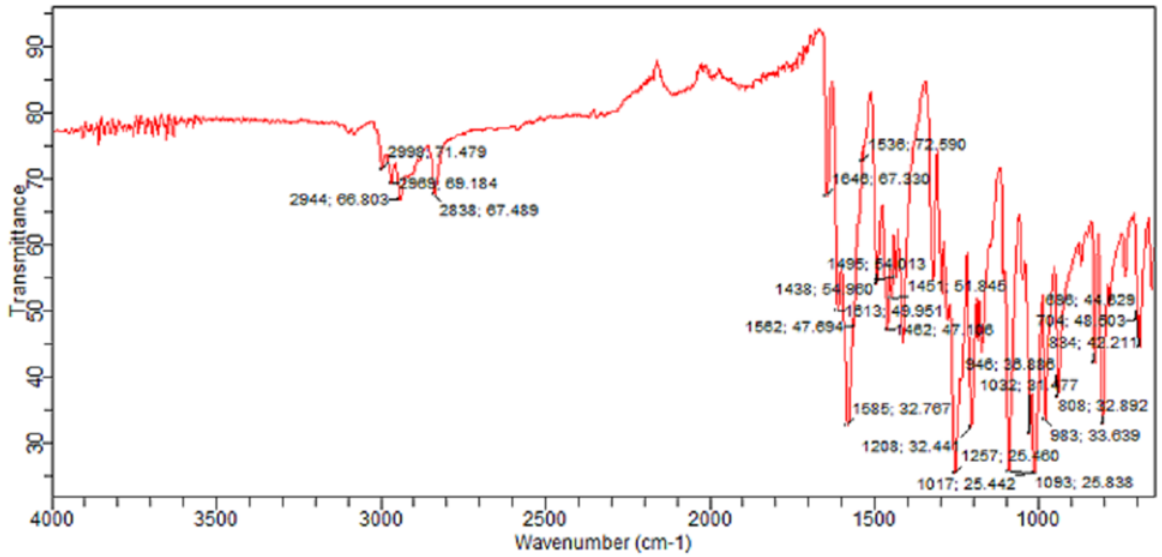


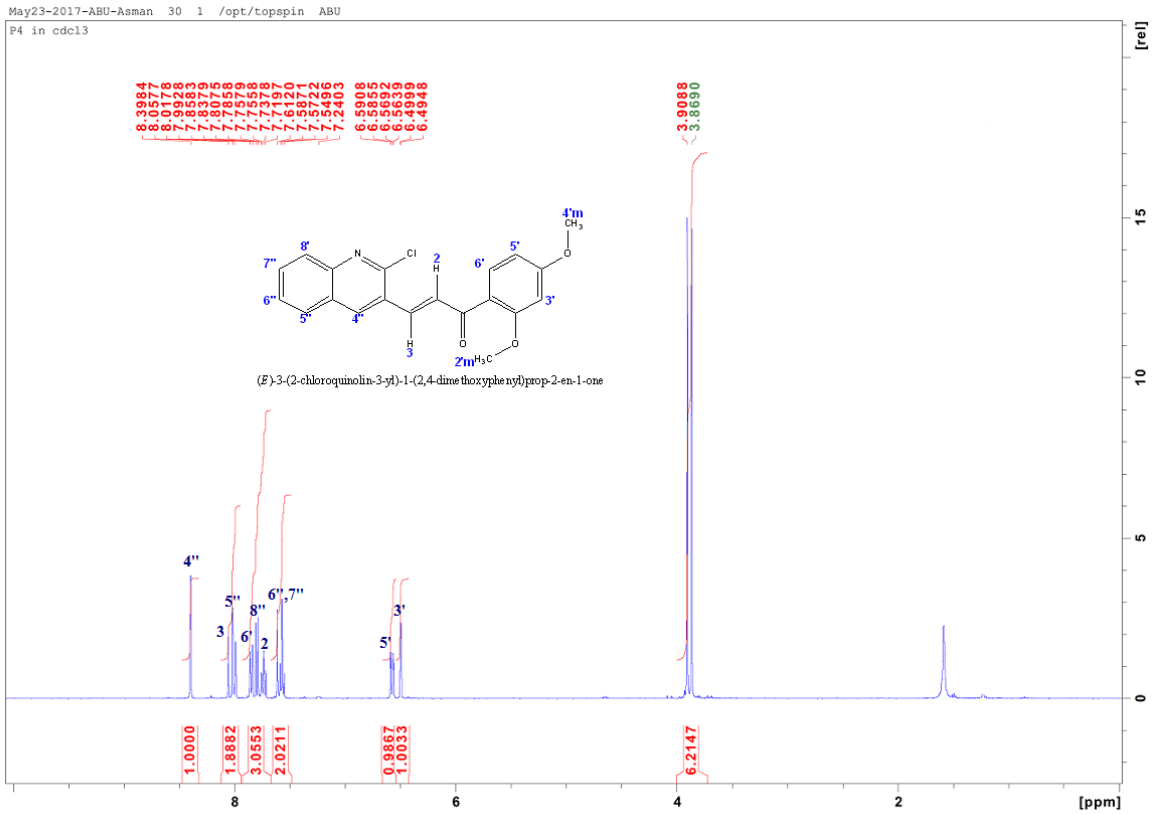
Figure: HSQC spectrum of compound P3

Appendix 31



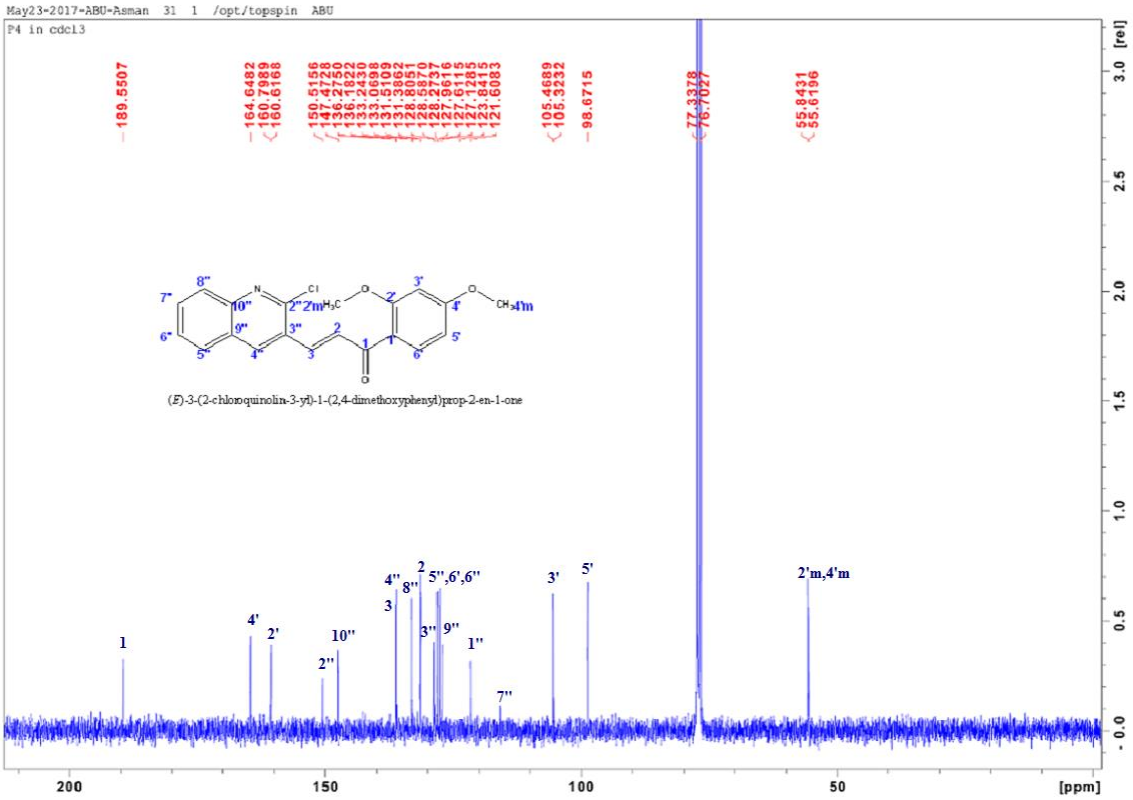
FT-IR Spectrum of P4

Appendix 32



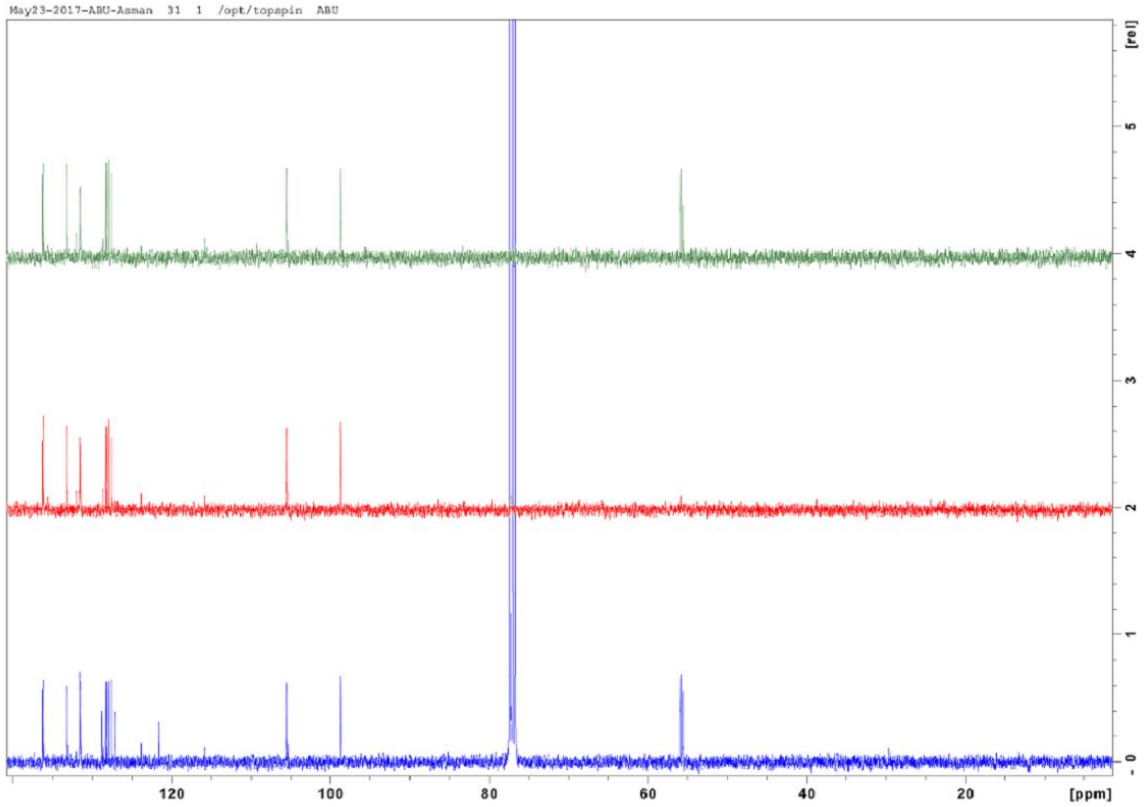
^{1}H NMR of compound P4

Appendix 33



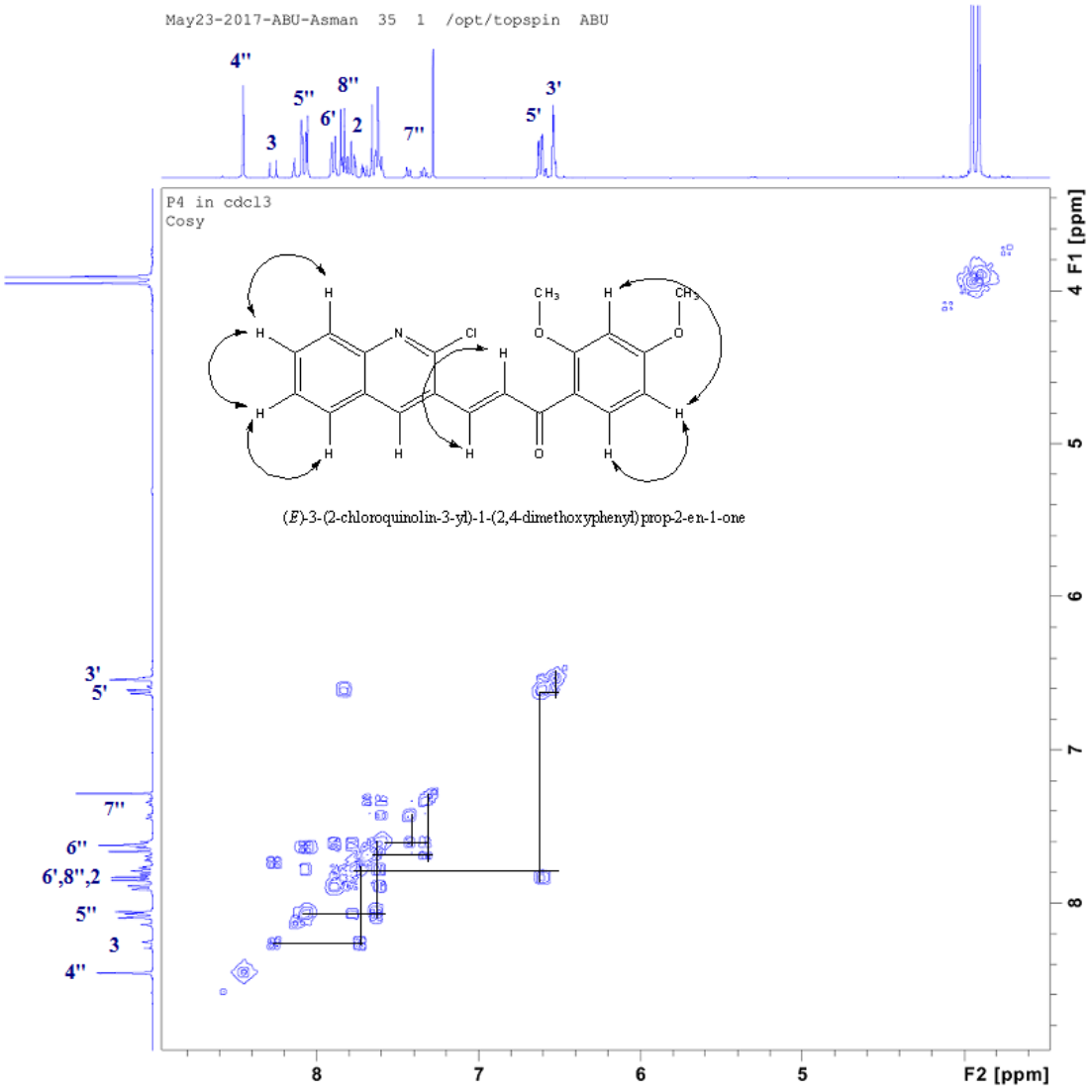
^{13}C NMR of compound P4

Appendix 34



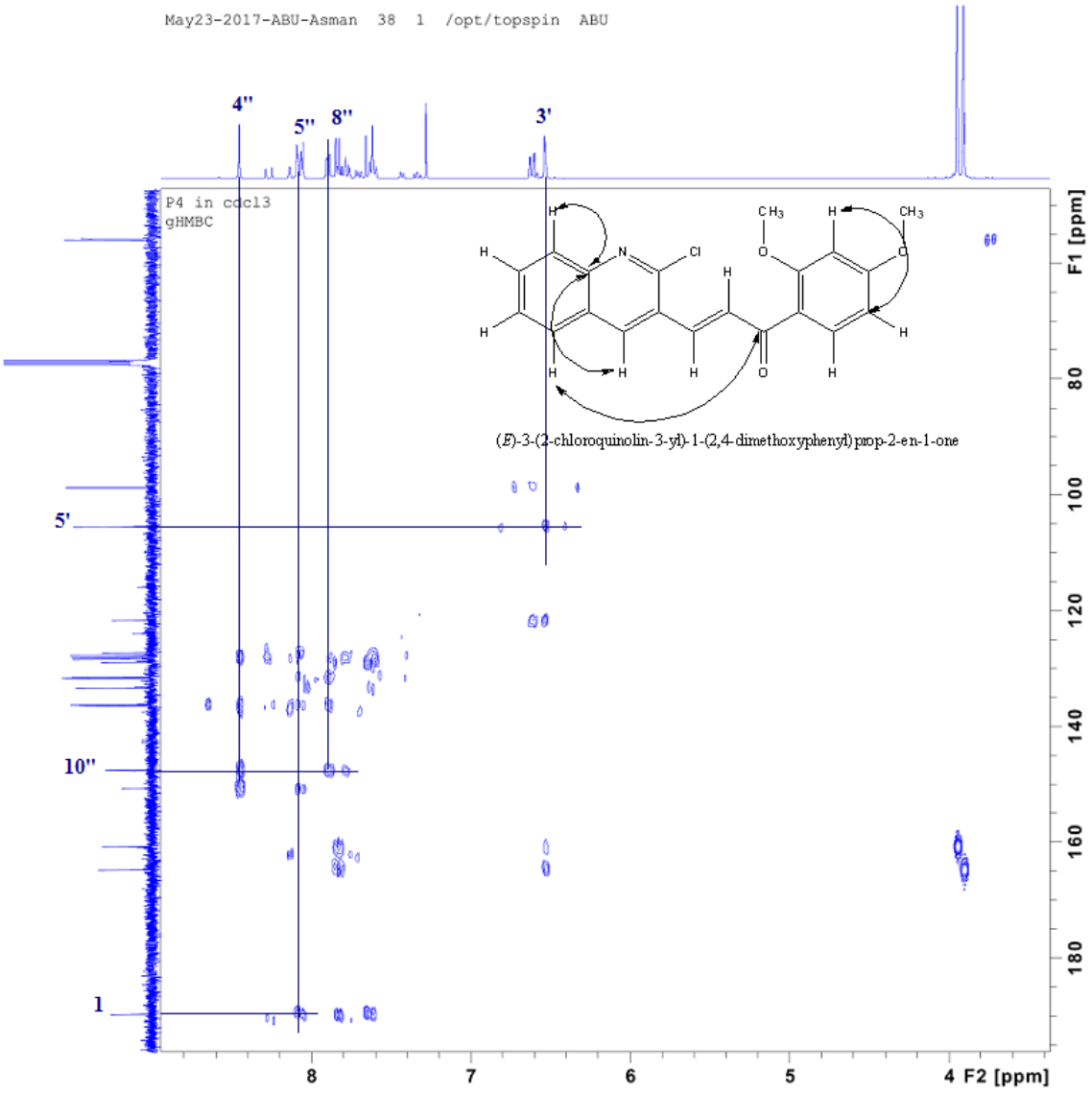
DEPT spectrum of compound P4

Appendix 35



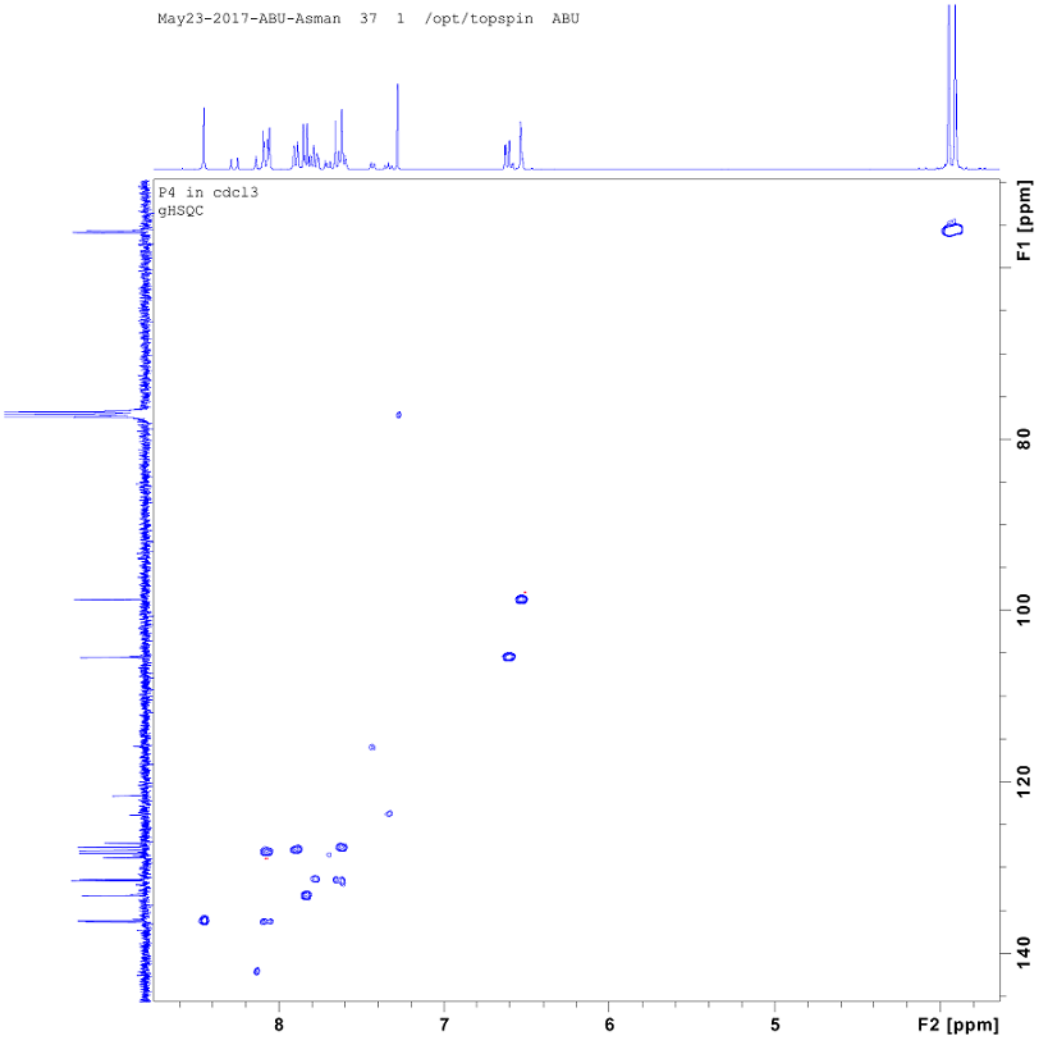
COSY spectrum of compound P4

Appendix 36



HMBC spectrum of compound P4

Appendix 37



HSQC spectrum of compound P4

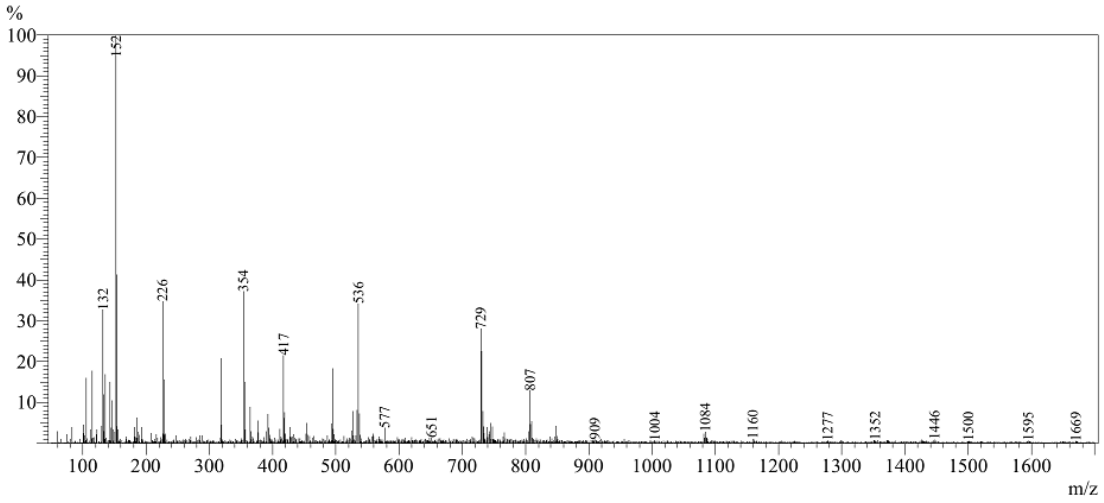
Appendix 38

Sample Information

Date Acquired	: 2017/05/30 11:21:35 AM
Sample Type	: Unknown
Sample Name	: p4f
Sample ID	: p4f
Data File	: p4f.lcd
Method File	: no column run.lcm
Report Format File	: DEFAULT.lsr
Tuning File	: 12042017 repeat repeat.lct

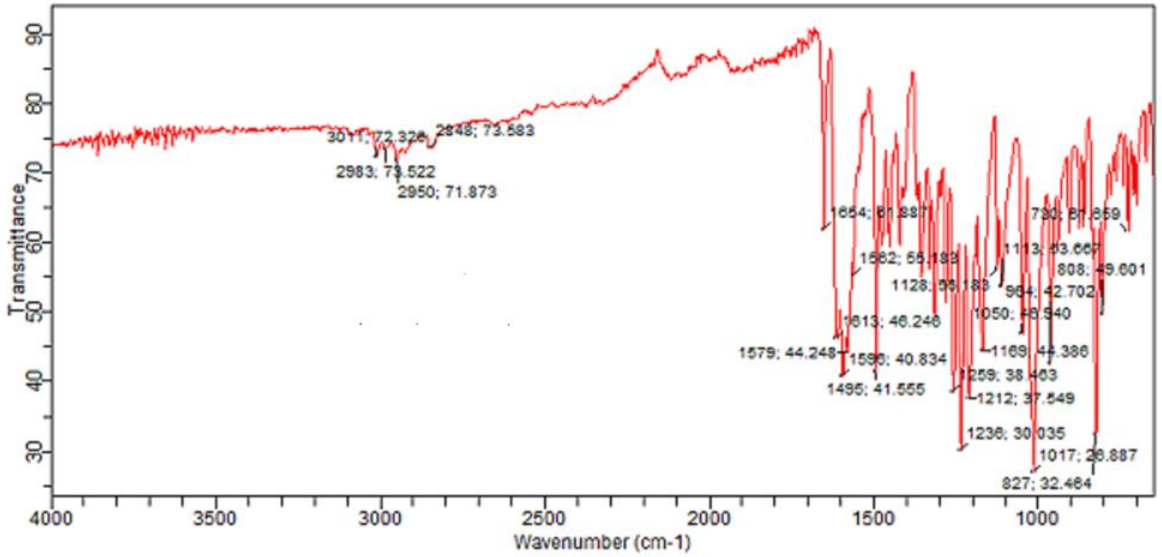
MS Spectrum

R.Time:1.067(Scan#:65)
MassPeaks:1716
Segment 1 - Event 1



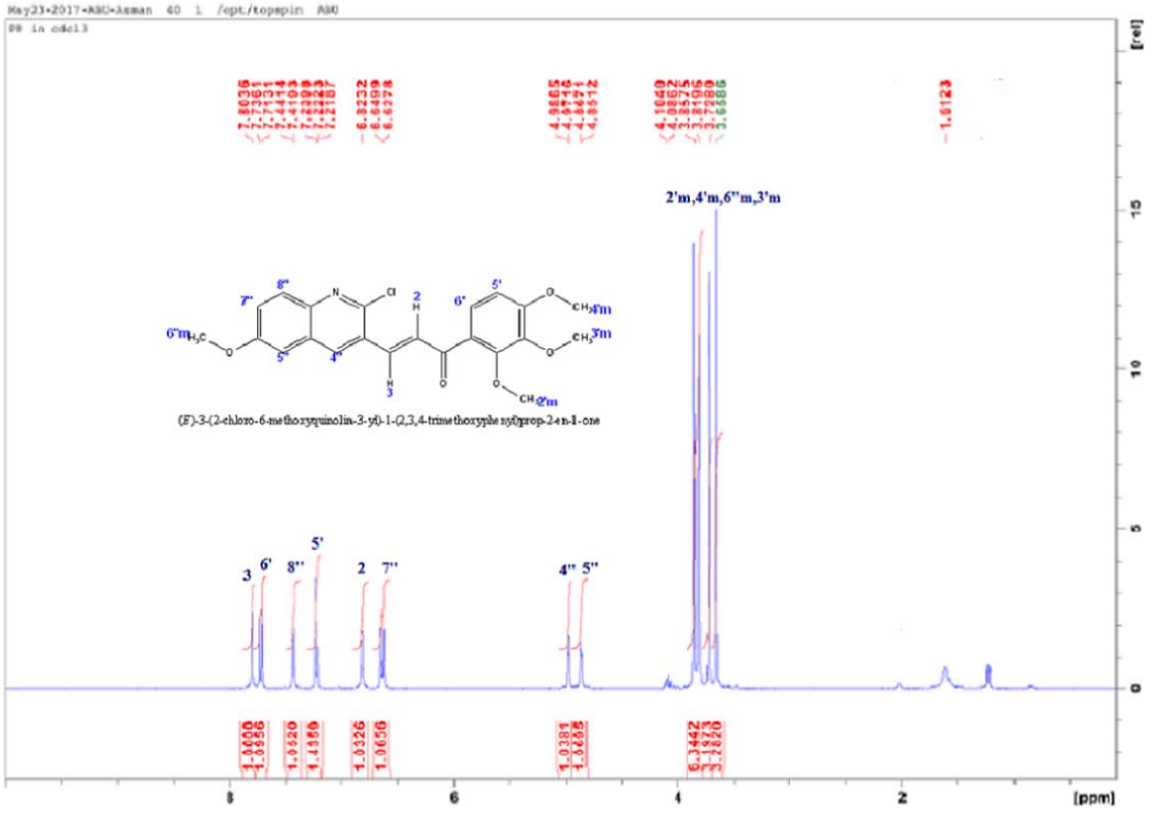
Mass spectrum of P4

Appendix 39



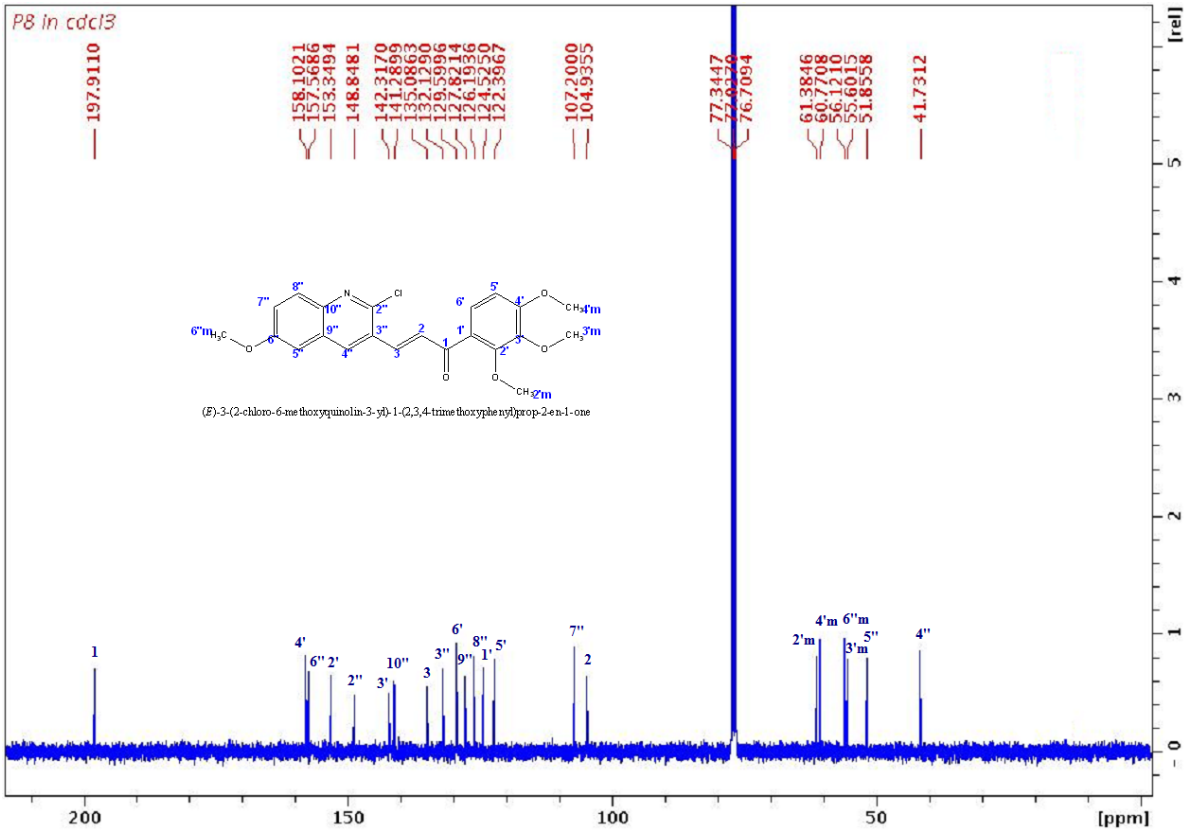
FT-IR Spectrum of P8

Appendix 40



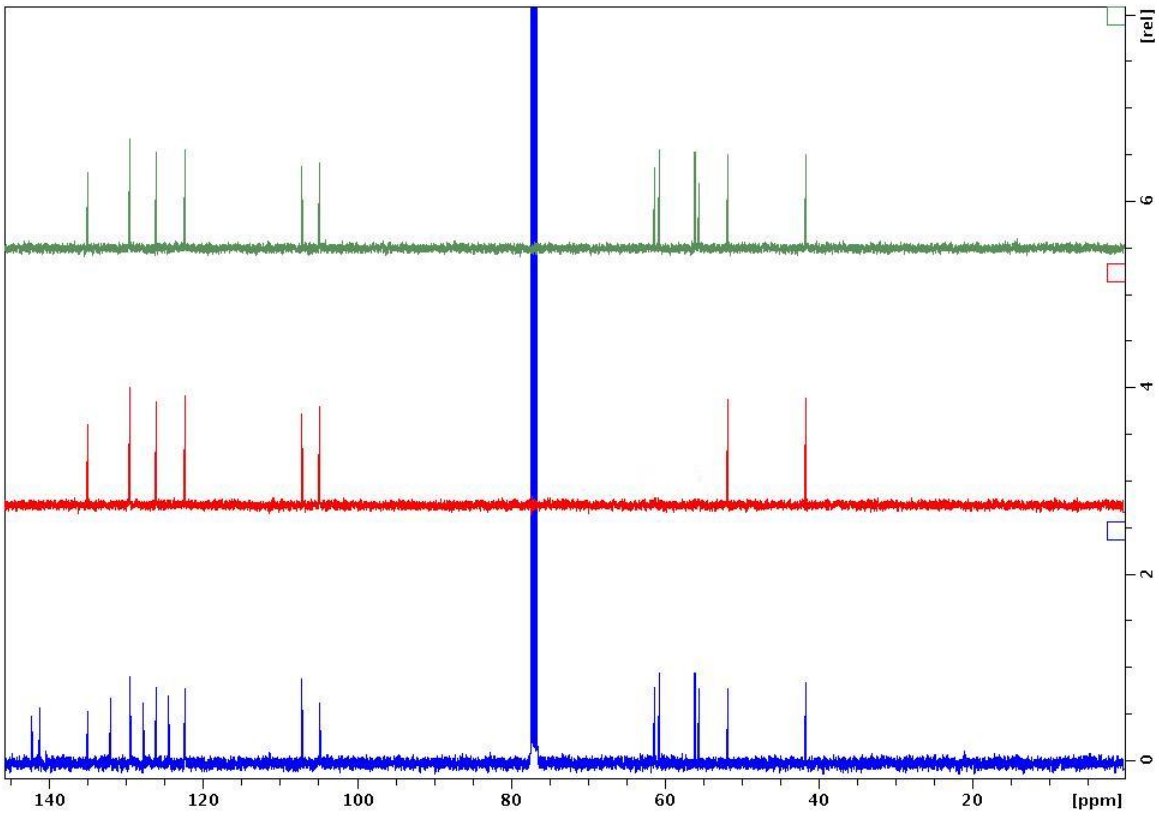
^{1}H NMR of compound P8

Appendix 41



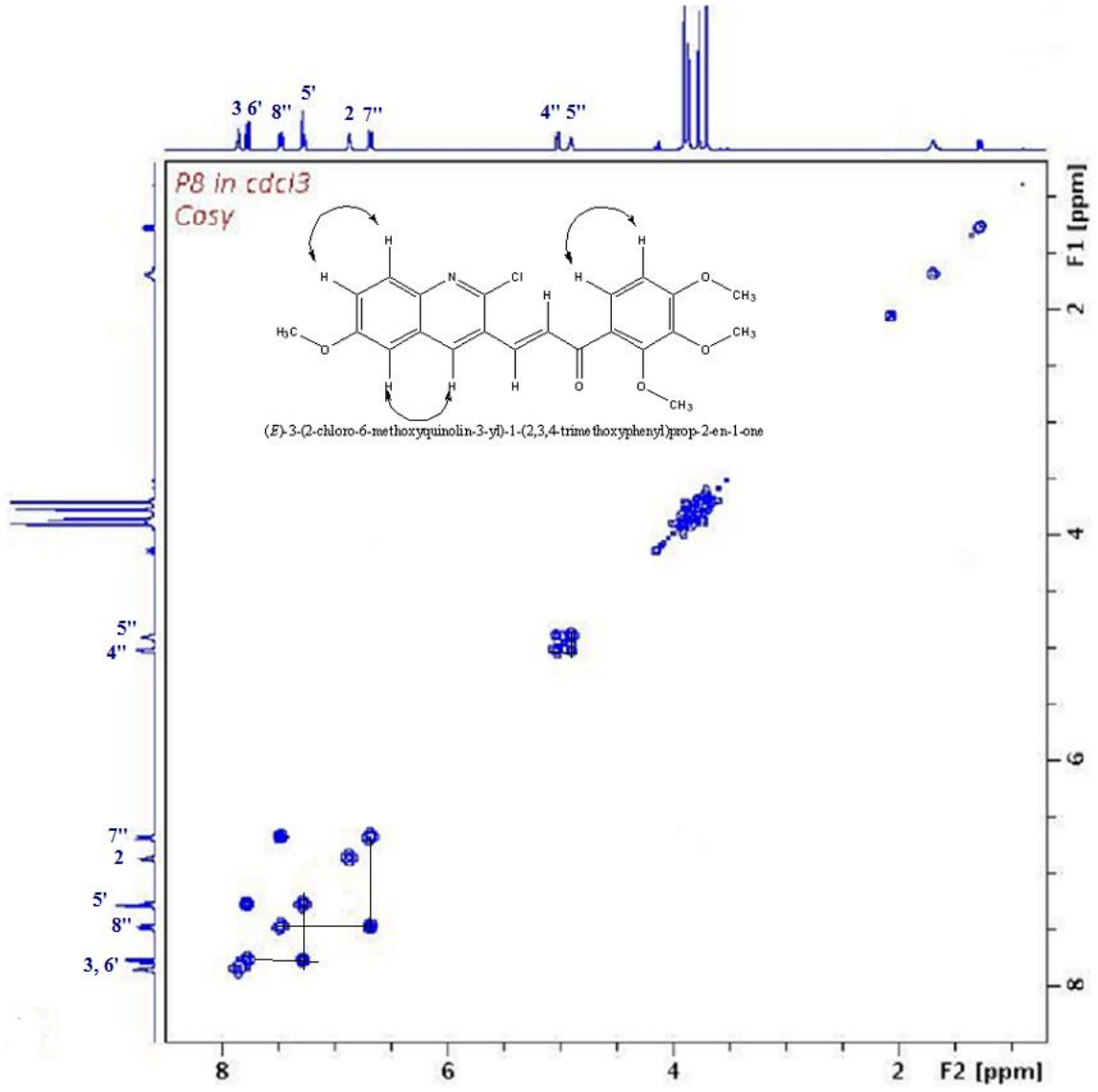
^{13}C NMR of compound P8

Appendix 42



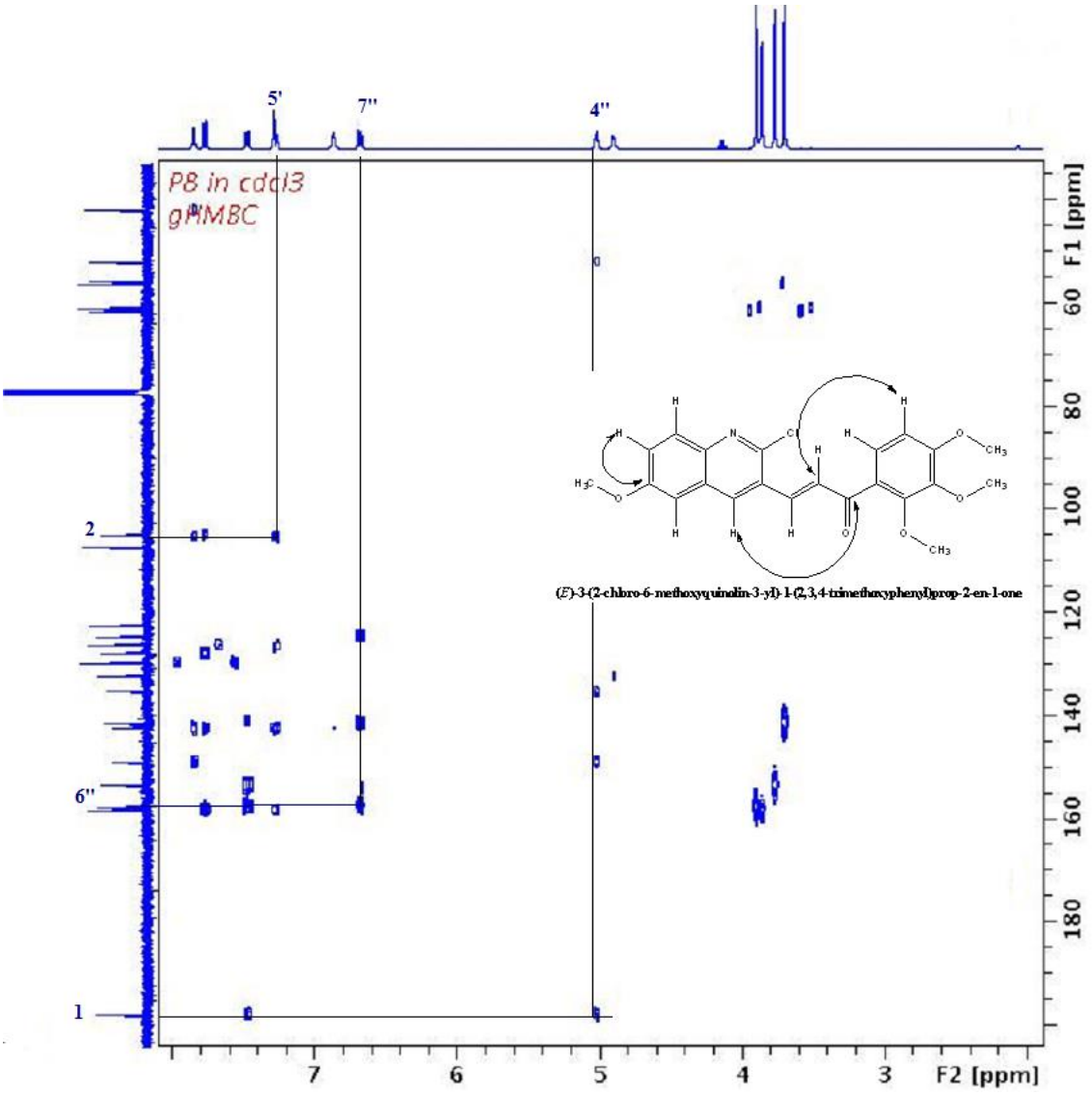
DEPT spectrum of compound P8

Appendix 43



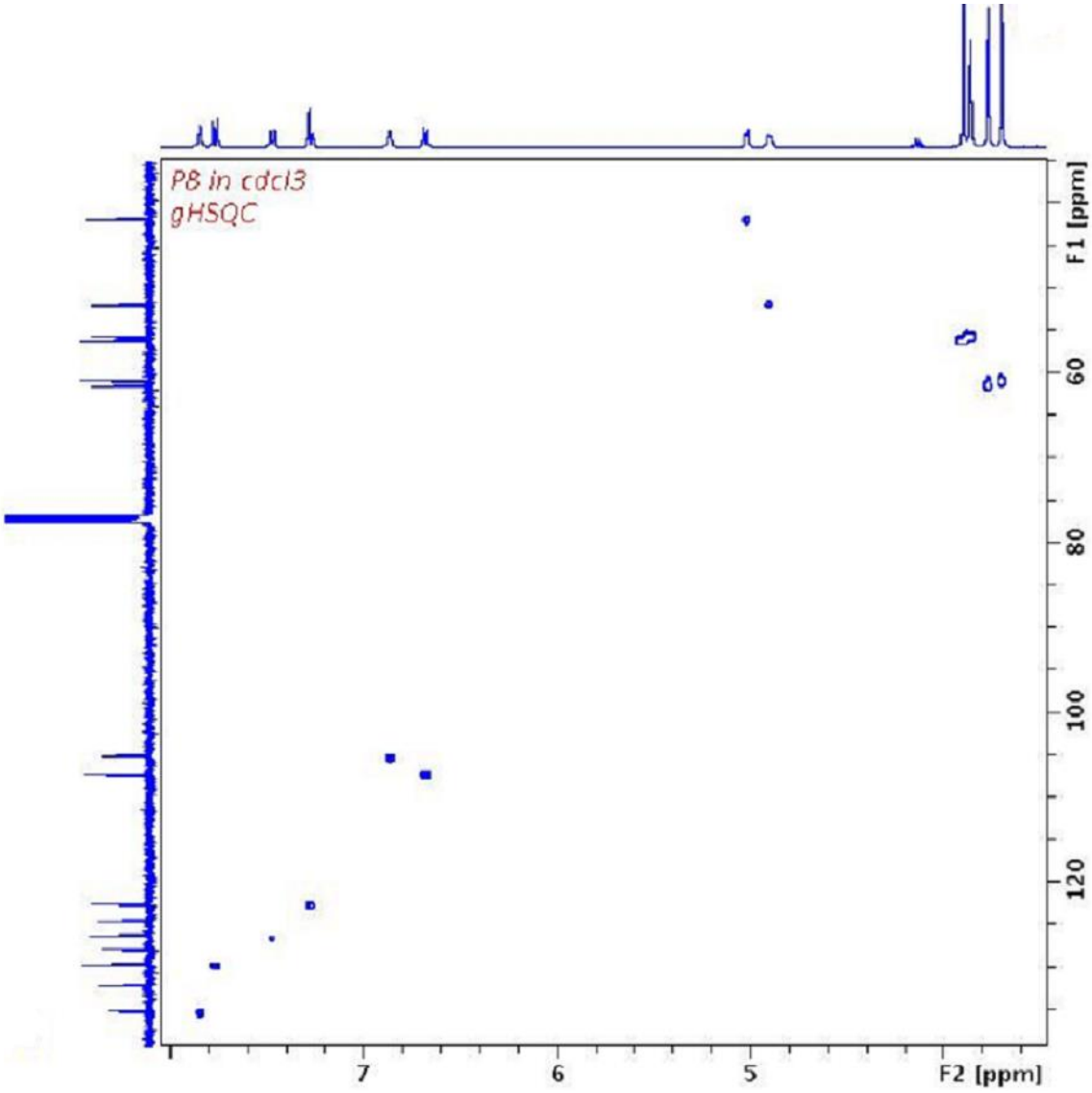
COSY spectrum of compound P8

Appendix 44



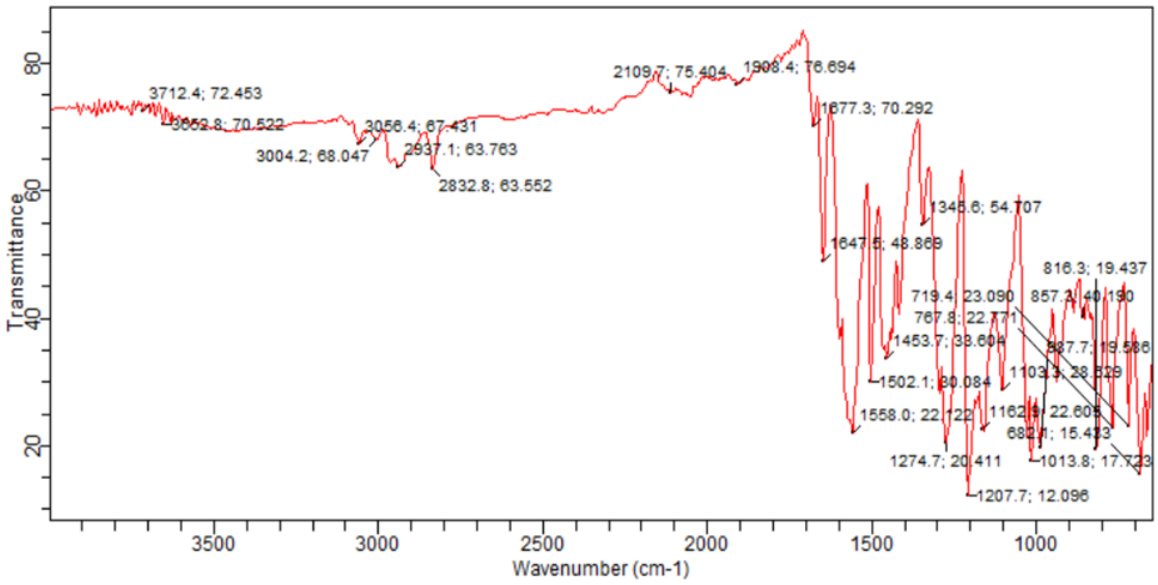
HMBC spectrum of compound P8

Appendix 45



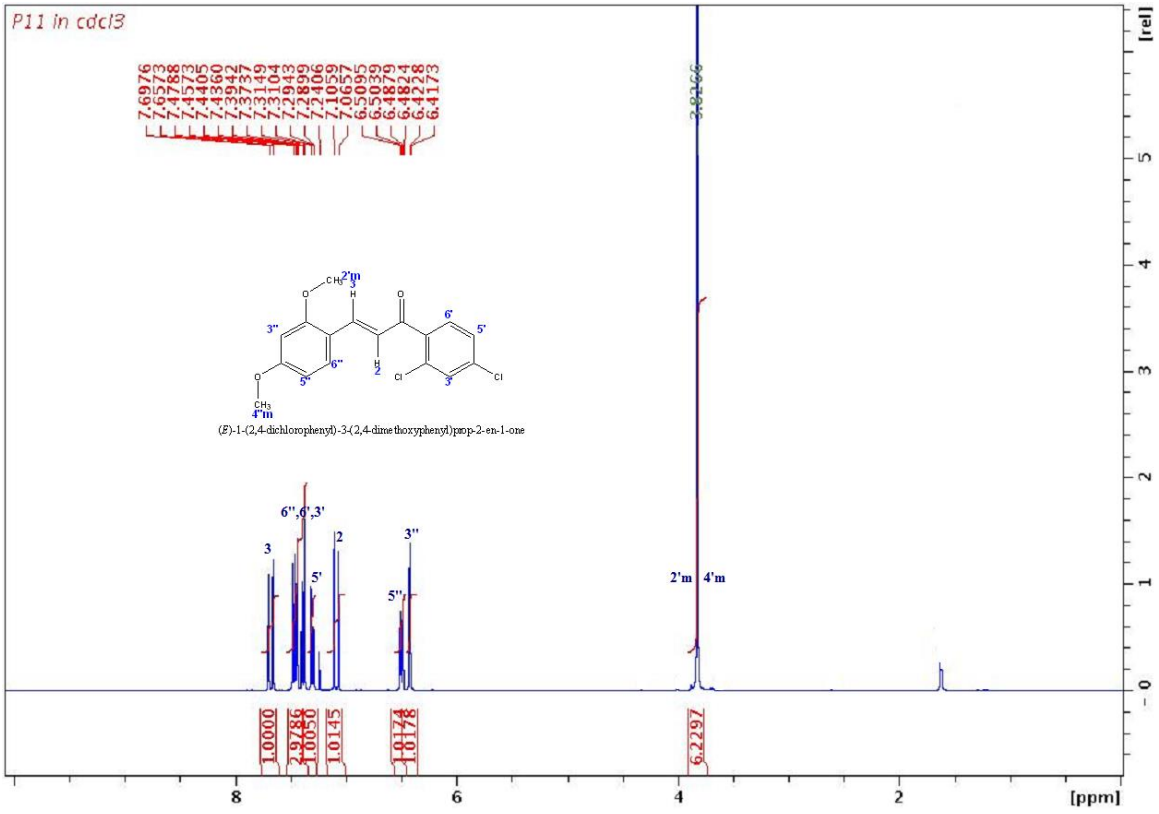
HSQC spectrum of compound P8

Appendix 46



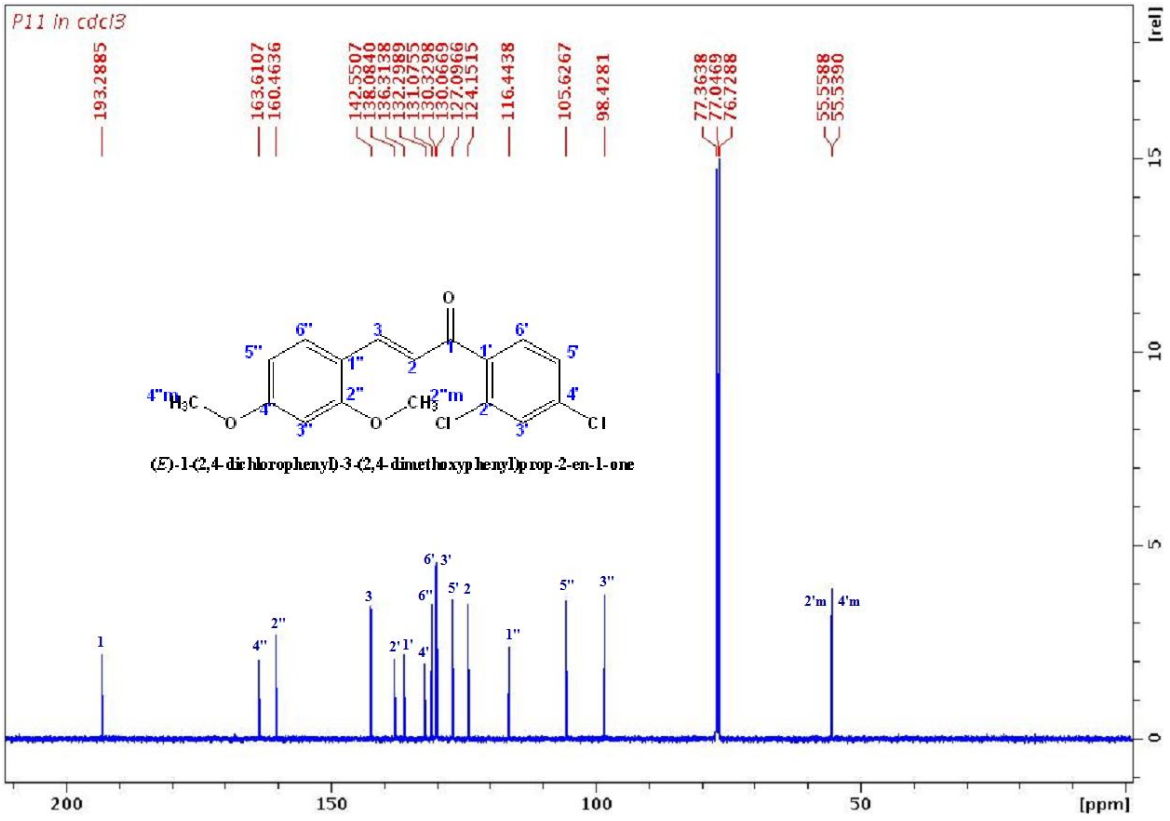
FT-IR Spectrum of P11

Appendix 47



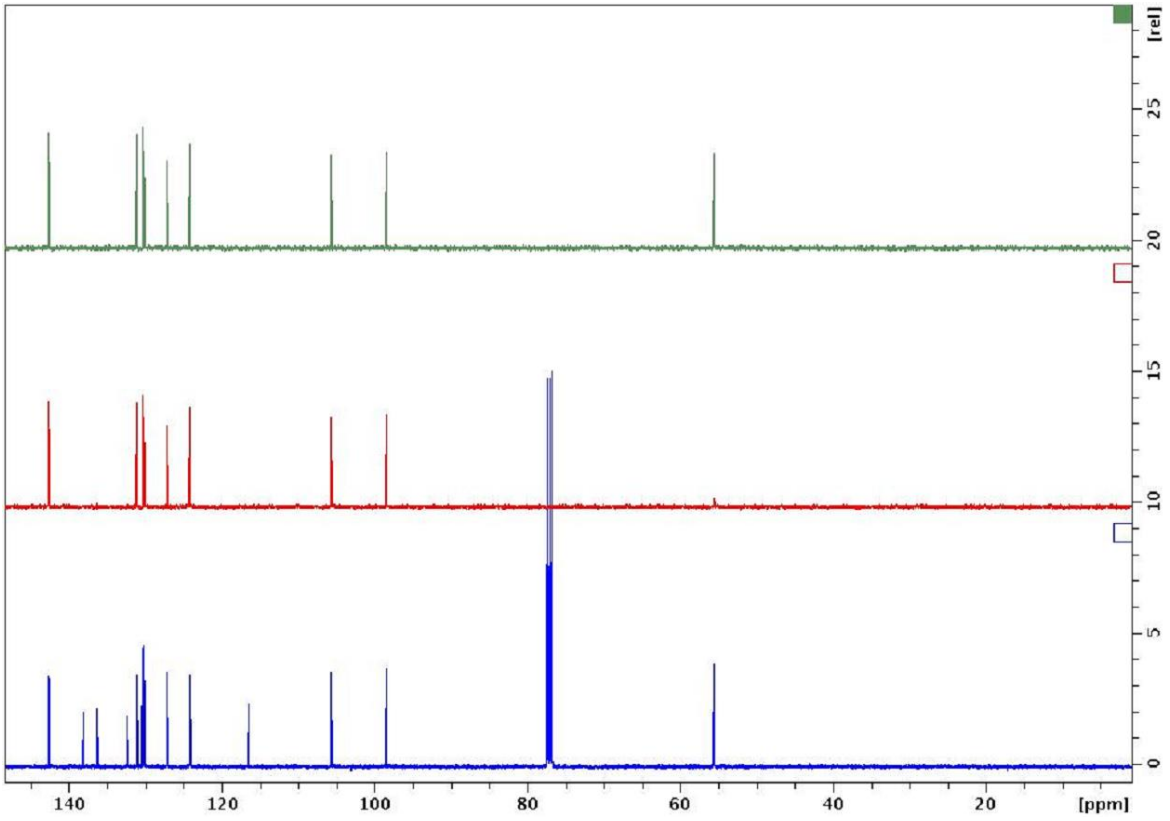
^{1}H NMR of compound P11

Appendix 48



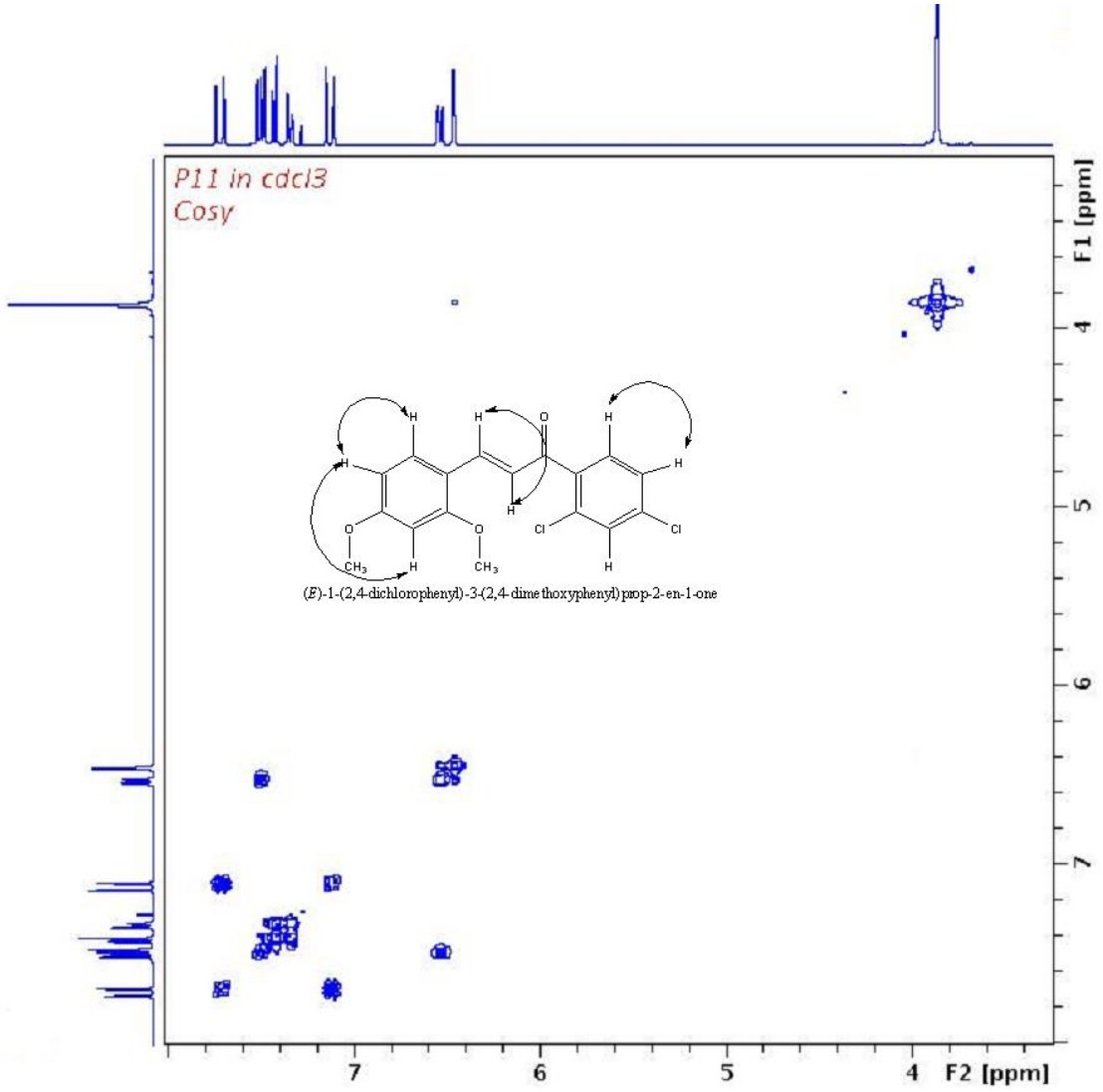
^{13}C NMR of compound P11

Appendix 49



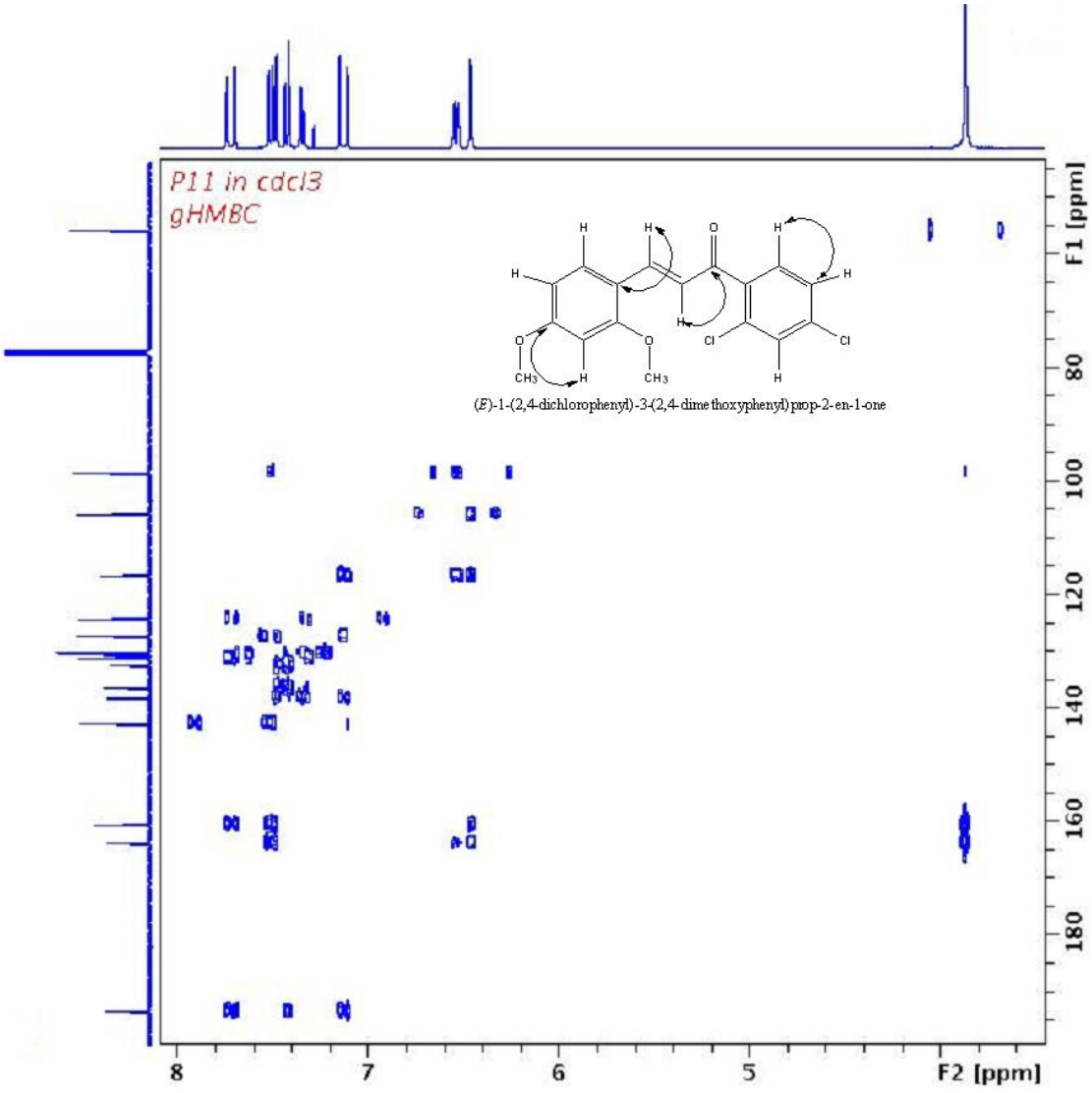
DEPT spectrum of compound P11

Appendix 50



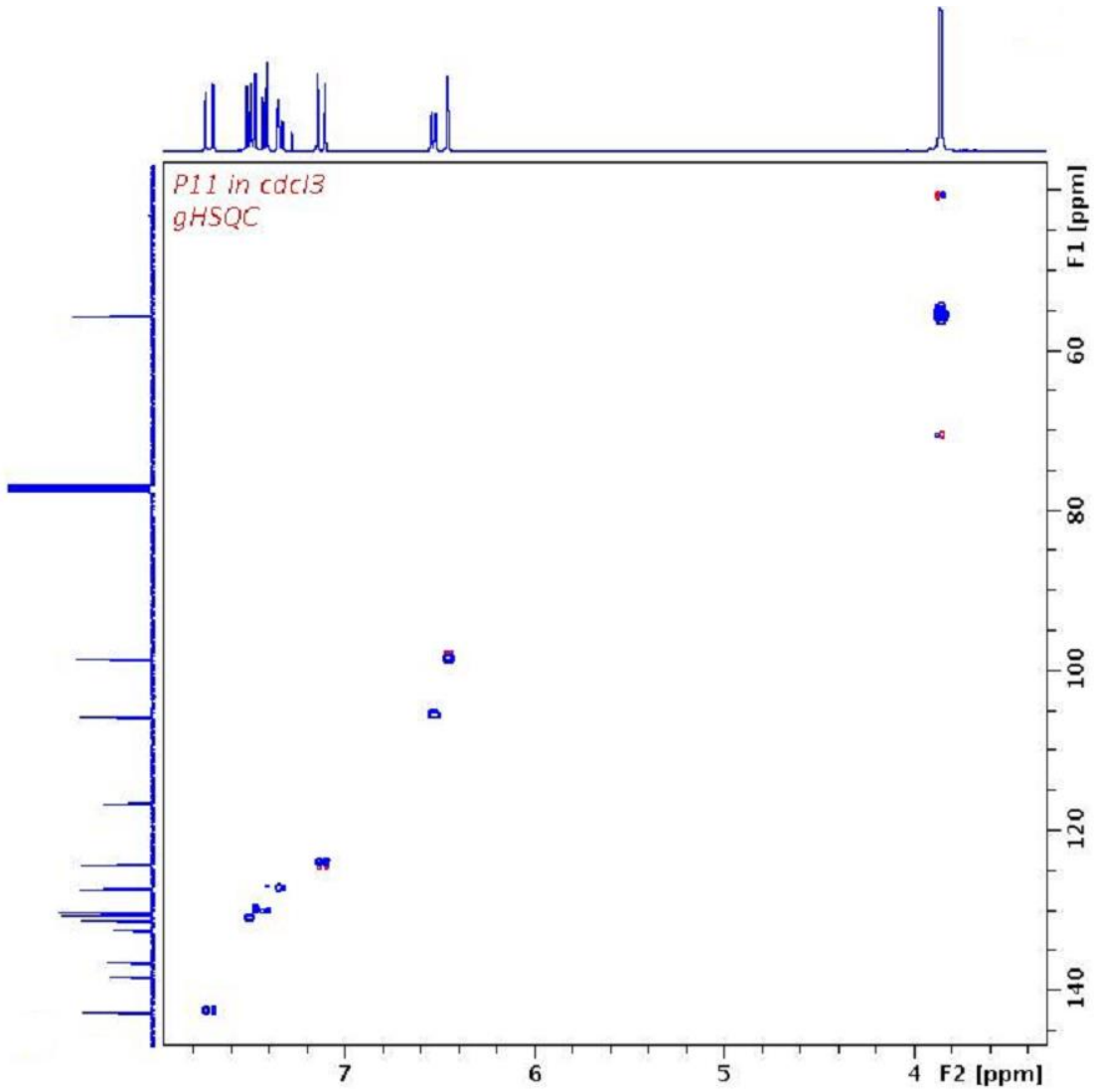
COSY spectrum of compound P11

Appendix 51



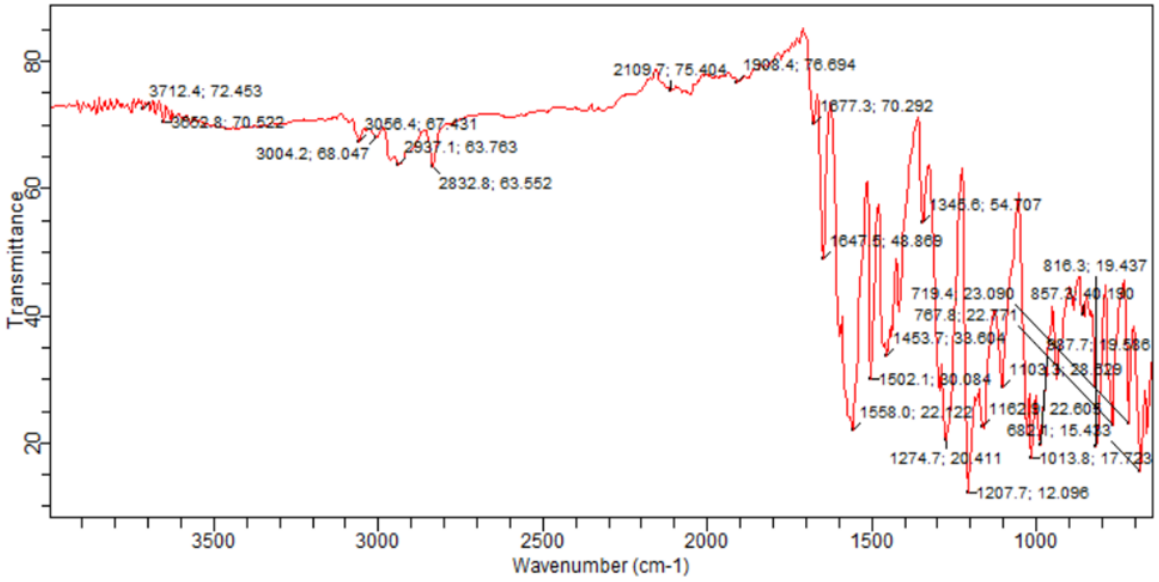
HMBC spectrum of compound P11

Appendix 52



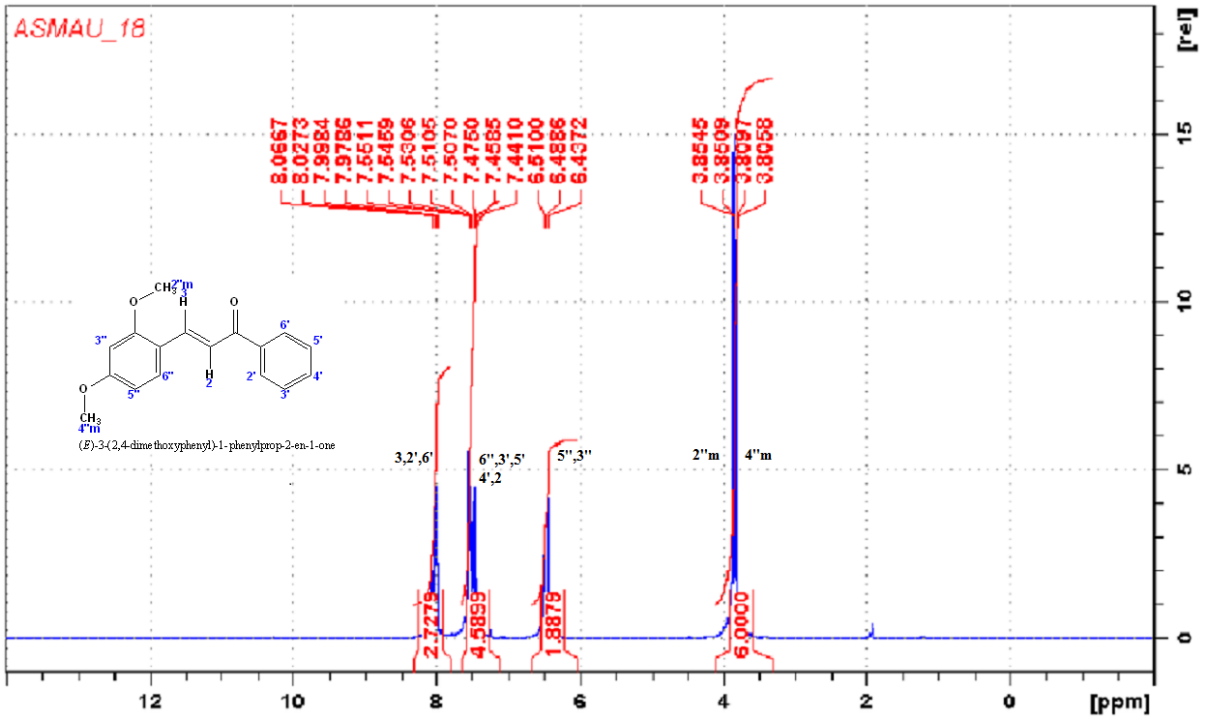
HSQC spectrum of compound P11

Appendix 53



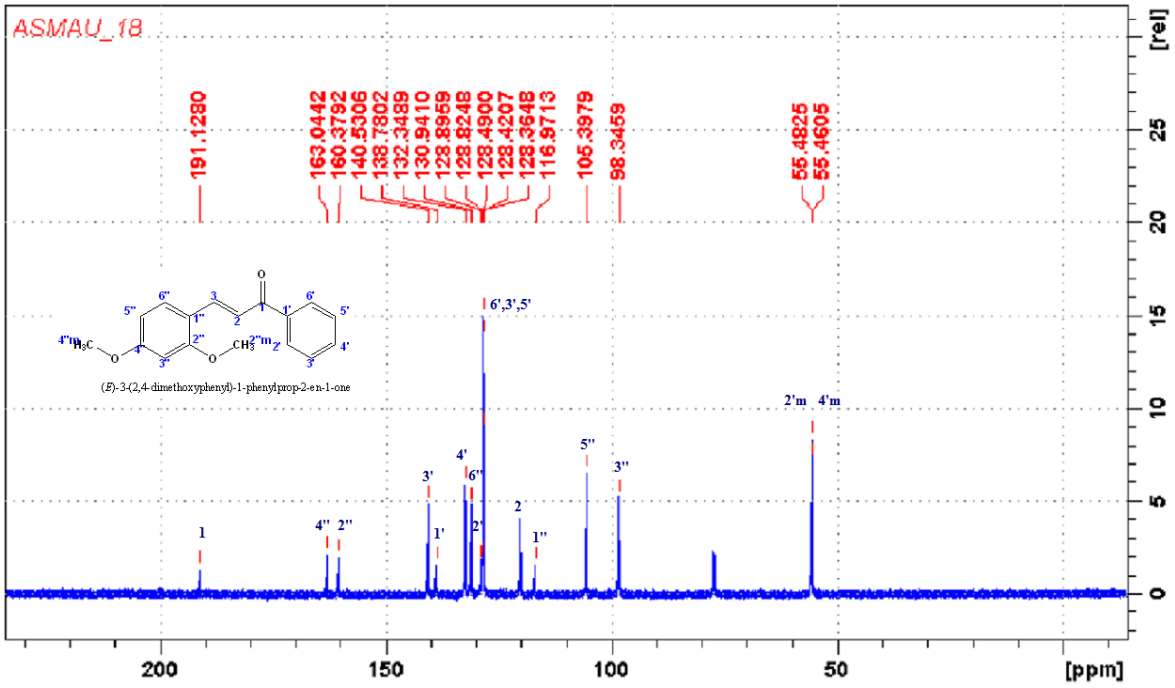
FT-IR Spectrum of P12

Appendix 54



^{1}H NMR of compound P12

Appendix 55



^{13}C NMR of compound P12

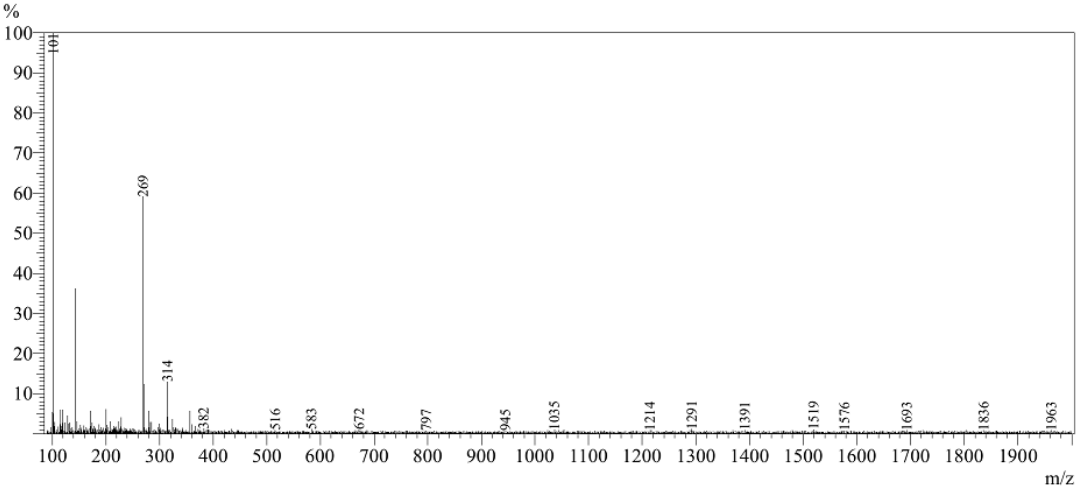
Appendix 56

Sample Information

Date Acquired	: 2017/05/30 09:20:58 AM
Sample Type	: Unknown
Sample Name	: p12
Sample ID	: p12
Data File	: p12.lcd
Method File	: lemien.lcm
Report Format File	: DEFAULT.lsr
Tuning File	: 12042017 repeat repeat.lct

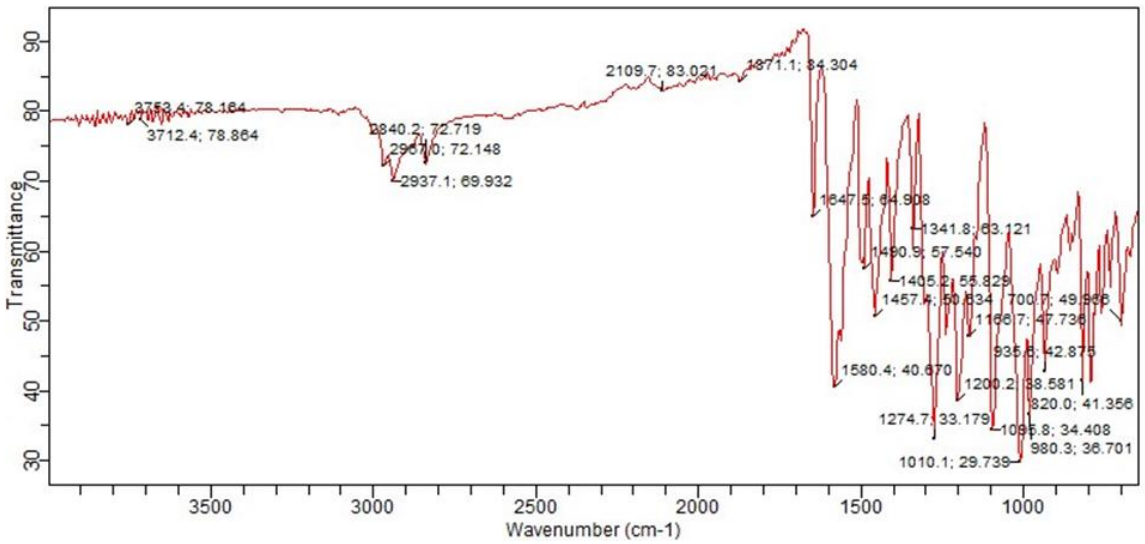
MS Spectrum

R.Time:1.067(Scan#:65)
MassPeaks:1929
Segment 1 - Event 1



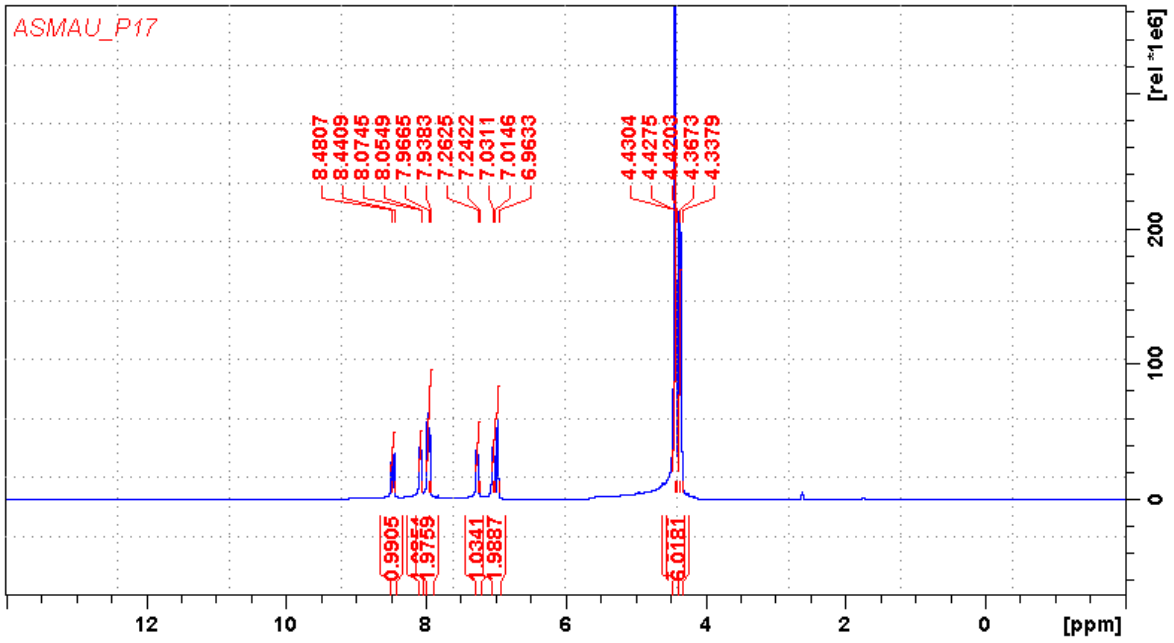
Mass spectrum of P12

Appendix 57



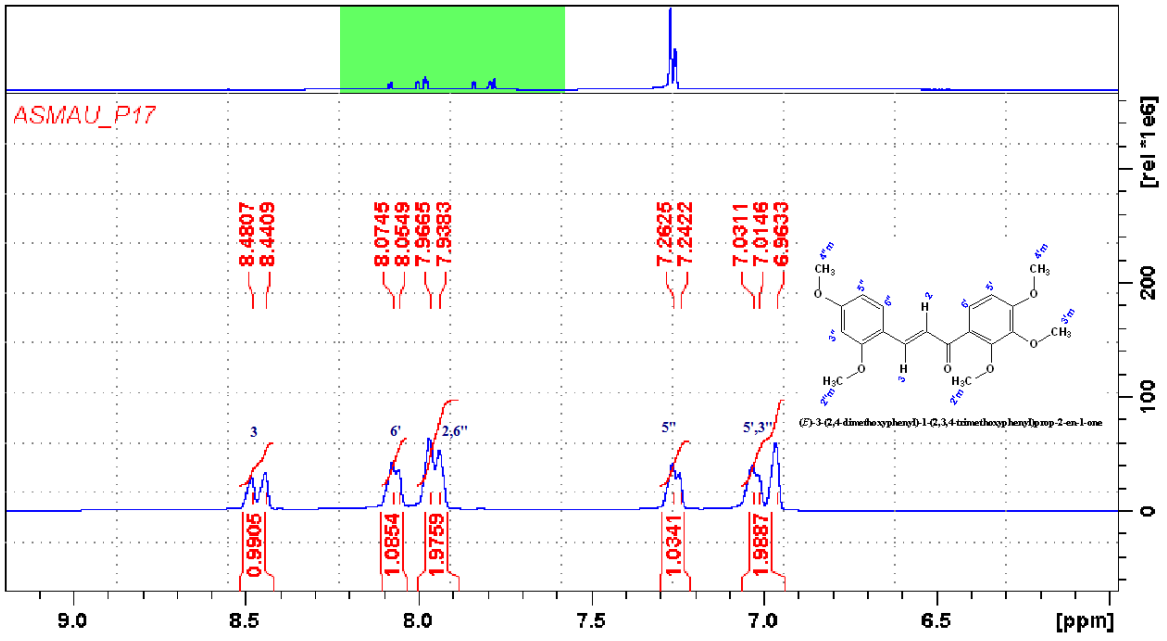
FT-IR Spectrum of P17

Appendix 58



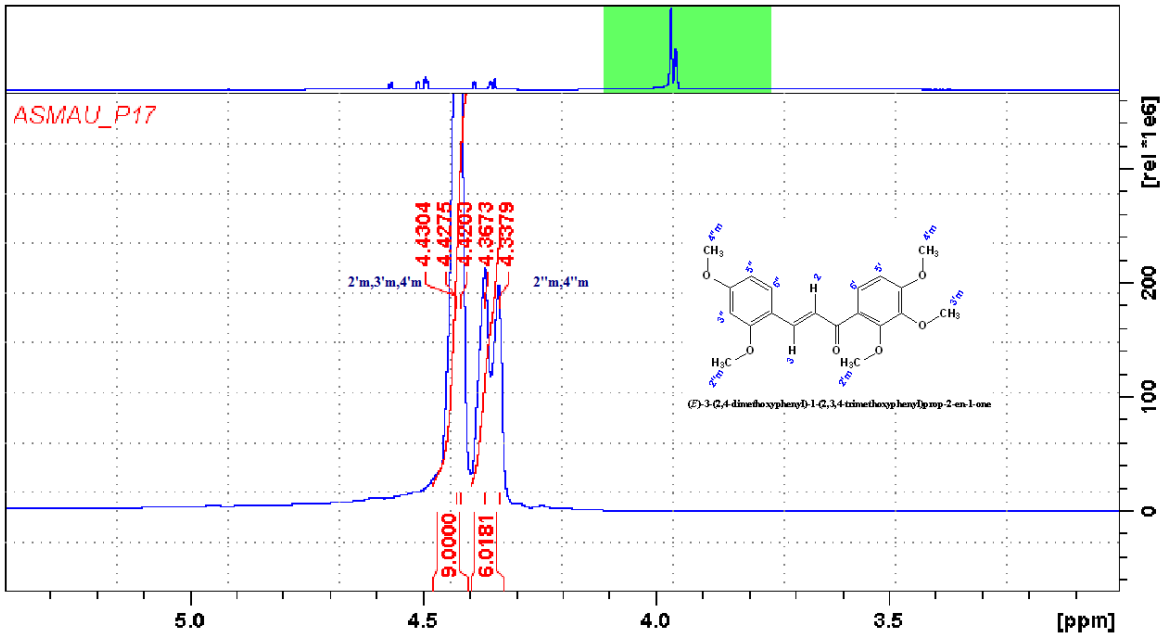
^{1}H NMR of compound P17

Appendix 59



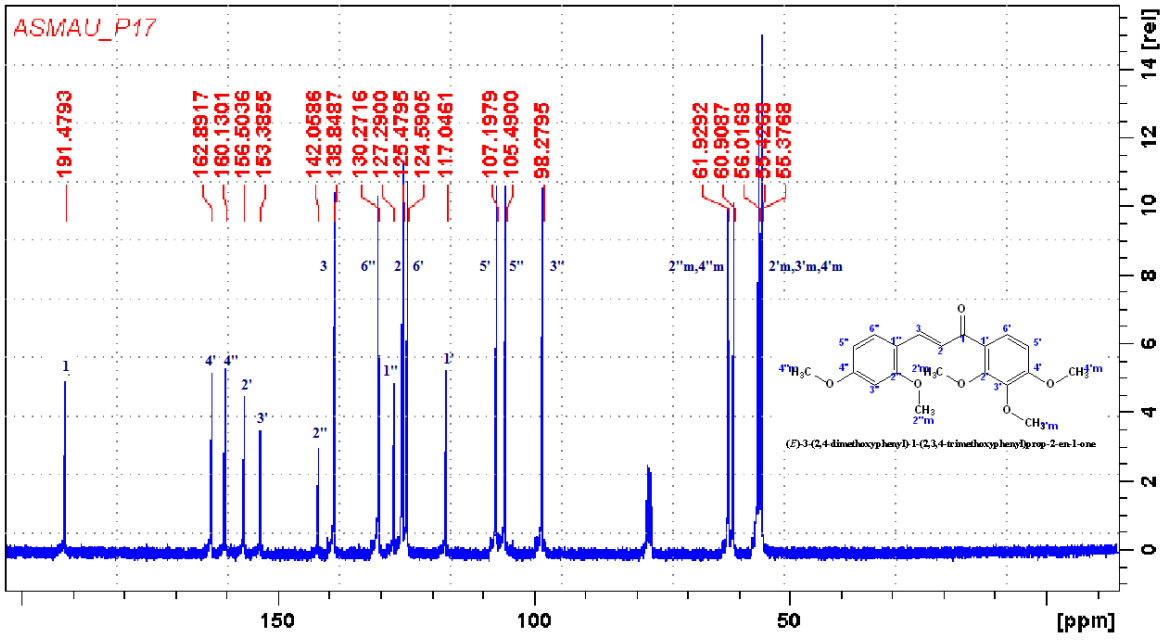
^{1}H NMR of compound P17 (Expanded)

Appendix 60



^{1}H NMR of compound P17 (Expanded)

Appendix 61



^{13}C NMR of compound P17

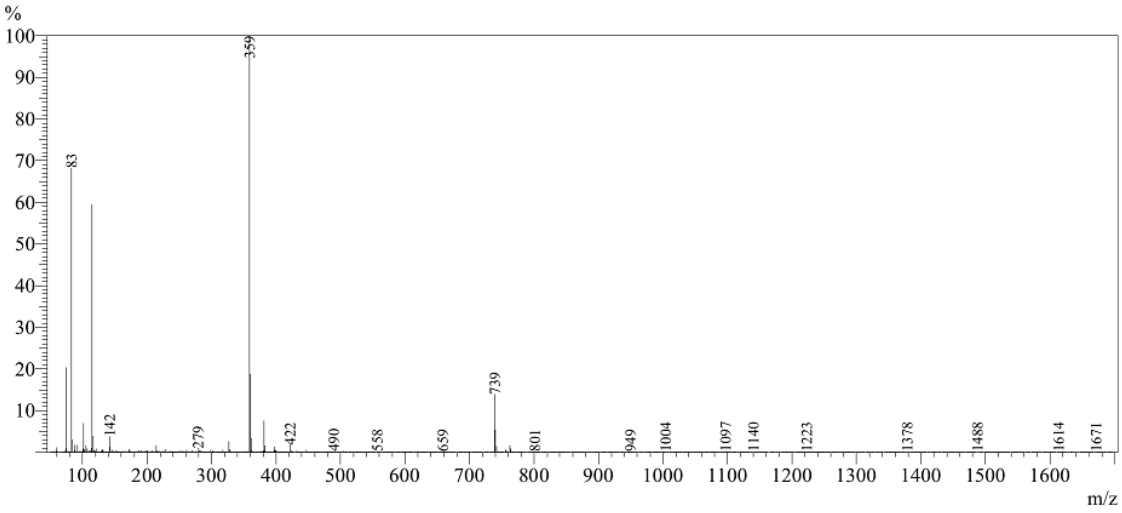
Appendix 62

Sample Information

Date Acquired	: 2017/05/30 10:26:50 AM
Sample Type	: Unknown
Sample Name	: p17
Sample ID	: p17
Data File	: p17.lcd
Method File	: no column run.lcm
Report Format File	: DEFAULT.lsr
Tuning File	: 12042017 repeat repeat.lct

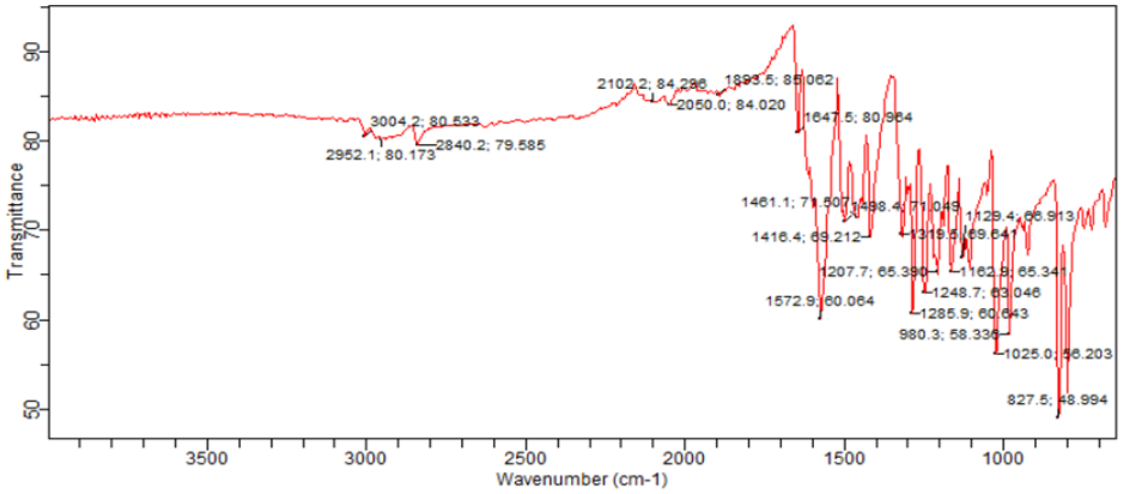
MS Spectrum

R.Time:1.067(Scan#:65)
MassPeaks:1667
Segment 1 - Event 1



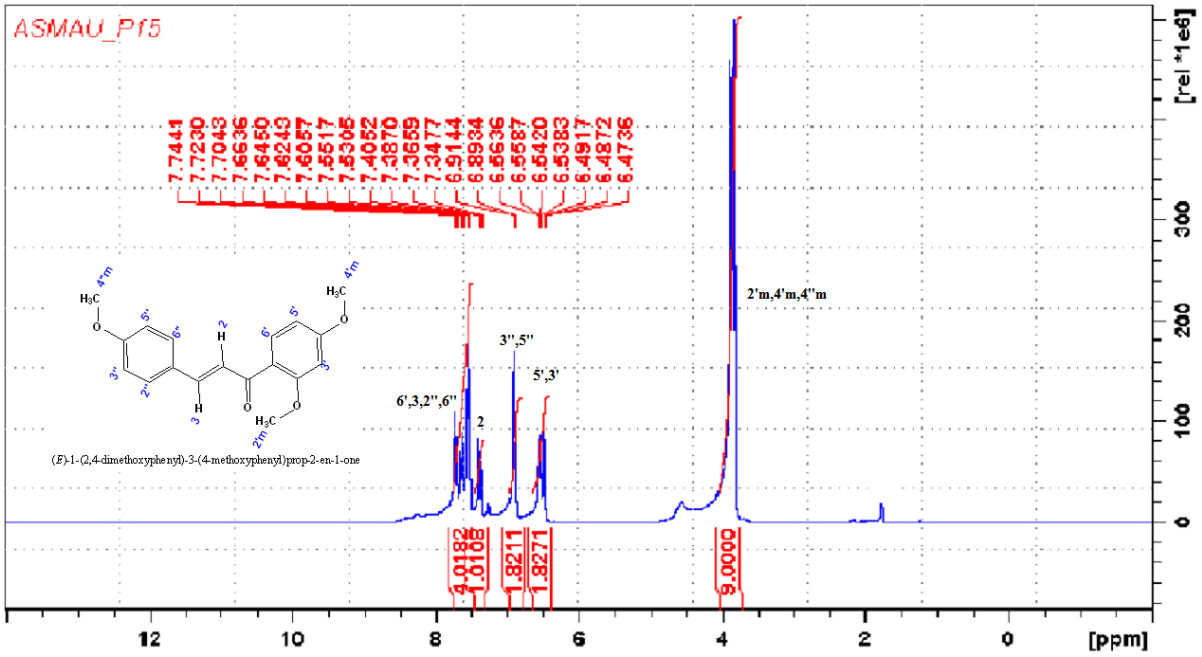
Mass spectrum of P17

Appendix 63



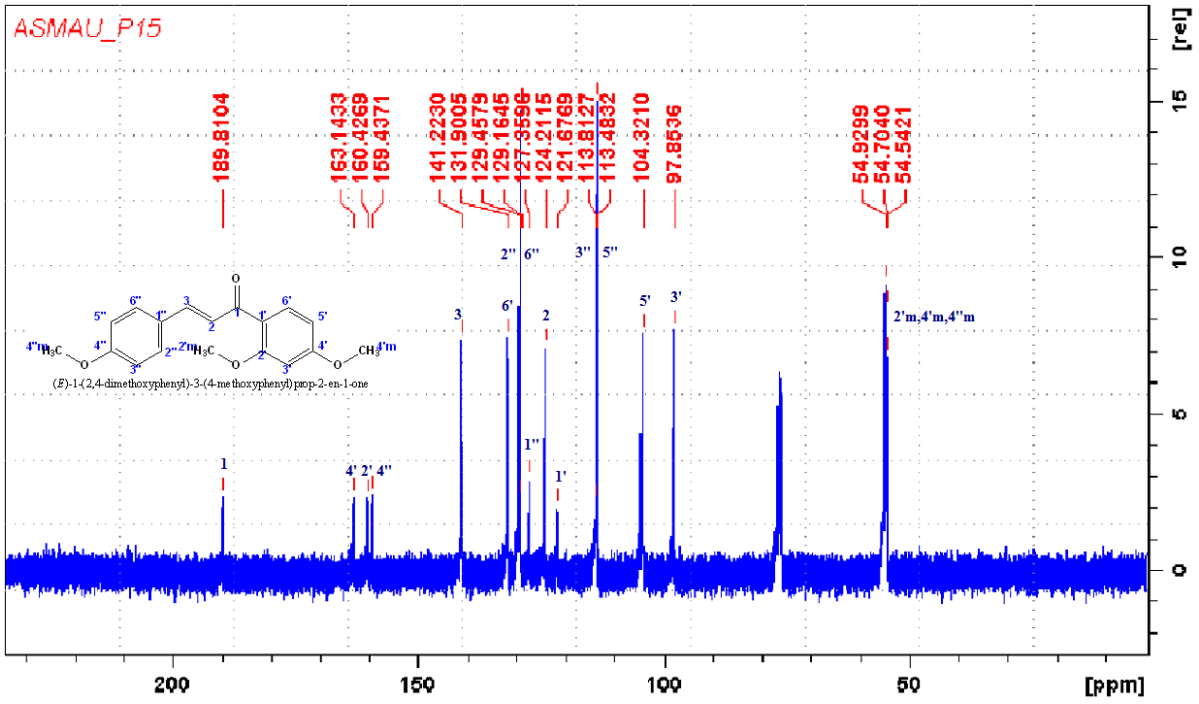
FT-IR Spectrum of P15

Appendix 64



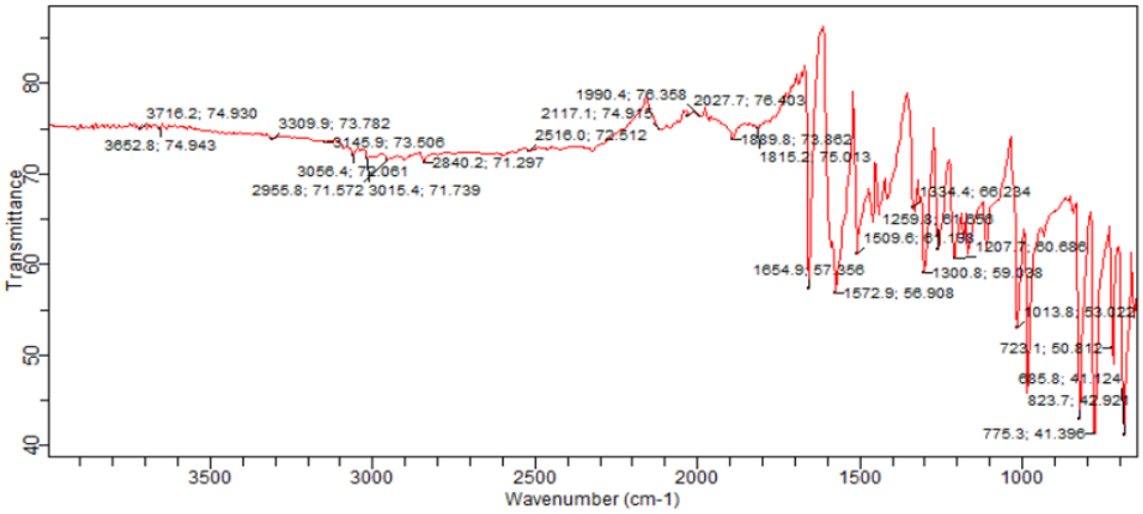
^{1}H NMR of compound P15

Appendix 65



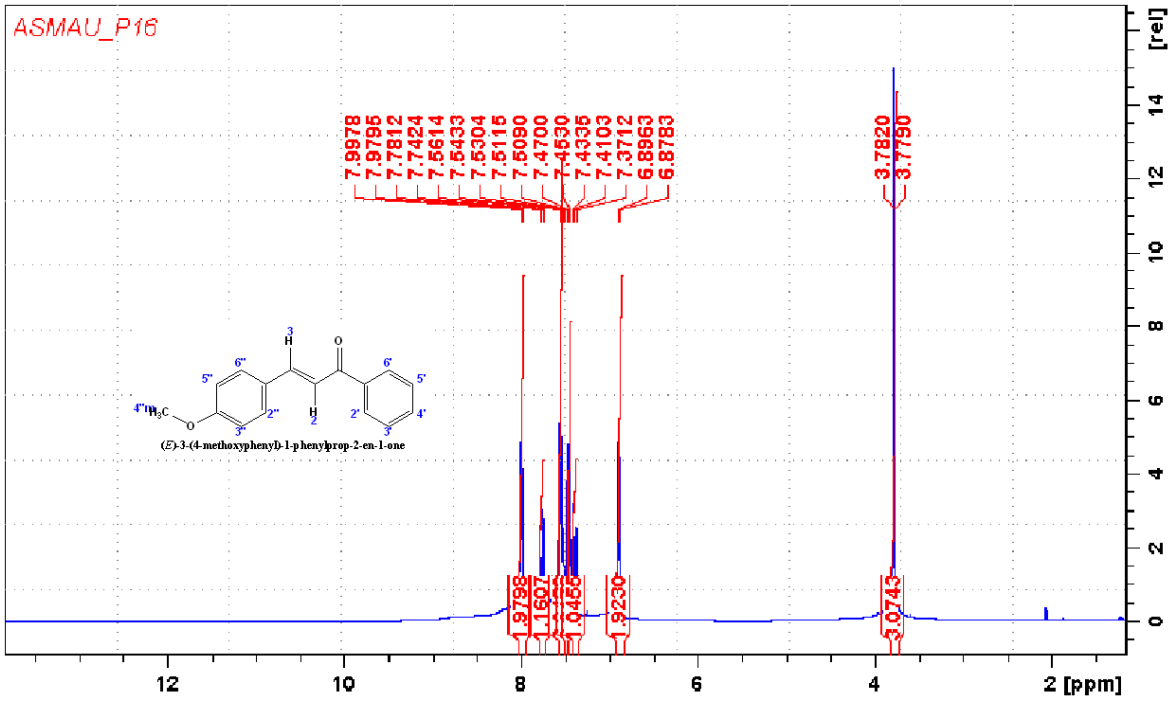
^{13}C NMR of compound P15

Appendix 66



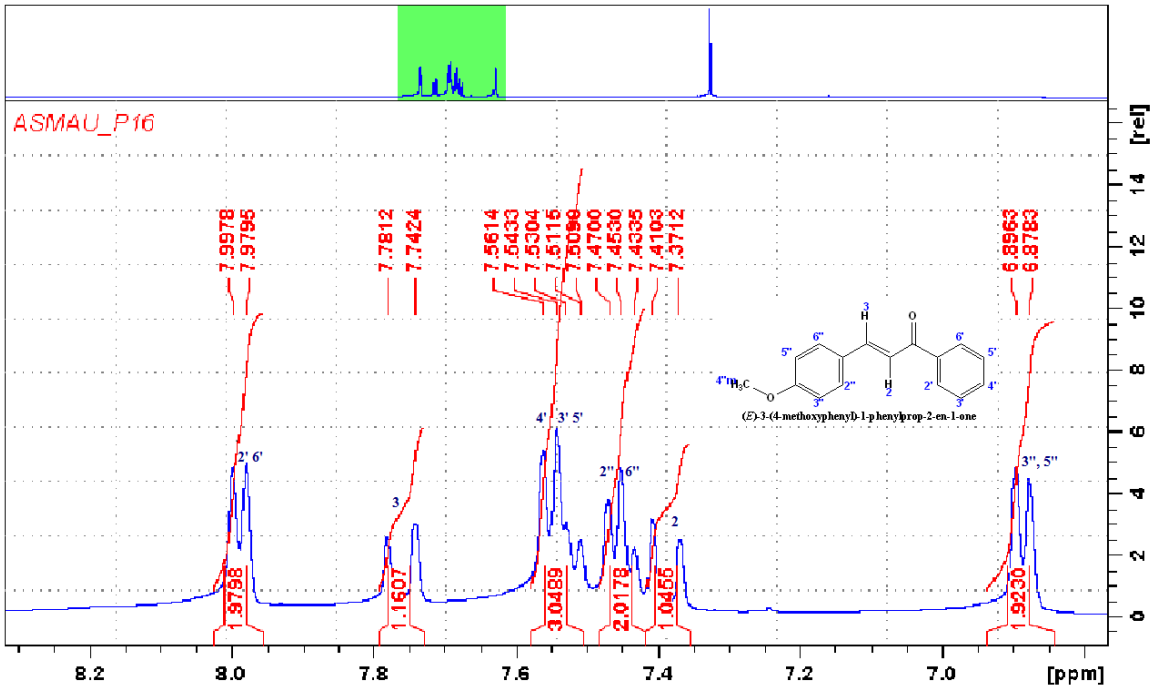
FT-IR Spectrum of P16

Appendix 67



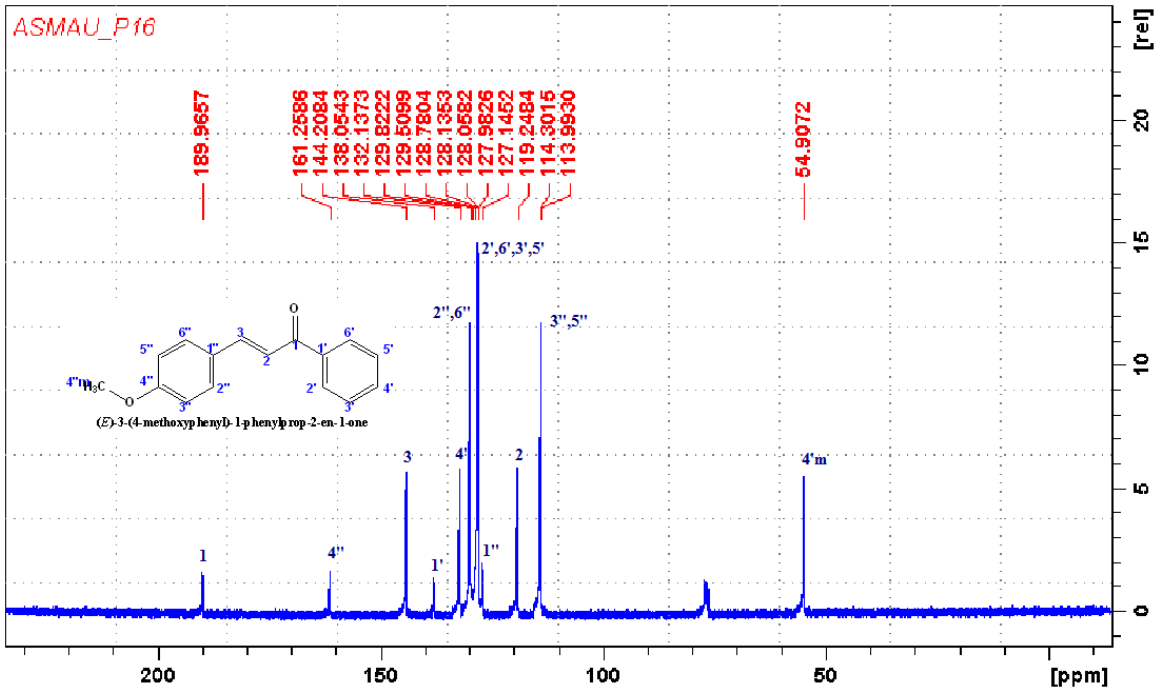
^{1}H NMR of compound P16

Appendix 68



^{1}H NMR of compound P16 (Expanded)

Appendix 69



^{13}C NMR of compound P16

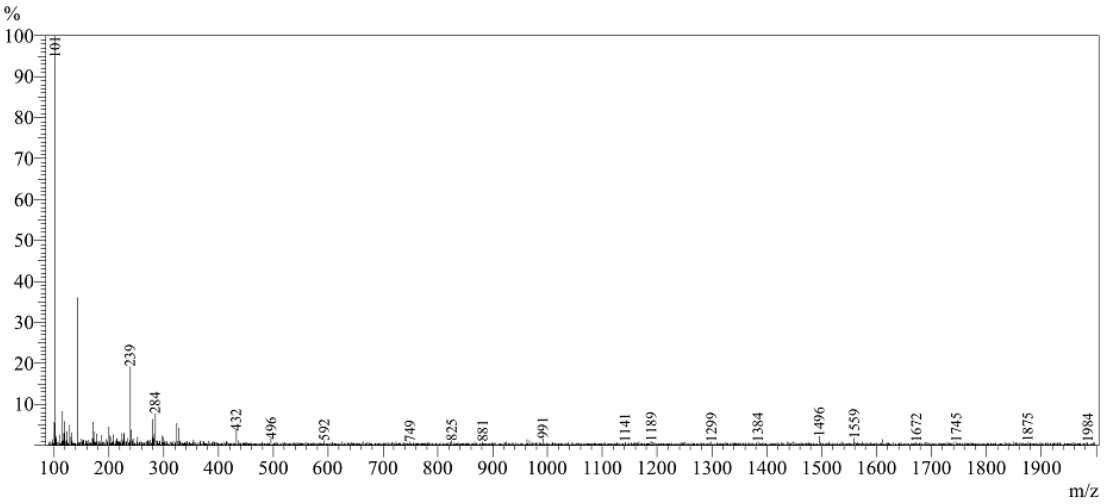
Appendix 70

Sample Information

Date Acquired	: 2017/05/30 10:16:19 AM
Sample Type	: Unknown
Sample Name	: p16
Sample ID	: p16
Data File	: p16.lcd
Method File	: lemien.lcm
Report Format File	: DEFAULT.lsr
Tuning File	: 12042017 repeat repeat.lct

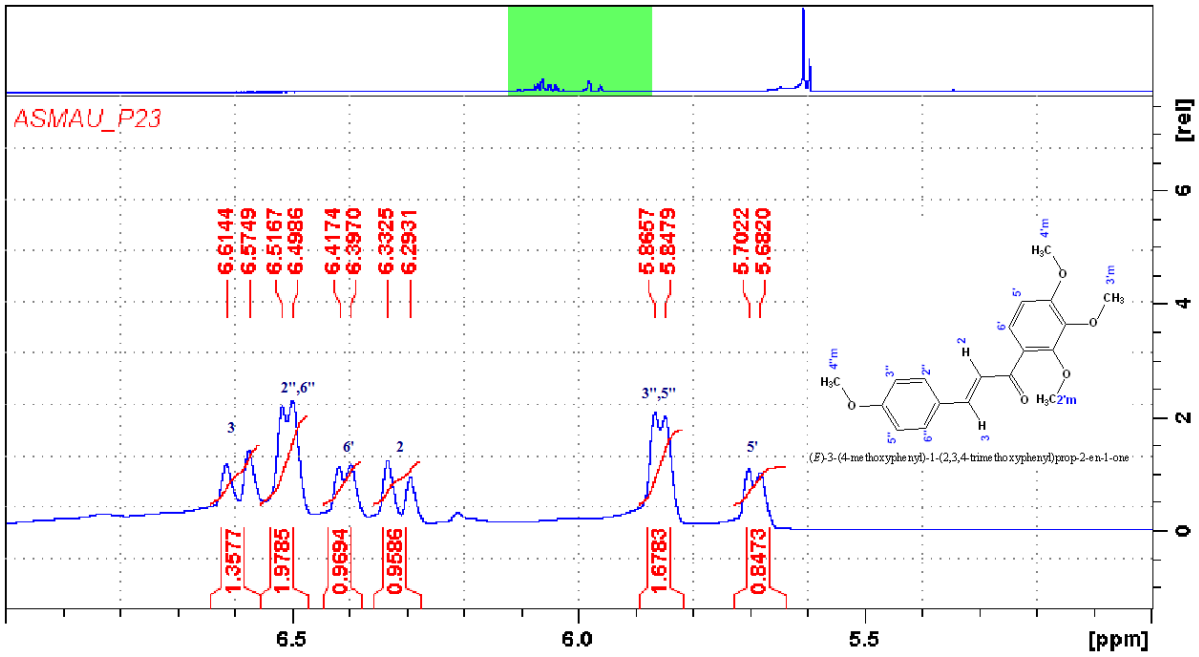
MS Spectrum

R.Time:1.067(Scan#:65)
MassPeaks:1923
Segment 1 - Event 1



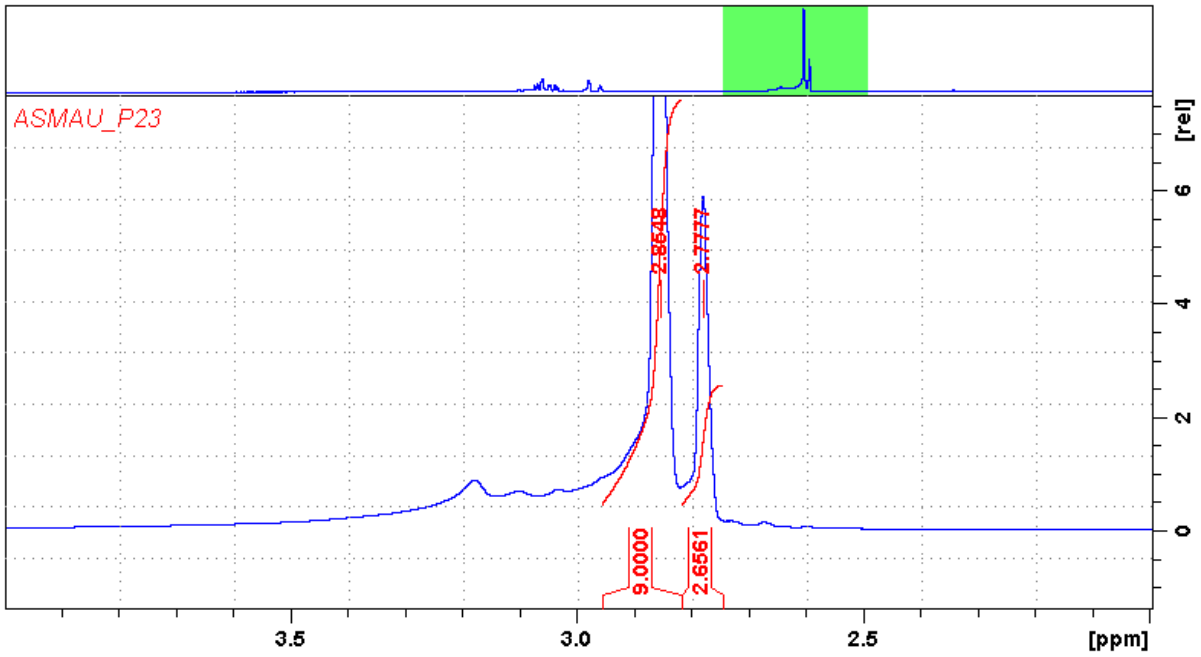
Mass spectrum of P16

Appendix 71



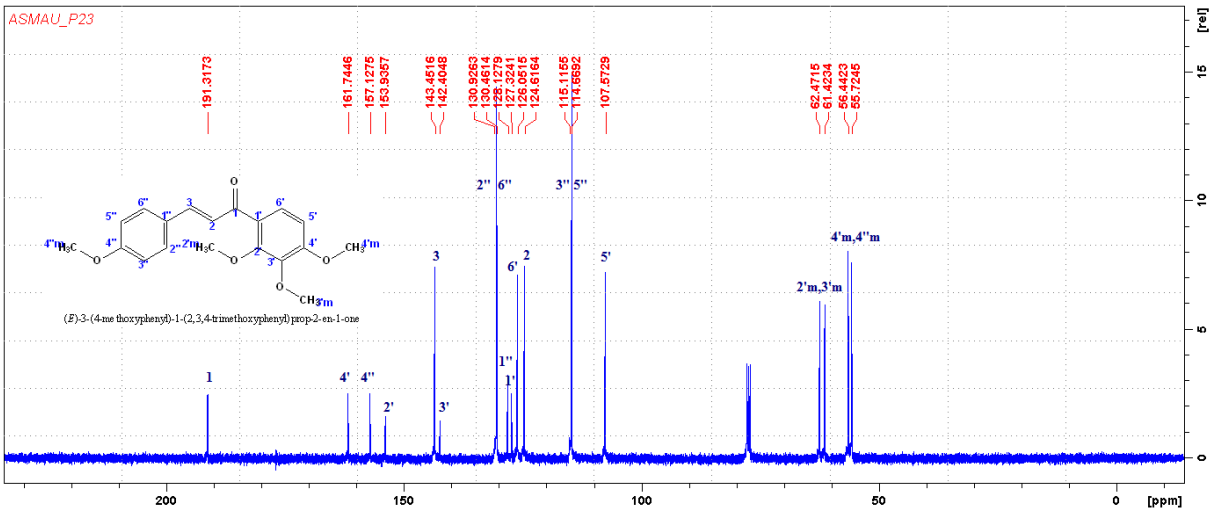
^{1}H NMR of compound 23

Appendix 72



^{1}H NMR of compound 23 (Expanded)

Appendix 73



^{13}C NMR of compound 23

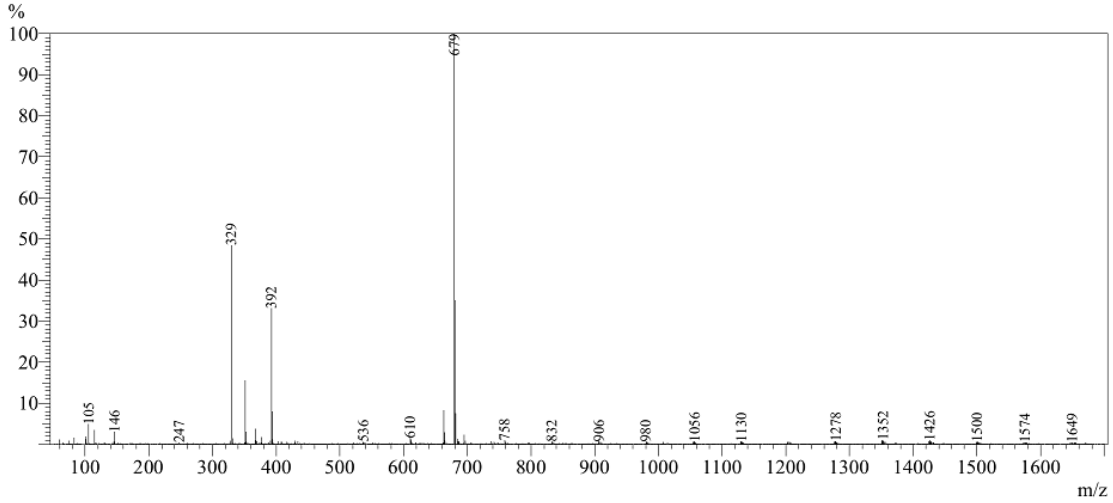
Appendix 74

Sample Information

Date Acquired	: 2017/05/30 10:53:23 AM
Sample Type	: Unknown
Sample Name	: p23
Sample ID	: p23
Data File	: p23.lcd
Method File	: no column run.lcm
Report Format File	: DEFAULT.lsr
Tuning File	: 12042017 repeat repeat.lct

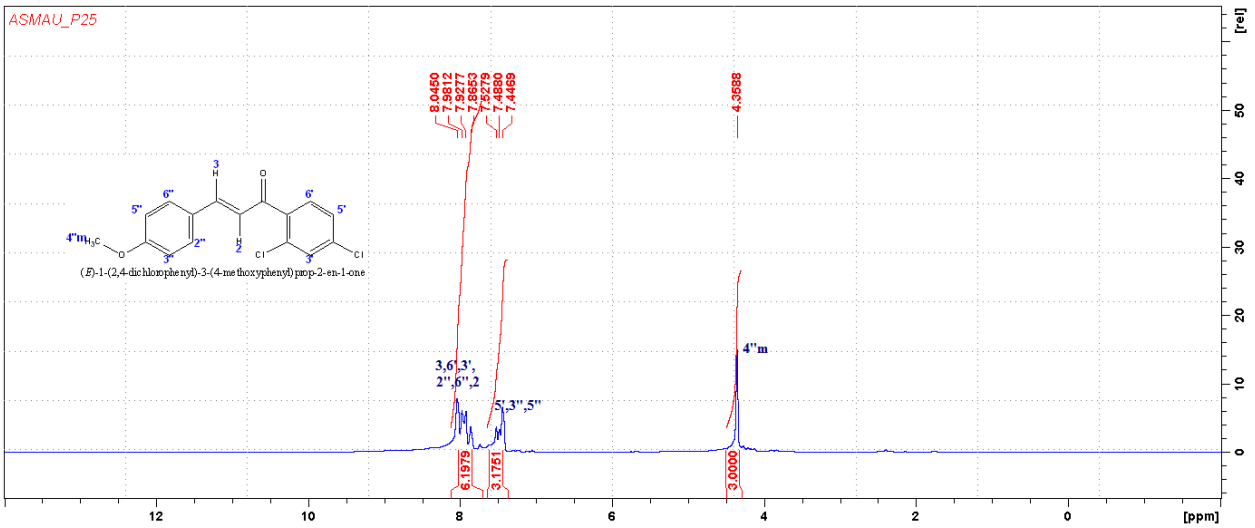
MS Spectrum

R.Time:1.067(Scan#:65)
MassPeaks:1722
Segment 1 - Event 1



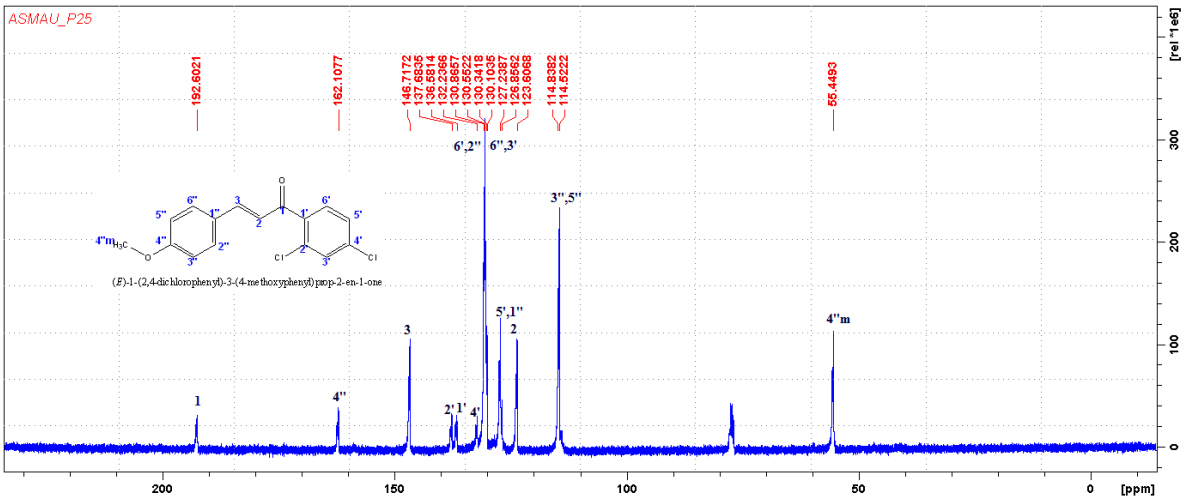
Mass spectrum of P23

Appendix 75



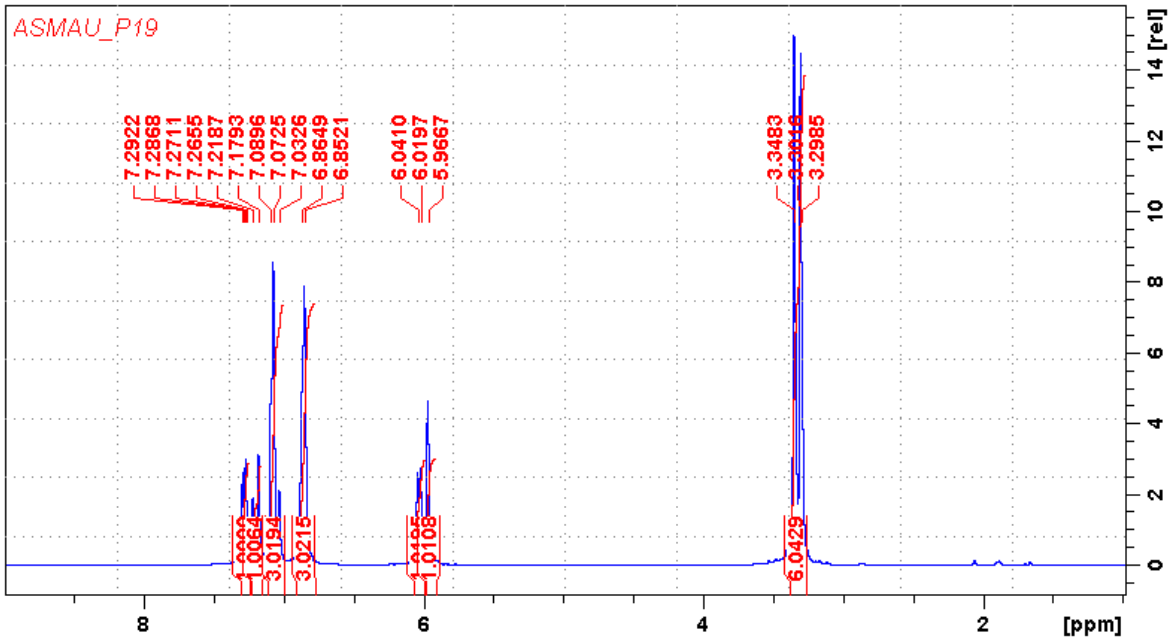
^{1}H NMR of compound 25

Appendix 76



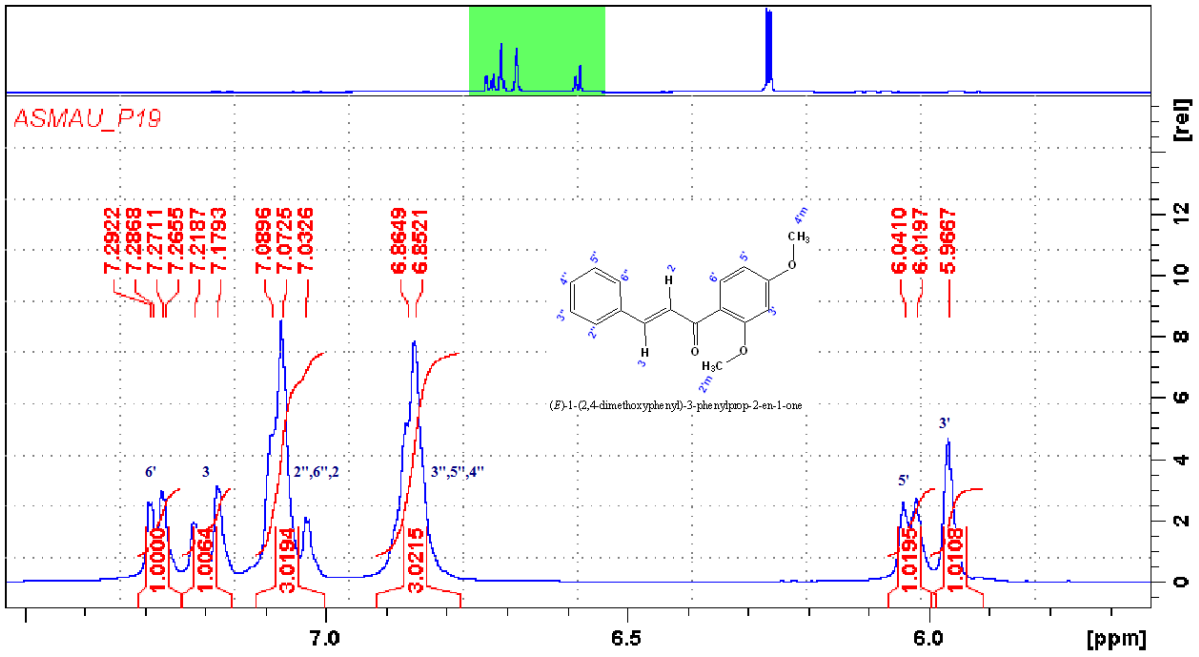
^{13}C NMR of compound 25

Appendix 77



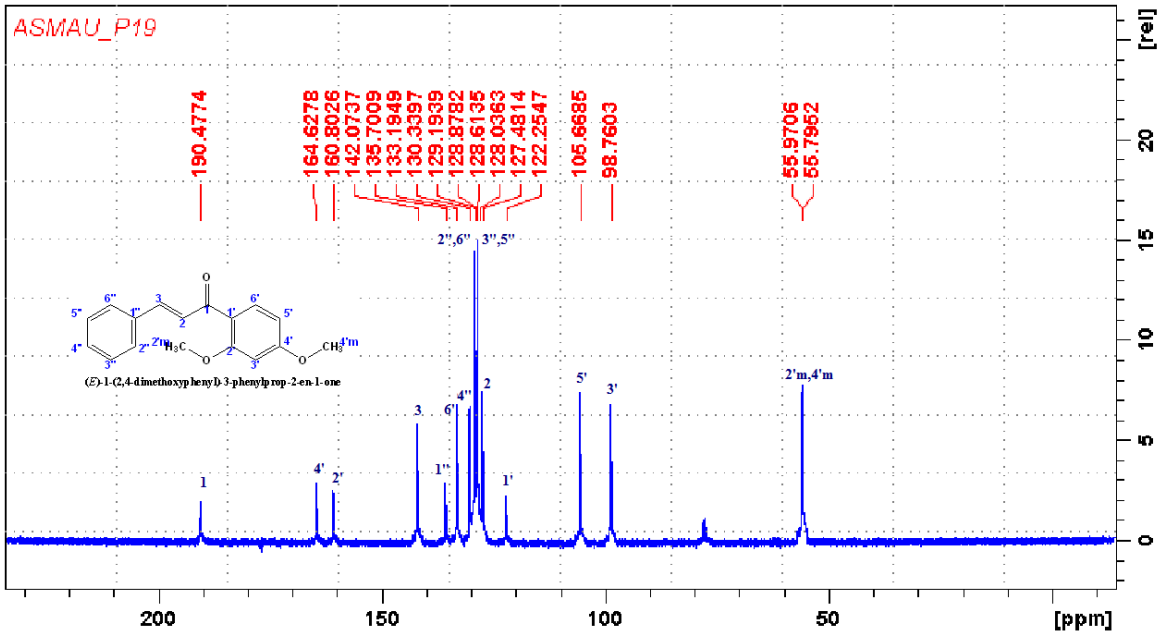
^{1}H NMR of compound P19

Appendix 78



^{1}H NMR of compound P19 (Expanded)

Appendix 79



^{13}C NMR of compound P19

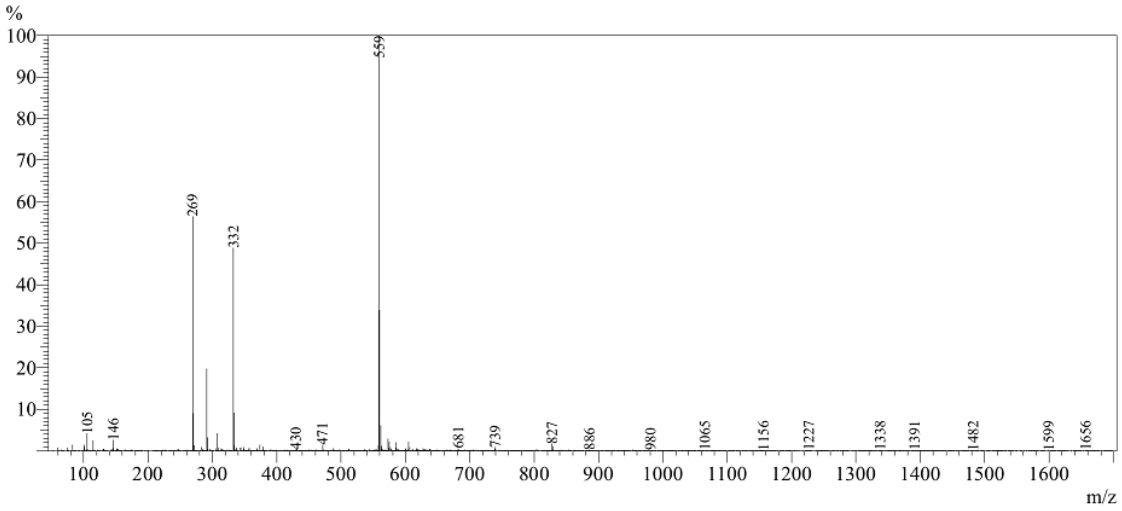
Appendix 80

Sample Information

Date Acquired	: 2017/05/30 10:35:41 AM
Sample Type	: Unknown
Sample Name	: p19
Sample ID	: p19
Data File	: p19.lcd
Method File	: no column run.lcm
Report Format File	: DEFAULT.lsr
Tuning File	: 12042017 repeat repeat.lct

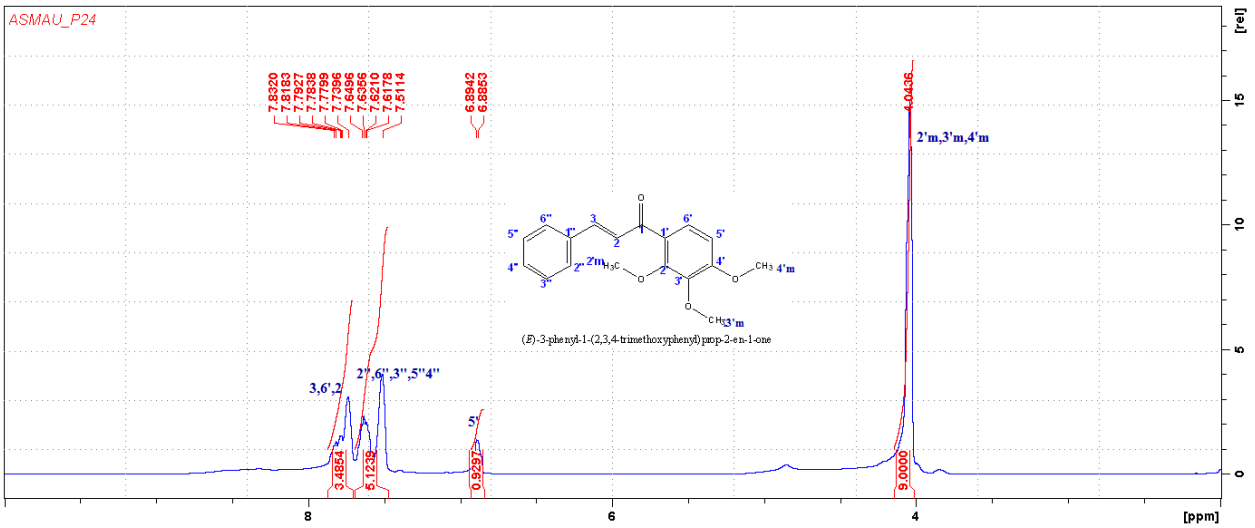
MS Spectrum

R.Time:1.067(Scan#:65)
MassPeaks:1711
Segment 1 - Event 1



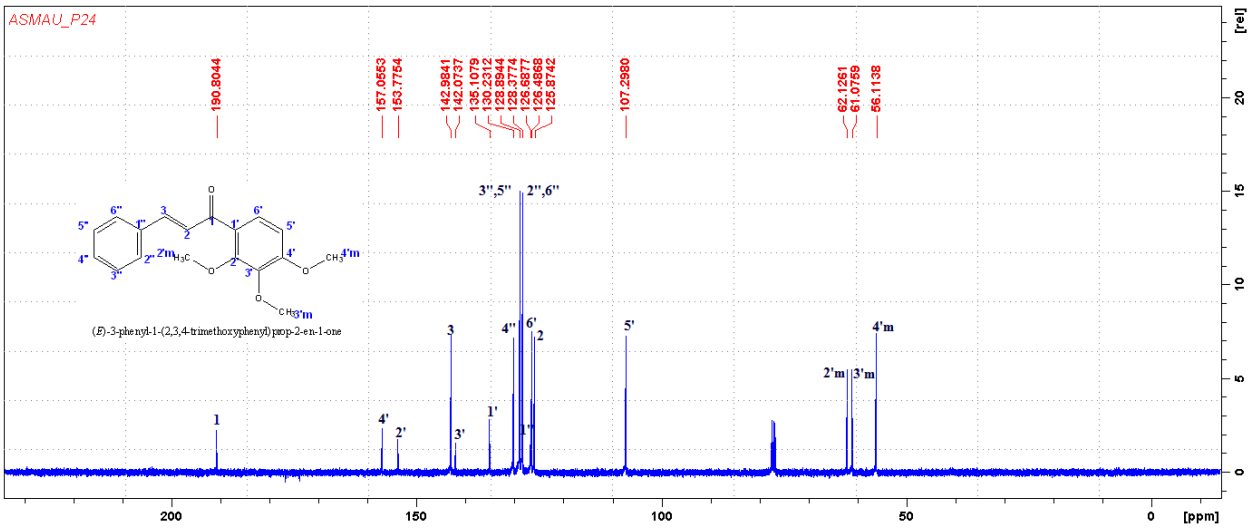
Mass spectrum of P19

Appendix 81



^{1}H NMR of compound 24

Appendix 82



^{13}C NMR of compound 24

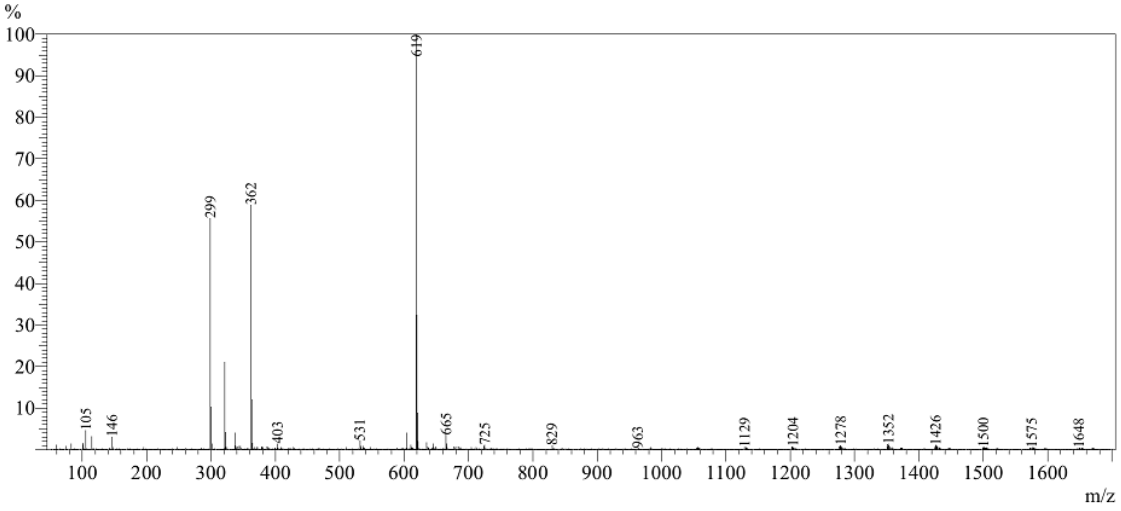
Appendix 83

Sample Information

Date Acquired	: 2017/05/30 10:57:47 AM
Sample Type	: Unknown
Sample Name	: p24
Sample ID	: p24
Data File	: p24.lcd
Method File	: no column run.lcm
Report Format File	: DEFAULT.lsr
Tuning File	: 12042017 repeat repeat.lct

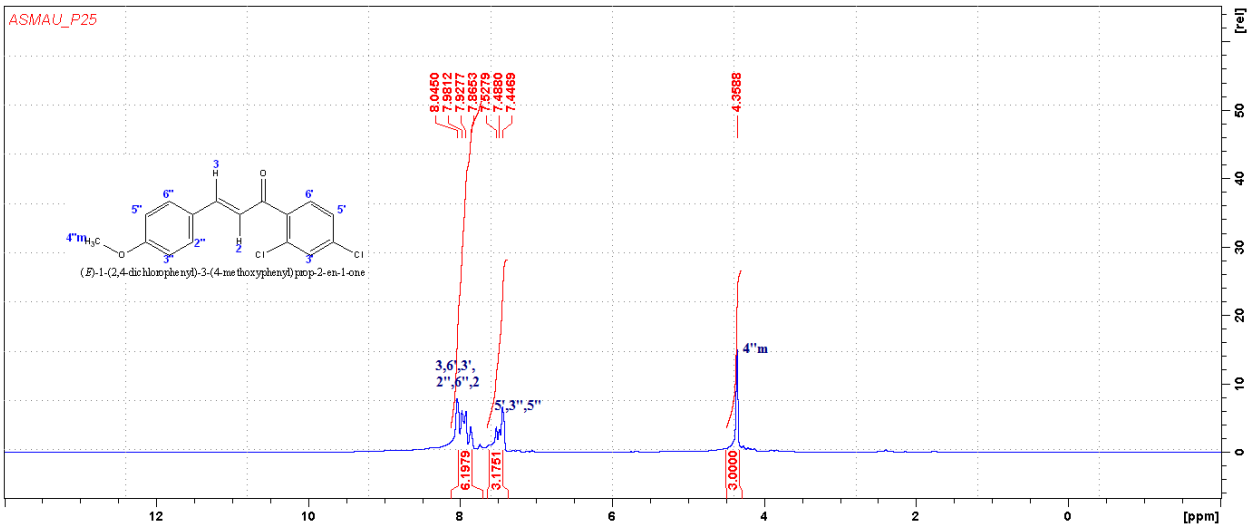
MS Spectrum

R.Time:1.067(Scan#:65)
MassPeaks:1703
Segment 1 - Event 1



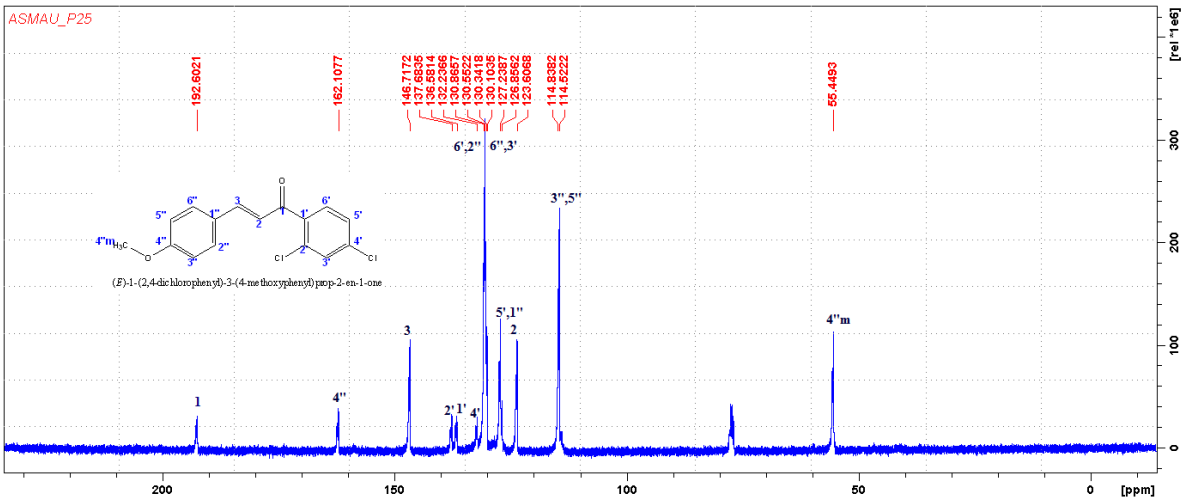
Mass spectrum of P24

Appendix 84



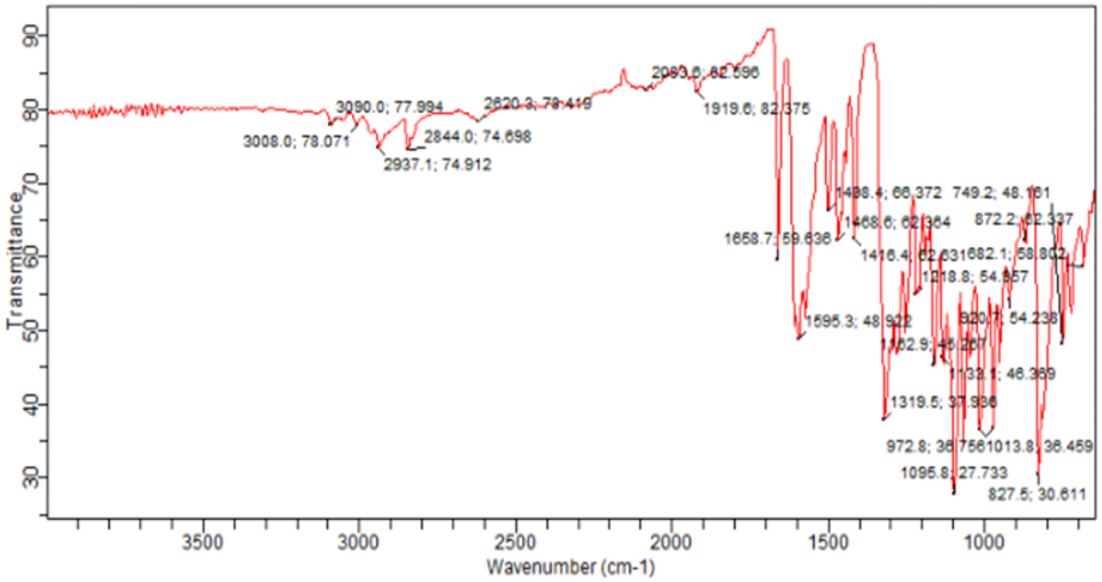
^{1}H NMR of compound 25

Appendix 85



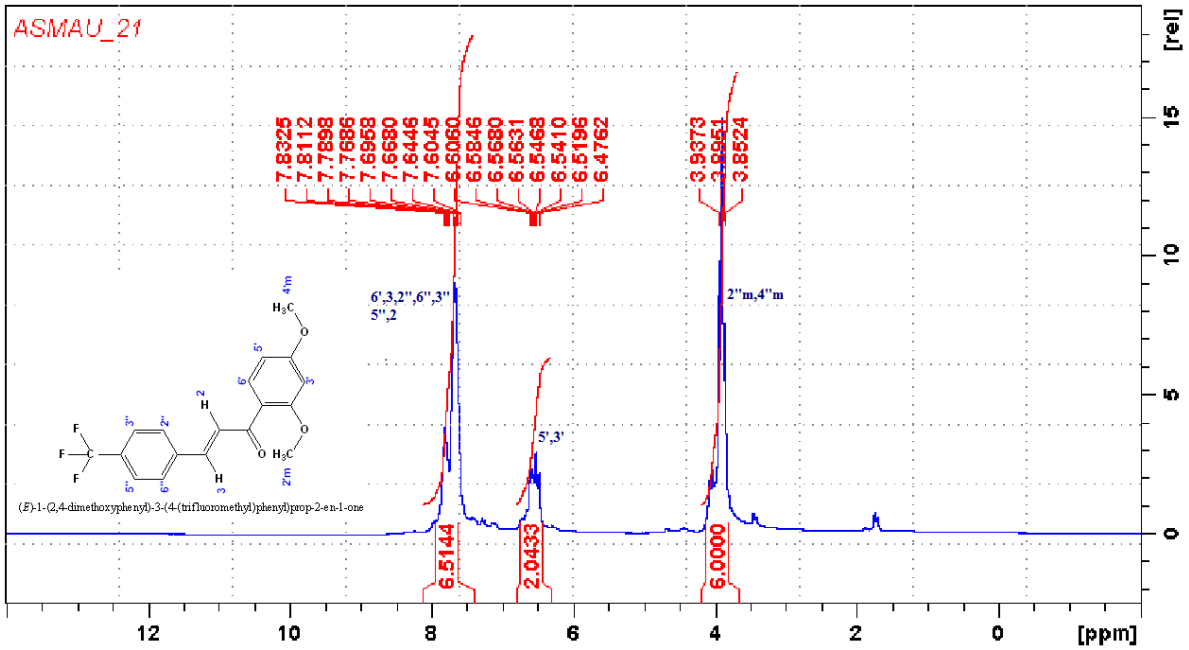
^{13}C NMR of compound 25

Appendix 86



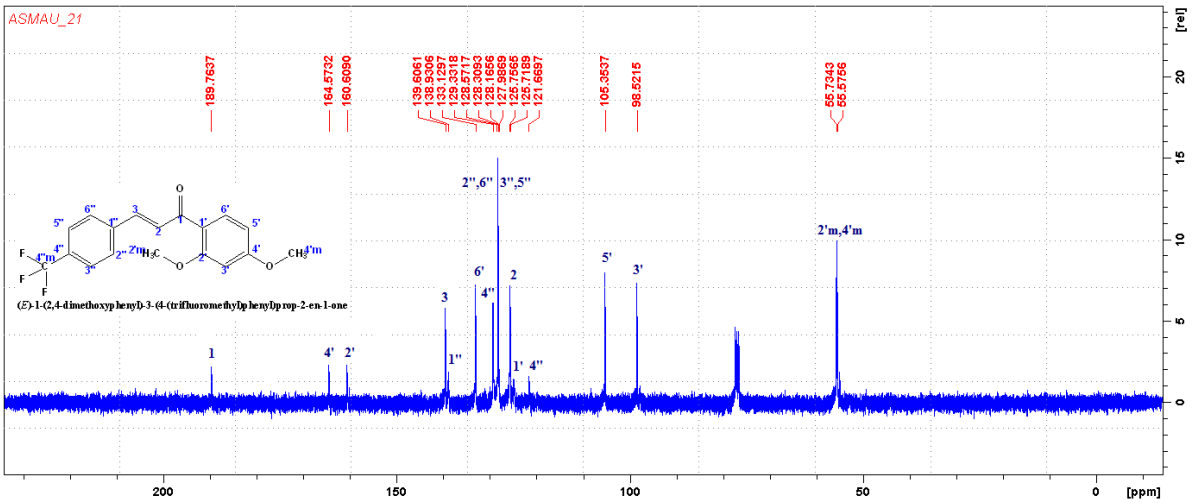
FT-IR Spectrum of P21

Appendix 87



^{1}H NMR of compound P21

Appendix 88



^{13}C NMR of compound P21

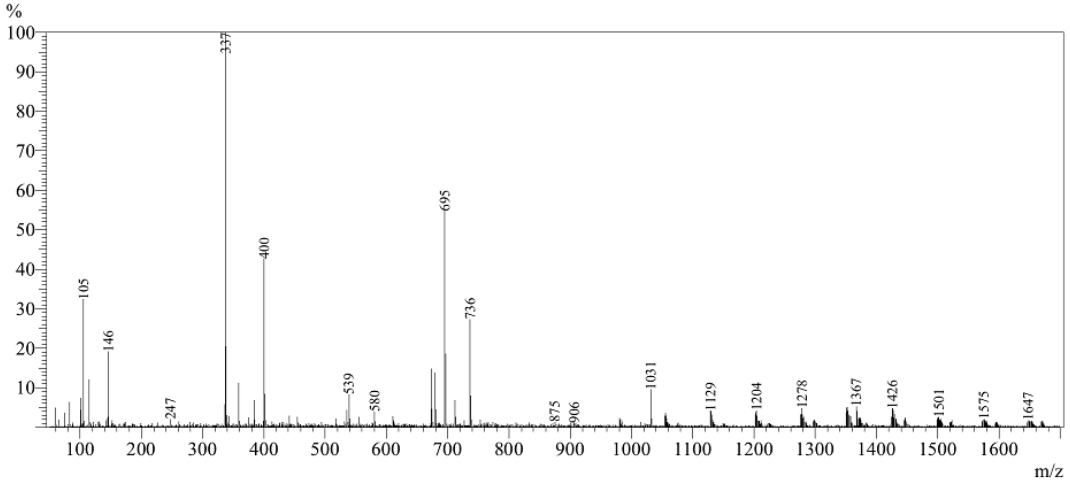
Appendix 89

Sample Information

Date Acquired	: 2017/05/30 10:44:32 AM
Sample Type	: Unknown
Sample Name	: p21
Sample ID	: p21
Data File	: p21.lcd
Method File	: no column run.lcm
Report Format File	: DEFAULT.lsr
Tuning File	: 12042017 repeat repeat.lct

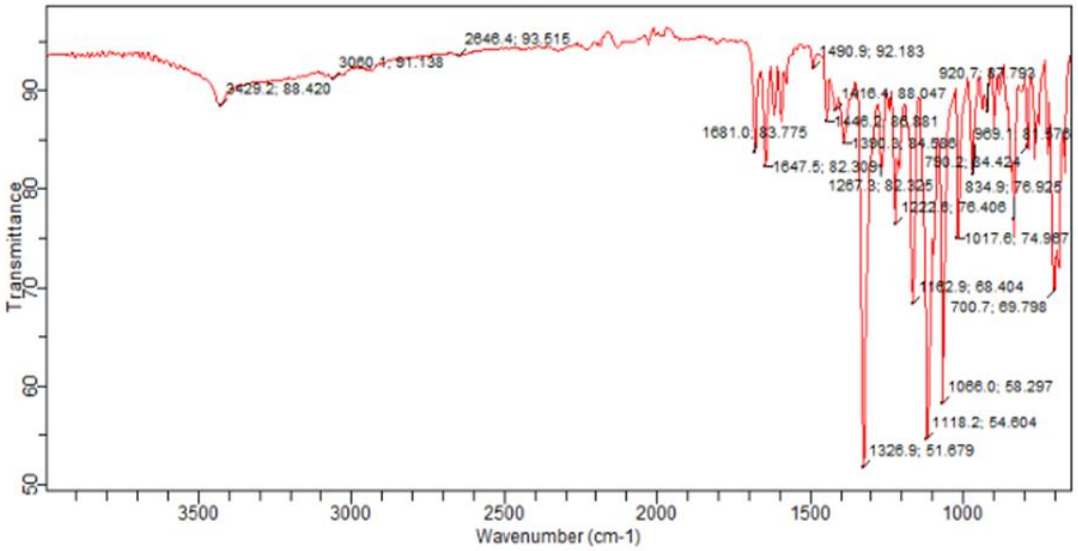
MS Spectrum

R.Time:1.067(Scan#:65)
MassPeaks:1713
Segment 1 - Event 1



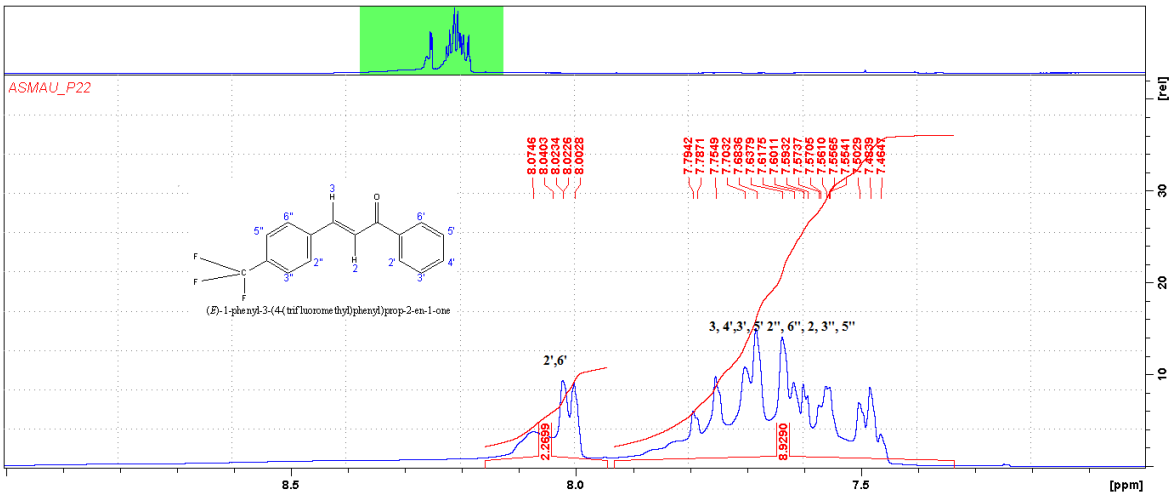
Mass spectrum of P21

Appendix 90



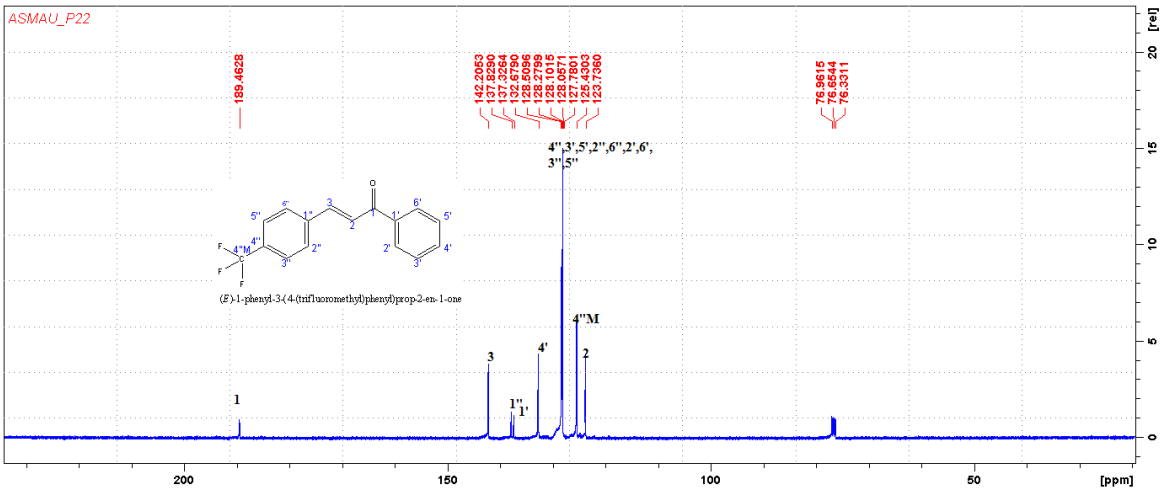
FT-IR Spectrum of P22

Appendix 91



^{1}H NMR of compound 22

Appendix 92



^{13}C NMR of compound 22

Appendix 93

TLC plates of substituted chalcones (n-Hexane : Ethyl acetate, 8:2)



Plate 1: P1

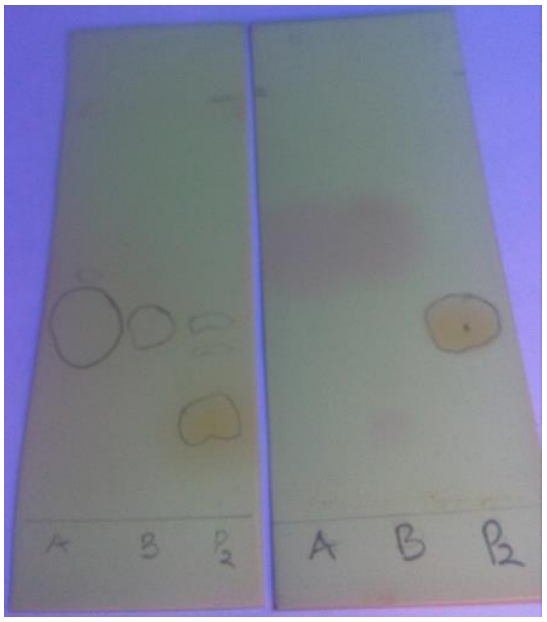


Plate 2: P2 purification

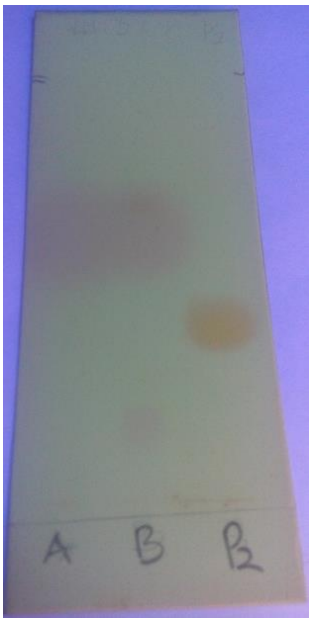


Plate 3: P2

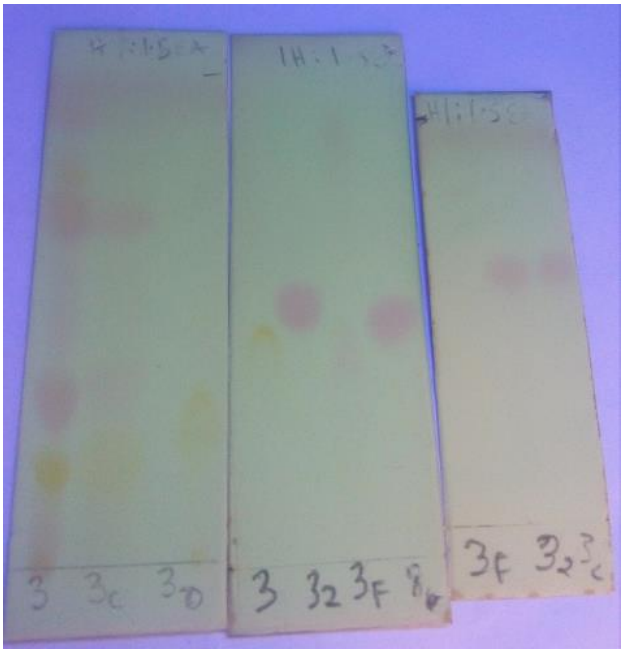


Plate 4: P3 purification

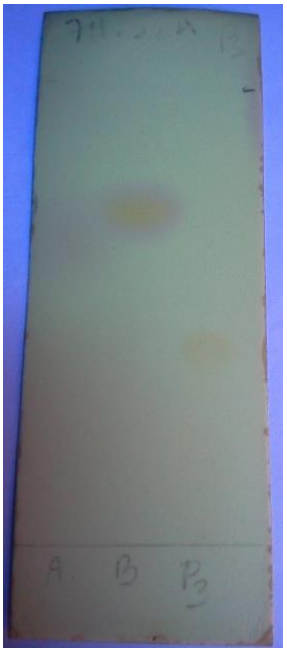


Plate 5: P3



Plate 6: P4

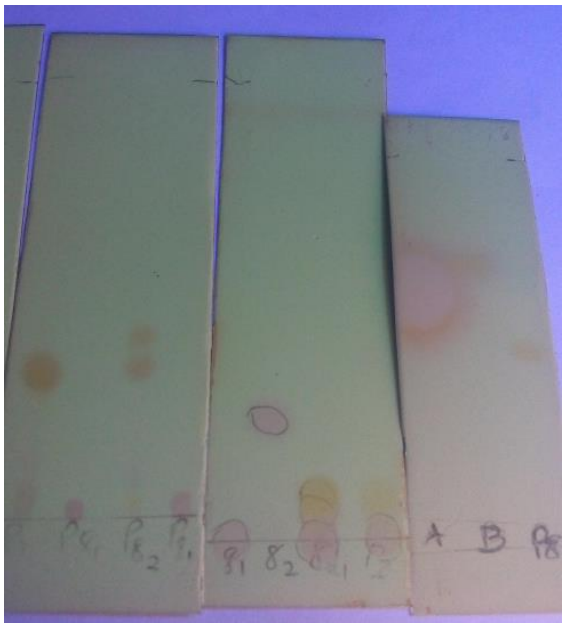


Plate 7: P8 Purification



Plate 8:P8



Plate 9: P11



Plate 10: P12



Plate 11: P13



Plate12: P15



Plate 13: P16

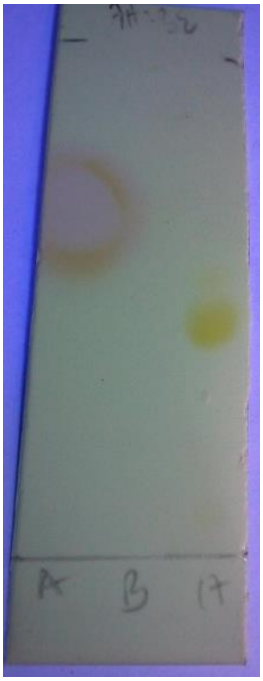


Plate 14: P17



Plate 15: P19



Plate 16: 22



Plate 17: P23



Plate 18: P24



Plate 19: P25